A COMPREHENSIVE FRAMEWORK TO MITIGATE SURFICIAL SLOPE FAILURES

by

BURAK BOLUK

Presented to the Faculty of the Graduate School of

The University of Texas at Arlington

in Partial Fulfillment of the Requirements

for the Degree of

DOCTOR OF PHILOSOPHY

THE UNIVERSITY OF TEXAS AT ARLINGTON

MAY 2021

ACKNOWLEDGEMENTS

I would like to express my sincere gratitude to my research supervisor Dr. Anand J. Puppala for his constant support, encouragement, vigilant guidance, and a great mentorship. Throughout my doctoral research, he shared his valuable time with me, maintained an open door, provided a patient supervision, and therefore facilitated great working conditions. In addition to this, his expertise in geotechnical engineering, passion, and hard work has inspired me immensely.

I would like to convey my sincere thanks to all the members of my PhD dissertation committee, Dr. Erick C. Jones, Dr. Xinbao Yu, and Dr. Srinivas Prabakar for reviewing my work and providing me insightful comments and valuable advices.

I would also like to express my gratefulness to Mr. Noel Paramanantham, P.E. and Mr. Dan Perry P.E. of Paris District, TxDOT, Mr. John Hajdasz, the head of the contractor company, and all other the engineers and staffs associated with the U.S. 75 Frontage Road rehabilitation work for their valuable contributions.

This research work has been supported by the Transportation Consortium of the South-Central States (TranSET) with the projects number of 17GTLSU04 and 18GTLSU06. I would like to thank to Dr. Navid Jafari and his research team at the Louisiana State University, for their invaluable cooperation in the TranSET projects.

I want to thank UTA College of Engineering and the Department of Civil Engineering for providing me the GTA and GRA scholarships and doctoral fellowships during my time at UTA. I also want to thank The State Hydraulic Works, which is a governmental agency under the Republic of Turkey Ministry of the Agriculture and Forestry, for their scholarships to pursue my research studies in UTA during my first year.

I would like to thank to Dr. Puneet Bhaskar and Dr. Sayantan Chakraborty for their friendships and unconditional support and advices during my research studies. Also, I would like to thank my friends, Dr. Shi He, Dr. Leila Mosadegh, Dr. Surya Congress, Dr. Santiago Caballero, Dr. Jasaswee Das, Dr. Anu George, Merlin Benedick, Nripojyoti Biswas, Manikanta Kartik, Ashrafuzzaman Khan, Prince Kumar, Nice Kaneza, Sandesh Gautam, Jose Bautista, Lam Le, and Jacque Bussey for their support, encouragement, and assistance during my research works. I also want to thank Dr. Ali Shafikhani for his very precious assistance on LIDAR surveys.

Like as always, above all, I am thankful to Allah for giving me an opportunity to meet and work with good people, successful completion of my doctoral dissertation and giving me a wonderful family. I am very grateful and would like to present my deepest thanks to my father, mother, brother, and fiancée. Their constant love, support, and unlimited trust on me during my research studies made me more dedicated and ambitious to pursue the doctoral program.

ABSTRACT

A COMPRHENSIVE FRAMEWORK TO MITIGATE SURFICIAL SLOPE FAILURES

Burak Boluk

The University of Texas at Arlington, 2021

Supervising Professor: Dr. Anand J. Puppala

Each year, numerous highway and dam slopes that are built with high plasticity clays experience shallow slope failures. Besides the high maintenance and repair costs, these failures negatively impact public life by interrupting the traffic flow and causing serious safety hazards. The development of desiccation cracks due to weathering cycles deteriorates hydro-mechanical properties of soil, increases water infiltration, and ultimately results in surficial slope failure.

Several slope rehabilitation methods have been developed to stabilize clayey soil slope sections affected by surficial failures. Lime stabilization is an effective treatment method that generally reduces the swell-shrink potential of expansive soil and enhances its engineering properties. However, exposure to wet-dry cycles negates some of the benefits of lime treatment and affects the extent of rainfall infiltration through the treated layer. Most lime treatment projects were primarily conducted without thoroughly estimating the impact of wet-dry cycles on the performance of the treated slopes. Proper consideration of long-term impacts of harsh environmental conditions on properties of treated soil in slope

stability analysis is needed to produce more resilient and promising slope rehabilitation projects.

In this research, the effectiveness of the lime treatment on both highway and dam slopes is assessed by incorporating the effect of detrimental changes in the hydro-mechanical properties of the treated soil due to wet-dry cycles. An experimental program is designed to estimate and compare the long-term strength parameters and durability of control and treated soils. The long-term stability of three lime-treated slopes is assessed numerically for various expected rainfall intensities and durations by conducting rainfall-induced unsaturated slope stability analyses. In order to assess the performance of lime-treated slope, field moisture probes and elevation survey techniques are used to monitor moisture fluctuation and deformation in slope with time, respectively. Also, the life cycle cost and benefit analysis for the current project is carried out to investigate the economic feasibility of the slope rehabilitation method using the lime treatment. The framework developed in this research study can be readily used by the geotechnical engineering fraternity to assess the long-term to address surficial slope stability issues.

TABLE OF CONTENTS

LIST OF FIGURES

LIST OF TABLES

Chapter 1

INTRODUCTION

1.1 Background

Numerous geotechnical engineering infrastructures, including highway and dam embankment slopes are built using expansive clayey soils (Kodikara et al. 2004, Al-Rawas and Goosen 2006, Jones and Jefferson 2012, Congress and Puppala 2020). Even though the initial factor of safety (FOS) of these slopes satisfy the design criteria, many of them experience stability issues in long-term due to detrimental impact of seasonal weathering cycles on hydro-mechanical properties of soil (Kayyal and Wright 1991, Jafari et al. 2019). Expansive soils typically undergo considerable amount of volume change and are often susceptible to desiccation cracks due to cycling drying and wetting (Zhao et al. 2020). The desiccation cracks damage integrity of soil and deteriorate its hydro-mechanical properties (Kodikara and Costa 2013, Jafari et al. 2019a). The desiccation cracks reach at greater depths after each wet-dry cycle, and the effects of desiccation cracks on hydro-mechanical properties of soil can extend up to 2.1m (7 ft) depth from the surface of slope (Anderson et al. 1985, Konrad and Ayad 2011).

The detrimental impacts of the desiccation cracking on the hydraulic properties of soil has been observed by many researchers (Lau 1987, Kodikara and Choi 2006, Peron et al. 2013, Louati et al. 2018). The rate of water flow is

significantly larger in a desiccated soil than that of the intact soil matrix (Köhne et al. 2002, Li et al. 2017). Albrecht and Benson (2001) reported that the increase in permeability value for clays due to development of desiccation cracks could be three orders of magnitude. The strength reduction of soil due to desiccation cracks has gathered great concern over several decades (Kayyal and Wright 1991, Wright et al. 2007, Stirling et al. 2017).

During the wetting period, the water easily seeps down to deeper soil layers through cracks and accumulates in the surficial layer due to underlying non-desiccated soils. The excessive wetting of soil leads to swelling and softening of clayey soil which ultimately decrease its shear strength to fully soften strength (FSS) (Skempton 1970; Skempton 1977; Jafari et al. 2019b). The degradation of shear strength of soil and increase in pore water pressure due to high infiltration rate causes surficial slope failure (Qi et al. 2020; Boluk et al. 2021). These failures are generally surficial in nature and are usually 1.2 to 2.4 m deep (Anderson et al. 1985, Konrad and Ayad 2011).

Lime stabilization is one of the most commonly used and effective methods to reduce swelling and shrinkage potential of expansive soils (Chakraborty and Nair 2018, Puppala et al. 2019a). The cementitious products, formed during soil-lime reactions, bind the soil particles and enhance its strength, stiffness, and durability significantly (Puppala et al. 1996; Hoyos et al. 2004). Althoguh the lime treatment significantly improve the soil properties, a very few studies have been

reported on the long-term performance of lime-treated soil. Rao et al. (2001) investigated the impact of wet-dry cycles on lime-treated soils and observed that liquid limit and clay fraction increases considerably due to breaking of cementitious bonding after each weathering cycle. Khattab et al. (2007) also pointed out that weathering cycles can cause a significant increase in swell potential and eventually decrease the effectiveness of lime treatment.

Though the lime stabilization method gives promising results in most of the cases, some attempts were resulted in with unsatisfied results in the past. Several recurring failures in lime-treated slopes in Texas were reported by Abrams and Wright (1972). Also, many of state departments were reported lime stabilized subgrade failures due to loss of benefits of treatment, or the treatment being ineffective over the time (Little et al. 2000). The exact reasons of the inadequate performance of lime stabilized projects are still debatable. Probable reasons of these failures include:

1. Inadequate comprehensive laboratory test program followed in the design phase,
2. Insufficient applied treatment dosages and depth of treatment,
3. Improper field conditions during the design phase,
4. Underestimation of the effects of the moisture changes due to the climatic fluctuations on the treated soils' hydro-mechanical properties, and
5. Inadequacy of the providing a proper drainage system.

An attempt has been made in the present research work is to investigate the long-term effectiveness of the lime treatment on the slopes by incorporating the effect of detrimental changes in the hydro-mechanical properties of soil and rainfall events. In this research study, a comprehensive framework is developed by addressing the abovementioned issues, and the long-term performance of lime-treated slope is evaluated.

1.2 Research Objectives

The main objective of this research study is to assess the effectiveness and permanency of lime treatment as a viable option to arrest and rehabilitate the skin slide type failures on highway and dam embankment slopes. This study is conducted by evaluating the long-term stability of lime stabilized slopes by considering climatic factors and the effect of cyclic wetting and drying cycles on hydro-mechanical properties of the treated soil. The performance of lime treatment method is assessed by using post-construction monitoring techniques. Moreover, the long-term economic aspect of the lime stabilization method for slope is investigated. In order to accomplish the main objective, several specific objectives have been formulated, and are listed following:

1. To investigate the effectiveness of treatment in term of long-term strength properties of selected soil with different dosages of lime and curing periods.

2. To examine the thickness of the surficial treated layer on the stability of slopes.
3. To study the effects of rainfall intensity and duration on the stability of untreated and lime-treated soil slopes and assess the need for drainage system.
4. To monitor the seasonal moisture changes of the treated and control soils in the stabilized slopes and measure the vertical changes occurred in the treated slope surface and pavement due to moisture fluctuations.
5. To study the expected expenditures and benefits of the lime-treated slope stabilization method by conducting a life cycle cost and benefit analysis.

These research tasks are conducted as per the developed flowchart as shown in Figure 1.1.

Figure 1.1 A comprehensive flowchart followed to in this research study

1.3 Organization of Dissertation

This dissertation was prepared as a final product of a comprehensive research study and consists of a total of seven chapters. The brief outline of dissertation and contents of each chapters are presented following.

Chapter 1 introduces the topic of research and provides some background information of the topic. The main research objective and specific tasks used to accomplish the goals are also presented. A description of each chapters is detailed, and the organization of the dissertation is also presented in this chapter.

Chapter 2 presents a compiled literature review on expansive soils, causes of surficial slope failures, several slope stabilization methods, as well as some of their limitations. The clay mineralogy, soil-water interactions, development desiccation cracks, and impacts of desiccation cracks on slopes are discussed in detail in this chapter. Also, the fundamental concepts of the unsaturated state soil, water flow in this soil, and slope stability analysis are presented. The lime stabilization method, the impact of lime stabilization on hydra-mechanical properties of soil, and the effects of weathering cycle on lime-treated soils' properties are also discussed.

Chapter 3 describes the observed failures on embankment slopes of U.S. 75 Frontage Road, Grapevine dam, and Joe Pool lake dam. In addition to this, the basic laboratory soil tests performed on the U.S. 75 Frontage Road slope to determine the main causes of this slope failure are presented, as well as their results

are included. Also, the previous research study conducted using these dam embankment slopes to assess and compare the performance of several different slope stabilization methods are presented in detail.

Chapter 4 details the experimental methodology and test procedures of soil-lime mix design studies performed for U.S. 75 Frontage Road slope rehabilitation work. Basic characterization tests, engineering tests, durability, and strength retention tests after subjecting wet-dry cycles. Additionally, a comparison of results of soils treated with different treatment dosages and cured for different periods, are provided in this chapter.

Chapter 5 provides the details of numerical analysis studies conducted to evaluate the long-term stability of unsaturated treated slopes under various expected climatic conditions. The effect of a drainage system on the stability of rehabilitated slope section is also studied. In addition to this, the inverse numerical analysis of the failed U.S. 75 Frontage Road embankment slope is also presented.

Chapter 6 presents the construction plans prepared and executed for stabilization of the failed section of U.S. 75 Frontage Road slope along with the details of field operations phases. Moreover, the post-treatment performance of rehabilitated slope section is assessed by using field instrumentation and conducting field total station and light detection and ranging (LIDAR) surveys. In addition to this, the economic aspect of the lime stabilization work is studied by

conducting life cycle cost and benefits analysis on the U.S. 75 Frontage Road slope rehabilitation work.

Chapter 7 summarizes the major findings and conclusions obtained from this research work. It also addresses the future scope of works and recommendations.

Chapter 2

LITERATURE REVIEW

2.1 Introduction

Expansive clayey soils are prevalent in many arid and semi-arid regions of the world (Al-Rawas and Goosen 2006, Jones and Jefferson 2012, Congress and Puppala 2020). These soils are often used to build man-made slopes including highway and railway embankments, levees, and dams (Jafari et al. 2019). Seasonal climatic fluctuations (wet-dry cycles) cause significant volumetric changes in clayey soil slopes (Banerjee 2017, Khan et al. 2017, Julina and Thyagaraj 2019). The swelling and shrinkage in the soil are caused by the events of precipitation, evaporation, and thawing. During the wet period, the expansive soil swell and in dry period, it tends to shrink (Zhao et al. 2020).

Restrained shrinkage causes the development of tensile stresses and when the tensile stress exceeds the soil tensile strength, soil experiences desiccation cracks (Acharya 2015, Al-Dakheeli and Bulut 2019). These desiccation cracks usually develop in the surficial layer of slope (active zone) (Wright et al. 2007, Wang et al. 2012, Caballero et al. 2016). In the rainy period, these cracks act as conduits and promote moisture intrusion into soil mass, subsequently resulting in a significant decrease in its effective strength (Prozzi and Luo 2007, Chen and Won 2007, Yang et al. 2019a, Zhang et al. 2020). This aforementioned

phenomenon results in numerous surficial slope failures (Qi et al. 2020, Boluk et al. 2021).

Many soil stabilization methods have been used in the past to prevent surficial slope failures. Lime stabilization is one of the most preferred and effective methods in minimizing the volumetric changes in expansive soils (Chakraborty and Nair 2018, Puppala et al. 2019a). Lime treatment generally reduces the swell-shrink potential of expansive soils, enhances the soil hydro-mechanical properties and affects the moisture infiltration characteristics (Locat 1996).

Most lime treatment slope stability projects are primarily conducted without thoroughly estimating the impact of rainfall on the slope degree of saturation by assuming the treated layer completely saturated or dry (Dronamraju 2008; Le 2013). Also, exposure to wet-dry cycles changes the engineering properties of treated soils and complicates the rainfall infiltration process (Akcanca and Aytekin 2014). These assumptions do not capture the actual field conditions and underestimate the effects of the seasonal variation of the rainfall on slope stability. There is a need to investigate the long-term effectiveness of the lime treatment on the slopes by incorporating the effect of detrimental changes in the hydro-mechanical properties of the treated soil due to wet-dry cycles and rainfall events.

This chapter reviews the available literature on desiccation cracking and its impacts on hydro-mechanical properties of expansive soil. It presents the

fundamental concepts of unsaturated soil mechanics with primary focus on hydro-mechanical properties and its estimation methods. The development mechanism of surficial slope failure is also discussed in conjunction with different rainfall characteristics. The salient information about soil lime admixtures: reactions and design considerations, the effect on soil properties, and performance under cyclic wet-dry cycles are thoroughly assessed in this chapter. All the compiled aforementioned literature is given in the following sections.

2.2 Expansive Soils

2.2.1 General

Expansive soils are prone to volume change when subjected to variation in moisture content. Because of this characteristic, these soils are also known as shrink-swell soils, expandable soils, cracking soils, or active soils. Expansive soils prevail across many regions of the world; countries including Australia, India, South Africa, Saudi Arabia, Turkey, and the US. It is commonly found in the areas with arid and semi-arid climates, where the annual precipitation is lower than the potential evapotranspiration (Kodikara et al. 2004, Sabtan 2005, Jones and Jefferson 2012). Approximately $1/4^{th}$ of the total land area in the US has expansive soil (Hedayati 2016). Figure 2.1 illustrates the distribution of expansive clays across the United States. Expansive soils are found throughout the areas from the Gulf of Mexico to Canada and Iowa to Pacific costs (Witczak 1972). Although the nature of expansive clays is unfavorable to build structures on them, the increase

in population and urbanization into reclaimed farmlands has made it difficult to avoid expansive clayey soil zones and many infrastructures are built by using on-site expansive soils as a borrow material (Williams 2003).

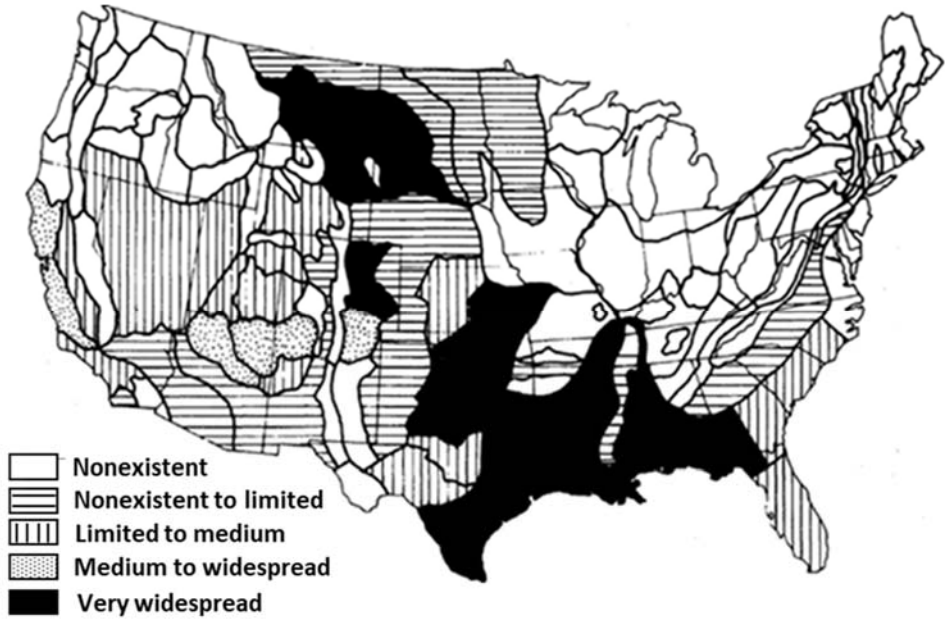

Figure 2.1 Expansive soil map of the USA (Witczak 1972)

The volumetric changes in expansive soil cause a significant amount of damage in embankment slopes, road pavements, pipelines, foundations, and irrigation channels (Tripathy and Rao 2009, Puppala et al. 2014a, Sharma and Sivapullaiah 2016). In a typical year in the USA, 13 billion dollars of worth of structural damages are caused by expansive clayey soils (Table 2.1) (Adem and Vanapalli 2013). In the state of Texas alone, the annual expenditure on repairs related to expansive soil touches one billion dollars (Punthutaecha et al. 2006, He et al. 2018). The annual overall financial loss due to expansive soils is more than

loss due to natural calamities such as earthquakes and tornados (Jones Jr and Holtz 1973, Puppala et al. 2011).

Table 2.1 Annual cost of damages caused by expansive clay (Adem and Vanapalli 2013)

Region	Damage per year	Reference
USA	$ 13 billion	Puppala and Cerato (2009)
UK	£ 400 million	Driscoll and Crilly (200)
France	€ 3.3 billion	Johnson (1973)
Saudi Arabia	$ 300 million	Ruwaih (1987)
China	¥ 100 million	Ng et al (2003)
Australia	$150 million	Osman et al (2005)

The swelling phenomenon in expansive soil is primarily attributed to the hydration of clay minerals. These volumetric changes generally occur in the surficial layer of soils within 3 meters from the ground surface (active zone). The degree of swell and shrinkage strain in soil depends on its density, void ratio, and initial water content, overburden stresses, and type and amount of clay minerals (Bell and Culshaw 2001, Patel 2019). Different types of clayey soils exhibit different degrees of swelling potential when hydrated. The soil containing mostly kaolinite or illite mineral undergoes little or no volumetric increase upon hydration. On the other hand, soil that contains smectite, montmorillonite or bentonite minerals could expand up to several times of its dry state volume (Norrish 1954). The physical and chemical characteristics of some of the common clay minerals are discussed in the following section.

2.2.2 Clay Mineralogy and Chemical Structure

The term ‘clay’ is referred to as particulate material that has a particle size smaller than 2 micrometers and has a group of minerals that have a common crystal structural characteristic and chemical composition (Velde 1995). These minerals belong to the family of phyllosilicates, silicate layers, and preliminary product of weathering of rock or soils (Deer 2011). Phyllosilicates have a layered structure that consists of layered atoms planes. Based on the coordination of these atom planes, there are 2 types of phyllosilicate clay minerals: tetrahedral and octahedral sheets (Figure 2.2). Clay minerals are formed in various sizes and can be identified with different techniques such as Infrared analysis, differential thermal analysis, microscopic examination, or X-ray diffraction.

A tetrahedron is formed by a cation (silicon or aluminum) that is surrounded by four oxygen atoms. Adjacent tetrahedrons share oxygen anions and form a hexagonal network of the tetrahedral sheet. Similarly, an octahedron is formed by a cation (generally aluminum, magnesium, iron) surrounded by six oxygen or hydroxyl anions. These octahedral units form the eight-sided block of octahedral sheets (Barton and Karathanasis 2002). The interlocking of these tetrahedral and octahedral sheets forms the clay mineral units of 1:1 layer (one tetrahedral and one octahedral sheet) and 2:1 layer (two tetrahedral and one octahedral sheet). Different configuration and composition within these sheet layers result in different groups of clay minerals with different physical and

chemical properties. The most commonly found and known clay minerals are kaolinite, illite, and montmorillonite.

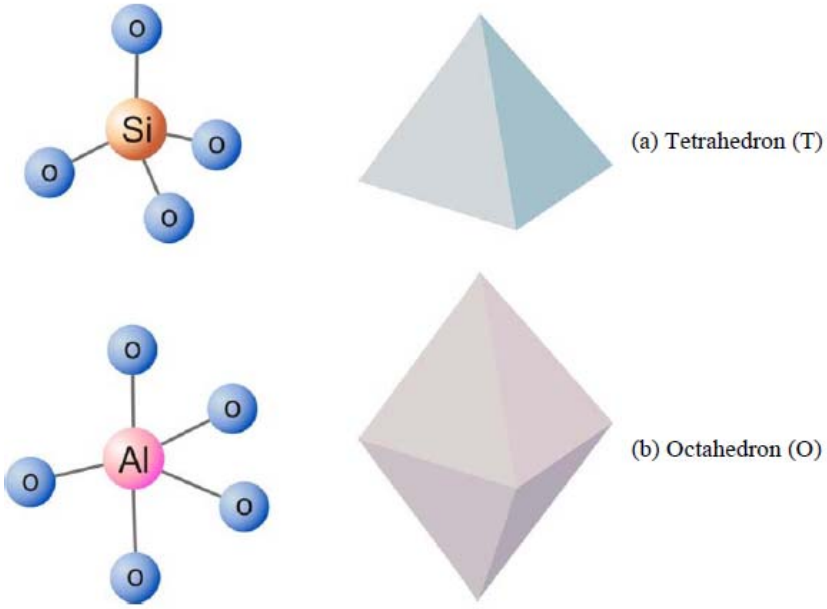

Figure 2.2 Structure of tetrahedral and octahedral sheets (Al-Ani and Sarapää 2008)

The kaolinite clay mineral ($Al_2Si_2O_5(OH)_4$), as shown in Figure 2.3a, has a 1:1 layered structure. It has a triclinic crystal structure with a diameter of 0.2 μm to 12 μm (Al-Ani and Sarapää 2008). Because of its small specific surface area (around 10-20 m^2/g) and strong hydrogen bonds between clay mineral sheets, kaolinite does not undergo high swelling (Deng et al. 2017). Illite (Figure 2.3b) clay mineral has a 2:1 layered structure and generally occurs after decomposition of feldspars, micas, and muscovite. The general formulization for illite is $K_yAl_4(Si_{8-y},Al_y)O_{20}(OH)_4$ (Mukherjee 2012). It is the primary component of

marine clay and shales and has a flaky shape with a particle size ranging from 0.1 μm to 2 μm (Al-Ani and Sarapää 2008). The specific surface area of illite clay mineral lies between 65 m^2/g and 100 m^2/g. Like kaolinite, illite also does not undergo an excessive swell strain due to interlayer cation of potassium, calcium or magnesium (K,Ca, or Mg) between phyllosilicates.

Montmorillonite (Figure 2.3c) has a general chemical formula of $(1/2Ca,Na)(Al,Mg,Fe)_4(Si,Al)_8O_{20}(OH)_4.nH2O$ with a 2:1 layered structure. Montmorillonite is formed by weathering of igneous rocks which are high in magnesium, iron, and calcium (Rapp 2002). These are platy irregular or hexagonal-shaped particles with an average thickness of 1 nm. Montmorillonite has specific surface area between 600 to 800 m^2/g and undergoes significant swelling strains due to weak van der Waals forces between silicate layers. The montmorillonite clay particles can expand up to 12–15 times upon hydration (Al-Ani and Sarapää 2008). Therefore, it is frequently used as mud in drilling operation and fill material to prevent leakage in dam slopes.

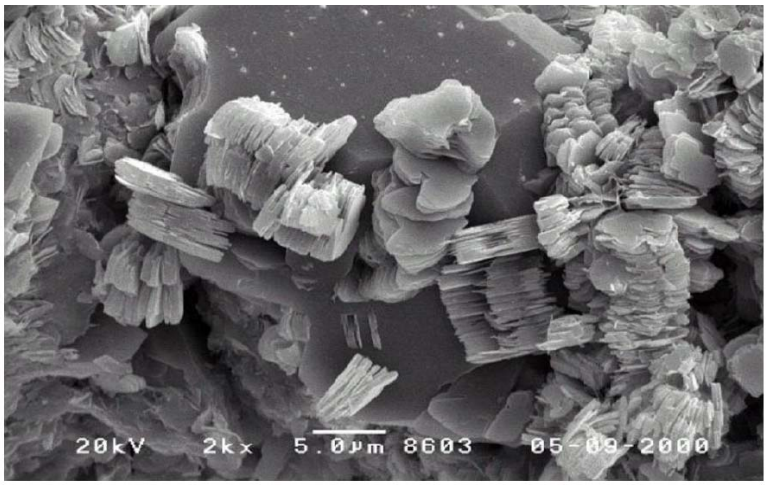

(a)

(b)

(c)

Figure 2.3 (a) SEM pictures of kaolinite, (b) illite, and (c) montmorillonite clay minerals (source: http://webmineral.com)

The soil that contains a larger amount of expansive clay minerals of montmorillonite, vermiculite, nontronite, saponite, hectorite, or beidellite, generally undergoes greater swell and shrinking strains. The volumetric increase of 10% is a typical value for expansive soils (Nelson and Miller 1992). Volumetric changes up to 30% can occur for soils containing a high amount of smectites (Al-Ani and Sarapää 2008).

2.2.3 Soil – Water Interaction

The swelling behavior of phyllosilicates in clay minerals is a function of broken bonds and the net negative charges in layers because of isomorphous substitution in either tetrahedral or octahedral sheets (He 2019). The structural alignment of the clay minerals changes due to the substitution of a cation with a

comparable size of another cation. Table 2.2 shows the ionic radius of the most common elements and their radii (Klein and Hurlbut 1993). In most of the clays, substitution of cation results in net negative charges on the surface of clay minerals (Xian et al. 2017). For example, when Si^{+4} cation is replaced with Al^{+3} in a tetrahedron, a negative charge is generated on the mineral surface.

Table 2.2 Physical properties of common elements (Klein and Hurlbut 1993)

Element	**Crustal Average (gkg ~)**	**Ionic radius (nm)**	**Volume (%)**
O^{-2}	466.0	0.140	89.54
Si+4	277.2	0.039	2.37
Al^{+3}	81.3	0.051	1.24
Fe^{+2}	50.0	0.074	0.79
Mg^{+2}	20.9	0.066	0.60
Na^{+2}	28.3	0.097	1.84
K^{+1}	25.9	0.133	1.84

The swelling and shrinkage phenomena in clayey soil are governed by the degree of soil-water interactions. The interaction of water with clay minerals occurs because of the following mechanisms (Mitchell 1976, Holtz and Kovacs 1981, Ural 2018):

1) Cation hydration: the net negative charges of clay surface attract the cations and water.
2) Hydrogen bonding: hydrogen bonds could be formed between the hydrogen present on clay surface and oxygen in the water and/or the hydrogen in water with oxygen on the clay surface.

3) Water dipole attraction: The positive side of water molecules get attached to the negatively charged clay surface. The negative side of water molecules attract the cations and hold the clay and water system together.
4) Attraction by osmosis: High concentration of negative charge on clay surface induces water molecules into clay by the process of osmosis.

Contrary to this, dehydration of clay minerals leads to a reduction in the space between silicate sheets and this is commonly known as shrinkage of clays.

2.2.4 Desiccation Cracks in Expansive Soil

2.2.4.1 General

The expansive clayey soils, particularly rich in smectite clay minerals, are prone to high shrinkage strains and desiccation cracking during the dry period (Omidi et al. 1996). The shrinkage and development of desiccation cracks in the soil are strongly related to the swelling potential of soil, amount of clay content, climatic factors, soil suction level, and presence of vegetation. (Morris et al. 1992, Day 1999). Lau (1987) showed that the desiccation cracks initiate at the suction level, less than 10 kPa for silty and clayey soils. The total cracked surface area is controlled by ambient temperature and an increase in temperature generally results in a higher evaporation rate and crack area (Tang et al. 2010). Soil with low swelling potential experiences fewer shrinkage cracks while the soil with high swelling characteristic undergoes a high shrinkage with wider cracks during dry periods (Zumrawi 2015).

The orientation and arrangement of desiccation cracks are highly random and unpredictable (Acharya 2015). Also, the exact estimation of the depth and width of the desiccation cracks is quite challenging. They may extend up to the depth of the active zone, where the seasonal moisture variation occurs in the ground (Morris et al. 1992). Desiccation cracks with up to 57 mm (2.2 in) width and 10 m (33 ft) deep from the ground surface have been reported in the literature (Nahlawi and Kodikara 2006; Chen and Won 2007). The dense network of desiccation crack serves as conduits and promotes moisture intrusion into soil mass, subsequently resulting in a significant decrease in its effective strength (Prozzi and Luo 2007, Chen and Won 2007).

Swelling and shrinking behavior of expansive soils cause irreversible results on soil properties (Jafari et al. 2019b). In the shrinking process, the silica sheets pull each other and create desiccation cracks. These desiccation cracks cannot be fully sealed during rewetting periods resulting in degraded soil properties (Fickies et al. 1979, Jones and Jefferson 2012). Therefore, the development of desiccation cracks damages the integrity of soil and causes detrimental changes in its hydro-mechanical, thermal, and physico-chemical properties (Kodikara and Costa 2013, Jafari et al. 2019a). Eventually, this leads to numerous problems in structures that are built with or on the soils prone to shrinkage.

2.2.4.2 Development Mechanism of Desiccation Cracks

Initiation and propagation of desiccation cracks are primarily associated with the shrinkage behavior of soil. When the soil starts to dry, there is an increase in soil suction and the volume of the soil starts shrinking (Jafari et al. 2019b). If soil is allowed to shrink freely without any internal constraint (moisture gradient, and non-uniformity in drying) or external constraint (interface friction and adhesion), there will not be any development of desiccation cracks (Nahlawi and Kodikara 2006, Kodikara and Costa 2013). As the tensile strength of the soil is generally very low, even a small value of tensile stress during drying can easily exceed the tensile strength resulting in the formation of desiccation cracks.

The effects of suction on the development of desiccation cracks in the soil mass have been studied by numerous researchers (Morris et al. 1992, Puppala et al. 2011, Tang et al. 2011, Wei et al. 2020). Tang et al. (2011) conducted a study on initially saturated samples to examine shrinkage and development of desiccation cracking by image processing technique. Figure 2.4 shows the schematic of crack initiation in a fully saturated soil (Tang et al. 2011). Due to loss in moisture content in the soil during drying, the water-air meniscus is formed in pores resulting in the development of capillary suction. With further drying, the curvature of water - air meniscus increases and the suction or tensile force that pull the clay particles towards each other, increases. If soil is constrained and there is no free shrinkage, the developed tensile stress exceeds the soil tensile strength and surface crack is formed.

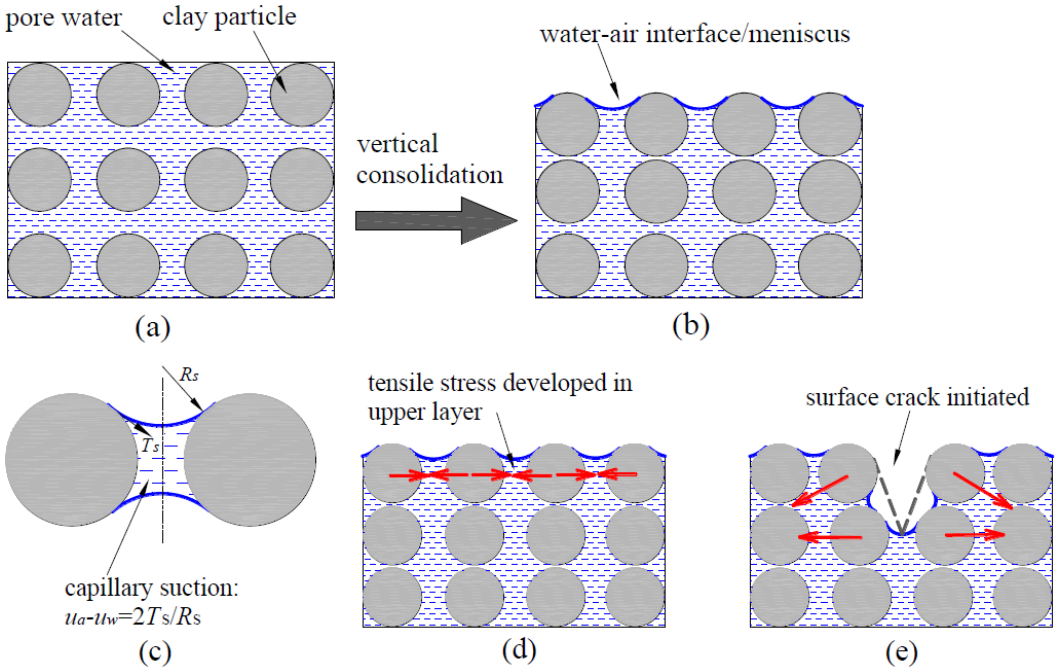

Figure 2.4 Initiation of desiccation crack in soil mass (Tang et al. 2011)

2.2.4.3 Effect of Desiccation Cracks on Engineering Properties of Soil

2.2.4.3.1 Effect on Hydraulic Conductivity

The effects of desiccation cracks on engineering properties of soil have been studied by numerous researchers (Elsbury et al. 1990, Daniel and Wu 1993, Albrecht and Benson 2001, Qiang et al. 2014, Louati et al. 2018). In regard to hydraulic properties of soil, desiccation cracks act like flow channels for water and hence increases the permeability of the soil. The majority of desiccation cracks that are developed in the dry season tend to reseal in the following wetting period. However, some cracks remain present because of the irreversible nature of swelling (He 2019). During the rewetting period, these cracks might get filled up

with some foreign material such as vegetation or granular material. This phenomenon leads to the formation of macro pores in soil mass resulting in a change in the permeability value of soil (Fickies et al. 1979).

Daniel (1984) conducted a study to investigate the permeability of the clay liners that are exposed to climatic variation in the field and found that there is a significant increase in permeability value (up to four orders in magnitude) with respect to permeability value measured in the laboratory. Boynton and Daniel (1985) investigated the permeability increase due to wet-dry cycles with respect to the increasing level of effective stresses. The author observed that the magnitude of the increase in permeability value due to desiccation decreased with an increase in effective stress. At an effective stress value higher than 8 psi (56 kPa), the coefficient of permeability of desiccated soil was found similar to the same before desiccation cracks development. The findings suggested that at the deeper soil layers, the presence of high overburden pressure might prevent the crack development and therefore mitigate the increase in soil permeability induced by desiccation cracks (Kleppe and Olson 1985).

Omidi et al. (1996) attempted to study the variation in permeability of desiccated soil with respect to volumetric shrinkage strain. The authors found that there was no significant increase in permeability up to 11 percent of shrinkage strain. The soils that exhibited high volumetric shrinkage strain underwent a significant increase in permeability due to high desiccation cracking (Figure 2.5).

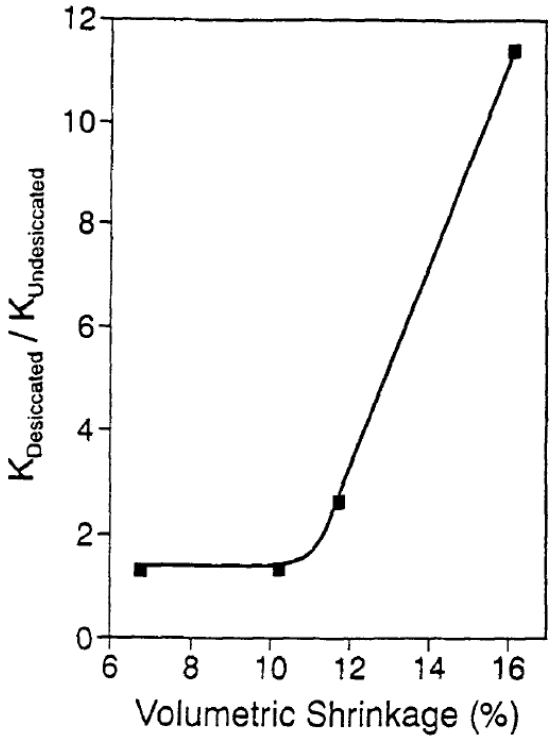

Figure 2.5 Rate of an increase in soil permeability with respect to soil shrinkage strain (Omidi et al. 1996)

Benson (2001) investigated the changes in the permeability of soils with various clay amount and plasticity index and compaction conditions under wet-dry cycles. The results showed that the soil specimens compacted at wet of optimum moisture content (OMC) experienced a higher increase in permeability than specimens compacted at OMC after a wet-dry cycle. Also, the authors observed that the soil with a high amount of clay content experiences more cracking and undergoes a higher increase in soil permeability value. The observed

increase in permeability water was almost 3 orders in magnitude after three drying and wetting cycles (Figure 2.6).

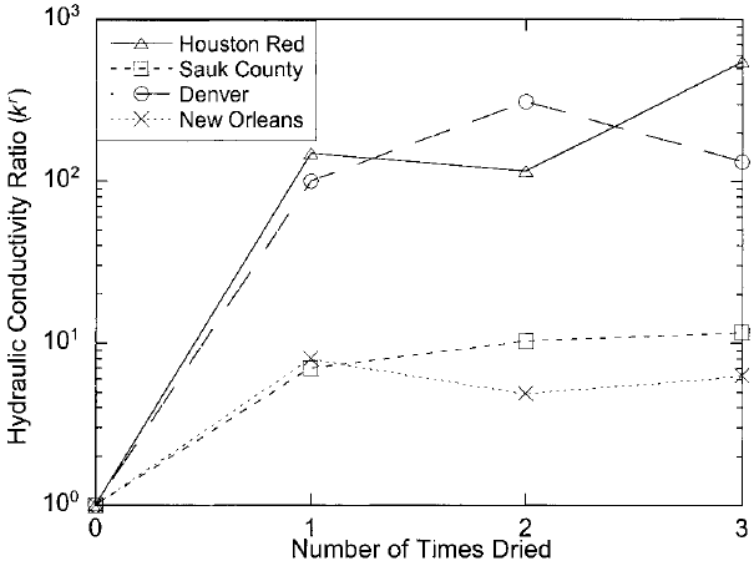

Figure 2.6 Variation in permeability soil under wet-dry cycles (Benson 2001)

2.2.4.3.2 Effect on Soil Strength

The development of desiccation cracks has an adverse effect on structures that are built with or built on expansive clays. This is mainly because of the reduction in the shear strength of soil due to desiccation cracks (Al-Zubaydi, 2011). During the wetting period, the water easily seeps down to deeper soil layers through cracks and accumulates in the surficial layer due to underlying non-desiccated soils. The presence of cracks leads to the development of positive pore water pressure during the wetting period and consequently causes a considerable decrease in effective stress in soil (Day 1994). Along with a reduction in effective

stress, desiccation cracks also damage soil integrity and reduces soil strength parameters (Boluk et al. 2021). The strength reduction due to desiccation cracks has gathered great concern over several decades. One of the earliest studies about soil strength reduction was conducted by Terzaghi (1936). Terzaghi (1936) attributed the cause of strength reduction in the clayey soils to the development of fissures. The author explained that during the wetting period, the fissured clayey soil swells freely due to the absence of confining pressure (Figure 2.7).

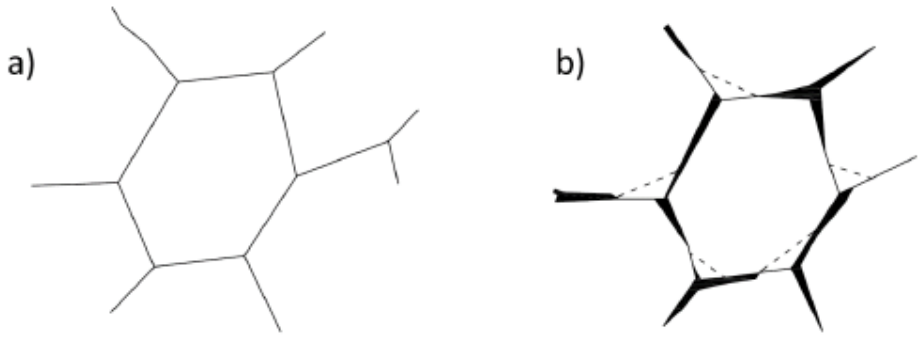

Figure 2.7 Crack propagation and weakening the soil (Terzaghi 1936, Castellanos 2014)

The similar phenomena of soil strength reduction occur for the soil that experiences desiccation cracks (Jafari et al. 2019a). Even though the desiccation cracks are resealed due to swelling during wetting period, there is a high probability that the desiccation cracks might occur at the same place where the initial cracks developed (Yong and Warkentin 1975). This leads to propagation of cracks to deeper layers and reduction in strength of soil (Yesiller et al. 2000,

Bordoloi et al. 2020). Rogers and Wright (1986) examined the reduction in soil strength properties after 30 shrink-swell cycles. The authors concluded that the cohesion intercept of the soil decreases drastically due to weathering cycles. It becomes negligible just after the 1st cycle of wetting-drying. Results also showed a significant decrease in friction angle of soil post wetting-drying cycles.

Kayyal and Wright (1991a) and Wright et al (2007) conducted studies on Paris, Beaumont, and Eagle ford clayey soils (Figures 2.8a, b, and c). A series of Triaxial consolidated undrained (CU) tests were conducted on specimens with three different initial conditions: 1) newly compacted specimens, 2) specimens subjected to wet-dry cycles, 3) specimens normally consolidated from the slurry condition. The first 2 sets of tests were conducted to study the effects of the wet-dry cycle on soil shear strength whereas, the third series of tests were performed to compare the shear test results with FSS results. The test results showed that the cohesion of soil decreases drastically (almost zero) at lower effective stresses for all the 3 soils after wet-dry cycles. The shear strength of Paris and Beaumont clay soil samples subjected to wet-dry cycles was found almost equal to the strength of the sample normally consolidated soil sample (Kayyal and Wright 1991). These results suggested that exposure to wet-dry cycles can cause a reduction of shear strength to FSS (Wright et al. 2007).

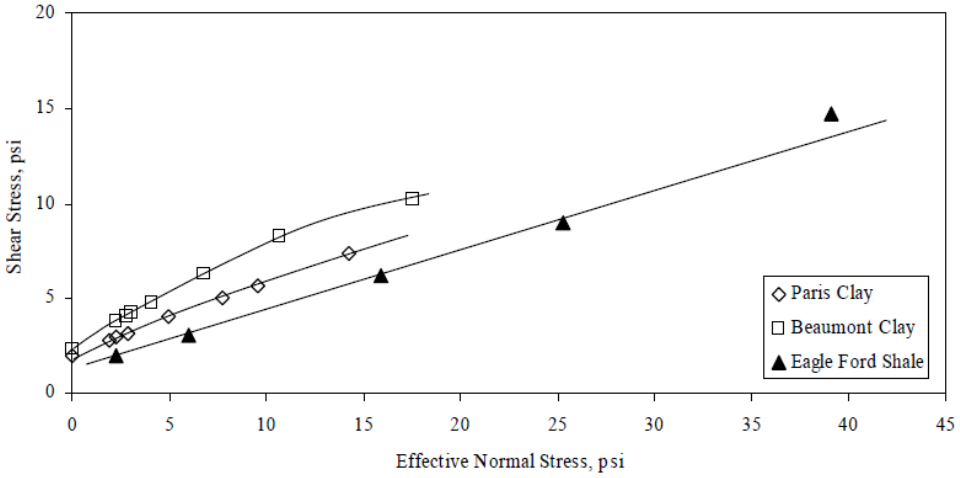
Shear Stress, psi
Effective Normal Stress, psi
Paris Clay
Beaumont Clay
Eagle Ford Shale

(a)

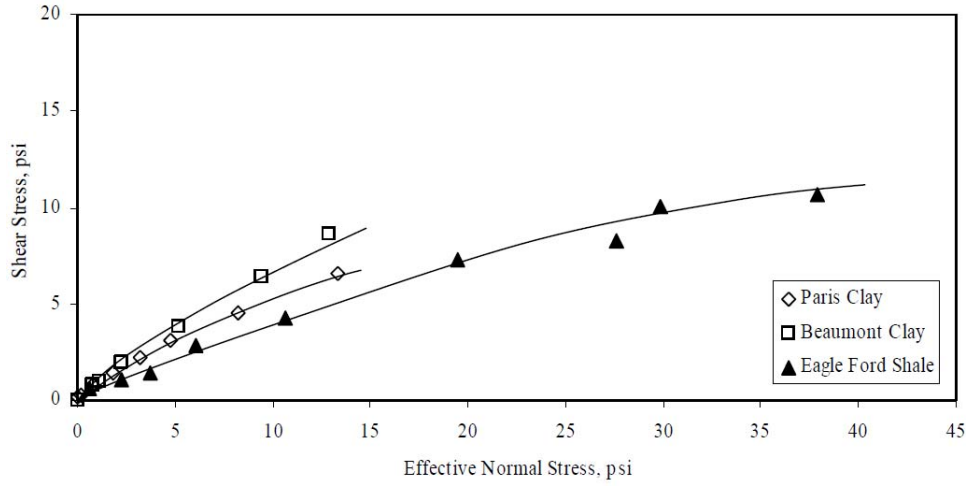
Shear Stress, psi
Effective Normal Stress, psi
Paris Clay
Beaumont Clay
Eagle Ford Shale

(b)

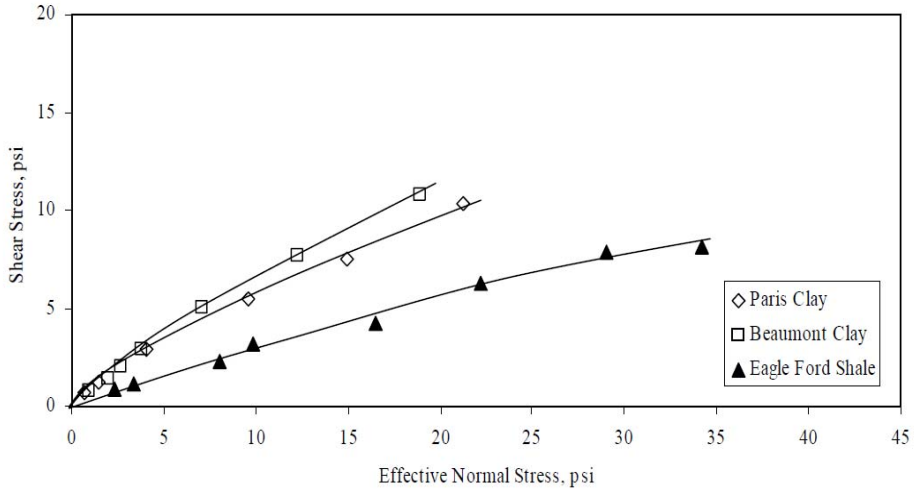

(c)

Figure 2.8 Shear strength of different soils: (a) compacted condition, (b) after wet-dry cycles, and (c) normally consolidated from slurry (Kayyal and Wright 1991, Wright et al. 2007)

2.2.4.4 Fully Softened Strength

2.2.4.4.1 General

In early studies on the shear strength of clayey soil, it was found that the peak shear strength of undisturbed clayey soil decreases significantly over the period of time (Taylor 1937, Skempton 1948, 1964, 1970). In a study conducted by Skempton (1964) on the failure of a natural slope of Jackfield, it was observed that the shear strength of London clay had experienced about 80% strength loss from its peak value to its residual strength value due to weathering cycles. The author also stated that the strength reduction of soil is generally caused by a drastic

loss of effective cohesion and a slight drop (1 to 2 degree) in the effective friction angle of soil. The FSS value of soil lies between peak and residual strength of the over-consolidated clayey soils (Figure 2.9) (Skemptom 1970). The author conducted back analyses for the first-time failures in stiff London clays and the analysis results showed the average mobilized shear strength of clayey soil at failure time of slope showed a prominent match with the FSS.

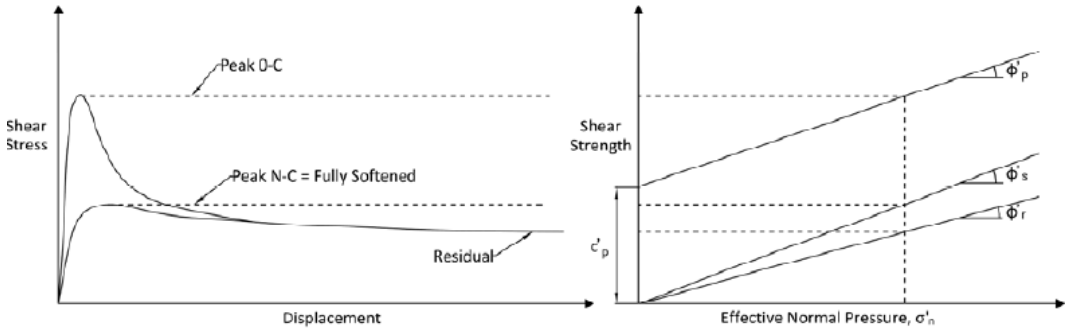

Figure 2.9 Comparison of the soil peak, FSS, and residual strength envelops (Skempton 1970)

From Skempton (1970) study, it can be concluded that the first failure of cut slopes is eventuated due to strength reduction of soil from peak strength to FSS. Furthermore, the study formulized FSS value as the peak strength value of normally consolidated clay. Though the conclusions made by Skempton (1970) were based on cut slopes, the concept of FSS can also be applied to fill embankments undergoing cyclic wetting and drying cycles (Kayyal and Wright 1991a). The fissures developed in cut slopes due to the release of overburden stress

can be considered equivalent to desiccation cracks in fill embankments due to weathering cycles (Kayyal and Wright 1991a). Also, the surficial soil zone, which experiences strength softening due to wet-dry cycles, is anticipated to coincide with the depth of the active zone, wherein moisture fluctuations are observed (Wright et al. 2007).

Castellanos et al. (2016) compiled a total of 142 slopes that experienced the first-time failure due to strength reduction in the long term. The authors attempted to study the effects of the consistency limits and type of soil on strength reduction. As shown in Figure 2.10, results indicated that the slopes in which failure is related to FSS have a liquid limit (LL) and plasticity index (PI) above 40 and 20 respectively. In a different study, the effect of soil mineralogy, composition, and consistency limits on FSS was evaluated by Tiwari and Ajmera (2011). The FSS value of soils was determined by using direct shear (DS) apparatus under different normal stress values.

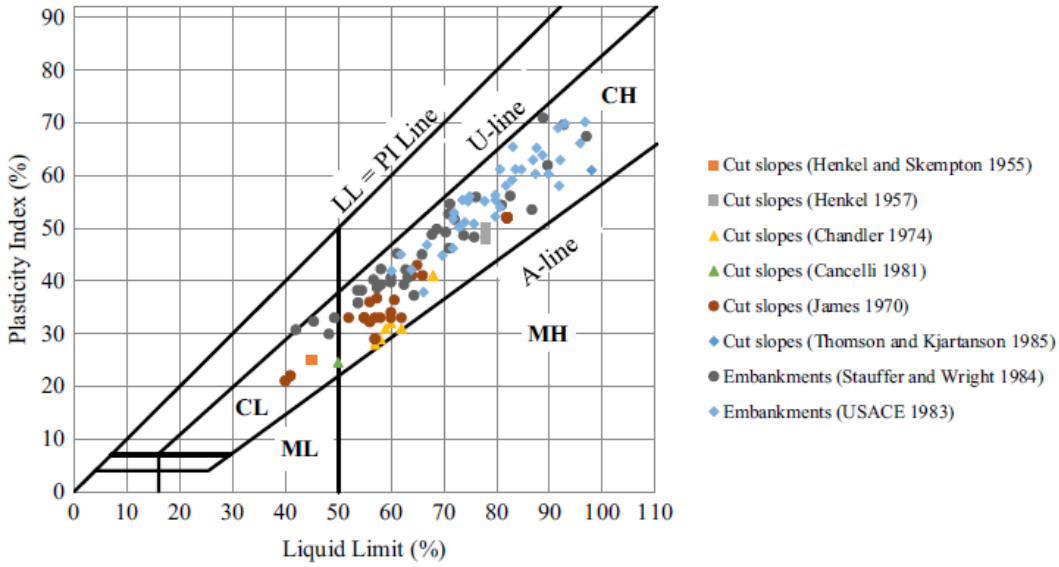

Figure 2.10 Compiled slope failures related to FSS (Castellanos et al. 2016)

The obtained correlation between FSS friction angle and clay content, LL, PI, and soil composition is presented in Figures 2.11a, b, c, and d, respectively. With an increase in the amount of montmorillonite and kaolinite in the soil, there was a decrease in soil FSS friction angle. Similarly, with an increase in the consistency limits of soil, a decrease in FSS friction angle value was observed. Also, variation in the amount of montmorillonite in soil was found to be a critical factor for FSS friction angle value.

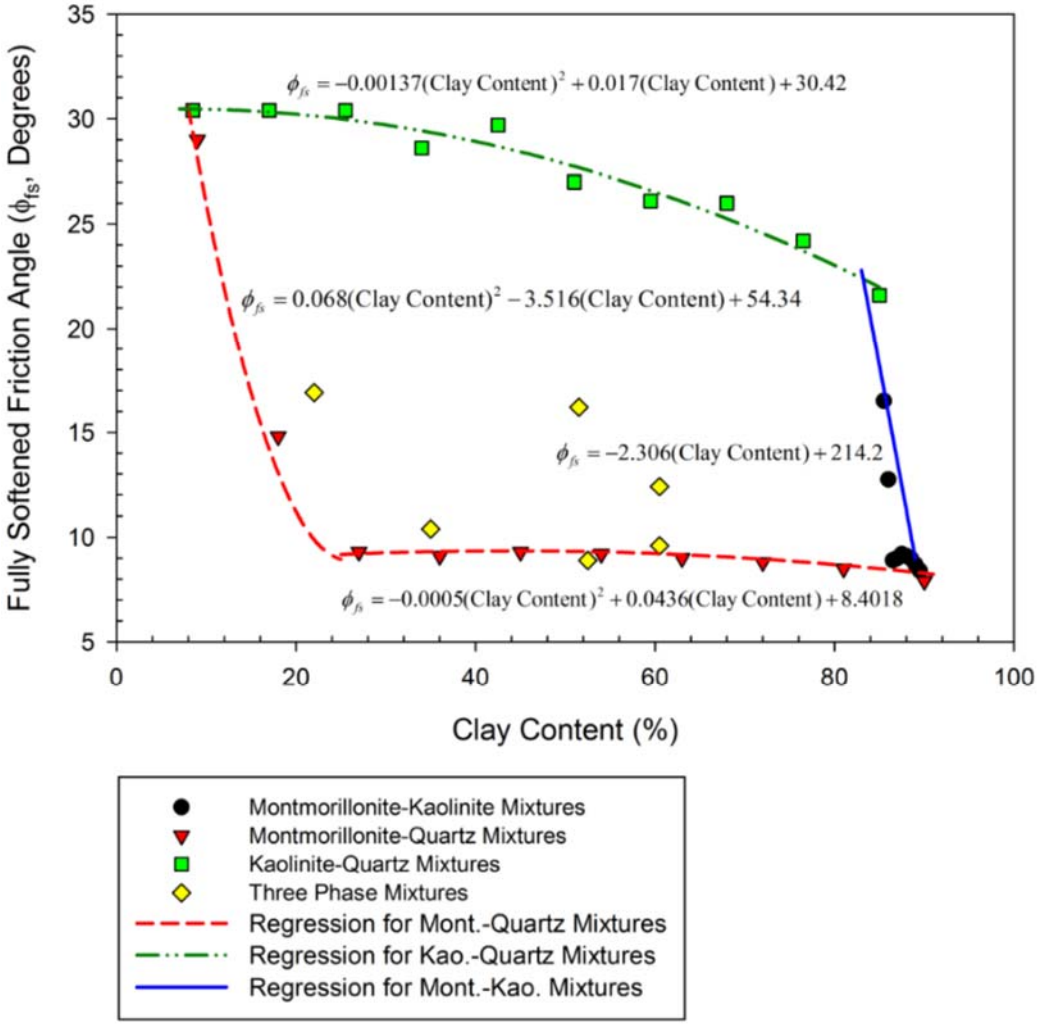
$\phi_{fs} = -0.00137(\text{Clay Content})^2 + 0.017(\text{Clay Content}) + 30.42$
$\phi_{fs} = 0.068(\text{Clay Content})^2 - 3.516(\text{Clay Content}) + 54.34$
$\phi_{fs} = -2.306(\text{Clay Content}) + 214.2$
$\phi_{fs} = -0.0005(\text{Clay Content})^2 + 0.0436(\text{Clay Content}) + 8.4018$
Fully Softened Friction Angle (ϕ_{fs}, Degrees)
Clay Content (%)
35
30
25
20
15
10
5
0
20
40
60
80
100
Montmorillonite-Kaolinite Mixtures
Montmorillonite-Quartz Mixtures
Kaolinite-Quartz Mixtures
Three Phase Mixtures
Regression for Mont.-Quartz Mixtures
Regression for Kao.-Quartz Mixtures
Regression for Mont.-Kao. Mixtures

(a)

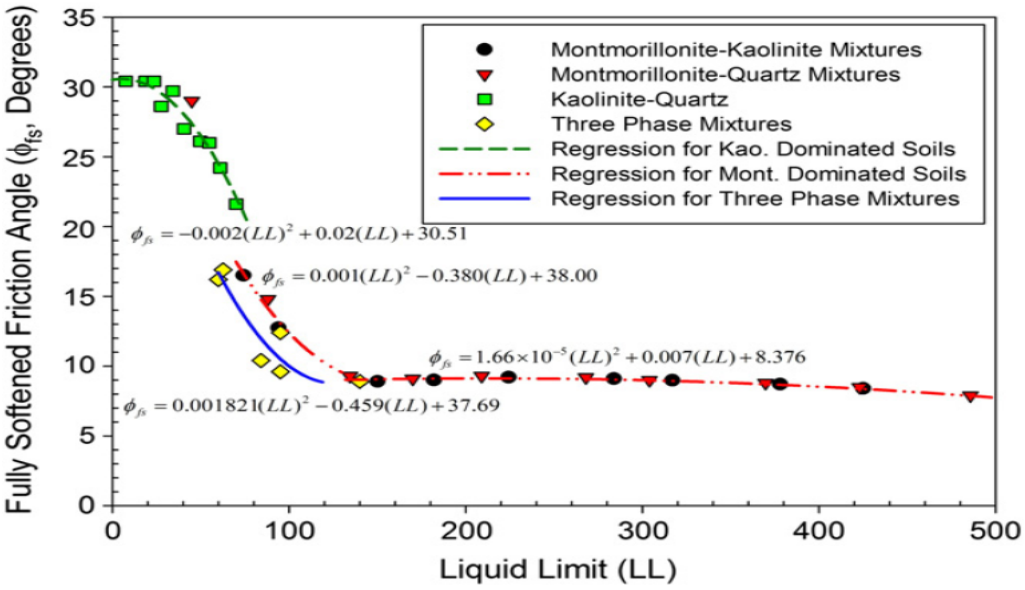
Fully Softened Friction Angle (ϕ_{fs}, Degrees)
Liquid Limit (LL)
Montmorillonite-Kaolinite Mixtures
Montmorillonite-Quartz Mixtures
Kaolinite-Quartz
Three Phase Mixtures
Regression for Kao. Dominated Soils
Regression for Mont. Dominated Soils
Regression for Three Phase Mixtures
$\phi_{fs} = -0.002(LL)^2 + 0.02(LL) + 30.51$
$\phi_{fs} = 0.001(LL)^2 - 0.380(LL) + 38.00$
$\phi_{fs} = 1.66\times10^{-5}(LL)^2 + 0.007(LL) + 8.376$
$\phi_{fs} = 0.001821(LL)^2 - 0.459(LL) + 37.69$

(b)

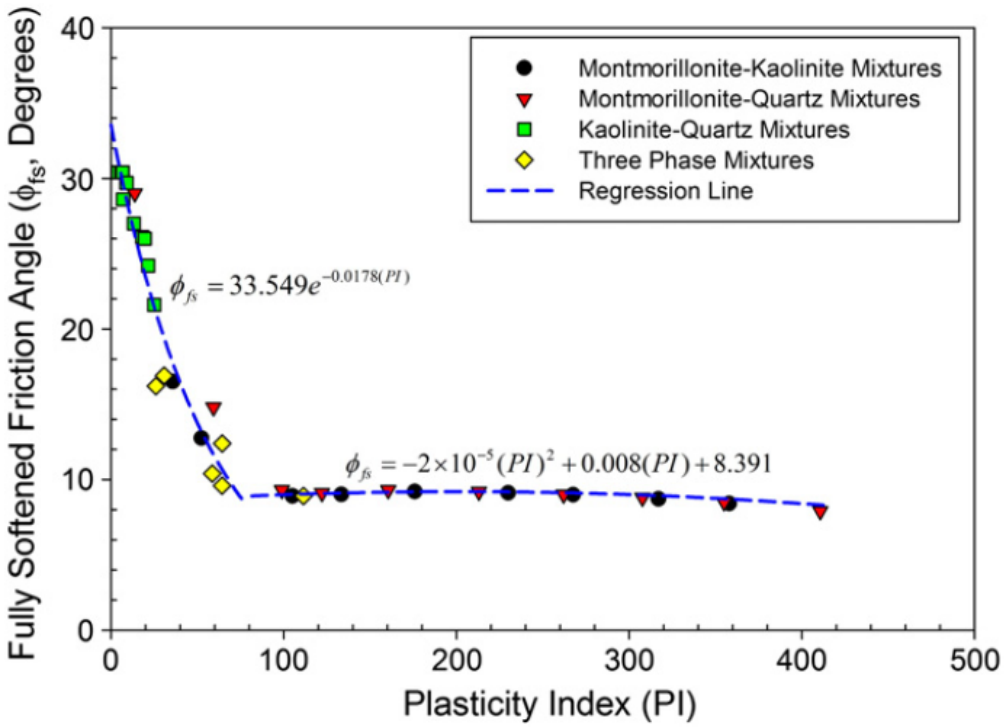
Fully Softened Friction Angle (ϕ_{fs}, Degrees)
Plasticity Index (PI)
Montmorillonite-Kaolinite Mixtures
Montmorillonite-Quartz Mixtures
Kaolinite-Quartz Mixtures
Three Phase Mixtures
Regression Line
$\phi_{fs} = 33.549e^{-0.0178(PI)}$
$\phi_{fs} = -2\times10^{-5}(PI)^2 + 0.008(PI) + 8.391$

(c)

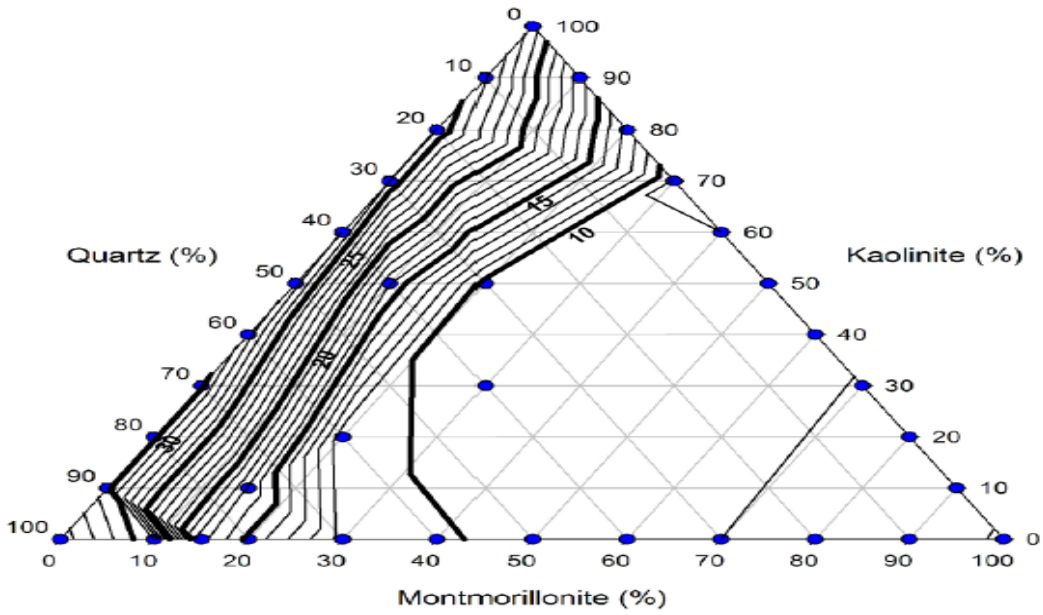

Figure 2.11 (a) Effects of soil composition, (b) clay content, (c) LL, and (d) PI on FSS friction angle value (Tiwari and Ajmera, 2011)

In the backdrop of desiccation cracks, the change in matric suction during drying period strongly effects the hydro-mechanical properties of soil (Morris et al. 1992, Omidi et al. 1996, Jafari et al. 2019a, Bhaskar et al. 2019a, Boluk 2021). There is a significant increase in soil strength and a decrease in its soil permeability with an increase in suction (Fredlund et al. 1978, Fredlund et al, 1994). Accurate assessment of rainfall-induced slope stability analysis requires the incorporation of soil suction in analysis (Bhaskar 2020). Therefore, it is important to study the effect of unsaturated soil properties and its impact on soil hydro-mechanical properties. The following section discusses the fundamental concepts of unsaturated soil mechanics relevant to the current research study.

2.3 Unsaturated State of Soil

2.3.1 Soil Suction

Soil is a particulate and porous material and consists of three phases: solid, water, and gas (air). However, Fredlund and Morgenstern (1977) suggested using the fourth phase of the water-air meniscus, the interface between water and air phase, which is formed in pores (Figure 2.12). At the molecular level, each water molecule experiences intermolecular cohesive forces from other water molecules. In the case of fully saturated soil, these forces get balanced out because of equal and opposite forces in all directions.

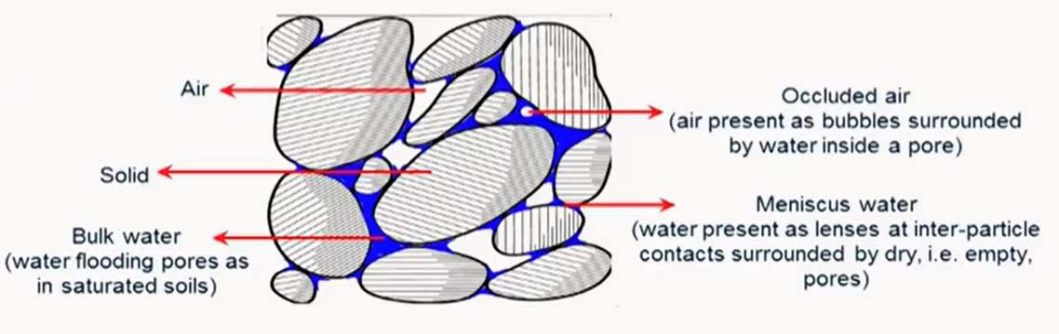

Figure 2.12 Schematic of unsaturated soil (Fredlund 1977)

However, in unsaturated soil, there are imbalanced forces due to the absence of cohesive forces at the air-water interface. This phenomenon creates a resultant inward force at the air-water interfaces as shown in Figure 2.13. This resultant unbalanced inward force causes surface tension which makes the interface look like a warped membrane (Figure 2.14).

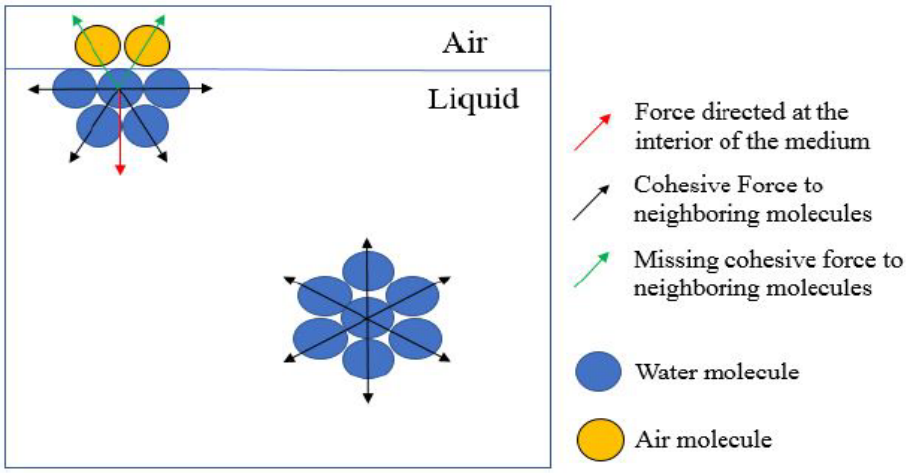

Figure 2.13 Development of the surface tension caused by imbalanced inter-molecular forces (Bhaskar 2020)

This pressure difference (Δu) of the three-dimensional surface can be calculated by using the following equation (2.1):

$$\Delta u = T_s\left(\frac{1}{R_1}+\frac{1}{R_2}\right) \tag{2.1}$$

Where,

Δu = pressure difference between two fluids in kPa,

Ts = Surface tension in kPa, and

$R1$ and $R2$ = radius of curvature of principal planes in m,

In unsaturated soils, the pressure difference between atmospheric air and water pressure is called matric suction ($u_a - u_w$) resulting in meniscus on the air-water interface which can be calculated by the following relationship (2.2):

$$\psi = (u_a - u_w) = \frac{2T_s}{R_s} \tag{2.2}$$

Where,

$(u_a - u_w)$ = soil matric suction in kPa, and

R_s = radius of curvature of contractile surface in m.

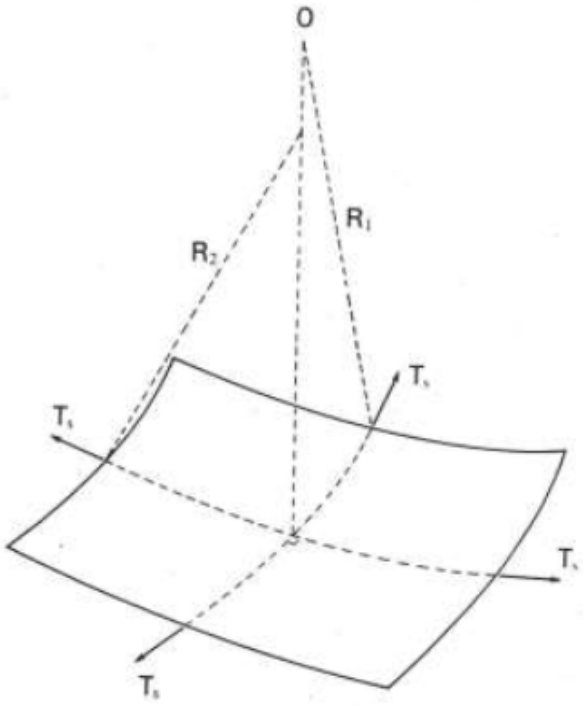

Figure 2.14 Surface tension on the air-water system (Fredlund and Rahardjo, 1993)

When the soil matric suction increases, the contractile skin becomes more curved and its radius of curvature decreases. On the other hand, the decrease in soil suction (in wetting period) leads to an increase in the radius of curvature to

infinity. In the saturated conditions, this curvature shape is eradicated due to balance in intermolecular forces.

The soil matric suction that is linked with moisture content generally experiences a seasonal fluctuation closer to the surface of the slope (Fredlund and Rahardjo 1993). During a dry period, soil matric suction level increases while in rainy periods the suction level decreases. The changes in soil unsaturated condition directly influence the soil properties including soil strength and hydraulic conductivity and consequently the safety of slope. During a dry period, the existence of high suction levels in soil reduces its hydraulic conductivity and increases its strength considerably. Whereas, in rainy seasons, the decrease in soil matric suction increases its permeability, reduces its effective strength and, thus increasing the probability of slope instability.

2.3.2 Suction – Water Content Relationships

2.3.2.1 General

Soil Water Retention Curve (SWRC) defines the relationship between the soil matric suction (ψ) and soil water content or degree of saturation. SWRC contains the fundamental idea of unsaturated soil and can be used to identify the basic soil properties of unsaturated soil (Fredlund and Rahardjo 1993). It is strongly related to soil properties including grain size distribution, soil type, density, and void ratio (Burger and Shackelford 2001, Zhou et al. 2012). Some of the correlations are developed for unsaturated soil parameters such as soil strength

parameters, stiffness, and hydraulic conductivity by incorporating the SWRC (Banerjee, 2018). SWRC curves can be determined by using soil gravimetric water content, soil volumetric water content, and degree of saturation. Soil gravimetric water content can be calculated using the following equation (2.3):

$$w = \frac{M_w}{M_s} \tag{2.3}$$

Where,

w = gravimetric water content,

M_w = weight of water, and

M_s = dry weight of soil.

Soil volumetric water content, θ, and degree of saturation, S, can be determined using the following equations of (2.4) and (2.5), respectively.

$$\theta = \frac{V_w}{V_v + V_s} \tag{2.4}$$

$$S = \frac{V_w}{V_v} \tag{2.5}$$

Where,

θ = volumetric water content,

S = degree of saturation,

V_w = volume of water,

V_v = volume of voids, and

V_s = volume of solids.

Gravimetric water content is a commonly used variable in geotechnical engineering. The main advantage of this variable is that it does not require any volume change measurement. It can be used with full confidence for soils that do not undergo volume change with the application of suction. Although the measurement of the accurate volumetric changes is complex in volumetric water content, it is preferred to be used in geotechnical soil science to estimate the unsaturated permeability values and in transient seepage analyses (Leong and Rahardjo 1997b).

2.3.2.2 Properties of Soil Water Retention Curve (SWRC)

A typical SWRC, as shown in Figure 2.15, is defined in 3 zones: boundary effect zone, transition zone, and residual zone (Fredlund 2006). In SWRC, air entry value (AEV) and residual soil suction value (ψ_r) demarcate these three zones. AEV of soil is defined as the minimum suction value at which air starts to draw into saturated pores of soils (Lu and Likos, 2004). In the boundary effect zone, up to AEV, the soil remains almost saturated under applied matric suction (Fredlund and Rahardjo 1993). After AEV, the air starts to draw into the soil and air pushes the water from larger pores. A small amount of increase in suction leads to a larger decrease in water content. In the transition zone, which lies between AEV and residual soil suction value (ψ_r), there is barely any reduction in the water content of the soil. In this zone, the SWRC becomes almost a straight line. The unsaturated

characteristics of soil are more prominent in the transition zone of SWRC as all three phases; solid, water and air phases are continuously present in it (Bao et al, 1998). Graphically, the intersection of slope line in the transition zone and horizontal line in the boundary effect zone provides the AEV of soil.

After residual matric suction, it becomes very difficult to remove additional water from the soil. In the residual zone, water is present in the pores in the form of thin film through adsorption (Vanapalli et al. 1998). Graphically, the intersection of the extended line from the slope portion of the SWRC and the tangent from the suction value of 1 GPa gives ψ_r value of soil. The parameters and shape of SWRC are directly controlled by soil type and properties. With an increase in soil PI and the amount of fine material in the soils, the AEV and saturated water content of soil increase, and the slope of SWRC in the transition zone decreases. Also, there is a significant effect of soil initial water content, soil stress history, and structure on the SWRC of soil (Fredlund and Xing 1994).

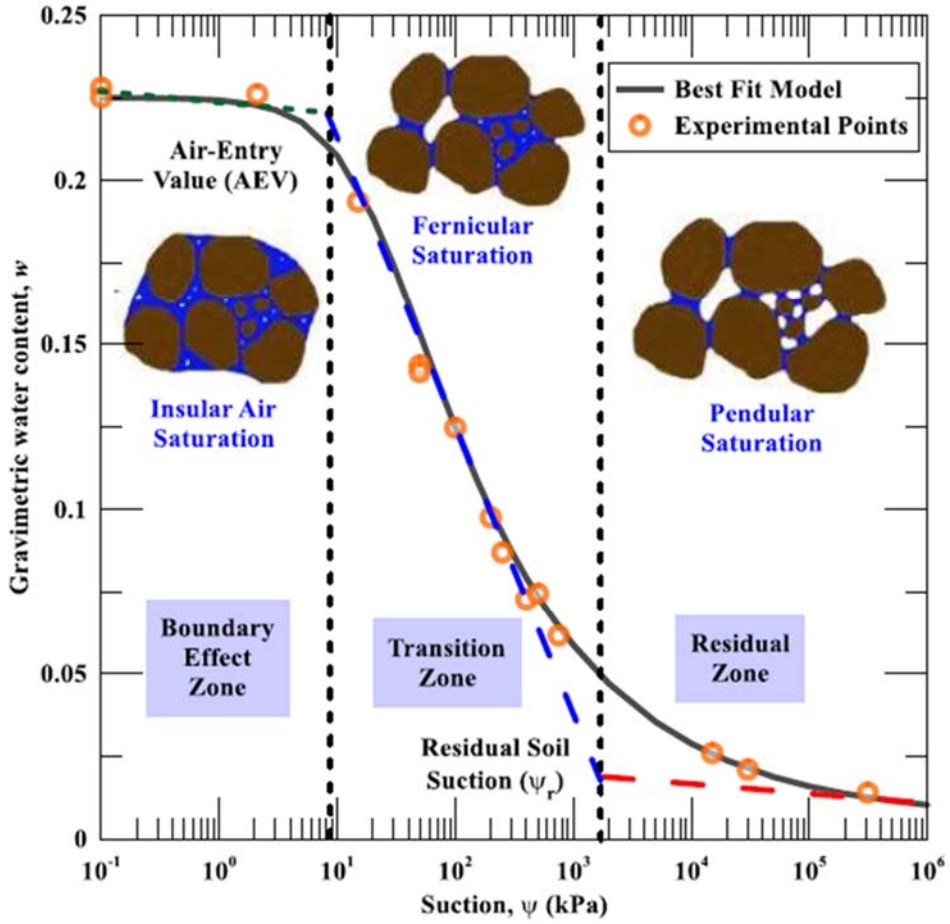

Figure 2.15 A typical SWRC of soil (Banerjee, 2018)

2.3.2.3 Determination Methods of SWRC

Various test methods have been developed for the determination of the SWRC of soil. Each method has its advantages and limitations and can be used to determine either the total and/or matric suction value. Table 2.3 represents several determination methods and suction measurement techniques and measurement ranges. Both Fredlund Tempe cell (Figure 2.16a) and pressure plate devices (Figure 2.16b) work using the same Axis-translation techniques and tests are

conducted with a high air entry value (HAEV) ceramic disk (Hilf 1956). The main advantage of the Fredlund Tempe cell is that it allows inducing normal stress on specimens during the testing process, on the other hand, the pressure plate device allows to conduct the test on several specimens at the same time. In these devices, the soil matric suction value (u_a- u_w) can be directly applied to the specimens that sit on the saturated HAEV disc while changing only the air pressure and maintaining the pore water pressure of the sample. The HAEV disc with very small pores prevents the air to pass through it and maintains air pressure in the apparatus. Therefore, at the corresponding suction level, the water present in the sample can only drain out. After the equilibrium stage is achieved, the water content of the sample is determined at the corresponding suction level. This technique can build up matric suction in the apparatus up to AEV of the HAEV disk.

Table 2.3 Overview of several SWRC measurement methods

Test method	**Technique**	**Soil Suction**	**Suction Range (10^3 kPa)**
Tempe cell	Axis-translation	Matric	0 - 1.5
Pressure plate	Axis-translation	Matric	0 - 1.5
Thermal conductivity sensor	-	Matric	0.01 - 1
Thermocouple psychrometer	Humidity measurement	Total	0.01 - 8
Chilled-mirror hygrometer	Humidity measurement	Total	1 – 450
Filter paper	Humidity measurement	Total	0 - 1000

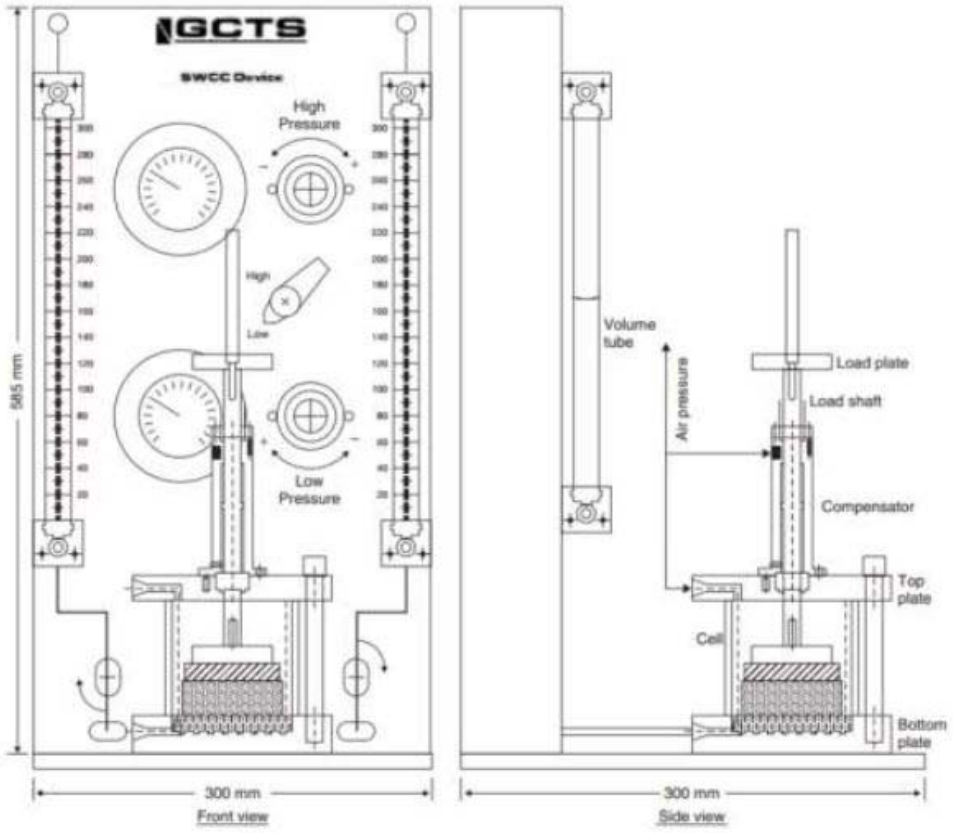
GCTS
SWCC Device
High Pressure
High
Low
Low Pressure
585 mm
300 mm
Front view
Volume tube
Air pressure
Load plate
Load shaft
Compensator
Top plate
Cell
Bottom plate
300 mm
Side view

(a)

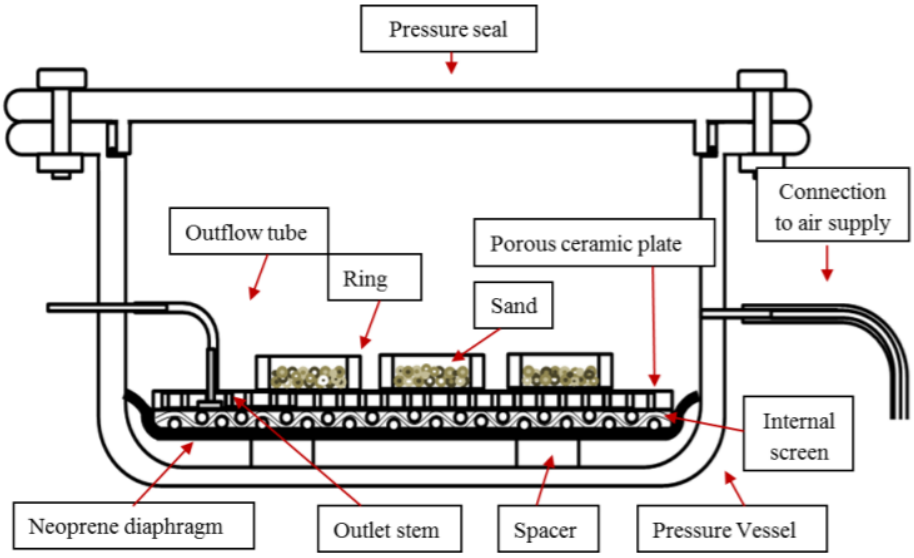

(b)

Figure 2.16 a) Cross section view of Fredlund's Tempe cell (Padilla et al. 2005) and b) typical pressure plate device (Azmi et al. 2019)

The principle of the Dew point potentiometer apparatus shown in Figure 2.17 is based on the chilled-mirror technique. In this technique, the relative humidity of the air that is inside the closed container is determined by using the optical and temperature sensors, and a mirror. Consequently, the total suction value is estimated based on the measured water vapor pressure above the soil sample (Leong et al. 2003).

Figure 2.17 Dew point potentiometer apparatus used in the research

2.3.2.4 Mathematical Equations for SWRC

The determination of the SWRC for a wide range of soil suction levels requires extensive laboratory work. Therefore, several empirical models are used to define SWRC over a wide range of suction levels. These empirical equations are formulated to best fit the available laboratory determined data. The adjustment and generating the best fitted SWRC are done, generally, using 2 or 3 fitting parameters. In Table 2.4, some of the most known mathematical equations are presented. Among all the available equations, van Genuchten (1980) and Fredlund and Xing (1994) equations best fit the measurement data with higher coefficient of correlation (Leong and Rahardjo 1997a).

Table 2.4 Mathematical equation to fit SWRC (Fredlund et al., 2012)

Reference	Equation	Description
Gardner (1958b)	$\Theta_d = \frac{1}{1 + a_g \psi^{n_g}}$ Where, $\Theta_d = \frac{w(\psi)}{w_s}$	a_g = fitting parameter which is related to AEV of the soil n_g = fitting parameter that is a function of the rate of water extraction from soil after AEV.
Brooks and Corey (1964)	$w(\psi) = w_s$ or $\Theta_n = 1 \; for \; \psi \leq \psi_{aev}$ $\Theta_n = \left[\frac{\psi}{\psi_{aev}}\right]^{-\lambda_{bc}} \psi > \psi_{aev}$ Where, $\Theta_n = \frac{w(\psi) - w_r}{w_s - w_r}$	ψ_{aev} = air entry value of soil λ_{bc} = pore size distribution index w_r = residual water content located through trial-and-error process that yields straight line on semi log plot of degree of saturation versus suction.
van Genuchten (1980)	$\Theta_n = \frac{1}{\left[1 + \left(a_{vg}\psi\right)^{n_{vg}}\right]^{m_{vg}}}$ Where, $\Theta_n = \frac{w(\psi) - w_r}{w_s - w_r}$	a_{vg} = fitting parameter primarily related to inverse of air-entry value (units equal to 1/kPa) n_{vg} = fitting parameter primarily related to rate of water extraction from soil once air-entry value has been exceeded. m_{vg} = fitting parameter primarily related to residual water content conditions.

Fredlund and Xing (1994)	$w(\psi) = C(\psi)\frac{w_s}{\left[\ln\{e + \left(\frac{\psi}{a_f}\right)^{n_f}\}\right]^{m_f}}$ Where, $C(\psi) = 1 - \frac{\ln(1 + \psi/\psi_r)}{\ln[1 + (10^6/\psi_r)]}$ $\Theta_d = \frac{w(\psi)}{w_s}$	a_f = fitting parameter which is primarily a function of air-entry value of soil. n_f = fitting parameter which is primarily a function of rate of water extraction from soil once air-entry value has been exceeded. m_f = fitting parameter which is primarily a function of residual water content. $C(\psi)$ = correction factor which is primarily a function of suction corresponding to residual water content.

2.3.3 Unsaturated Hydraulic Conductivity

2.3.3.1 General

In the soil matrix, the water flow can only occur in the connected and saturated pores (Figure 2.18a). By inducing the soil matric suction, the water stored in big pores is replaced with air. Therefore, water flow is enforced to occur in a smaller size of pores (Figure 2.18b). This phenomenon increases the tortuosity of the flow path resulting in a significant decrease in soil permeability value (Ng and Menzies 2014). Further increase of soil matric suction can reach the soil to the residual zone and water flow start to occur only in vapor form (Figure 2.18c).

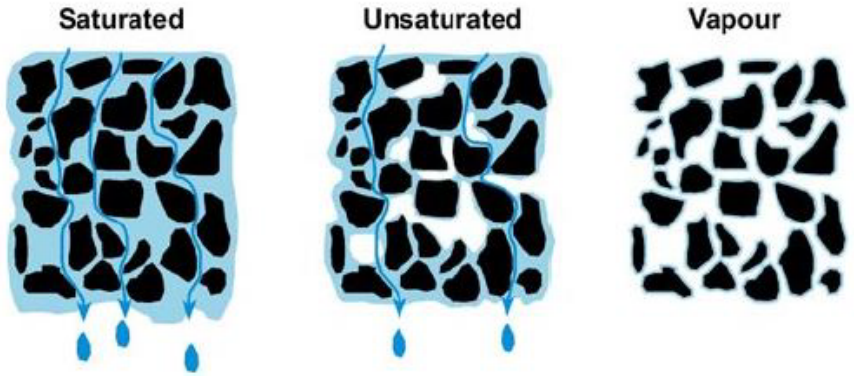

(a) (b) (c)

Figure 2.18 Water flow phenomena in saturate and unsaturated soil ("water flow UNSW", 2007)

The aforementioned characteristics of water flow show the influence of the water content and suction level of soil on the permeability. As SWRC defines the relationships between soil water content and suction, the hydraulic conductivity of unsaturated soil can be estimated by using its SWRC (Fredlund et al. 1994).

2.3.3.2 Estimation of Unsaturated Permeability

The unsaturated hydraulic conductivity function of soil can either be measured in the laboratory or estimated by using the mathematical models based on SRWC. The direct measurement methods are expensive and require an excessive amount of time and work, whereas permeability estimation models provide faster and economical solutions (Zhai and Rahardjo 2015). Although the permeability estimating models provide approximate results, they are generally adequate for unsaturated state soil problems (Fredlund et al. 2012). There are a

variety of existing models available to estimate the unsaturated hydraulic conductivity of soil (Rahimi et al. 2015). These models are broadly categorized as 1) empirical models and 2) statistical models. Tables 2.5 and 2.6 present some of the commonly used models for estimating permeability of soil.

Table 2.5 Empirical permeability functions to predict the permeability of unsaturated soil (Leong and Rahardjo, 1997)

Type	Permeability Functions	Reference
$k = f(\theta_w)$	$k_w = a\theta_w^b$	Gardner (1958)
	$k_w = k_s\left(\frac{\theta_w}{\theta_s}\right)^{2b+3}$ and $b = \frac{\Delta\, log\, \psi}{\Delta\, log\theta_w}$	Campbell (1973)
	$k_w = k_s \exp[b(\theta_w - \theta_s)]$	Dane and Klute (1973)
$k = f(\psi)$	$k_w = a + b\psi$	Richards (1931)
	$k_w = a\psi^{-b}$	Wind (1955)
	$k_w = \frac{k_s}{1 + a\left(\frac{\psi}{\rho_w g}\right)^b}$	Gardner (1958)
	$k_w = a\exp(b\psi)$	Christensen (1943)
	$k_w = k_s$ $for\ (u_a - u_w) \le (u_a - u_w)_b$ $k_w = k_s\left[\frac{(u_a - u_w)_b}{(u_a - u_w)}\right]^\eta$ $for\ (u_a - u_w) > (u_a - u_w)_b$	Brooks and Corey (1964)

Note: In the table, *a* and *b* are constants; *k* is coefficient of permeability where subscripts *w* and *s* denote unsaturated and saturated conditions, respectively; ψ is the matric suction; θ_w is the volumetric water content.

Table 2.6 Statistical models to estimate permeability of unsaturated soil

Burdine (1953)	$k_r(\theta) = \frac{k(\theta)}{k_s} = \Theta^q \frac{\int_{\theta_r}^{\theta} \frac{d\theta}{\psi^2(\theta)}}{\int_{\theta_r}^{\theta s} \frac{d\theta}{\psi^2(\theta)}}$ where, $\Theta = \frac{\theta - \theta_r}{\theta_s - \theta_r}$ q=2	$k(\theta)$ =calculated permeability for a specified water content, k_s = saturated permeability, Ψ = suction level, θ_s = saturated volumetric water co content, θ_r = saturated residual water content, and q = specific soil-fluid parameter
Kunze et al, (1968)	$k_r(\theta_i) = \frac{k_s}{k_{sc}} \frac{T_s^2 \rho_w g}{2u_w} \frac{\theta_s^p}{n^2} \sum_{j=i}^{m} \left[(2j+1-2i)\psi_j^{-2}\right]$ where, i = 1,2,…m	T_s = Surface tension, $k_r(\theta_i)$ = calculated permeability for a specified water content, k_{sc} = saturated permeability ρ_w = density of water, u_w = viscosity of water, g = gravimetric acceleration, *i,n,m*= initial,total number and last interval number, respectively. p = constant parameter related with variation in pore size

Mualem (1976)	$k_r(\theta) = \frac{k(\theta)}{k_s} = \Theta^q \left(\frac{\int_{\theta_r}^{\theta} \frac{d\theta}{\psi(\theta)}}{\int_{\theta_r}^{\theta_s} \frac{d\theta}{\psi(\theta)}} \right)^2$ $\Theta = \frac{\theta - \theta_r}{\theta_s - \theta_r}$ where, q=0.5	$K(\theta)$ = calculated permeability for a specified water content k_s = saturated permeability, θ_s = saturated volumetric water content, θ_r= saturated residual water content, and Ψ = suction level.

Empirical models use the similarity between SWRC and hydraulic conductivity function of soil to develop equations. Most of the empirical equations are in exponential form and use information from the SWRC of soil through a curve fitting procedure. These equations can be used in engineering applications if measured data of coefficient of permeability against suction or water content is available (Fredlund and Rahardjo, 1993). In statistical models, the permeability function is calculated by the integration of suction values along the SWRC. The matric suction is always expressed as a function of volumetric water content in statistical models (Fredlund et al., 1994). In these models, permeability function of soil uses a few discrete points instead of a continuous mathematical model. The accuracy of these models highly depends on the number and locations of these discrete points (Zhai and Rahardjo, 2015).

The direct measurement methods are quite time consuming whereas, SWRC based statistical models provide fast and reliable results (Fredlund et al. 2012; Zhai and Rahardjo 2015). In this study, the unsaturated permeability

function of all the soil and mix design soils is predicted with Fredlund et al, (1994a) equation as shown in Equation 2.6.

$$k_{\psi} = k_s \frac{\frac{\sum_{i=j}^{N} \Theta(e^{y}) - \Theta(\psi)\,\Theta'(e^{y_i})}{e^{y_i}}}{\frac{\sum_{i=1}^{N} \Theta(e^{y}) - \Theta_s\,\Theta'(e^{y_i})}{e^{y_i}}} \quad (2.6)$$

Where,

ks = saturated permeability value of soil in m/s,

kψ = unsaturated state permeability value of soil in m/s,

Θs = saturated volumetric water content,

e = 2.71828,

y = a dummy variable,

i = the internal between *j* to *N,*

j = the minimum suction value described by the final function,

N = the maximum suction value described by the final function,

Ψ = suction, and

Θ' = 1st derivative of the equation.

2.3.4 Unsaturated Shear Strength

In unsaturated conditions, the developed matric suction in soil contributes to its shear strength. This contribution is introduced to soil strength with two stress state variables of extended Mohr-coulomb equation as seen in Equation 2.7 (Fredlund et al. 1978).

$$\tau = c' + (\sigma_n - u_a)\, tan\, \varphi' + (u_a - u_w)\, tan\, \varphi^b \quad (2.7)$$

Where,

c' is effective cohesion in kPa,

φ' is the effective internal friction angle in degrees,

$(\sigma_n - u_a)$ is net normal stress in kPa,

u_a is pore-air pressure in kPa,

u_w is the pore-water pressure in kPa,

$(u_a - u_w)$ is matric suction in kPa, and

φ^b is an internal friction angle with respect to matric suction.

The development of the matric suction is contributed to the equation with φ^b value represented in the failure envelope with the 3rd stress space (Figure 2.19). The rate of increase in soil shear strength due to soil suction is not linear which suggest that the φ^b value is not constant (Escario and Saez 1986). And, determination of it requires significant laboratory work over a wide range of suction. Therefore, it is correlated with SWRC parameters and several recommendations are made by Zhang et al. (2014):

1) If soil AEV is smaller than 1 kPa, the contribution of suction value can be ignored by assuming φ^b is 0.
2) If the soil AEV is in between from 1 to 20 kPa, the unsaturated shear strength of soil should be determined by nonlinear equations.

3) If the soil AEV is in between from 20 to 200 kPa, the contribution of suction value can be made by assuming φ^b is 15°.

4) If the soil AEV is greater than 200 kPa the φ^b value can mostly be assumed as same as soil effective friction angle.

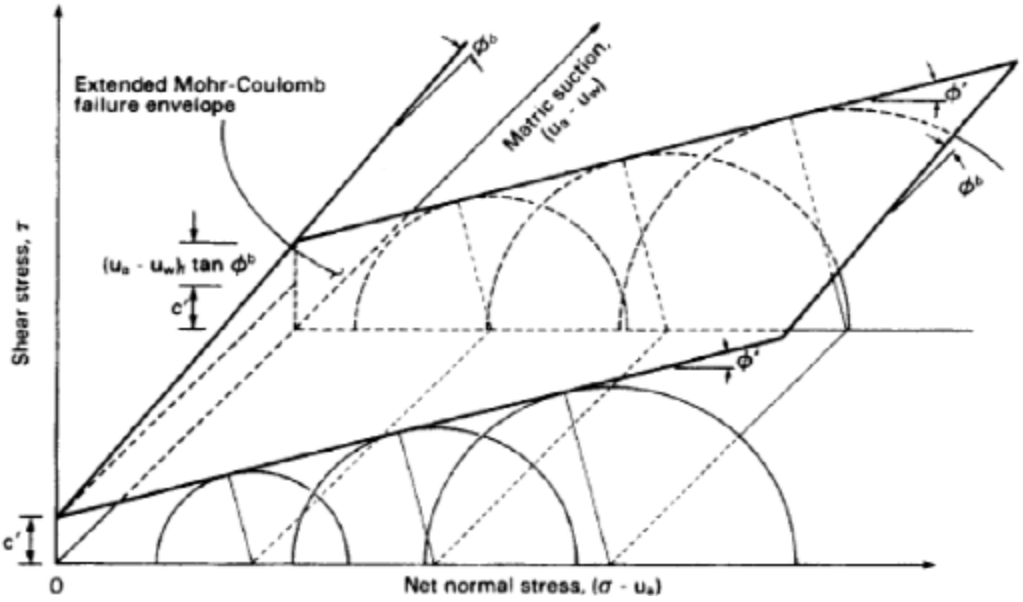

Figure 2.19 Extended Mohr-Coulomb failure envelope of unsaturated soil (Fredlund and Rahardjo, 1993)

2.4 Engineered Slopes

2.4.1 General

Modern infrastructures including highways, railways, and dams are essential for urban development. Building these structures usually requires construction of engineered earth slopes. Engineered slopes, also known as manmade slopes, can be categorized into two different groups: earth fill

embankments slopes, excavated or cut slopes (Figure 2.20). In a fill embankment, a volume of fill material is compacted and raised to the surface elevation. The fill embankments are generally built by using economic earthen materials available from nearby borrow sources or any adjacent excavated cuts. They are generally granular material (sand, rock, and gravel), cohesive fine material (silt, clay, and shale), a mixture of soils, and sometimes random material. Because of high compressibility, soft clays and organic materials are usually avoided as fill material. The poorly graded coarse material is usually placed at deeper layers near the base of the embankment and the well-graded soils are used in upper layers to support the overlying structures.

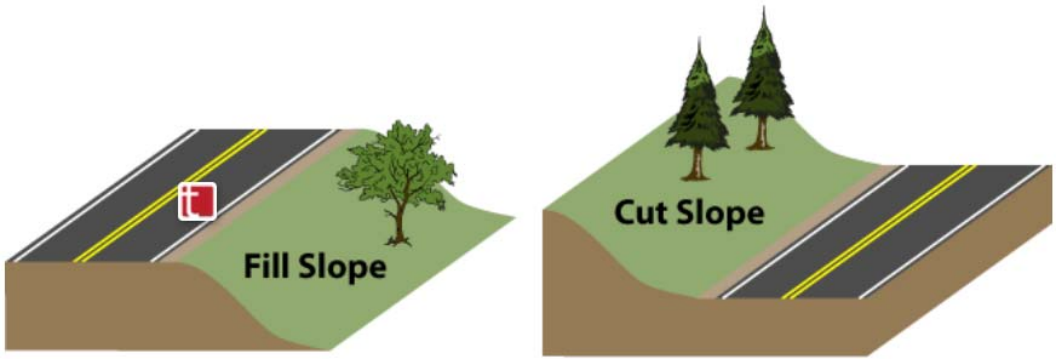

Figure 2.20. A typical fill and cut slopes (source: https://www.sddc.army.mil/sites/TEA/Functions/SpecialAssistant/TrafficEngineeringBranch/BMTE/calcRoadside/roadsideSafetyTutorials/typesOfSlopes/Pages/default.aspx)

Cut slope, also known as back slope, involves cutting and excavating the natural slope or original ground surface to a lower elevation. This type of slope is generally built to shorten the length of the route by constructing straight roadways in the same grade. It also creates extra spaces for city urbanization and industrial site developments. The uncertainties in the soil properties of natural ground cause difficulties in the design of cut slopes.

2.4.2 Design of Engineered Slopes

Design criteria and factor of safety of the engineered slopes are determined based on the loads, usage, and the conditions that are possibly expected throughout its service life span. Some of the conditions that are considered in the design process of engineered slopes are:

- Stability during the construction and at the completion of construction.
- The long-term conditions after completion of construction including strain-softening in the soil due to rapid excavation and desiccation cracks and fissures.
- Steady-state seepage phenomena and rapid (or sudden) drawdown.
- The natural event including hurricane, storms, flash floods, snows, and rainfall.
- The tolerable settlement, and differential displacements.

The precise slope design heavily depends on the accuracy of measured or estimated soil properties used in the analysis. Therefore, a significant amount of

laboratory and field investigation is involved in the design process to assess the quality and the safety factor of the slopes (Table 2.7).

Table 2.7 Standard test methods for fill embankment and cut slopes

Soil Property	Standard Test Method	Reference
Unit weight	Standard test method for bulk density ("unit weight") and voids in aggregate	ASTM C29
Specific gravity	Standard test methods for maximum index density and unit weight of soils using a vibratory table	ASTM D4253
Relative density	Relative density of cohesion less soils	ASTM D2049
Gradation	Standard test method for particle-size distribution (gradation) of fine-grained soils using the sedimentation (hydrometer) analysis	ASTM D7928
	Standard test methods for particle-size distribution (gradation) of soils using sieve analysis	ASTM D6913
	Standard test methods for determining the amount of material finer than 75-μm (no. 200) sieve in soils by washing	ASTM D1140
Soil dry unit weight-moisture characteristic	Standard test methods for laboratory compaction characteristics of soil using standard effort (12,400 ft-lbf/ft3 (600 kn-m/m3))	ASTM D698
	Standard test methods for laboratory compaction characteristics of soil using modified effort (56000 ft-lbf/ft^3 (2700 kn-m/m3))	ASTM D1557

Compacted in-situ unit weight	Standard test method for density and unit weight of soil in place by sand-cone method	ASTM D1556
	Standard test methods for in-place density and water content of soil and soil-aggregate by nuclear methods (shallow depth)	ASTM D6938
	Standard test method for density and unit weight of soil in place by the rubber balloon method	ASTM D2167
Shear strength	Standard test method for unconsolidated-undrained triaxial compression test on cohesive soils	ASTM D2850
	Standard test method for direct shear test of soils under consolidated drained conditions	ASTM D3080
	Standard test method for consolidated undrained triaxial compression test for cohesive soils	ASTM D4767
	Standard test method for torsional ring shear test to measure drained fully softened shear strength and stress dependent strength envelope of fine-grained soils	ASTM D7608
	Standard test method for torsional ring shear test to determine drained residual shear strength of cohesive soils	ASTM D6467
Bearing capacity	Standard test method for California bearing ratio (cbr) of laboratory-compacted soils	ASTM D1883
Permeability	Standard test method for permeability of granular soils (constant head)	ASTM D2434
	Standard test methods for measurement of hydraulic conductivity of saturated porous materials using a flexible wall permeameter	ASTM D5084

SWRC	Standard test methods for determination of the soil water characteristic curve for desorption using hanging column, pressure extractor, chilled mirror hygrometer, or centrifuge	ASTM D6836
Consolidation	Standard test methods for one-dimensional consolidation properties of soils using incremental loading	ASTM D2435
	Standard test method for one-dimensional consolidation properties of saturated cohesive soils using controlled-strain loading	ASTM D4186

2.4.3 Safety Factors of Engineered Slopes

The most common definition of the factor of safety (FOS) is the ratio of shear strength of soil to the shear stress in the soil at the potential failure plane. Also, there are alternative definitions of FOS detailed below (Gedney and Weber Jr 1978).

1) The ratio between the resisting moments to driving moments at a particular point.
2) The ratio between the available resisting forces to driving forces in the potential failure plane.
3) The factor by that shear strength parameters might be decreased to result in limit equilibrium along to potential slip surface.

The unity (1.0) in FOS calculations is refer to the condition in which slope failure is imminent. In the design phases, the required minimum FOS is chosen by considering the degree of uncertainties and the consequence of the possible failure

of the slope being analyzed. The safety factors of the slope are determined for all possible cases are expected during the entire life span of the slope as the soil parameters and groundwater conditions are not stable (Gedney and Weber Jr 1978).

Numerous federal regulatory agencies have recommended value of FOS for different anticipated scenarios. This minimum FOS threshold is based on the experiences from the past projects that were built with similar exploration techniques and design processes (Duncan and Wright 2005). For instance, the recommended minimum FOS of an embankment slope is 1.5 for long-term and steady-state seepage conditions (EM-1110-2-1902). Likewise, for the design of highway slopes, the Texas Department of Transportation (TxDOT) "Geotechnical Manual 2020" requires a minimum of 1.3 FOS for the slope. Furthermore, if a slope supports any structure and critical utilities, the minimum FOS value of 1.5 is required. Also, based on the past shallow slope failures experiences, Table 2.8 tabulates the upper limit of PI of soil for different slope ration required to maintain the FOS of 1.3. However, there is no specific FOS recommendation has been made for the slopes with soil having a higher value of PI than given in Table 2.8.

Table 2.8 Range of Soil Plasticity Index for different slope angles (TxDOT Geotechnical Manual 2020)

Slope Ratio	**Plasticity Index, PI (%)**
2.5H:1V	<5
3H:1V	<20

3.5H:1V	<35
4H:1V	<55
4.5H:1V	<85

2.4.4 Slope Stability Analysis

2.4.4.1 General

Slope safety is one of the most critical issues in the field of geotechnical engineering. Many methods have been developed in the last several decades to assess the stability of slopes. The slope stability analysis methods incorporate soil mechanics and characteristics of soil or rock (Duncan and Wright, 2005). The earlier hand-performed analysis methods were based on simplified calculations and highly conservative assumptions. Due to advancements in computers and calculations methods, more sophisticated and accurate methods have been developed. Despite the availability of a variety of methods, it is very important to use the suitable analysis method based on the field conditions and expected failure mechanism. It is important to know the theoretical fundamentals of the methods to determine the most appropriate slope stability analysis method to be used for a given problem. These methods can be broadly classified as (1) limit equilibrium methods (LEM) and (2) numerical methods.

2.4.4.2 Limit Equilibrium Methods

The limit equilibrium method is considered as a fundamental approach to slope stability analysis. Most of the early slope stability analysis methods are based

on the limit equilibrium approach. The main features of LEM in slope stability analysis are given below (Van Impe and Verastegui, 2007):

- Selection of a trial slip surface.
- Calculation of the applied shear stresses.
- Calculation of mobilized shear strength along the postulated slip surface.
- Determination of the FOS of slope (ratio of the calculated shear strength and shear stress).
- Determining the lowest FOS (the most critical slip surface) and failure mechanism by numerous iterations.

The method of slices in LEM is the most commonly used approach in slope stability analysis. In this method, the trial slip surface is divided into slices and the internal equilibrium of each slice is individually assessed. Several shapes of slip surfaces including plane, circular, and logarithmic can be assumed depending upon slope geometry. In the various alternative method of slices methods, the static equilibrium is computed by taking into account the interslice forces and satisfying force equilibrium and/or the moment equilibrium. (Fredlund and Krahn 1977).

The most appropriate method to be used is needed to be selected based on the field conditions and expected failure mechanism. Table 2.9 gives an overview of the more commonly used methods in slope stability studies by detailing the equilibrium equations, the shape of slip surface, and fundamental assumptions.

Table 2.10 points out the applicability of some of the commonly used slope stability analysis methods.

Table 2.9 Overview of various LE based method (Duncan and Wright 2005)

Procedure	**Equilibrium Condition Satisfied**	**Shape of slip surface**	**Assumptions**
Swedish Circle	Moment equilibrium about center of circle, Force equilibrium is implicitly satisfied	Circular	Friction angle is zero
Logarithmic Spiral	Moment equilibrium about center of circle, Force equilibrium is implicitly satisfied	Logspiral	-
Ordinary Method of slices	Moment equilibrium about center of circle, Force equilibrium is implicitly satisfied	Circular	The forces on the sides of the slices are neglected
Simplified Bishop	Vertical force equilibrium, Moment equilibrium about center of circle	Circular	All interslice shear forces are zero
Spencer's Method	Vertical force equilibrium, Horizontal force equilibrium, Moments equilibrium on any point	Any shape	Interslice forces are parallel, The normal force acts at the center of the base of the slice
Morgenstern and Price's	Vertical force equilibrium, Horizontal force equilibrium,	Any shape	Interslice shear force is related to interslice normal force by: $X = f(x)E$,

	Moments equilibrium on any point		The normal force acts at the center of the base of the slice

Table 2.10 Overview of the applicability of various Limit Equilibrium Methods on slope (Duncan and Wright 2005)

LE Based Method	**Applicability**
Swedish Circle	Applicable to slopes where ø = 0 (i.e., undrained analyses of slopes in saturated clays).
Logarithmic Spiral	Applicable for homogeneous slopes. Useful for developing slope stability charts and used some in software for design of reinforced slopes.
Ordinary Method of slices	Applicable to non-homogeneous slopes and c-ø soils where slip surface can be approximated by a circle. Very convenient for hand calculations. Wrong results for effective stress analyses with high pore-water pressures.
Simplified Bishop	Applicable to non-homogeneous slopes and c-ø soils where slip surface can be approximated by a circle. Calculations feasible by hand or spreadsheet. More accurate than Ordinary Method of slices, especially for analyses with high pore-water pressures. Improper and inaccurate for noncircular slip surfaces
Spencer's Method	Accurately applicable to any slope geometries and profiles. The simplest complete equilibrium procedure for computing factor of safety.
Morgenstern's and price	Accurately applicable to any slope geometries and profiles, well-established equilibrium procedure.

2.4.4.3 Numerical Method

The improvement in computer and technology-aided the development of many sophisticated numerical methods to calculate the FOS value of the slope.

Numerical methods do consider both mobilized soil deformations and stresses. The strength reduction method and the gravity increase method are most known and used numerical methods to compute slope FOS (Le 2013).

In the gravity increase method, material properties are considered to be constant and, the mobilized external forces (i.e., weight) are assumed to increase due to an increase in gravity. Therefore, the gravity increase method is more useful to assess the stability of the fill embankment slope during the construction stages (Le 2013). In this method, the FOS is defined as the ratio between the gravitational acceleration at the time of the failure and the actual gravitational acceleration. In the strength reduction method, the gravity loads of the soil mass are kept unchanged and the soil strength parameters are reduced systematically until the slope experiences instability problem. The FOS is defined as the ratio between the actual soil strength parameters and the reduced soil strength parameters at the failure.

The main benefits of the numerical methods over LEM on slope stability analysis are: 1) there is no restriction on the shape and location of the failure surface, and 2) numerical methods take into consideration changes in the deformations and generates more precise results. However, conventional LEMs are also able to produce reliable and accurate results (Matthews et al. 2014). The comparison between the FOS values of slopes computed with LEM and numerical

methods of strength reduction method showed good agreement (Van Impe and Flores 2007, Moni and Sazzad 2015).

2.5 Surficial Slope Failures

2.5.1 Introduction

The issue of slope instability in highway embankments, dams, and other engineered and natural slopes has always been an area of concern for geotechnical engineers. The slope failures are generally associated with property damages, loss of life, and interruption in the routine services. The design studies of the slopes are generally based on laboratory test results on compacted soil samples. However, variation in soil properties and slope conditions, and environmental activities over a period of time result in loss of stability. A large number of the reported slope failures attribute to rainfall events (Rogers and Wright 1986, McCleskey 2005, Le 2013, Castellenos 2016). In the case of rainfall-induced failure in expansive soil slope, the depth of failed section is usually low, and failure is termed as a surficial slope failure (Fleming et al. 1992, Days 1996, Duncan et al. 2011). The surficial slope failures are generally observed between the crown and mid-slope.

The depth and nature of slope failure are governed by soil type, soil profile, and geometry of slope (Titi and Helwany 2007, Mizal-Azzmi et al. 2011, Jafari et al. 2019c). As shown in Figure 2.21, slope failure can be rotational, translational, and a combination of both rotational and translational (Craig 2004). In the case of rainfall-induced surficial slope failure, the slip surface is usually translational in

nature. The translational type of slip can be seen as a slide that is parallel to the slope surface and at shallow depths (Abramson et al. 2001). The nature of slip surface depends on the degree of homogeneity in soil profile of slope (Abramson et al. 2001). With decrease in homogeneity in soil profile, the radius of curvature of failure surface tends to increase.

In the case of slopes with high plastic clayey soil, there is a gradual loss of shear strength in the surficial layer due to the development of desiccation cracks (Jafari et al. 2019). The mechanism of desiccation crack is discussed in soil slopes detail in the following section. Because of the decrease of homogeneity in soil profile due to the presence of weaker surficial soil layer over relatively stronger soil layer, translational type of failure usually occurs in slope with high plastic clayey soil during rainfall. These failures are generally shallow in nature with depth of slip surface, D, less than 10 ft and depth to length ratio, D/L, of failed section less than 0.15 (Figure 2.22) (Abramson et al. 2001).

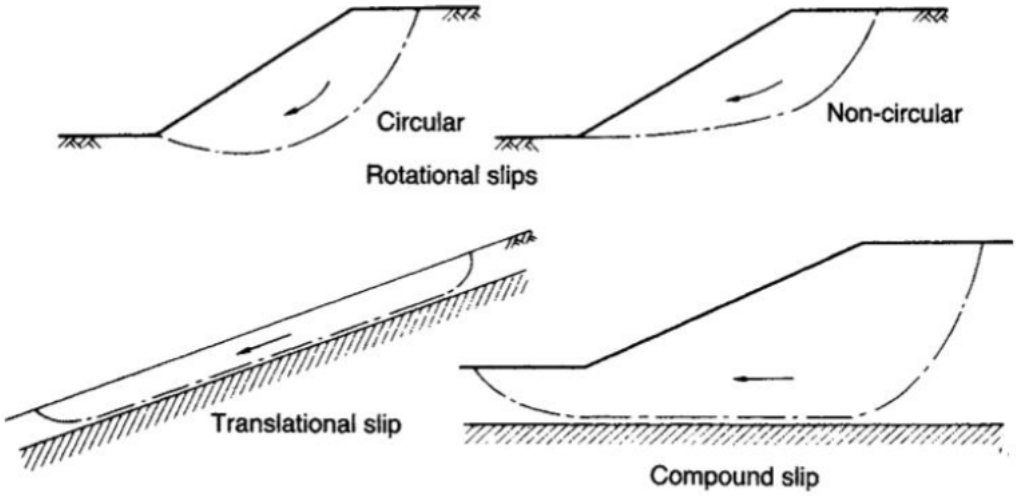

Figure 2.21 Slope failure types observed (Craig, 2004)

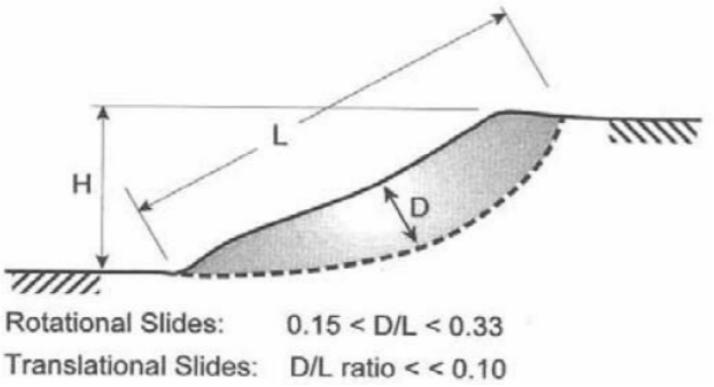

Figure 2.22 Slope failure type based on the aspect ratio of the failed zone (Abramson et al., 2002)

2.5.2 Mechanisms of the Surficial Slope Failures During Rainfall

Surficial failure in a clayey soil slope is primarily caused by the presence of desiccation cracks developed due to the weathering cycle (Jafari et al. 2019c). The hot and dry period leads to high shrinkage strain and results in the formation

of desiccation cracks in the soil. During a rainfall event, these desiccation cracks serve as conduits and allow the water to infiltrate abruptly into the inner layer of the slope. When the infiltrate water encounters a low permeable underlying layer, it starts to accumulate in the surficial layer. This phenomenon of infiltration causes swelling and softening of the expansive soil. If the rainfall intensity is higher than the soil permeability and rainfall lasts for long period, there is generation of pore water pressure in the surficial layer resulting in the formation of a perched water table (Abramson et al. 2001).

This process results in a decrease in effective stress in the soil at shallow depths and ultimately causes slope failure. As the shallow slope failure plane is generally parallel to the slope surface, it is commonly analyzed as an infinite slope failure (Day and Axten 1989). Based on the field investigations, it has been found that the rainfall-induced pore water pressure is a critical factor in surficial slope failures (Johnson and Sitar 1990). Therefore, many researches have focused on the impact of rainfall characteristics and its pattern on surficial slope stability.

2.5.3 Effects of Rainfall Characteristic on Surficial Slope Failures

The effects of rainfall intensity and duration on the failure of surficial slopes have been studied by numerous researchers (Rahardjo et al. 2001, Lee et al. 2009, Li et al. 2013, Garg and Maji 2014, Ran et al. 2018, George et al. 2018, Jafari et al. 2019c). These studies indicated that the effect of rainfall characteristics on slope failure is closely related to hydraulic properties of the soil (Cai and Ugai

2004, Gofar et al. 2007, Rahardjo et al. 2007a). Cai and Ugai (2004) evaluated the effect of rainfall intensity and its duration on the safety factor of a slope for soils with different permeability values. In their study, the Glendale clayey loam (GCL), Uplands silty sand (USS), and Bet Degan loamy sand (BLS) have a permeability value of 1.52×10^{-6} m/s, 1.83×10^{-5} m/s, and 6.38×10^{-5} m/s respectively.

The results of the study conducted by Cai and Ugai (2004) showed that for the slopes built with low permeable soil, the rainfall duration is more critical than the rainfall intensity (Figure 2.23). The slopes with low permeable soil might fail only when the rainfall lasts for a long period of time with considerable intensity. However, for the slopes with relatively higher permeable soil, a higher intensity rainfall event for a short duration induces failure. The authors also pointed out that the slope with higher initial volumetric water content or water retention capacity experiences a faster rise in pore water pressure during a rainfall event.

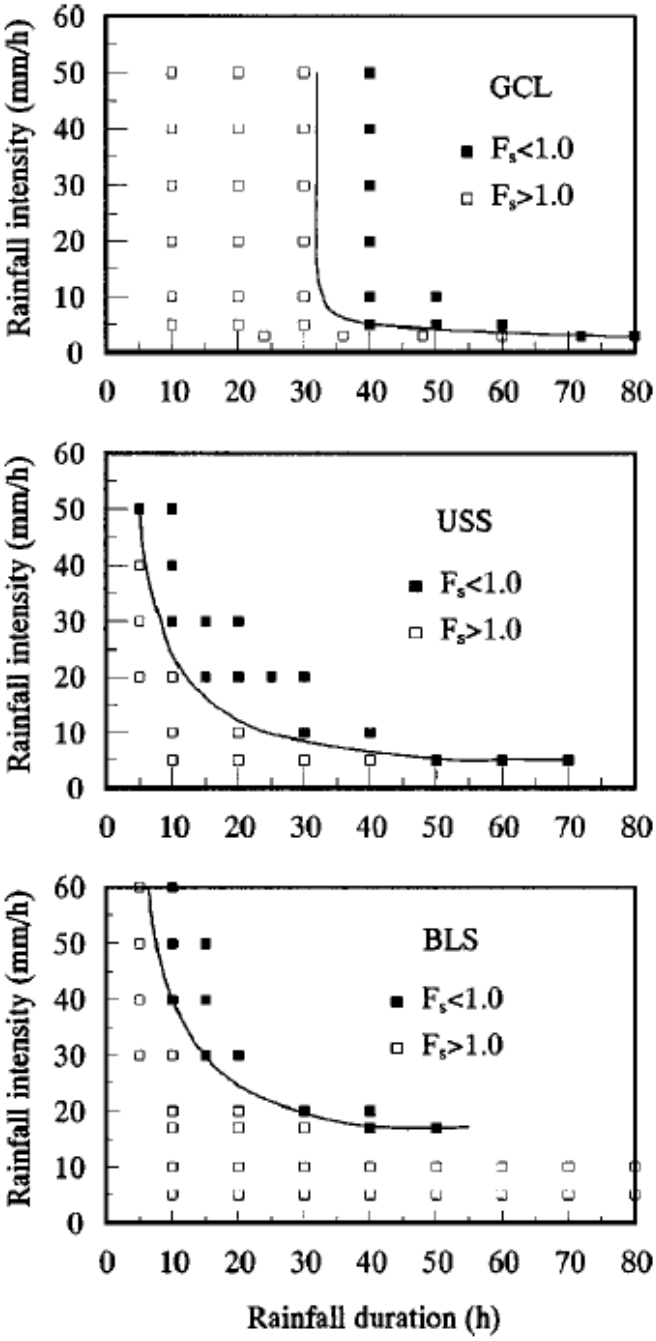

Figure 2.23 Effects of rainfall duration and intensities of slope safety (Cai and Ugai 2004)

Rahardjo et al. (2007) conducted a research study to examine the effect of slope geometry, location of the water table, and soil properties on slope stability for different rainfall intensities. The study suggested that soil permeability and rainfall intensity played a major role in the variation of the FOS value of slope with homogenous soil. The slope geometry and location of the water table are secondary factors and control the FOS value only just before the rainfall event (Figure 2.24). Also, the authors concluded that the soils having low permeability value (less than 10^{-6} m/s) does not experience instability problem up to 24 hours rainfall regardless of the rainfall intensity. In a different study, Gofar and Rahardjo (2017) observed that for the slopes with low permeability, the pore water pressure changes continue after the rainfall event and the critical conditions can occur up to 72 hours after rainfall. However, for slopes with soil having higher permeability value, the decrease in FOS could continue up to 12 hours and the FOS of the slope can be recovered back fast.

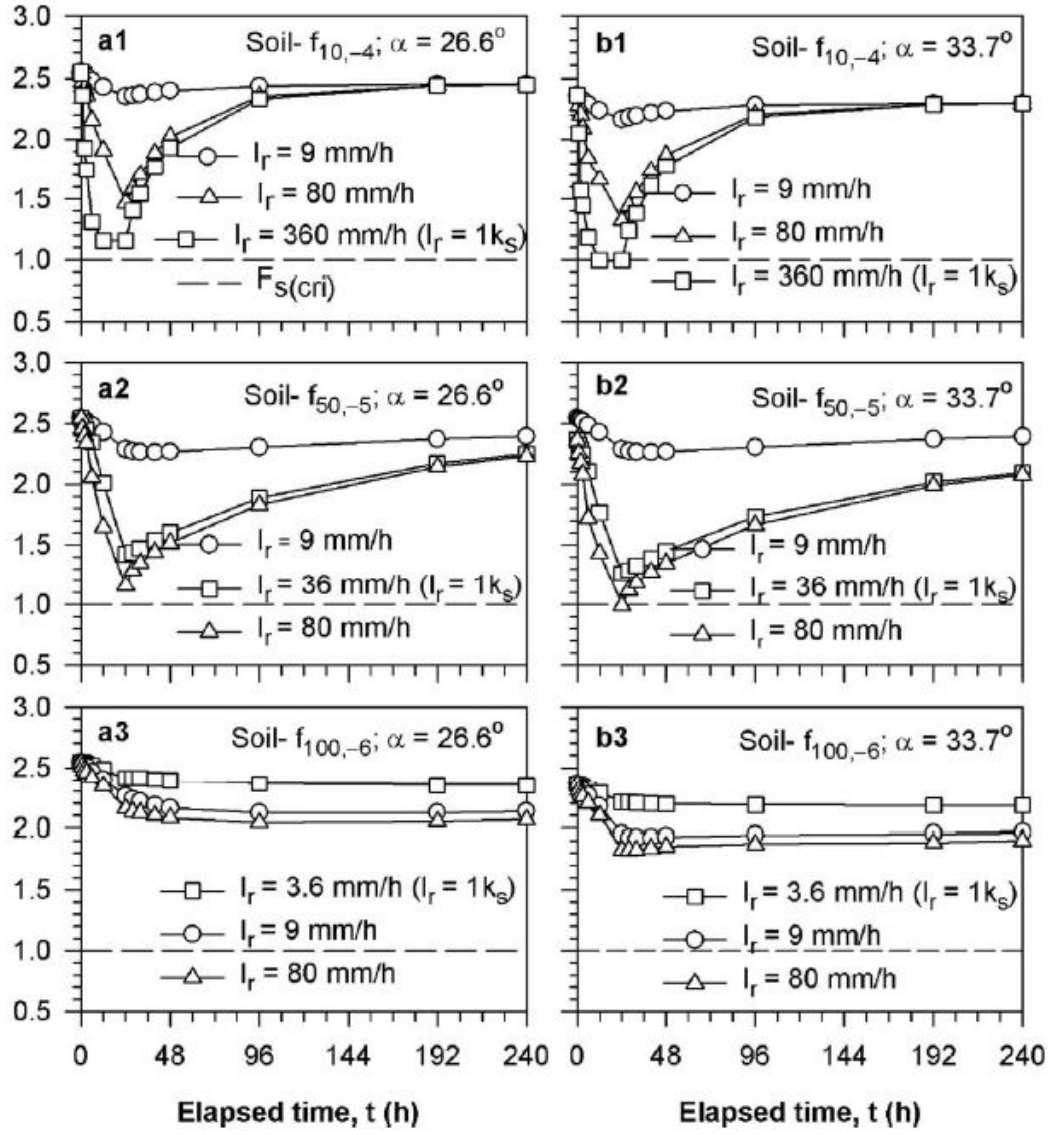
a1
Soil- $f_{10,-4}$; α = 26.6°
I_r = 9 mm/h
I_r = 80 mm/h
I_r = 360 mm/h (I_r = 1k_s)
$F_{s(cri)}$
b1
Soil- $f_{10,-4}$; α = 33.7°
I_r = 9 mm/h
I_r = 80 mm/h
I_r = 360 mm/h (I_r = 1k_s)
a2
Soil- $f_{50,-5}$; α = 26.6°
I_r = 9 mm/h
I_r = 36 mm/h (I_r = 1k_s)
I_r = 80 mm/h
b2
Soil- $f_{50,-5}$; α = 33.7°
I_r = 9 mm/h
I_r = 36 mm/h (I_r = 1k_s)
I_r = 80 mm/h
a3
Soil- $f_{100,-6}$; α = 26.6°
I_r = 3.6 mm/h (I_r = 1k_s)
I_r = 9 mm/h
I_r = 80 mm/h
b3
Soil- $f_{100,-6}$; α = 33.7°
I_r = 3.6 mm/h (I_r = 1k_s)
I_r = 9 mm/h
I_r = 80 mm/h
3.0
2.5
2.0
1.5
1.0
0.5
0
48
96
144
192
240
Elapsed time, t (h)
Elapsed time, t (h)

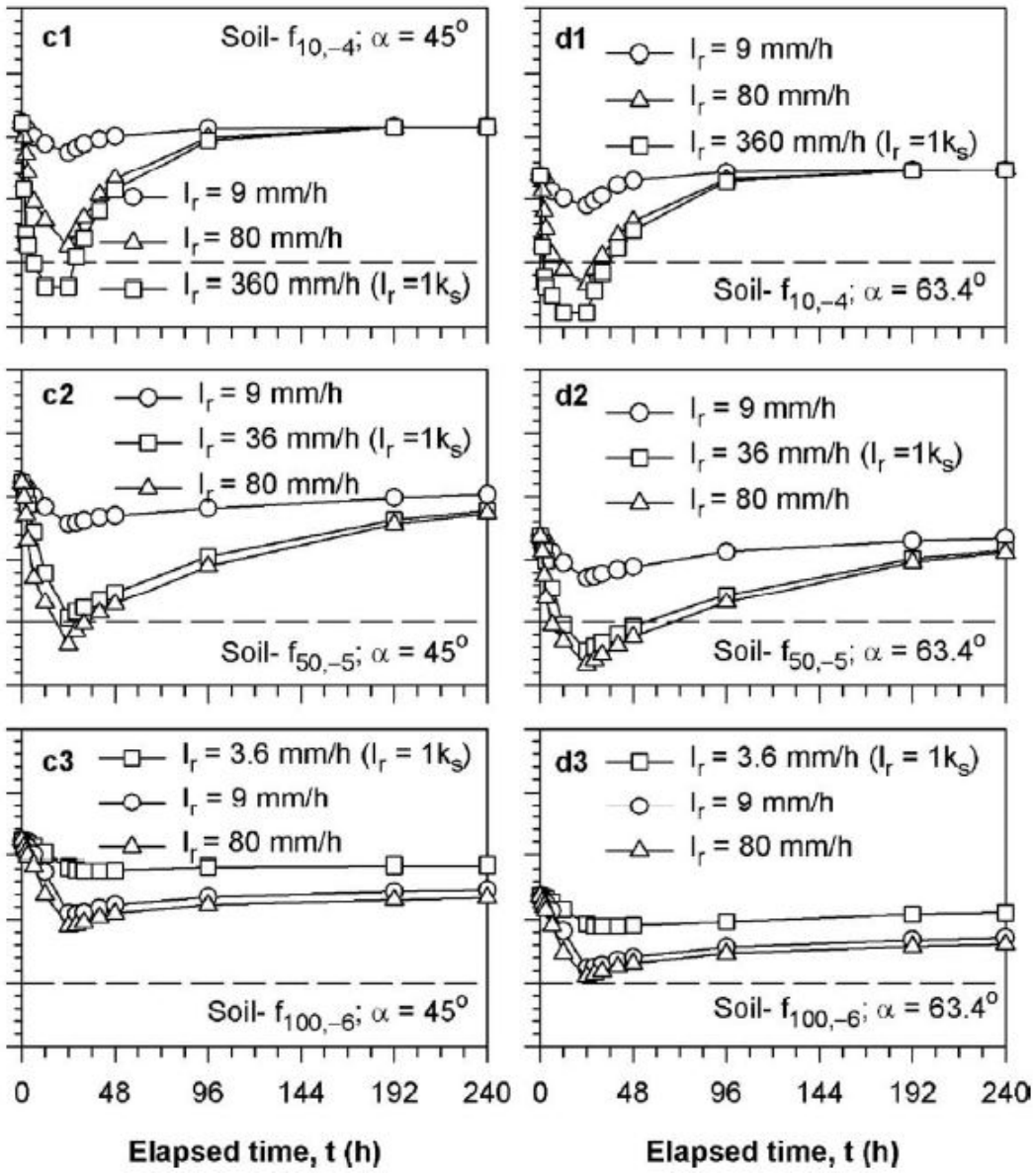

Figure 2.24 Relative effect of slope angle, soil permeability, and rainfall intensity on the variation of FOS under 24h rainfall (Rahardjo et al. 2007)

2.5.4 Effects of Antecedent Rainfall on Surficial Slope Failures

The surficial slope failure generally takes place during or just after a long rainy period. Antecedent rainfall is referred to as the total amount of rain that occurred just before the single significant storm that caused slope failure (Au 1998). Rahardjo et al. (2001) conducted a study to investigate the impact of antecedent rainfall on slope instability problem by inducing 5 days of continuous antecedent rainfall preceding the major storm rainfall. The research result suggests that the stability of slope depends on both daily rainfall event and the antecedent rainfall. The initial degree of saturation and coefficient of permeability before the major rainfall event is controlled by antecedent rainfall. Results showed that a combination of 5 days of antecedent rainfall that is exceeding 60 mm and a major storm that is exceeding 90 mm (i.e., a continuous rainfall greater than 150 mm over 6 days) result in a slope failure.

Tsaparas et al. (2002) investigated the influence of rainfall patterns on rainfall-induced slope failures. Figure 2.25 shows the different scenarios of rainfall patterns opted for the study. Results demonstrated that different rainfall patterns with the same amount of rainfall create different pore water pressure distribution in slope. It was found that the worst pore water pressure profile was observed in the case of evenly distributed rainfall (Scenario 3 and 4). For scenario 3, where 25 mm of antecedent rain was evenly distributed in 5 days before the major rainfall event, around 1.20 m deep wetting front (saturated zone) was observed in the

slope. In a scenario where the total rainfall amount (265 mm) was evenly distributed over 5-days and 4h without any major rainfall event, the pore water pressure distribution changed drastically. The depth of the wetting front was observed to be 4 m depth from the surface with a small value of negative pore water pressure of 4.5 kPa.

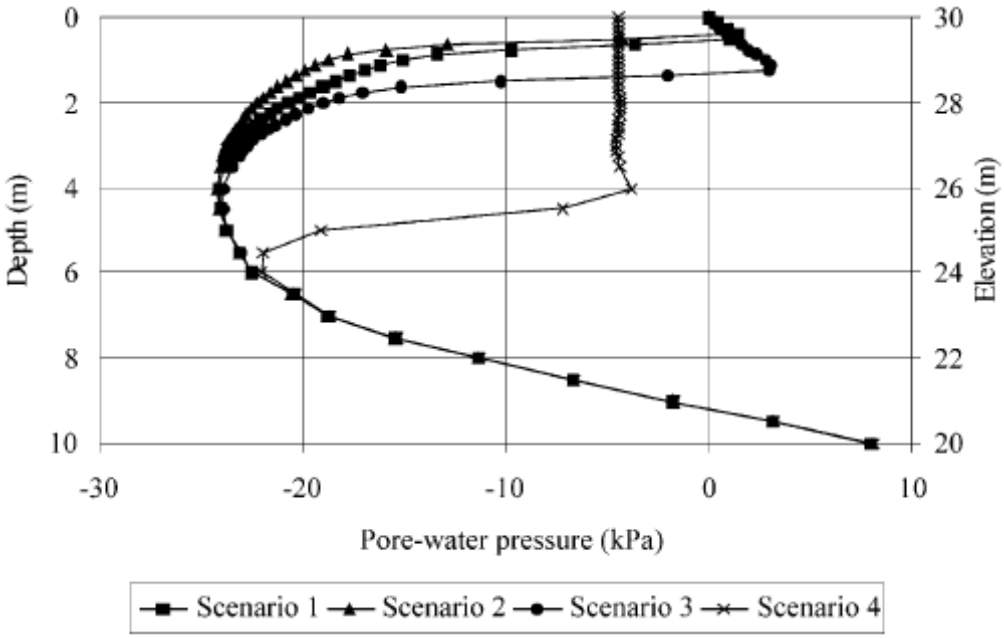

Scenario 1: 1mm/h rain for 5 h daily for 5-days and 240mm rain in 4 h on 6th day
Scenario 2: 5mm/h rain for 1 h daily for 5-days and 240mm rain in 4 h on 6th day
Scenario 3: even distribution of 25 mm rain in 5-days and 240mm rain in 4 h on 6th day
Scenario 4: even distribution of 265 mm rain in 5-days and 4 h

Figure 2.25 Pore-water pressure variation under the different pattern of rainfall event (Tsaparas et al. 2002)

Rahardjo et al. (2008) investigated the slope response to antecedent rainfall events with the help of comprehensive site instrumentation. Their study concluded

that the slope with soil rich in fines and a low permeability value requires a higher amount of antecedent rainfall than a slope with higher permeability value to build critical pore water pressure in the slope. Rahimi et al. (2011) from their studies concluded that the antecedent rainfalls influence the stability of soil slope regardless of the permeability value. However, the impact of antecedent rainfall on FOS of the slope with high permeable soil is comparatively smaller than slope with low permeable soil. The reduction in FOS of the slope was found to be 45% and 13% for the low and high permeability soil, respectively.

2.6 Slope Stabilization Methods

The safe design of the engineered slope requires proper consideration of soil properties, slope geometry, expected loads, and changes in soil properties due to environmental factors during the life span of a slope (Gedney and Weber Jr 1978, Abramson et al. 2001, Castellanos 2014). Sometimes, due to change in soil properties with time, constraints in slope geometry, and unforeseen long-term environmental conditions the expected slope performance cannot be achieved. To enhance the stability of slopes, various methods have been developed in the past decades (Day 1996b, Holtz and Schuster 1996, McCleskey 2005, Le et al. 2015). The slope stabilization techniques can be categorized under three main approaches as follow (Holtz and Schuster 1996):

- Avoiding the possible problem.
- Reduce the driving forces that trigger soil movement.

- Increase the resisting forces against the potential movement.

Avoiding problems can be achieved by removing and replacing the partially or completely unstable material or changing the location of the project. However, this approach may not economical or feasible for many slopes and changing project location generally is not practical for rehabilitation projects (Holtz and Schuster 1996). In the second approach, reduction in driving forces can be achieved by providing surface and underlying drainage system in a slope, reducing the weight of slope by using lightweight fill material or with some earthworks including changing the line and grade or slope by flattening and benching the slope (Nelson and Allen 1974, Abramson et al. 2001, Saftner et al. 2017a).

An increase in resisting forces against the potential movements is generally made by providing a resisting external force or boosting the strength of the soil. This is usually done by using buttress, counterweight fills at the toe, installation of structural systems (i.e., precast concrete walls, timbers, sheet and soldier piles), and building gravity walls (Highland and Bobrowsky 2008). Boosting the internal soil strength can be achieved by using various procedures including, reinforcing the backfill material, installing in situ reinforcement (i.e., nails, anchors, micro piles), or mixing the soil with additives such as calcium-based stabilizers, fibers, or compost materials (Day 1996b, Dronamraju 2008, He 2019). This research study is conducted to mitigate surficial slope failures problems that occurred due

to highly plastic clayey soil. Therefore, the following section focuses on the miscellaneous stabilization methods for surficial slope stability problems.

2.6.1 Excavating and Recompacting the Failed Slopes

In the case of surficial slope stabilization, excavation, and recompaction of the soil of the failed slope is the most common method (Sutterer 2000). This method is applied by the following steps listed following:

- Excavation of the failed mass of slope.
- Removal of the organic materials from the slope.
- Stocking the soil excavated in a designated area and leaving it to dry.
- Transferring back the soil to the same failed zone and compacting in layers after reaching the optimum moisture content value.

The repair costs of skin failures are a few hundred thousand dollars (Le 2015). Although this method requires the least design work and is one the most economical solution, this method does not promise success for all the repair works. As this method does not increase the soil strength, recurring failures were reported in most of the stabilized slopes (Day 1996, Le 2015). Apart from it, this method also requires high maintenance and operation costs in the long-term (Stauffer and Wright 1984, McCleskey 2005).

2.6.2 Steel Pipe Piles and Wood Lagging Repair Method

The use of piles with wood lagging technique is a combination of hollow galvanized steel pipe piles and timber lagging (i.e., wood beams). The repair procedure is listed following (Day 1997).

- Removal of failed soil mass and stock it off-site.
- Cutting the slope and creating benches in slope (Figure 2.26).
- Driving steel pipe pile into firm natural fill or filling the boreholes with concrete.
- Installation of the wooden plate across the placed piles.
- Re-construction of the slope with fill material.

The shallow slope failures could be rebuilt using this technique without advanced construction equipment. However, in this stabilization method, frequent bending failures in the pile system have been reported because of the mobilized force in the surficial layer. These bending failures are due to the low flexural capacity of the steel piles used. (Day 1997, Titi and Helwany 2007). In this stabilization method, attention is given to the timber lagging system as it transfers to loads to steel piles. The piles need to be designed against shear force and bending failure.

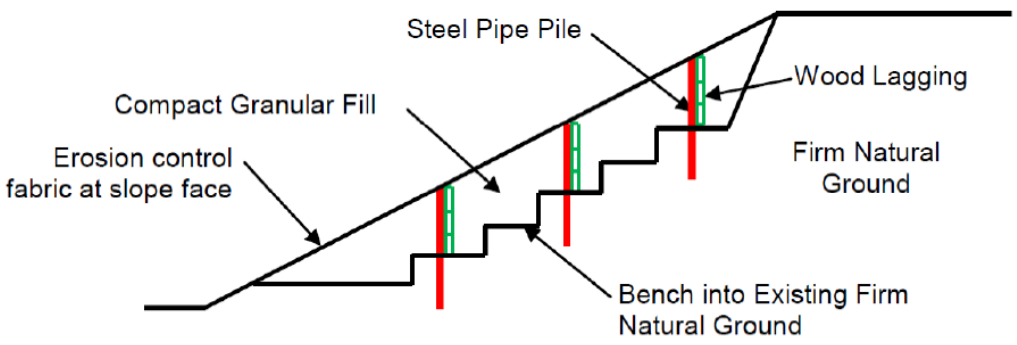

Figure 2.26 Steel pipe pile and wood lagging rehabilitation method (Day, 1997; Sapkota 2019)

2.6.3 Geo-grid Using for Repair Surficial Slope Failures

Geo-grids are fabricated from polyethylene terephthalate (PET), high-density polyethylene (HDPE), polypropylene (PP), and polyvinyl alcohol (PVA) polymers (Yeo and Hsuan 2010). Because of its material properties and design, geogrids can be used in slope as a reinforcing element (Onur et al. 2016). Repairing the slopes with geo-grid is considered to be a cost-effective and innovative method (Titi and Helwany 2007, Ooi and Tee 2011). Figure 2.27 shows a schematic of a typical slope stabilization using geo-grids. The repair procedure is listed the following:

- Disposal of the surficial failure mass off site.
- Removal of the failed soil mass and stock it off site.
- Cutting the slope and creating benches on the slope.
- Installation of horizontal drains along the length of the slope.

- Re-construction of the slope with layers of geogrid and fill material.

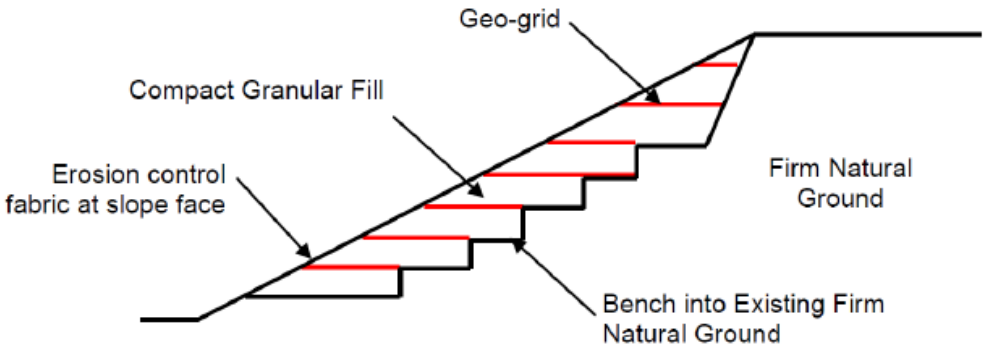

Figure 2.27 Typical slope stabilization project designed with geo-grid (Day, 1997; Sapkota 2019)

There are a lot of considerations involved in the design of a geo-grid stabilized slope. It requires detailed knowledge of properties and design of geo-grid, properties of the fill soil, slope ratio, benching in existing slope, and the geometry of the potential failure mass. Any discrepancy or wrong judgment in any of the considerations could lead to the failure of geo-grid reinforced soil slopes (Day 1996a, Berg et al. 2020).

2.6.4 Launched Soil Nails to Repair Surficial Slope Failures

In this method galvanized or non-galvanized solid or hollow steel bars are placed into slope using special equipment of soil nail launcher. These nails are required to install beyond to critical slip surface to a resistant zone at least depth of 1 m (3.3 ft) (USDA Forest Servi 1994). Launched nails act as reinforcement on the soil mass and increase the shear resistance and tensile strength against

mobilized driving forces as seen in Figure 2.28 (Titi and Helwany 2007). In this method, the nails can be installed till 8 to 11 m (26 to 36 ft) below the ground without any excavations (Steward and Ribera 1995).

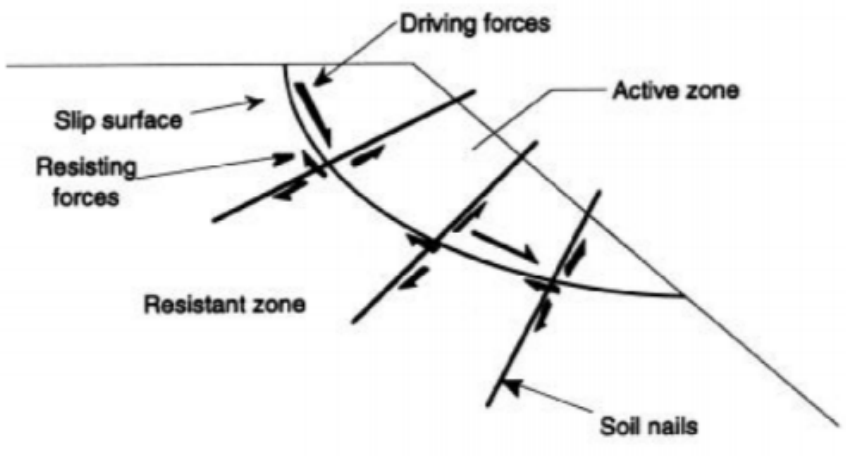

Figure 2.28 Slope repair using soil nails (FHWA, 2003; Titi and Helwany 2007)

The design studies of this method re quire consideration of various soil nail type, spacing, length, and the number of nails used, and environmental impact on nails. The analytical methods need to be carried out similar to laterally loaded piles as well as considering local shear bearing capacity and soil flowing problem along with the rigid material. It has been reported that the failure is more critical at shallow depths and with narrow nails as the nails are not wide enough to prevent it (Fabius et al. 2008).

2.6.5 Earth Anchors to Repair Surficial Slope Failures

Earth anchors have been widely used in earth retaining structures and slopes to resist the loads that cause instability (Das and Shukla 2013). This method

strengthens the slope and constrains the possible soil movement using tension-resisting elements. These earth anchors are sometimes called as Tie-backs (Deaton 1984). Earth Anchors system includes a wire rope, mechanical earth anchor, bearing plate, and the end anchorage plate. The shallow slope repair procedure with earth anchors is listed following (Titi and Helwany 2007):

- Excavation of the failed soil and rebuilding slope with the same soil or new granular material.
- Seeding the slope surface and installation of earth erosion systems
- Inserting the mechanical anchors into the slope beyond the failure slip surface.
- Pulling the wire rope and tightening the anchors.
- Locking the tight wire rope to endplates (Figure 2.29).

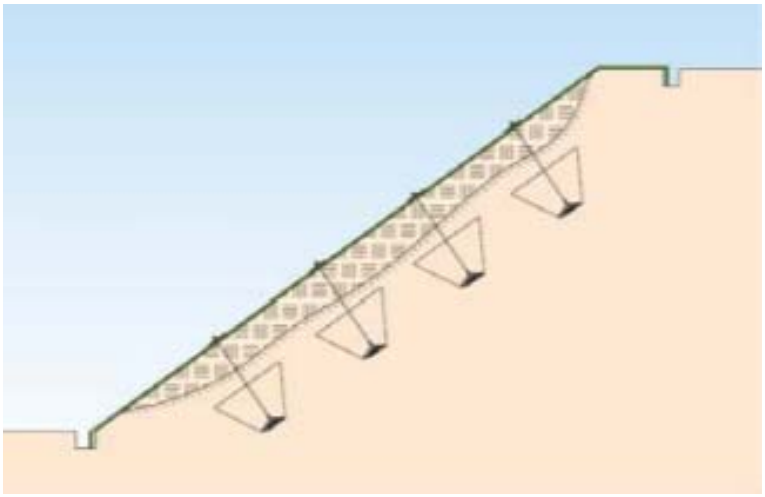

Figure 2.29 Earth anchors for slope stabilization (Titi and Helwany 2007)

2.6.6 Plate Piles

Plate pile is a relatively new technology to mitigate the surficial slope failures. In this method, various dimensions of (36-66 inch in height x 12 inches in width x ¼" in) plates are welded to a steel pile (Taliaferro 2016) and the combination of works in the same manner of pile slope system (Figure 2.30) (Collins and Short 2006). Plate piles are driven beyond the potentially unstable slope layer with the help of a vibratory hammer. The system transmits the shear stress from the slip surface to the underlying stiffer deep layer (Taliaferro 2016).

Although the field test results for the plate piles have proven the effectiveness of this method, it is still limited to stabilize the soil layers up to 3 ft of depth (Fay et al. 2012). Another drawback of this method is that the process of driving the plate piles becomes very challenging if the slope material is hard silt or clay. Also, as this is a new technology, there is a very limited number of technical persons available for field implementation (Taliaferro 2016).

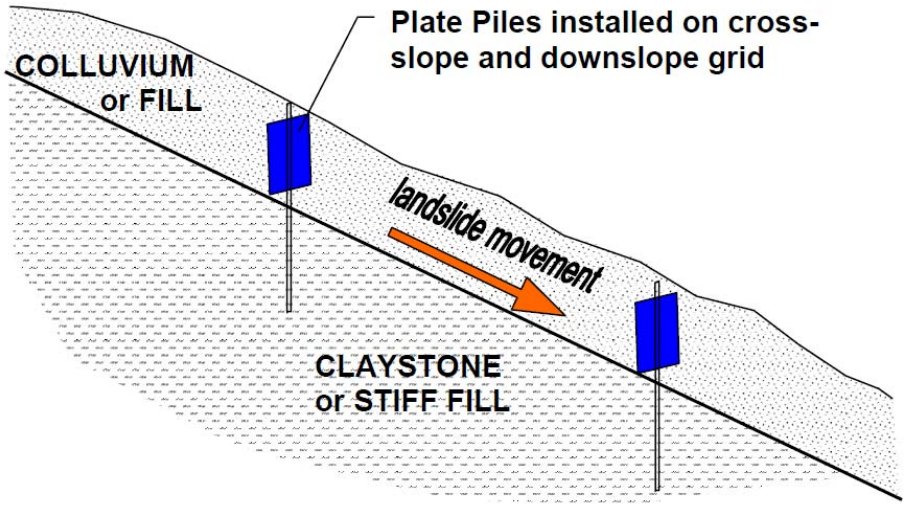

Figure 2.30 Plate pile slope stabilization concept (Short and Collins, 2006)

2.6.7 Using Compost, Fiber, and Calcium-based Additives

The stability of the slope and its durability against challenging environmental factors can be enhanced by using additives. Compost, fiber, and calcium-based additives are mixed with soil in a certain amount to improve the soil properties. These additives boost the strength of soil, reduce compressibility, and volumetric shrinkage and ultimately mitigate the detrimental effect of desiccation cracks in clayey soil slopes. For example, compost enhances the soil moisture retention capacity (hydrophilic characteristics) and therefore limits the shrinkage strains of expansive soil (Dronamraju 2008). Fibers blending in the soil act as reinforcement material by increasing the interlocking of soil particles and decreasing the soil tensile strains (Maher and Gray 1990, Kumar and Singh 2008). Mixing of calcium-based stabilizers in the soil creates cementitious products and

prevents volumetric changes, increase soil durability, stiffness, and strength (Hoyos et al. 2004, Collin et al. 2008). One of the major concerns in this stabilization method is the non-uniform blending of additive in soil throughout the slope (Day 1996b). However, as these methods have been extensively used, a variety of high-quality construction equipment and procedures have been developed in the recent past.

2.7 Soil Lime Admixtures

Lime stabilization is one of the oldest and reliable methods of soil stabilization to improve soil properties economically (Pedarla et al. 2011, Puppala 2016, Puppala et al. 2019b). The use of lime stabilization of clay in construction is 5000 years old (Khattab et al. 2006). The application of lime in road construction started in Roman roads which date back more than 2,000 years (McDowell 1959). The abundant studies conducted over the several decades have concluded that lime treatment is an effective soil treatment method in mitigating volumetric changes in embankment slopes, road subgrades, and lightweight structures (Puppala et al. 1996, Elkady 2016, Wang et al. 2016, Chakraborty and Nair 2018a, 2018b, Elkady and Shaker 2018). Also, lime stabilization offers an economical solution by cutting down the transportation cost of the of borrow fill material due to the use of locally available soils (Reddy 2002). According to Corathers and Apodaca (2017), the USA used 1.35 million metric tons of lime for soil stabilization in 2017.

Lime treatment technique can be applied to a wide range of soils including dirty sands, silts, and plastic clays which contains at least 7% clay and has the minimum PI value of 10 (Bell 1996, Association 2004, Collin et al. 2008). However, it is not an effective method in the case of coarse material and soil with high soluble sulfate content. In the case of sulfate-rich soil, lime treatment results in significant heaving (Puppala et al. 2005, 2019c).

Adding lime additives to soil results in two main phenomena: short-term reactions that cause modification of soil physico-chemical characteristics and long-term reactions that enhance soil engineering properties. Short term reactions immediately improve the workability of the soil by blending a small amount (1 to 4 %) of lime into it (Lime Association 2004). On the other hand, long term reactions improve the strength and compressibility characteristics of the soil. These reactions generally happen over a long period of time (several years) and require a larger amount (more than 4 %) of lime. Different reactions that occur between soil and lime are briefly described in the following section.

2.7.1 Soil Lime Reactions

The lime used in soil stabilization can either be quicklime (CaO) or hydrated lime ($Ca(OH)_2$). When lime is mixed with active clayey soil (with negative charges), the primary short-term reactions including hydration, flocculation-agglomeration, and cation exchange take place (Basma and Tuncer 1991, Nelson and Miller 1997, Rajasekaran et al. 1997, Puppala and Musenda

2000, Khattab et al. 2007, Wang et al. 2017b, Hotineanu et al. 2015, Wang et al. 2015, 2016, Elkady 2016, Elkady and Shaker 2018, Bhuvaneshwari et al. 2019). The negative charges in soil attract the calcium ions (Ca^{+2}) from hydrated lime and Ca^{+2} ions displace water and other ions such as K, Na or Mg ions. In this process, electrically charged particles form a floc or larger agglomeration resulting in more friable and granular soil texture. This initial process generally requires a small amount of lime and occurs in few hours to days based on the type of clay minerals in the soil (Bell 1996, Al-Rawas et al. 2005, Puppala et al. 2013). For this reason, 1 to 4 days of mellowing time are recommended. It improves soil workability and constructability significantly and makes it workable even in wet conditions.

When lime is blended with the soil, the pH value of the soil-lime mixture increases which leads to the release of silica and alumina. The released free silica and alumina from clayey soil reacts with Ca^{+} from lime to form calcium-silicate-hydrate (C-S-H) and calcium-aluminate-hydrate (C-A-H) (Chittoori 2008, Elkady and Shaker 2018). The developed CSH and CAH bind the soil particles and improve the strength properties, volumetric changes characteristic, and durability of soil significantly (Puppala et al. 1996). These pozzolanic reactions in lime stabilized soil occur for several days to years.

2.7.2 Estimation of Optimum Percentage of Lime

In lime stabilization projects, the optimum lime content is determined based on pH test methods. This test is developed to determine the required amount

of lime and pH value to satisfy the initial cation exchange reactions and sustain a high pH environment for pozzolanic reactions (Eades and Grim 1966). Different agencies follow Eades & Grim test method to determine the optimum lime content for their mix design projects including the US Army and Air Force Department, Indiana Department of Transportation, and TxDOT. Also, some agencies suggest conducting durability tests and unconfined compressive strength tests to check that the determined percentage satisfies the strength criterion and ensures the stabilization effects are lasting (TxDOT 121, U.S. Army TM 5-882-14/AFM 32-1019). If the results of these studies are not satisfying the requirements, a greater percentage of lime content is selected.

2.7.3 Effect of Lime Treatment on Soil Hydraulic Properties

Numerous studies have been conducted to study the effects of lime treatment on the permeability of soil (McCallister and Petry 1992, Nalbantoglu and Tuncer 2001, Rajasekaran and Narasimha Rao 2002, Le Runigo et al. 2011, Al-Mukhtar et al. 2012a, Bhaskar et al. 2019b). As the lime treatment includes short term modification reactions and long term pozzolanic reactions and these reactions highly depends on soil mineralogy, the research findings are quite variable. Broms and Boman (1977) conducted in situ testing on the permeability of lime columns and compared these results with untreated soil. After the lime treatment, the permeability increased 100 to 1000 times and the authors suggest that these cylindrical columns act as vertical drains. Evans and Bell (1981)

explained the soil modification in texture and increase in particle size resulting in soil permeability.

El-Rawi and Awad (1981) observed that the permeability increase rate in cohesive clayey soil depends on clay fraction size. Soil with higher clay fraction exhibits higher permeability value after lime treatment. Khattab et al. (2007) observed an increase in soil permeability value by more than two orders in magnitude after treating the soil with 4% lime. The authors attributed this increase to an increase in the total pore volume of soil due to the flocculation of clay particles after lime clay reactions. Nerincx et al. (2016) observed that if the lime-treated soil is prepared on the wet side of OMC and compacted with kneading (using sheep foot roller), the permeability value remains unchanged.

Al-Kiki et al. (2008) investigated the effects of lime content and curing time on the coefficient of permeability of the soil. In their study, all the treated soil samples exhibited higher permeability value than the untreated soil and the rate of increase in the permeability coefficient dropped down with an increase in lime content. Also, in the early curing periods (less than 4.2 days), the permeability value was found to increase for all lime percentages. The longer curing period leads to a decrease in the permeability value of soil.

The permeability of soil is also influenced by the dosage of lime. Some researchers observed that the permeability value of lime stabilized soil increases only at a low dosage of lime. At higher dosages, treated soil exhibits lower

permeability value than untreated soil (Galvão et al. 2004; Kassim and Uuey 2000; Locat et al. 1996; Quang and Chai 2015). The treated soil has high permeability than untreated soil because of the flocculation of clay particles (Locat et al., 1996). The further addition of lime in the soil causes filling of pores with cementitious products (i.e., CSH) resulting in a decrease in average pore radius. This reduction in pore size eventually starts to decrease the permeability value of soil.

2.7.4 Effect of Lime Treatment on Soil Strength

The strength properties of soil change significantly after lime treatment. When soil is mixed with lime, there is an immediate increase in its strength due to initial soil modification reactions (Thompson 1965, Neubauer Jr and Thompson 1972). If there is an adequate high pH environment (more than 10.5), pozzolanic reactions and formation of CSH and CAH cementitious gels contribute to strength development. This pozzolanic reaction occurs over a long curing period and the strength increases are mostly controlled by the curing period rather than dosages (Bhattacharja and Bhatty 2003, Al-Mukhtar et al. 2010). The strength increase in the soil is generally influenced by soil clay mineralogy, silica-alumina percentage, soil pH, compacted moisture content, type of lime, and environmental conditions (Mallela et al. 2004). Ghobadi et al. (2014) found that the unconfined compressive strength value of soil can be increased by up to five times of untreated soil UCS value after curing 30 days curing period. Extended curing periods might lead to

continuing to increase the UCS value (Al-Mukhtar et al. 2012b, Hotineanu et al. 2015).

Similarly, many researchers observed that lime treatment leads to a significant increase in soil cohesion and the internal friction angle. The increase in soil friction angle is attributed to the coagulation in soil particles (Szendefy 2013). The cohesion value increase is considered due to the presence of coarse-grained and strongly bonded particles in soil mass, cementation, and pozzolanic reactions developed between soil and lime (Ola 1978, Lees et al. 1982, Bell 1996). Gay and Schad (2000) conducted a study by using 2-8% lime content with 3,7,14, and 28 days of curing period. The authors found that after mixing lime, the soil strength parameters experienced a significant increase within short term curing days (3 days) for all the lime percentage. Also, the authors observed that the cohesion value of treated soil with low lime content did not increased significantly over further curing conditions. A prominent cohesion value improvement based on curing time started to be observed for higher lime content (6 percent). Also, authors observed that the friction increase only up to 4% of lime and beyond this dosage the friction angle increase start to decrease for the same curing period.

A similar kind of trend observed for the soil cohesion increase, the cohesion value of 6% lime-treated soil obtained higher than 8 percent lime-treated soil. Qiang and Chen (2015) observed the same effects of high lime dosage. The authors concluded that for the low dosage of treatment, the limes only present in

pores created by soil skeleton, however higher lime dosages, result in separation of the soil particles. The excess lime can fill into these pores between soil particles. And, due to insufficient friction properties of the lime, it acts as lubricating material that causes a reduction in cohesion and internal friction angle.

2.7.5 Effect of Weathering Cycle on Lime-Treated Soil

Although lime treatment successfully enhances soil properties, exposure to wet-dry cycles can affect its engineering properties. Rao et al. (2001) examined the beneficial effects of lime-treated soils under four continuous wet-dry cycles. The results showed that wet-dry cycles result in some partial breakdown of cementitious bonding that leads to an increase in clay content of the soil. And, this phenomenon is attributed to a slight to moderate increase in LL and a considerable increase in soil PI and swelling capacity.

Khattab et al. (2007) conducted a similar kind of study by comparing two different orders of wet-dry cycles (i.e., starting the cycles first from wet or dry conditions). The authors found that the starting of the wet-dry cycles from the drying period causing a constant increase in swelling strains and almost complete loss in benefits of lime treatment. The authors suggest that to take measures against sunlight and heat for lime stabilization projects conducted during the hot season.

Akcanca and Aytekin (2014) and Song et al. (2020) investigated the changes in the permeability of lime stabilized soil during wet-dry cycles. Both researchers concluded that the permeability of lime-treated soils decreased

considerably and, therefore, the negative impacts of lime additives on the permeability value of treated samples partially lost. This permeability recovery is attributed to a reduction in voids size due to the development of cementation products that is occurred during wet-dry periods.

2.8 Summary

This chapter reviews the available literature on expansive soils and identifies stability issues in high plastic clayey slope due to the presence of desiccation cracks induced by wet-dry cycles. The clay mineralogy, swelling and shrinkage phenomena, and the development of desiccation cracks and its consequences on the clayey soil slopes were discussed. The slope failures are generally observed in unsaturated soil therefore, the fundamental concepts of unsaturated soil mechanics, effects of suction on hydro-mechanical properties of soil, rainfall-induced slope stability analysis methods were reviewed.

Several slope stabilization methods have been developed to prevent and repair the surficial slope failures. Different stabilization methods with their applicability and advantages and disadvantages were briefly described. The lime stabilization method is one of the most preferred and quite effective in mitigating the swelling and shrinkage strains in expansive soils. The soil lime reactions, the applicability of lime, soil mix design, the effect of lime on soil hydro-mechanical properties were studied in detail. Exposure to wet-dry weathering cycles degrades the engineering properties of lime-treated soils. Most lime treatment projects are

primarily designed without enough consideration of the impact of wet-dry cycles on the soil properties. The design assumptions do not portray the actual field conditions and underestimate the effect of the seasonal variation of the rainfall. Hence, it becomes important to investigate the long-term effectiveness of the lime treatment on the slopes by incorporating the effect of detrimental changes in the hydro-mechanical properties of the treated soil due to wet-dry cycles and rainfall events.

Chapter 3

SALIENT FINDINGS OF FAILED SLOPES AND CAUSES OF FAILURE

3.1 Introduction

The main purpose of this research work is to evaluate the long-term effectiveness of lime treatment in preventing surficial slope failures. To achieve this objective, a repaired slope of the U.S. 75 Frontage Road in North Texas, which was stabilized using the lime treatment, is considered in this research study. The slope experienced a surficial failure in December 2015 after heavy rainfall (21.87 cm) that month. In May 2020, the failed section of this slope was stabilized with lime and reconstructed. It is believed that the development of desiccation cracks in the soil after numerous seasonal wet-dry cycles resulted in shallow slope failure. In the present study, a comprehensive laboratory test program is designed and executed to investigate the causes that led to this slope failure. In the preliminary studies, physical and engineering tests were conducted on the soil collected from the scarp of the failed slope. The detailed procedure along with test results for all physical and engineering tests are illustrated in this chapter. Results of these preliminary studies were later used in numerical analyses to investigate the conditions that resulted in the failure.

This chapter also highlights salient findings of the case studies of Grapevine and Joe Pool dams where similar kinds of surficial slope failures were reported. Both Grapevine and Joe Pool dams are located in North Texas and have a close proximity to U.S. 75 Frontage Road. These earthen dams also experienced surficial slope failures during or after an intense rainfall event (McCleskey 2005). In the studies conducted by McCleskey (2005) and Dronamraju (2008), the efficacy of several stabilizers including lime, fibers, and compost additives in slope stabilization was evaluated through laboratory tests and numerical studies. In their analyses, the fluctuation in the moisture content of soil due to rainfall was not considered and the top 0.51 m (20 in.) surficial soil layer of the slope was assumed to be fully saturated. Also, the stability of the slope was analyzed using residual shear strength parameters in the surficial layer instead of fully softened strength parameters. The pertaining slope information and soil properties of Grapevine and Joe Pool dam provided in this chapter are later used in numerical studies of slope stability with proper consideration of moisture fluctuation and soil strength reduction due to rainfall.

3.2 Surficial Slope Failure on U.S. Highway 75 Frontage Road

3.2.1 General

The U.S. Highway 75 (US 75) is a part of the U.S. Highway System that runs from Interstate-345 in Dallas, Texas to the Oklahoma state border. In the present study, the surficial slope failure that occurred in Denison, Texas along the

southbound U.S. 75 Frontage Road, was investigated. The failed section of the U.S. 75 Frontage Road is located between State Highway 91 and Randell Lake Road. The location of the failed slope section is shown in Figure 3.1. Before the occurrence of failure, the section of the slope was 11.58 m (38 ft) in height with three horizontals to one vertical (3H: 1V) slope ratio.

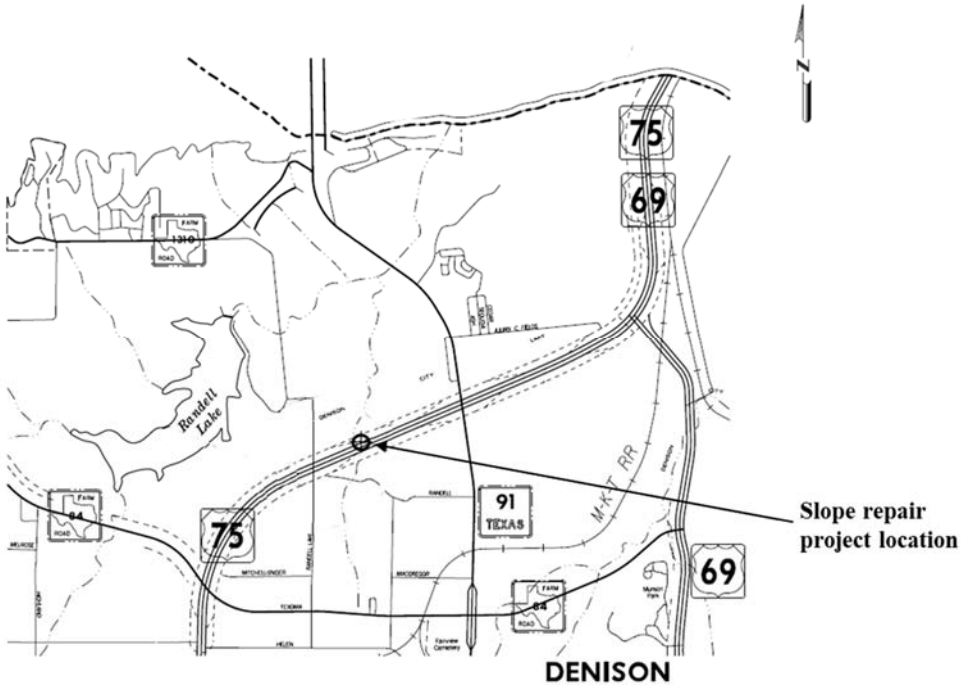

Figure 3.1 Location of the failed U.S. 75 Frontage Road slope (source: TxDOT)

According to the TxDOT officials, a number of surficial failures were observed nearby the site location. These failures mostly occurred near the crown of the slope and shoulder of the highway. The noticeable desiccation cracks were observed in the slope for the first time in November 2014, but no major failure was observed at that time. In December 2015, a total of 21.87 cm (8.61 in.) rainfall

was recorded by the nearest rainfall station (NOAA). The significant amount of rainfall that occurred in that month is believed to have caused this failure. This major surficial failure in the embankment slope extensively damaged the overlying pavement structure and resulted in the closure of the frontage road.

The University of Texas at Arlington (UTA) research team conducted the first site investigation in December 2017. In that site visit, the dimensions of the failed section of the slope, as shown in Figure 3.2a, were measured. The longitudinal extent of the failed section was about 18.3 m (60 ft) long along the pavement section with a vertical scarp height of approximately 1.8 m (6 ft). With time, the failure propagated and extended in both lateral and longitudinal directions due to the impact of wet-dry cycles. By June 2019, the length of the failed slope section had increased by more than 8 times to approximately 134.7 m (442 ft) and slope failure propagated to both lanes of the pavement as shown in Figure 3.2b.

(a)

(b)

Figure 3.2 Failed slope condition in (a) December 2017 and (b) June 2019

The investigation of this failure was carried out by conducting comprehensive laboratory studies on the soil samples collected from the failed slope section. The samples were collected from the failure scarp after removing 30 cm (1 foot) of topsoil from the surface as it was contaminated with vegetation remains, chemical fertilizers, and coarse material from pavement structure. The collected soil samples were transferred to the laboratory in sealed buckets. To identify possible causes of the failure, several classification and engineering tests were conducted prior to stabilization mix design studies.

3.2.2 Laboratory Studies on U.S. 75 Frontage Road Slope Soil

3.2.2.1 General

In order to determine the basic properties of soil collected from failed embankment slope U.S. 75 Frontage Road, several physical and engineering laboratory tests were carried out. The physical tests, including Atterberg limits, grain size distribution, and standard Proctor compaction test, were conducted for classification of soil and determination of its index properties. The laboratory engineering tests were performed to determine the strength and swell-shrinkage characteristics of the soil. The engineering tests conducted in this study include one dimensional (1D) swell test, shrinkage strain test, direct shear test, and torsional ring shear test. All the laboratory tests were conducted according to ASTM and TxDOT standards. The test procedure and results for each test are provided in detail in the following sections.

3.2.2.2 Physical Properties Tests

3.2.2.2.1 Atterberg Limits Tests

The Atterberg limits of a soil, Liquid Limit (LL) and Plastic Limit (PL), provide an idea about plasticity characteristics and swelling potential of fine-grained soil. The LL value of the soil is the water content which marks its transition from a plastic state to a liquid state. Similarly, PL defines the consistency at which soil passes from semisolid state to plastic state. Both LL and PL tests were performed on soil passing through number No. 40 sieve (425-μm). The LL of soil was determined using the Casagrande apparatus (Figure 3.3a) as per ASTM D4318-17. The soil used for the liquid limit test was air dried and reused to perform the PL test. An E-180 PL rolling device developed by TxDOT was used to determine the PL of the soil following the procedure of ASTM D4318 (Figure 3.3b).

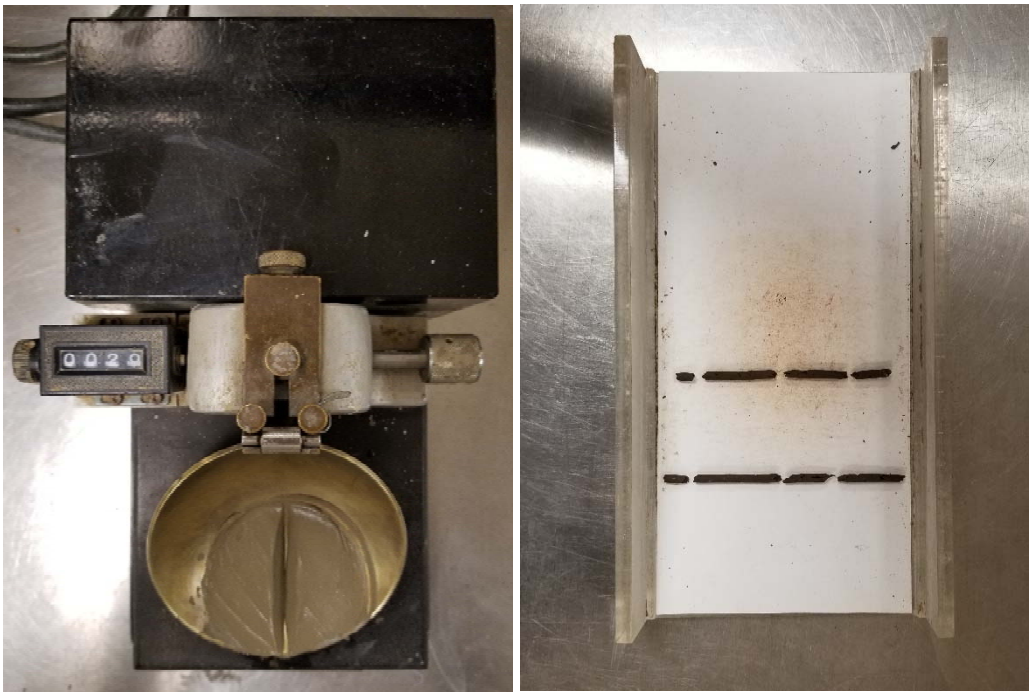

(a) (b)

Figure 3.3 Atterberg limits test: (a) Casagrande LL apparatus (b) E-180 PL rolling device

3.2.2.2.2 Soil Grain Size Distribution

The grain size distribution data of soil along with its consistency limits can be used to classify it based on the Unified Soil Classification System (USCS). Determination of the soil gradation curve was achieved by performing wet sieve analyses and hydrometer tests according to techniques outlined in ASTM D1140 - 17 and D7928 – 17, respectively. The grain size distribution curve of untreated soil is shown in Figure 3.4.

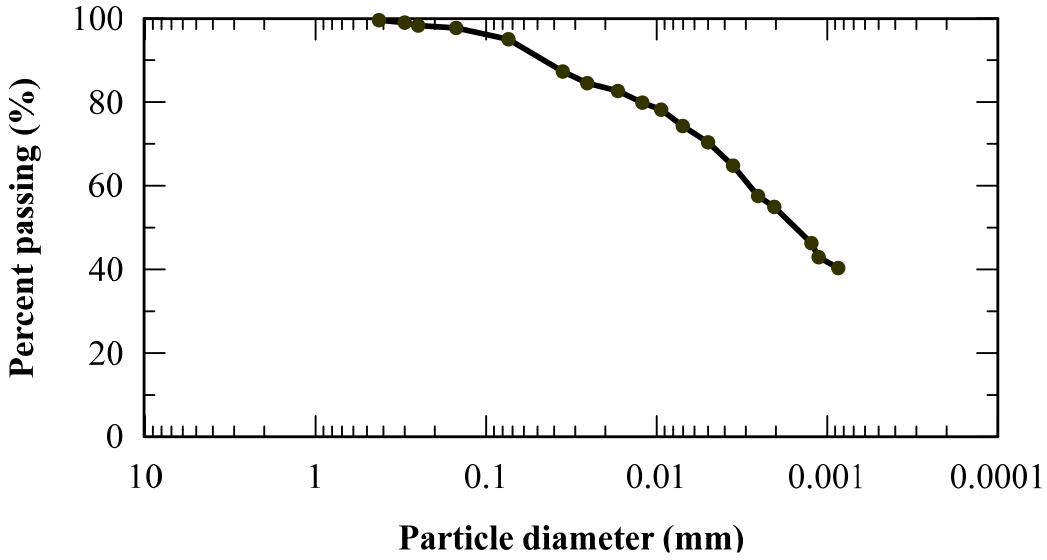

Figure 3.4 Grain size distribution of untreated U.S. 75 Frontage Road slope soil

3.2.2.2.3 Standard Proctor Compaction Test

The relationship between soil moisture content and dry unit weight was determined by conducting the standard Proctor compaction test. The dry soil samples were mixed with different percentages of water and compacted in the standard mold in three layers as per the procedure mentioned in ASTM D698-12. After oven drying process, the moisture content and dry unit weight of trial samples were calculated and plotted as shown in Figure 3.5. The peak point of the plotted curve is defined as the OMC and the corresponding dry density is called as the maximum dry density (MDD) or maximum unit weight.

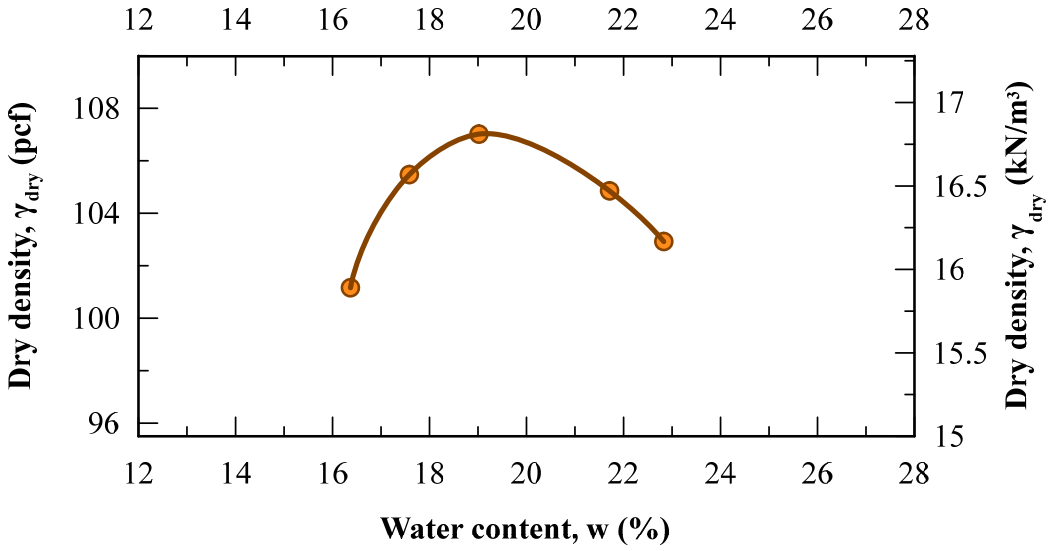

Figure 3.5 Relationship between dry unit weight and moisture content for untreated U.S. 75 Frontage Road slope soil

3.2.2.3 Engineering Tests

3.2.2.3.1 One Dimensional (1D) Swell Strain Test

The 1D swell test provides the degree of affinity of soil to water. It measures the amount of wetting-induced swelling in soil specimen. In this test, a cylindrical specimen of 63.5 mm (2.5 in.) diameter and 25.4 mm (1 in.) height was used. The specimen was statically compacted in the laboratory at its OMC and 95% of its MDD and the test was conducted using a conventional odometer apparatus (Figure 3.6) as per ASTM D 4546 standards. The specimen was inundated with water and the change in height was recorded using two manual dial

gauges. The test was continued until there was no observed change in the dial gauge reading. 1D swell strain was determined as the percentage increase in height of the specimen with respect to the initial height of the specimen. The test result of the 1D swell test is presented in Figure 3.7.

Figure 3.6 1D swell strain test setup

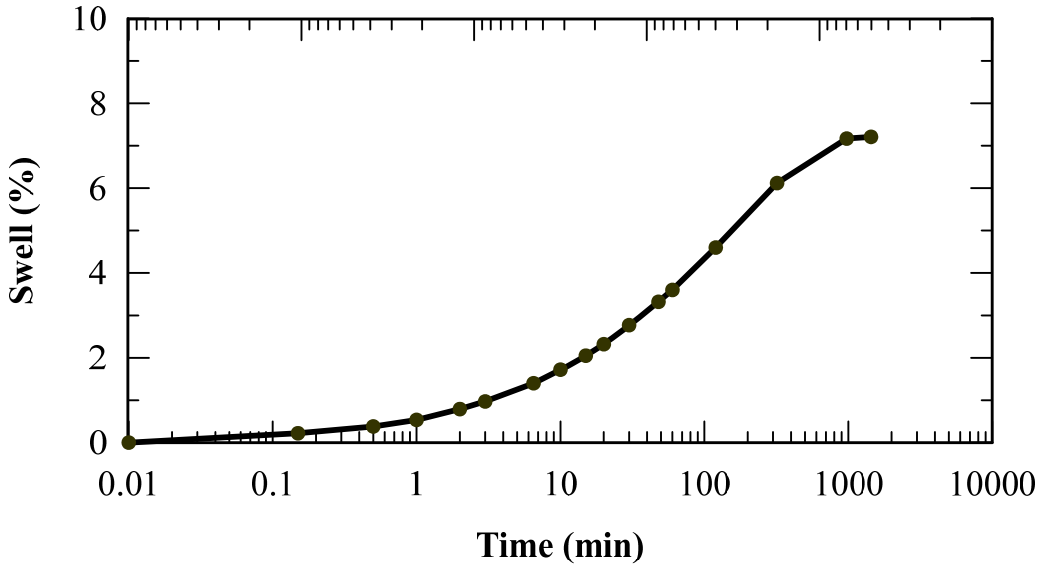

Figure 3.7 1D swell test result of untreated U.S. 75 Frontage Road slope soil

3.2.2.3.2 One Dimensional (1D) Shrinkage Strain Test

The linear shrinkage potential of soil was determined by measuring the decrease in linear length of soil specimens due to drying. This test was conducted in accordance with the Tex-107-E procedure with soil passing number 40 sieve. The soil was thoroughly mixed with a certain amount of water to obtain the target soil consistency specified in Tex-107-E. The soil specimens were placed in standard linear bar molds that were greased with petroleum jelly (Figure 3.8a). Before placing the molds in oven for drying, they were kept at room temperature until there was a slight change in the color of soil specimens. Once the specimens were dry, the length of dried specimens was measured using Vernier caliper and linear shrinkage strain was calculated with respect to the initial length of soil specimen (Figure 3.8b).

(a) (b)

Figure 3.8 1D linear shrinkage test specimens (a) before oven drying and (b) after oven drying

3.2.2.3.3 Direct Shear Test

The shear strength parameters of soil are the key parameters in design and analysis of slopes. In this study, DS tests were conducted to determine the peak shear strength parameters of the soil. These tests were conducted based on the procedure given in ASTM D3080 standards using a computerized DS testing equipment as shown in Figure 3.9a. The cylindrical soil specimen with 63.5 mm (2.5 in.) diameter and 25.4 mm (1 in.) (Figure 3.9b) were statically compacted at its OMC to 95% of its MDD. The DS tests were conducted at three different normal stress of 50 kPa, 100 kPa, and 150 kPa (1044, 2089, and 3133 psf). Before the shearing, the test specimens were fully saturated and consolidated under the designated normal loads. The test specimens were sheared at a slow shearing rate

of $4.4x10^{-3}$ mm/min ($1.73x10^{-4}$ in./min) to allow the excess water to dissipate easily and therefore, to ensure drained conditions. The measured peak strength of the results of 3 different DS tests was combined together and soil cohesion and friction angle value were calculated.

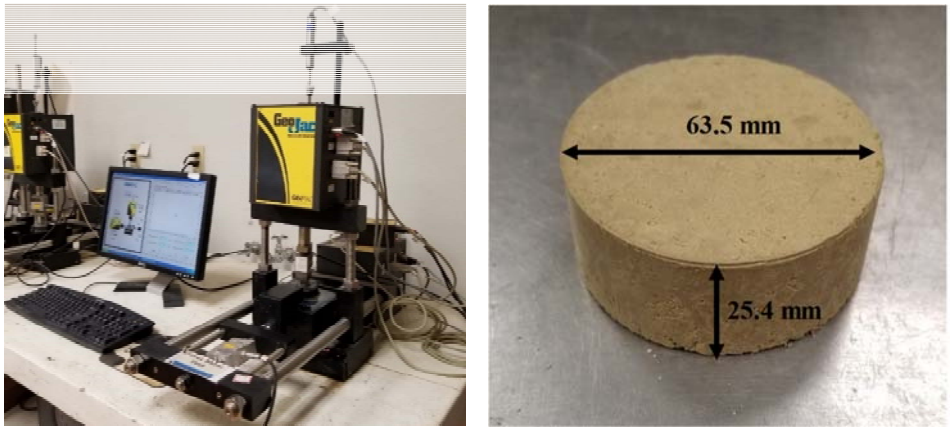

(a) (b)

Figure 3.9 (a) Computerized DS test apparatus and (b) DS test specimen

3.2.2.3.4 Torsional Ring Shear (TRS) Test

The long-term environmental factors, particularly wet-dry cycles, cause the development of desiccation cracks and a significant loss in shear strength of the soil. From the back analysis of failed slopes, it has been observed that the strength of soil may reduce from peak strength to fully softened strength. The reduction in soil strength parameters from peak to FSS needs to be quantified to better demonstrate the causes of failure. The FSS parameters of soil can be better measured by using the TRS test instead of DS or Triaxial tests (Skempton 1964, 1970, Kayyal and Wright 1991, Castellanos 2014, Jafari et al. 2019).

In the present study, TRS tests were conducted as per ASTM D7608-10 standards. A Bromhead ring shear testing equipment, as shown in Figure 3.10a, was used to perform the TRS test. In this test, the soil specimen was prepared in slurry condition by mixing the dry soil with distilled water corresponding to 1.5 times of its LL. The slurry specimen was then placed into an annular mold, as shown in Figure 3.10b, with an inside diameter of 70 mm (2.75 in.) and an outside diameter of 100 mm (4 in.). After placing the specimen in mold, a preconsolidation pressure of 6.25 kPa (130.5 psf) was applied with a load increment ratio of one. Each load increment was kept until the completion of the primary consolidation of soil or achieving the target normal stresses. In this study, TRS tests were conducted at a normal stress of 50 kPa, 100 kPa, and 150 kPa (1044, 2089, and 3133 psf). Once the consolidation was over, the specimens were sheared at a rate of 0.018mm/min (7.09×10^{-4} in./min) (Figure 3.10c). This small shear rate was chosen to ensure complete dissipation of excess water pressure in specimen.

(a)

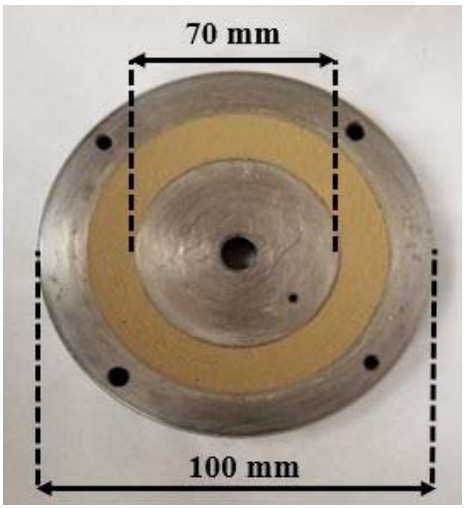

(b)

(c)

Figure 3.10 (a) Bromhead torsional ring shear apparatus, (b) annular mold used, and (c) specimen before shearing

3.2.3 *Results of Laboratory Studies*

This section presents and discusses the results of physical and engineering tests conducted on soil specimens from the U.S. 75 Frontage Road slope. The soil was found to have a high LL value of 58 and a plasticity index value (PI) of 37. A significant percent of clay fraction (CF) in the grain size distribution curve corroborates this finding. Based on the USCS classification, soil can be classified as a high plasticity clay (CH). The results of 1D free swell and shrinkage tests highlight the expansive nature of this clayey soil. Test results showed that the soil experienced a significant percentage of 1D swell strain (7.2%) and shrinkage strain (17.7%). Again, this trend in the swell-shrinkage characteristic can be explained by high CF and high PI value of soil. The test results of soil are summarized and presented in Table 3.1. The high value of the Atterberg limit, severe swell-shrink potential, and the presence of a high amount of clay content show the soil's susceptibility to degradation of hydro-mechanical properties due to wet-dry cycles.

Table 3.1 Summary of the test results of untreated U.S. 75 Frontage Road slope soil

Property	**Value**
Specific Gravity, G_s	2.69
Sand Content (%)	5

Silt Content (%)	40
Clay Fraction, CF (%)	55
Liquid Limit, LL (%)	58
Plastic Limit, PL (%)	21
Plasticity Index, PI (%)	37
USCS Classification	CH
Optimum Moisture Content, OMC (%)	19.5
Maximum Dry Density (kN/m^3/pcf)	16.8 /107
1D Free Swell Strain (%)	7.2
1D Linear Shrinkage Strain (%)	17.7

The Figures 3.11a and 3.11b presents the results of the DS and TRS tests conducted on the untreated U.S. 75 Frontage Road slope soils at different normal stresses, respectively. The values of cohesion and friction angle of soil, obtained from the DS and TRS tests, are tabulated in Table 3.2. A 23.7 degree of soil effective friction angle were obtained from the DS test results, which were performed to determine the peak strength of soil in the newly compacted condition. The TRS tests results showed that the expected friction angle of soil will drop down slightly to 23.4 degree when it subject to numerous weathering cycles. Unlike the angle of friction, there was a drastic change observed in the cohesion value. The expected soil cohesion value decreased from 13.2 kPa to 1.28 kPa due to softening behavior of soil after exposing the weathering cycles.

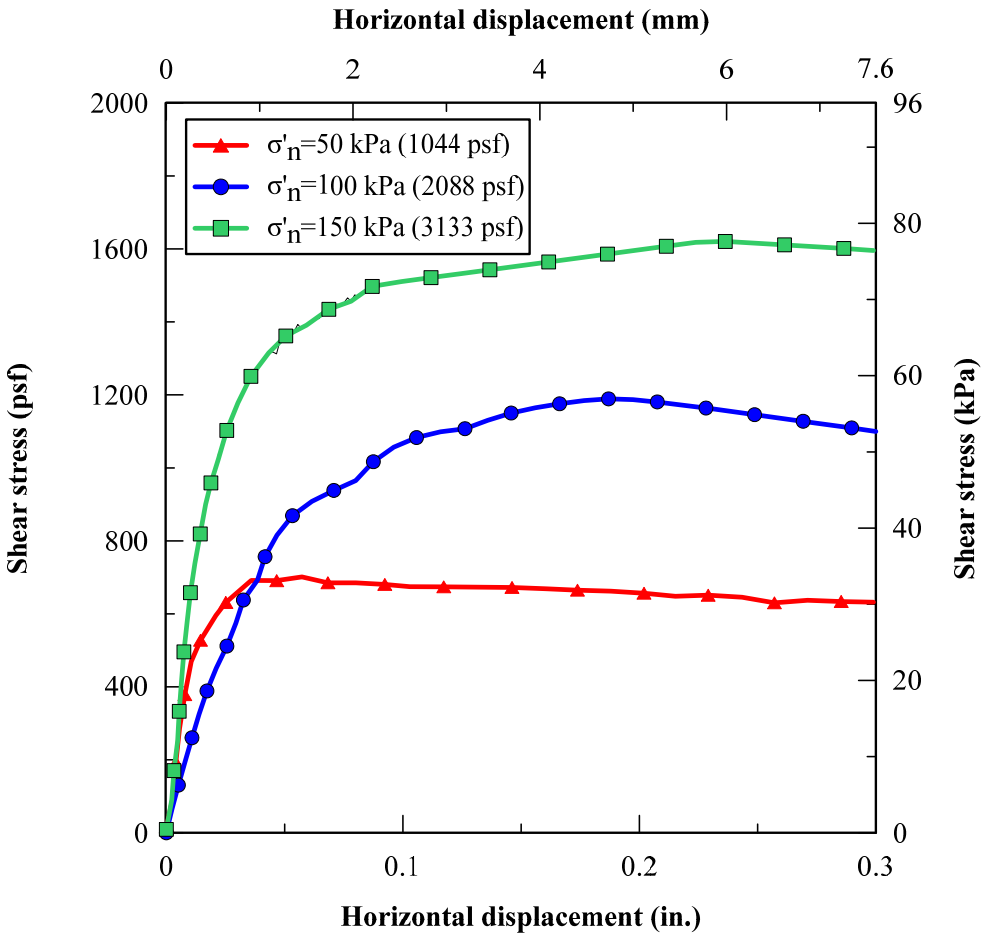
Horizontal displacement (mm)
0
2
4
6
7.6
2000
1600
1200
800
400
0
96
80
60
40
20
0
σ'n=50 kPa (1044 psf)
σ'n=100 kPa (2088 psf)
σ'n=150 kPa (3133 psf)
Shear stress (psf)
Shear stress (kPa)
0
0.1
0.2
0.3
Horizontal displacement (in.)

(a)

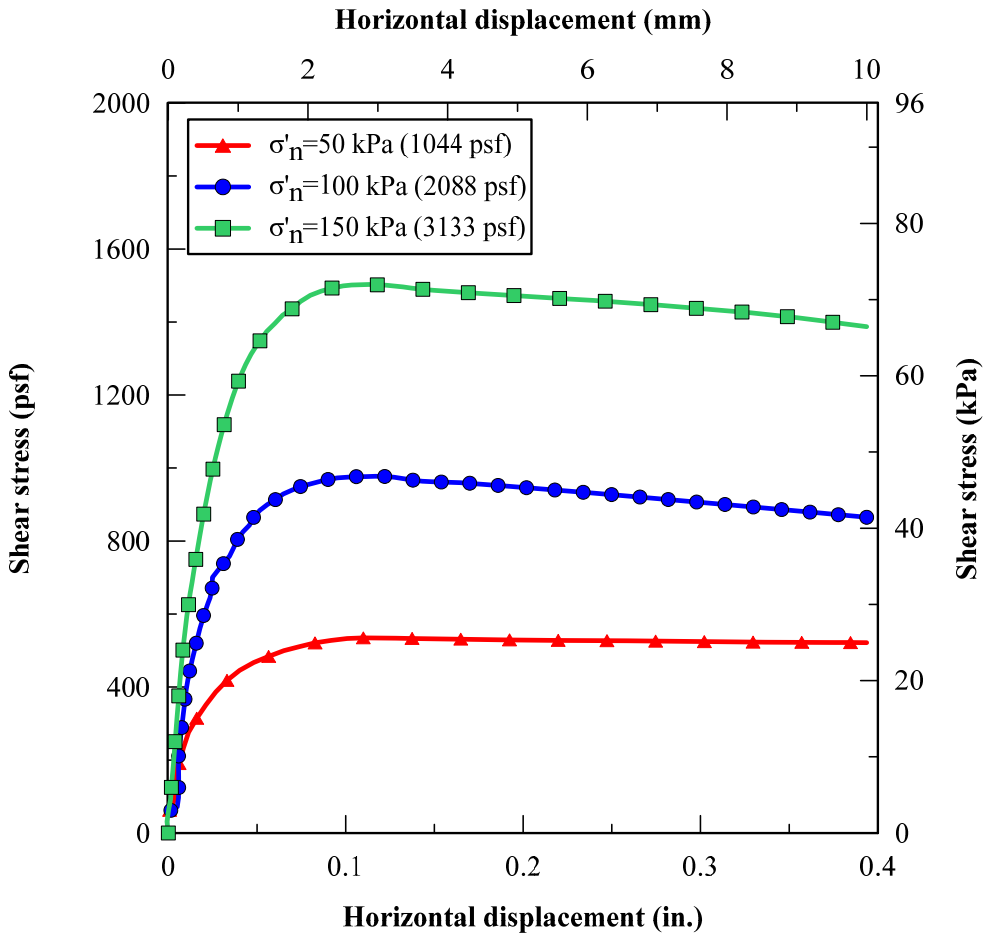

(b)

Figure 3.11 (a) DS test results and (b) TRS test results for untreated soil used in U.S. 75 Frontage Road slope

Table 3.2 Measured peak shear strength and FSS parameters for untreated U.S. 75 Frontage Road slope soil

Strength Type	Test Type	c' (kPa / psf)	ϕ' (degree)
Peak shear	Direct shear	13.20 / 275.3	23.7
Fully softened	Torsional ring shear	1.28 / 26.8	23.4

This observed softening behavior of soil highlights the fact that the long-term shear strength of soil after numerous weathering cycles is governed by its friction angle. In a surficial layer of the slope, the soil shear strength is mainly contributed by cohesion and very little contribution is made by its friction angle due to low effective overburden pressure. The decrease in cohesion value of soil after weathering cycles could lower down its shear strength to a value smaller than shear stress and could ultimately result in a surficial slope failure. This observed reduction in strength of soil from laboratory test results are supporting evidence for the surficial slope failure problem occurred in the embankment slope of the U.S. 75 Frontage Road. The measured strength parameters are also used as an input parameter in rainfall-induced slope stability studies in this research work.

3.3 Surficial Slope Failure on Grapevine and Joe Pool Dams

3.3.1 General

Both Grapevine and Joe Pool dams are located close to Dallas, Texas and are operated by the United States Army Corps of Engineers (USACE) Fort Worth district. The salient features of these dams are presented in Table 3.3. Slope instability problem has been historically an issue for these dams and each of the dams has experienced a significant number of surficial slope failures (Figures 3.12a and 3.12b) (McCleskey 2005). Though these slope failures were not a critical threat to the integrity of the dam, it caused high maintenance costs for repairs.

Table 3.3 Details of Grapevine and Joe Pool dams (Source: USACE)

Item	**Grapevine Dam**	**Joe Pool Dam**
Location	Grapevine, Texas	Grand Prairie, Texas
Year of Construction Completion	June 1952	April 1986
Age of the Dam (years)	68	34
Length of Dam	3764.0 m (12349.0 ft)	6760.0 m (22178.5 ft)
Max. Height of Dam	39.0 m (127.9 ft)	33.1 m (108.5 ft)
Width of Crest	8.5 m (27.9 ft)	9.1 m (29.9 ft)
Crest Elevation	179.2 m (588.0 ft)	172.1 m (564.5 ft)
Slope of Dam	2.5H:1V	2.8H:1V

(a)

Figure 3.12 Typical slope failures occurred (a) Grapevine and (b) Joe Pool dam (Courtesy: USACE, Fort Worth District; Dronamraju 2008)

The construction of the Grapevine dam embankment was completed in 1952. The dam started to experience slope failures after 13 years in 1965 and the dam embankment has experienced more than 20 surficial failures. Some of the failures are tabulated in Table 3.4 (McCleskey 2005). Although detailed information about the failure depth for all the slope failures is not available, these failures generally occurred at a depth of between 0.6-1.8 m (2-6 ft).

Table 3.4 Observed surficial slope failures on the Grapevine dam slope (McCleskey 2005, Dronamraju 2008)

Date of Slide	**Slide Width × Length (m)**	**Height of Failure Scarp**
26 Feb 1965	30 x 12	N/A
05 Jun 1970	38 x 14	1.2 m (4 ft)

09 Feb 1973	24 x 5	0.9 m (3 ft)
23 Apr 1973	23 x 11	0.6 m (2 ft)
03 Apr 1974	60 x 21	N/A
10 Apr 1974	15 x 11	0.3 m (1 ft)
Jun 1976	18 x 21	1.8 m (6 ft)
Jun 1976	27 x 21	1.8 m (6 ft)
17 Jan 1977	45 x 20	N/A
07 Feb 1977	42 x 15	N/A
27 Oct 1981	16 x 21	N/A
10 Jan 1982	46 x 21	N/A
13 Mar 1989	30 x --	N/A
04 Nov 2004	45 x 23	0.6-1.2 m (2-4 ft)

N/A: Not available

The construction of Joe Pool Dam was completed in 1986 and the slope of the dam experienced failure after 2 years of its completion in 1988. In the past several decades, the dam slope has experienced numerous numbers of shallow failures. The repair cost of these failures was ranging, generally, between $10,000 for temporary repairs to over $100,000 for more thorough repairs (McCleskey 2005). In 2009 during a period of severe storms, a total of 10 slides were observed at the slope of the Joe Pool dam. The repair cost of the failures occurred in Joe Pool dam in 2009 was around $2 million 2009 (USACE). However, the dams experienced repeated slides in the same areas, which shows the ineffectiveness of the adopted rehabilitation method.

Previously, researchers at UTA have conducted comprehensive research to study more efficient and economical rehabilitation techniques to repair future

slides with the financial support from USACE, Fort Worth District (McCleskey 2005, Dronamraju 2008). Details of these studies are given in the next section.

3.3.2 Earlier Studies on Grapevine and Joe Pool Dams

3.3.2.1 Introduction

The literature review conducted by researchers indicated that the surficial failures were mainly attributed to desiccation cracks developed in the active zone of slopes due to weathering cycles. These cracks allow penetration of rainwater deeper into the slope and cause saturation of its surficial layer. These aforementioned phenomena emphasize the need for mitigation of desiccation cracks that will eventually reduce the soil suction decreases of the surficial layer. Hence, promises higher shear strength that is contributed by soil suction.

The comprehensive research studies conducted by McCleskey (2005) and Dronamraju (2008) investigated the efficacy of different stabilizers in several combinations and proportions in rehabilitation and prevention of surficial slope failures at Grapevine and Joe Pool dam. These techniques are aimed at the utilization of locally available soil and promise economic and safe solutions in long-term conditions. The details of the stabilizers used in these studies are given in the following section.

3.3.2.2 Stabilizers Used in the Studies

In their research study, McCleskey (2005) and Dronamraju (2007) used lime, polypropylene fiber, and bio solid compost in different combinations and

proportions to stabilize the failed slope. The chemical treatment of lime has been considered as one of the most effective and economic stabilization methods. Unlike lime, polypropylene fiber is used in soil stabilization as a reinforcement material as the randomly oriented fibers could increase the strength of the soil and boost its resistance towards swelling strains. Apart from lime and fibers, researchers also evaluated the efficacy of bio solid compost in stabilizing expansive soil. The additive of the bio solid compost has been chosen as it can absorb water from the surrounding environment and retain a significant amount of moisture content in soil and ultimately can reduce the development of desiccation cracking. The impacts of these stabilizers were thoroughly investigated with comprehensive laboratory and field studies and the obtained results are presented in the following section.

3.3.2.3 Results of Studies

3.2.2.3.1 Results of Laboratory Tests

A summary of the laboratory test results obtained by McCleskey (2005) is presented below. The stabilization studies were conducted using the control soil samples and index properties are tabulated in Table 3.5.

Table 3.5 Basic soil properties of Grapevine and Joe Pool dam soils

(McCleskey 2005)

Property	**Grapevine Dam**	**Joe Pool Dam**
% Passing No. 200 sieve	57.5	69.4
% Clay fraction	15.5	10.5
Liquid limit	30	58
Plastic limit	17	24
Plasticity index	12	34
USCS classification	CL	CH

In the studies several combinations and proportions of stabilizers used and their notations are tabulated in Table 3.6.

Table 3.6 Notation of various treated soils (McCleskey 2005)

Treatment Type	Notation	
	Grapevine Dam	**Joe Pool Dam**
Control soil	GV-CTRL	JP-CTRL
Soil with 0.15% polypropylene fibers	GV-F0.15	JP -F0.15
Soil with 0.30% polypropylene fibers	GV-F0.30	JP -F0.30
Soil with 0.40% polypropylene fibers	GV-F0.40	JP -F0.40
Soil with 4% hydrated lime	GV-L4	JP -L4
Soil with 8% hydrated lime	GV-L8	JP -L8
Soil with 0.15% polypropylene fibers and 4% lime	GV-F0.15-L4	JP -F0.15-L4
Soil with 0.15% polypropylene fibers and 8% lime	GV-F0.15-L8	JP -F0.15-L8
Soil with 0.30% polypropylene fibers and 4% lime	GV-F0.30-L4	JP -F0.30-L4
Soil with 0.30% polypropylene fibers and 8% lime	GV-F0.30-L8	JP -F0.30-L8
Soil with 20% bio solid compost	GV-020	JP -020

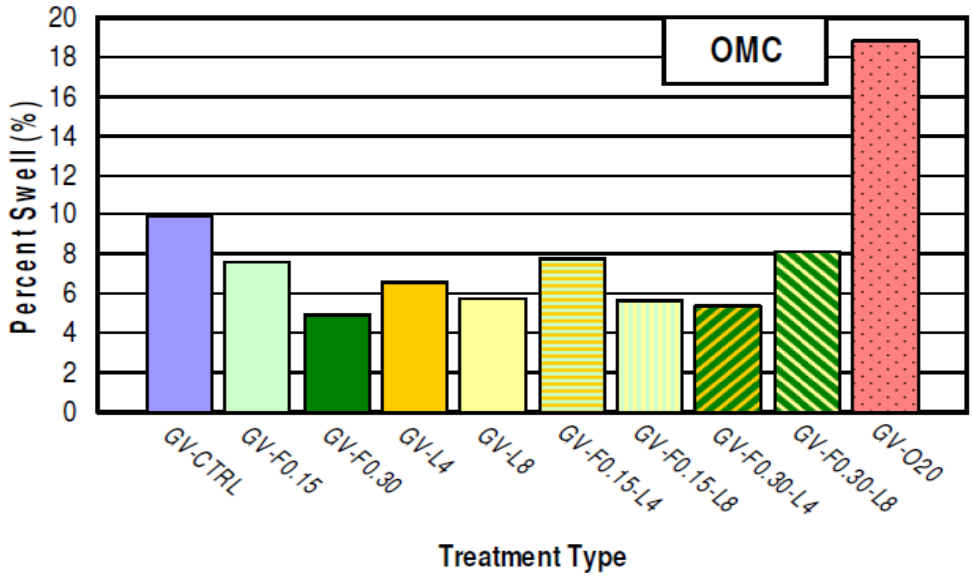

(a)

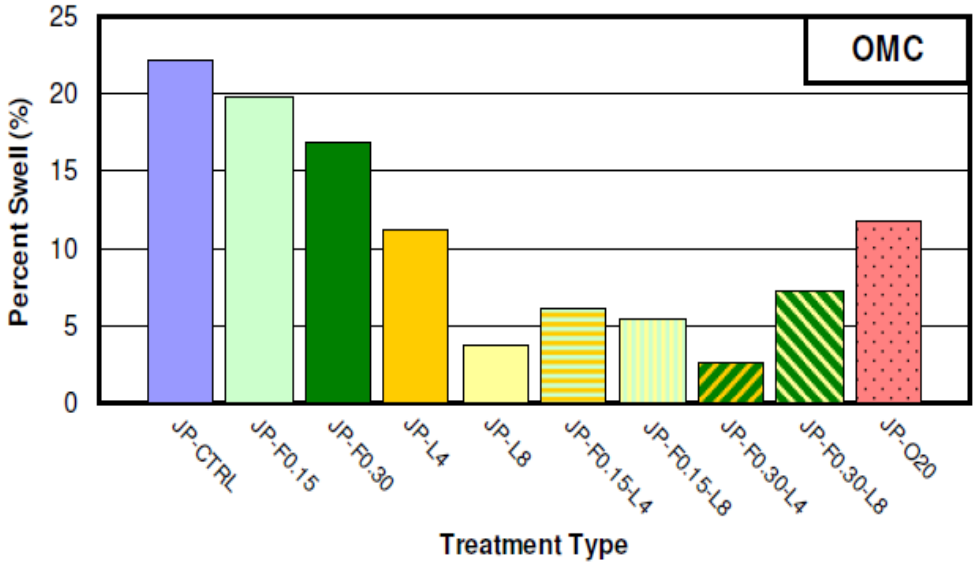

(b)

Figure 3.13 Swell strain test results: (a) Grapevine and (b) Joe Pool dam soils

(McCleskey 2005)

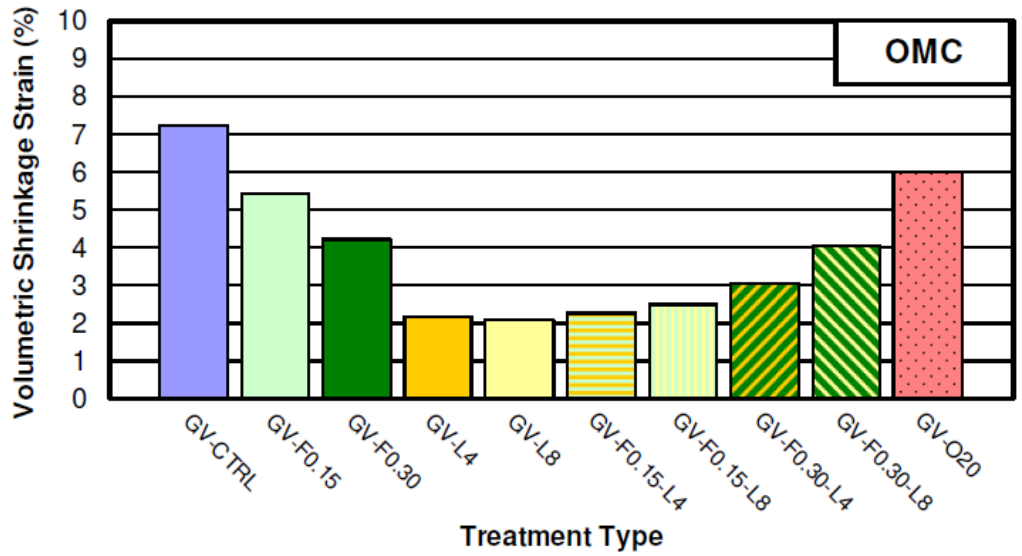

(a)

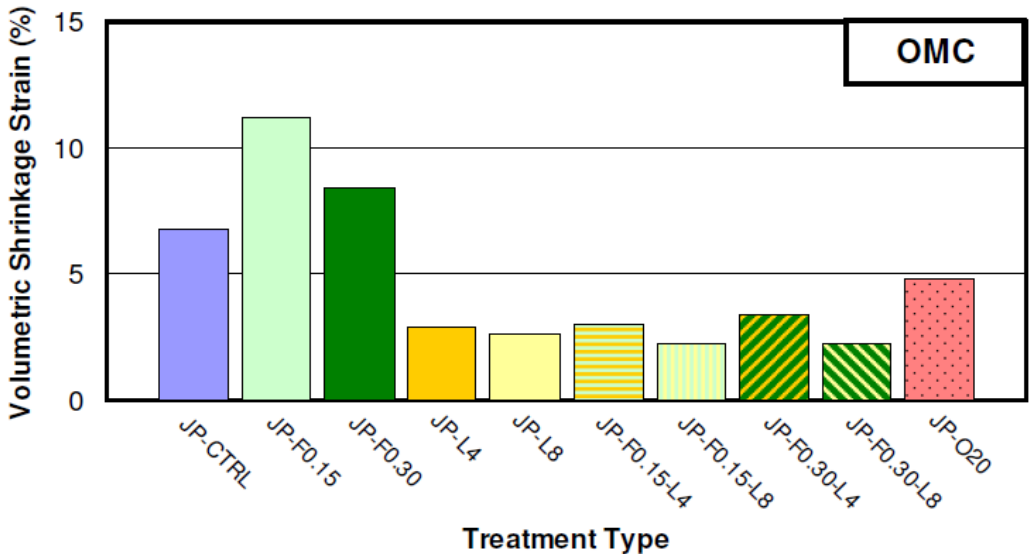

(b)

Figure 3.14 Volumetric shrinkage strain test results of (a) Grapevine and (b) Joe Pool dam soils (McCleskey 2005)

The short-term and long-term strength improvements due to soil stabilization were investigated by conducting the DS and TRS tests. Undrained DS tests were conducted to determine the peak strength parameters of soil which were not experienced any desiccation cracks whereas TRS tests were conducted to estimate soil residual shear strength parameter values (Dronamraju 2008). These obtained test results are tabulated in Table 3.7.

Table 3.7 Strength parameters of Grapevine and Joe Pool dam soils (Dronamraju 2008)

Treatment	**TRS Test**				**DS Test**	
	Grapevine Dam		**Joe Pool Dam**		**Joe Pool Dam**	
	Cohesion kPa (ksf)	Friction Angle (degrees)	Cohesion kPa (ksf)	Friction Angle (degrees)	Cohesion kPa (ksf)	Friction Angle (degrees)
Control	0 (0)	18	0 (0)	20	80 (1.67)	36
20% Compost	3.4 (0.07)	20	2.9 (0.06)	19	86 (1.80)	40
4% Lime with 0.30% Fibers	10.5 (0.22)	35	10.5 (0.22)	33	57 (1.20)	38
8% Lime with 0.15% Fibers	16.3 (0.34)	40	16.8 (0.35)	39	62 (1.30)	42
8% Lime	12.9 (0.27)	38	12.5 (0.26)	36	105 (2.20)	43

Based on the performance of the tested treatment types given above, the Grapevine and Joe Pool dam slopes were stabilized using the stabilization methods of soil+20% compost, soil + 4% lime + 0.3% fiber, soil + 8% lime + 0.15% fiber,

and soil + 8% lime. The field implementation studies were conducted by treating the top 46 cm (18 in) of dams' core soil after removing the top soil for vegetation cover with the-above mentioned additives. A total of 5 sections, four treated sections and one control section, were constructed on Grapevine and Joe Pool dams. Each of the sections was in dimensions of 18.3 m x 7.6 m (60 ft x 25 ft) as layout shown in Figure 3.15. The moisture content variation, lateral movements of newly built sections had been monitored with embedded sensors and inclinometers. The vertical movements were investigated with several total station surveys.

Figure 3.15 Layout of the treated test sections for Grapevine and Joe Pool dams

3.3.2.3.2 Results of Field Studies

The field performance investigation studies were conducted on Joe Pool dam slope by Dronamraju (2008) for over a period of one year. In each of stabilized and control test section, the moisture probes were installed at a depth of 25 cm (10 in.) (top probe) and 50 cm (20 in.) (bottom probe) from the top surface. The lateral displacements were monitored with a total of 10 vertical inclinometers installed (i.e., 2 inclinometers per section). Swelling and shrinkage strains of each section were monitored by conducting monthly elevation surveys with the help of total station. A summary of the field investigation results obtained by Dronamraju (2008) is presented below. Figures 3.16a and 3.16b represent the average annual moisture content measured by both top and bottom probes, respectively. Figure 3.17 shows the elevation survey results for each test section. Also, the summary of annual vertical inclinometer measurements is tabulated in Table 3.8.

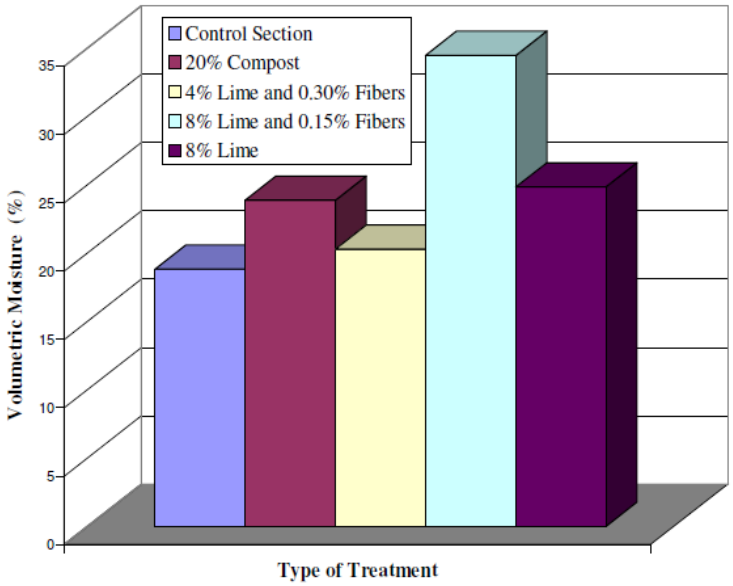

(a)

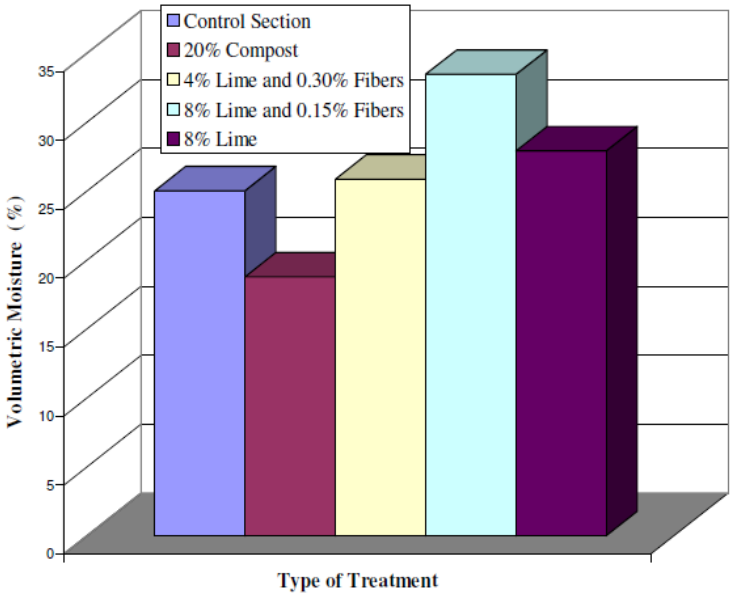

(b)

Figure 3.16 Average annual volumetric moisture content variation of (a) top probe and (b) bottom probe (Dronamraju 2008)

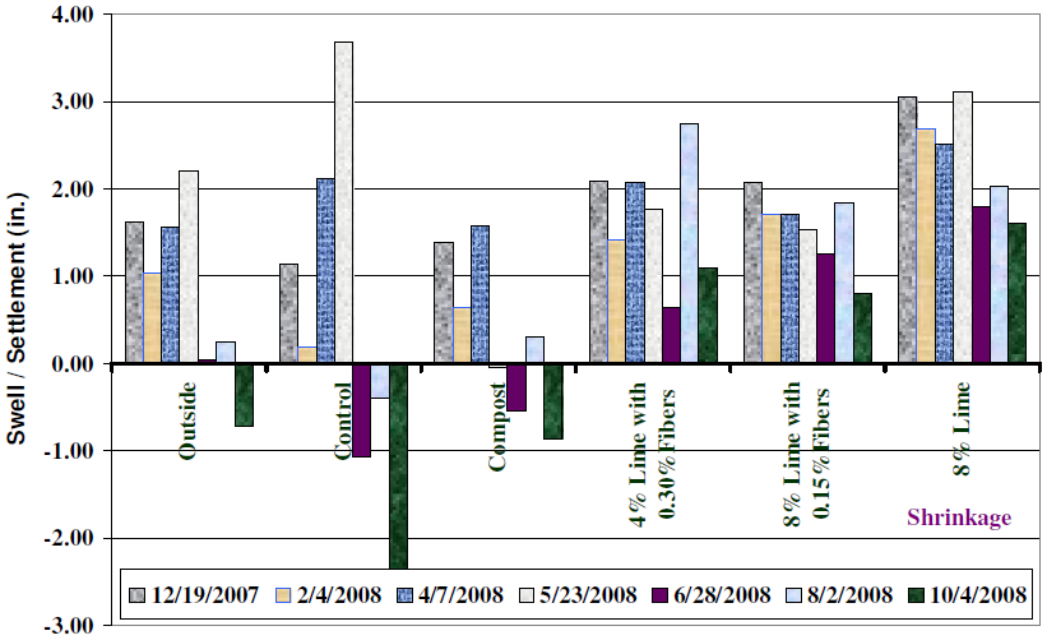

Figure 3.17 In-situ vertical displacement measurements (Dronamraju 2008)

Table 3.8 Summary of lateral displacement measurements (Dronamraju 2008)

Test Section	Inclinometer Name	Maximum Movement, mm (in.)	Movement After 1 Year, mm (in.)
Control	1	61 (0.24)	8 (0.03)
	2	147 (0.58)	97 (0.38)
20% Compost	3	53 (0.21)	3 (0.01)
	4	147 (0.58)	147 (0.58)
4% Lime with 0.30% Fibers	5	89 (0.35)	51 (0.20)
	6	132 (0.52)	135 (0.53)
8% Lime with 0.15% Fibers	7	51 (0.20)	36 (0.14)
	8	86 (0.34)	76 (0.30)
8% Lime	9	56 (0.22)	-15 (-0.06)
	10	66 (0.26)	51 (0.20)

*Negative value implies the inward movement

Analysis of results of these studies was made by researchers McCleskey (2005) and Dronamraju (2008) also several conclusions and recommendations were made based on the above given results. The following section is included these conclusions and recommendations.

3.3.2.4 The Conclusion Made by McCleskey (2005) and Dronamraju (2008)

The interpretations of results of the laboratory studies were made by McCleskey (2005) and Dronamraju (2008) whereas, the field implementation results were analyzed by Dronamraju (2008). McCleskey (2005) concluded that the swelling strains of clayey soils were reduced significantly by lime and lime with fiber treatment. The addition of fiber did not further reduce the swelling potential of soil significantly. Also, the compost bio solid treatment could not improve the swelling properties of soil impressively. The shrinkage strain test results showed that lime and lime with fiber treatment were quite effective to reduce shrinkage cracks. The presence of fiber additives generally improved soil shrinkage properties. The addition of lime to soil resulted in a significant improvement in soil strength. Reduction in the development of desiccation cracks in the soil can be achieved by reducing volumetric changes tendencies besides enhancing the soil shear resistance. Hence, lime (L8) and lime with fiber treatments (F0.15-L8 and F0.30-L4) were found the most effective treatment types to restrain swelling and shrinkage strains besides increasing soil strength.

The field investigations conducted by Dronamraju (2008) showed that lime, lime with fiber, and compost treatment methods cause the soil to hold higher moisture content than other methods. The total displacement caused by swelling and shrinkage strains was quite high (6.20 cm or 2.44 in.) in the section treated with compost bio solids as compared to the same in sections with lime and fiber treatment. Based on the site investigation studies, the section treated with 8% lime with 0.15% showed the best results (Dronamraju 2008). As the fiber construction method is relatively new and cumbersome, therefore, 8% lime treatment was considered as the best stabilization based on overall improvement in soil characteristics and easy constructability (USACE Forth Worth district). The recommended treatment method can be used at dam sections where desiccation cracks are formed. Using this method, the owners of this infrastructure could save millions of dollars in operation and maintenance costs by minimizing reoccurring stability issues (USACE).

3.4 Summary

This chapter provides the details of a failed slope selected for the purpose of the current research study. All basic laboratory tests were performed to characterize the soil collected from the site. Along with that, a series of 1D swell-shrinkage strain tests, direct shear, and torsional ring shear tests were performed to evaluate swell-shrinkage and softening behavior of this soil and to investigate the cause of surficial slope failure. The test results showed that high plastic clay

from the failed slope experienced severe volumetric changes and is highly susceptible to the development of desiccation cracks due to wet-dry cycles. The development of desiccation cracks led to a drastic decrease in the shear strength of soil particularly, the cohesion value. This significant decrease in soil strength parameters probably led to this surficial slope failure during an intense rainfall.

Additionally, the details of Grapevine and Joe Pool dam slope, which are built with clayey soil and have similar soil properties, are presented in this chapter. Likewise, the slope of US 75 Frontage Road, these dams also experienced surficial slope failure during heavy rainfall periods. Some of the earlier research work conducted by McCleskey (2005) and Dronamraju (2008), including laboratory and field investigation studies, is also included.

Chapter 4

SOIL MIX DESIGN STUDIES

4.1 Introduction

One of the main objectives of the present research study is to rehabilitate the failed section of the U.S. 75 Frontage Road with a lime stabilizer to mitigate volumetric swell and shrink related changes and thereby prevent the development of desiccation cracking in the surficial layer of the slope. As a part of this research work, a comprehensive laboratory testing program was designed and executed to assess the mechanical and hydraulic properties of the lime-stabilized soil. Also, the long-term performance of the lime-stabilized soil under wetting and drying cycles was evaluated to assess the permanency of the treatment. Based on the results of laboratory tests, an appropriate lime stabilization design was made for field implementation.

A series of chemical, engineering, and durability tests were conducted as per ASTM and TxDOT test standards. For lime stabilization related studies, the determination of the amount of the soluble sulfate ions in the soil is very important. The sulfate ions react with the calcium ions in the lime and form the ettringite mineral that ultimately results in significant heaving in soils (Kota et al. 1996, Puppala et al. 2014, 2018). Hence, prior to the determination of the properties of

lime-stabilized soil, the amount of soluble sulfate in the soil was measured using laboratory testing.

In a conventional lime treatment project, the dosage of lime is determined by conducting soil pH tests. The required dosage should be enough to induce a high pH environment (i.e., pH $\geq$ 12.4) for sustaining long-term pozzolanic reactions. However, the determined lime content based on the pH test does not provide any insights into the permanency of the lime stabilization. Therefore, in most cases, a higher lime dosage is required to satisfy the strength and durability criteria. In the present research work, although, the minimum required dosage of lime for the U.S. 75 Frontage Road slope soil was measured to be 5%, the soil mix design studies were conducted for both lime dosages of 5% and 8%. Several similar laboratory tests were performed on the untreated and lime treated soils to assess the benefits of lime stabilization in enhancing their properties. This chapter provides the details and results of the tests conducted in the testing program.

4.2 Chemical and Basic Soil Tests

4.2.1 Determination of Soluble Sulfate in Soil

The amount of soluble sulfate in the untreated soil was obtained by using the procedure outlined in the Tex-145-E test standard. This method indirectly measures the amount of soluble sulfate ions in the soil samples by determining the proportion of the light absorbance of cloudiness triggered by soluble sulfates in solutions. The collected soil samples were dried in an oven at 60 ± 5°C (140 ±

9°F) and pulverized. For this test, 20 g of dry soil passing US sieve number 40 was added to 400 mL of distilled water. The soil-water solution was shaken vigorously for at least a minute to solubilize the sulfate salts. After keeping the solution at room temperature for 12 hours, it was thoroughly mixed and passed through a fine porosity filter paper. In a glass vial, a barium chloride tablet was added and dissolved in 10 ml of the filtrate solution. The amount of sulfate ion in the solution was then measured with a colorimeter (Figure 4.1).

Figure 4.1 Colorimeter used in this study

The obtained value of sulfate was adjusted based upon the dilution ratio of the solution used in the test. The soluble sulfate determination test was conducted three times and the average soluble sulfate content in the control soil was found to be 480 parts per million (ppm). As per the guidelines of the National Lime

Association (2000), the obtained sulfate amount in the soil has a negligible risk of ettringite-induced heaving after lime stabilization (Table 4.1).

Table 4.1 Guidelines for use of lime in sulfate-bearing soils (National Lime Association 2000)

Risk Level	Soluble Sulfate Level
Low risk	Below 3000 ppm
Moderate risk	Between 3000-5000 ppm
Moderate to high risk	Between 5000-8000 ppm
High to unacceptable risk	Above 8000 ppm

4.2.2 Soil pH Test

The initial required lime content was obtained as per the procedure described in Tex-121-E. The soil, passing through sieve No. 40, was mixed with distilled water and the mixture was heated up to 45 - 60° C (112 - 140° F). A total of 210 g of dry soil was placed equally in 7 high-density polyethylene bottles and mixed with different dosages of lime (0%, 2%, 4%, 5%, 6%, 8%, and 10%). 150 ml of hot distilled water was added to each of the soil-lime mixtures and stirred vigorously (Figure 4.2a). To disperse the soil well, the samples were stirred every 15 minutes for a total of an hour test. The pH values of supernatants were determined by a pH meter apparatus. Figure 4.2b shows the plotted graph of pH versus the percentage of lime of mixtures with respect to the dry weight of soil.

The pH of 12.4 was achieved at 5% or more percentage of lime additives. Therefore 5% lime is considered as the minimum required amount of lime needed

for the soil mix design studies. However, Tex-121-E method is based on Eades and Grims' test method which relies on the pH of the soil-lime mixture, and this method does not provide any insights into the quantitative enhancement in soil properties or durability.

The laboratory mixture design studies need to provide a significant improvement in engineering and materials properties of soil to mitigate cracking and other distresses associated with soil behavior. In some projects, depending upon the soil mineralogy, soil composition, and organic material content, an extra amount of lime beyond this minimum dosage of lime is required. Hence, the laboratory soil design studies were conducted using the minimum lime content of 5% and 8% (3% extra lime beyond the minimum required dosage of 5%).

(a)

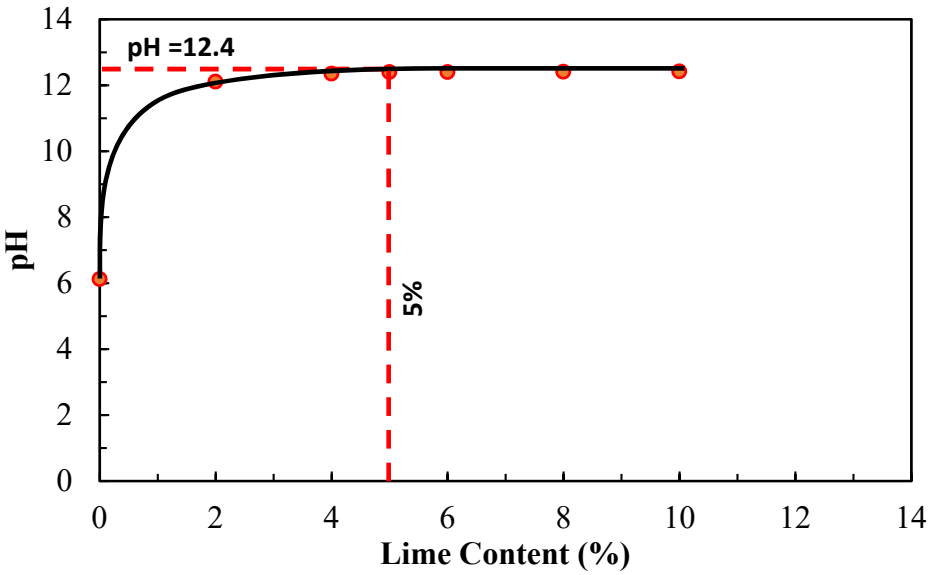

(b)

Figure 4.2 (a) pH test setup and (b) results

4.2.3 Compaction Test Studies

The moisture-density relationships for lime-treated soils were determined by following the Tex-113-E test standard. The main difference between the standard compaction Proctor test and the Tex-113-E compaction test method is the compaction energy. In the standard Proctor test, the compaction effort is soil 600 kN-m/m^3 (12,400 ft-lbf/ft,^{3}) whereas, in Tex-113-E method, the compaction effort is 1,100 kN-m/m^3 (22,913 ft-lbf/ft^3). All compaction tests on treated soils were conducted after one day of mellowing period. Upon mixing lime with soil, the sulfate ions in soil react with calcium ions in the lime stabilizer and reactive alumina available from clay minerals in the elevated pH environment to form

ettringite minerals, which are known to cause soil heaving (Kota et al. 1996, Puppala et al. 2014, 2018). One day mellowing period is allocated before compaction of the soil to allow the formation of ettringite minerals. After the mellowing period, the ettringite minerals are broken during the remixing process of the soil, and the further formation of ettringite minerals after compaction is prevented (Harris et al. 2004, Puppala et al. 2019). The compaction test results of treated soils along with the result of the untreated soil, which was previously presented in Chapter 3, are shown in Figure 4.3.

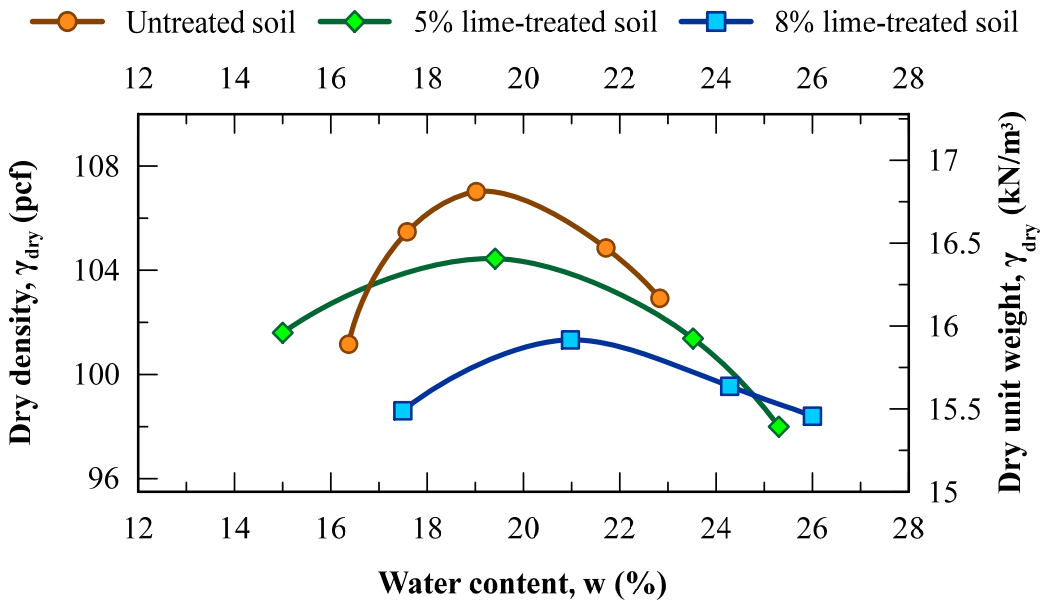

Figure 4.3 Moisture-dry density compaction curves for untreated, 5% and 8% lime-treated soils

Results show that the addition of lime decreased the density of soil and increased its water content. The MDD of soil dropped down from 16.8 kN/m^3

(107.0 pcf) to 16.4 kN/m^3 (104.4 pcf) and 15.9 kN/m^3 (101.3 pcf) after adding 5% and 8% lime respectively. Also, the OMC of soil increased from 19.0% to 19.5% and 21.0% for 5% and 8% lime-treated soils, respectively. A similar trend in the moisture – density relationship of lime-treated soil has been observed by numerous researchers (Remus and Davidson 1961, Bell 1996, McCleskey 2005, Bhaskar 2020). This phenomenon can be attributed to the formation of the flocculated soil structure due to initial soil-lime reactions. The addition of lime in the soil causes a reduction in the thickness of the water layer around the clay particles and increases sliding resistance between them. This additional water acts as a lubricant between particles and facilitates to overcome this resistance.

Engineering tests including soil strength, permeability, SWRC, durability, and strength retention after exposure to wet-dry cycles were conducted on both untreated and treated compacted specimens. In all the studies, untreated specimens were statically compacted at their OMC and 95% of respective MDD. The lime-treated soil specimens were prepared after one day of mellowing period on the wet side of the OMC (OMC+2%) and the respective MDD. The details of the procedures of the engineering tests are given in the following section.

4.3 Engineering Tests

4.3.1 Shear Strength Tests

The shear strength parameters of soil are the key parameters in analyzing the safety of slopes against shear stresses. In Chapter 3, the peak strength and FSS

parameters of the untreated soil determined by DS and TRS tests were presented. A significant decrease in strength properties, particularly in cohesion, was observed in post-wetting-drying cycles. Similar sets of DS and TRS were conducted on lime-treated soil specimens to investigate the effect of lime on the strength properties of soil (Figure 4.4). These tests were conducted on both the 5% and 8% lime-treated soil samples by following the procedure discussed in Section 3.2.2.3.3 and Section 3.2.2.3.4.

As the 'increase in strength' due to the formation of CSH and CAH cementitious products is typically achieved after longer curing periods, it is important to assess the short curing periods for lime-treated soil. Therefore, in this research study, short curing periods were focused. The DS and TRS tests were conducted after three and seven days of curing periods. The treated soil specimens were cured at room temperature for three and seven days in air-tight bags (no moisture loss) at almost 100% relative humidity. These test results were used as input parameters in numerical analyses studies that details of them are provided in Chapter 5.

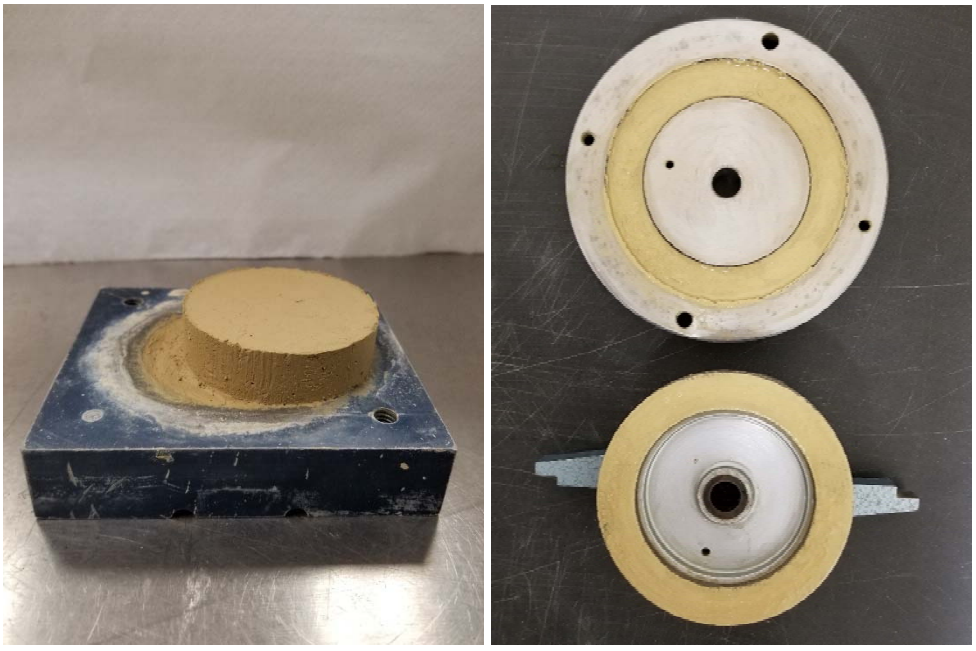

(a) (b)

Figure 4.4 Sheared soil specimens of (a) DS test and (b) TRS test

4.3.2 Soil Permeability Test

The saturated hydraulic conductivity values of newly compacted untreated and treated soils were measured with the modified triaxial equipment by following the procedure provided by Bhaskar et al. (2019). The permeability tests were conducted on compacted soil specimens of 38.1mm (1.5 in.) height and 71.1mm (2.8 in.) diameter. Before the test, the soil specimens were subjected to capillary soaking in a split mold. The main purpose of capillary soaking is to remove air bubbles from the specimen and expedite the backpressure saturation process. The specimens were then weighed and carefully mounted on the base pedestal of the equipment along with porous stones at the top and bottom. To prevent clogging of

porous stones by fine soil, filter papers were placed between porous stone and soil specimens. After covering the specimens with a latex membrane, the equipment was assembled, and the cell was filled with de-aired water (Figure 4.5). A seating load of 10 kPa (0.15 psi) was applied at the top to ensure proper contact between the soil specimens and top cap.

The specimens were saturated using back-water pressure and the degree of saturation was continuously monitored using Skempton's '*B'* parameter. In this research, the specimens were considered as saturated at *B* value of 0.95. Once the specimens were saturated, the permeability tests were commenced by applying a hydraulic gradient across the specimens. A head difference resulting in a hydraulic gradient of 35 was applied and sustained across the specimens throughout the test. Both inflow and outflow rates of water were continuously measured using volume change measurement devices. The tests were performed until the flow became steady and the rate of inflow and outflow became almost the same. After achieving a steady-state flow condition, the coefficients of permeability were calculated using Darcy's law.

Figure 4.5 The modified triaxial apparatus used for permeability test

The permeability test results showed that the untreated clayey soil has a low permeability value of 3.02×10^{-10} m/s (9.90×10^{-10} ft/s). After lime treatment, the permeability of soil was found to increase significantly. The saturated permeability of 5% and 8% lime-treated specimens were 3.94×10^{-9} m/s (1.29×10^{-8} ft/s) and 1.50×10^{-8} m/s (5.00×10^{-8} ft/s) respectively. The increase in permeability of lime-treated soil is mainly because of changes in the void pattern due to flocculation and agglomeration after chemical reactions. However, over time, the interconnected pores are partially filled with pozzolanic products and the permeability of soil might drop down gradually. As the specimens were tested after

seven days of the curing period, this phenomenon was not observed in the present case.

As discussed earlier in Chapter 2, several studies have reported a significant increase in untreated clayey soil permeability value of newly compacted samples (up to 10^4 times) after the weathering cycles (Daniel 1984, Albrecht and Benson 2001, Hughes et al. 2009). In the present research work, the long-term permeability value of untreated soil subjected to the weathering cycles was approximated as per the existing literature. Therefore, the permeability value of untreated soil of U.S. 75 frontage road slope that subjected to the weathering cycle was assumed 10^4 times higher than the permeability value of soil in a newly compacted condition. Also, the permeability value of lime-treated soil exposed to wet-dry cycles was assumed 15 times higher than the permeability value of soil in a newly compacted condition. These coefficients of permeability of untreated and treated soils were later used as input parameters in numerical analysis studies in Chapter 5.

4.3.3 Soil Water Retention Curve test

4.3.3.1 General

During a rainfall event, the change in soil suction primarily depends on the unsaturated hydraulic conductivity of the soil. In this study, the saturated permeability value and SWRC of soil were together used to estimate unsaturated soil hydraulic conductivity rate. The drying path of SWRC of untreated, seven

days cured 5% lime-treated, and 8% lime-treated soils were determined using both the Tempe cell and Dew point potentiometer apparatus. The details of the testing procedure are given following.

4.3.3.2 Tempe Cell Apparatus

Fredlund's Tempe cell apparatus uses the axis translation technique proposed by Hilf (1956). The soil specimen, 25.4 mm (1.0 in.) in height and 63.5 mm (2.5 in.) in diameter, was statically compacted at its OMC and 95% of the respective MDD. To ensure uniform moisture distributions in the specimen, it was kept in a humidity-controlled room with 100% relative humidity for two days. For saturation, the specimen was confined in a stainless-steel split mold and was submerged in led water. Simultaneously, a 500 kPa high air entry value (HAE) ceramic disk was saturated inside the Tempe cell at a pressure of 150 kPa. After ensuring there is no weight increase in the soil specimen due to saturation, the specimen was placed on the saturated HAE ceramic disk (Figure 4.6a).

The water content and suction relationship of the specimen was determined by applying air pressure on the specimen in the Tempe cell apparatus (Figure 4.6b). For each suction level, the constant air pressure was applied and sustained until no additional water was expelled from the specimen. At the equilibrium condition, the total amount of water drained out from the specimen was measured and the water content of the specimen was calculated. The Tempe cell was flushed every 12 hours to remove accumulated air beneath the ceramic disk during the test.

The SWRC test was conducted in the Tempe cell at different values of matric suction up to 500 kPa. For higher suction levels (>500 kPa), the SWRC of soil was determined using a Dew point potentiometer apparatus.

(a) (b)

Figure 4.6 (a) Tempe cell apparatus and (b) specimen placed top of HAE value ceramic disc

4.3.3.3 Dew Point Potentiometer Apparatus

After conducting tests in the Tempe cell apparatus, the soil from the same specimen was used in Dew Point Potentiometer WP4 apparatus to obtain SWRC at high suction values (Figure 4.7). The principle of the Dew point potentiometer apparatus is based on the chilled-mirror technique and its details are given in

ASTM D6836. In this test program, the specimen that is 25.4 mm (1.0 in.) in height and 63.5 mm (2.5 in.) in diameter, was cut into a smaller size and placed in the closed container of Dew Point Potentiometer. After placing approximately 7 cm^3 of specimens in the container, the relative humidity of inside air was determined by using the optical and temperature sensors, and a mirror. The value of total suction value was determined from the measured water vapor pressure above the soil sample in the apparatus. When the equilibrium stage was obtained, the displayed suction level was recorded. The specimen was then transferred to the oven and the water content of the specimens was determined.

Figure 4.7 WP4 apparatus used in this study

The experimentally obtained SWRC data from both Tempe cell and WP4 apparatus were plotted together and best fitted with Fredlund and Xing (1994) function. The fitting parameters of Fredlund and Xing (1994) equation were then

used with the saturated permeability value of soils and unsaturated hydraulic conductivity functions were determined as per Krahn (2004).

4.4 Durability and Strength Retention Studies

Each year, in semi-arid regions such as Texas, the soil in the slopes is subjected to a significant number of weathering variables particularly, wetting and drying cycles. Exposure to harsh environmental conditions could lead to irreversible changes in soil volume and can cause desiccation cracks in the soil. Therefore, it is important to incorporate the effects of wet-dry cycles in soil mix design studies to assess the permanency of treatment. The effect of recurring wetting and drying cycles on soil properties can be investigated with the laboratory durability test. This test provides insights into the impact of climatic variation on the long-term performance of soil. In the current study, the durability studies were conducted on untreated, 5%, and 8% lime-treated soil specimens as per ASTM D-559. The improvement in soil permanency against wet-dry cycles was assessed and the results were compared with the same of untreated soil.

In order to investigate the effects of curing time, durability tests were conducted on lime-treated specimens after 3, 7, and 28 days of curing periods. The soil specimens that were 116.3 mm (4.6 in.) in height and 101.6 mm (4.0 in.) in diameter were statically compacted in 3 layers. Just after the compaction, the lime-treated specimens were placed in air-tight bags and allowed to cure at room temperature and 100% relative humidity.

In the laboratory durability test, each weathering cycle consists of 5 hours of wetting followed by 42 hours of drying. Wetting is performed by fully submerging the soil specimen in the water at room temperature (Figure 4.8a) and drying is done by placing specimens in an oven at 71 ± 3°C (Figure 4.8b). The diameter and height of the specimen were measured, and volumetric strains were calculated after each wet and dry cycle. The test was performed for 14 cycles or until the specimen experienced failure.

Also, the strength retention characteristic of samples after 5% and 8% lime treatments were determined by performing the UCS tests after pre-decided cycles (0, 3, 7, and 14 cycles). The UCS tests were conducted following the procedure outlined in ASTM D2166 at the constant strain rate of 1mm/min ($3.9x10^{-2}$ in/min). Both durability and strength retention test results were studied and an optimum dosage of lime in mix design studies was determined based on both improvements in soil properties and the permanency of the treatment.

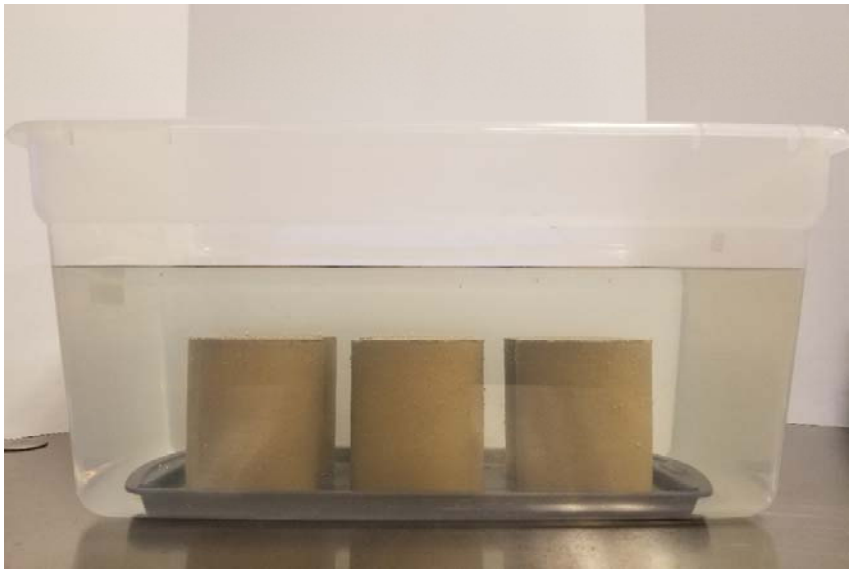

(a)

(b)

Figure 4.8 (a) Wetting and (b) drying process of durability and strength retention studies

4.5 Soil Mix Design Studies Results

4.5.1 Introduction

The effectiveness of lime treatment on the U.S. 75 Frontage Road slope was investigated by conducting an array of engineering characterization tests by following the different test methodologies detailed in the above sections. Several sets of DS, FSS, permeability, SWRC, durability, and strength retention tests after exposing wet-dry cycles were performed considering the combined effect of altering wet-dry cycles and climatic factors in hydro-mechanical properties and permanency of the treated soil. These studies were performed on untreated, 5%, and 8% lime-treated soils. In this section, the results of the stabilization studies are presented for assessing the effectiveness of lime treatment as a viable option to rehabilitate the shallow slope failures that occurred on highway embankment slopes.

4.5.2 Shear Strength Parameters

The peak and FSS shear strength parameters obtained from DS and TRS tests are presented and compared in this section. Test results showed that there were significant losses in the soil strength parameters for the untreated and lime-treated soils due to the effect of weathering cycles. These strength reductions were observed more drastically in the cohesion values. Also, the maximum strength degradation was observed in the case of untreated soil. While the lime-treated soils

maintained a considerable amount of cohesion value (5.2 to 6.6 kPa) after the wet-dry cycles, the cohesion value of untreated soil decreased to almost zero value. The cohesion loss in the soil is very critical at the shallow depths of slopes for surficial slope failures where there is a low amount of effective normal overburden pressure. During a rainfall event, the mobilized shear strength, mainly contributed by the soil friction angle, might not be sufficient to resist the shear stresses, which are increased due to saturation of soil mass and this ultimately causes a surficial slope failure.

Figures 4.9a and 4.9b show the peak strength parameters of untreated, 5% lime-treated, and 8% lime-treated soils obtained from DS tests. The consolidated drained DS test results revealed that the soil peak shear strength parameters experienced an enormous increase after both 5% and 8% lime treatment. After three days of the curing period, the friction angle of soil increased significantly from 23.7^{o} (untreated soil) to 40.7^{o} and 39.1^{o} for 5% and 8% of lime treatment, respectively. As these tests were conducted after a short period of curing time (three and seven days), these soil strength properties' improvements, particularly in soil friction angle, are mainly contributed by short-term soil reactions and flocculation of clay particles. Also, for the same curing period, the cohesion value increased from 13.2 to 37.4 and 29.0 kPa for 5% and 8% of lime-treated soils, respectively. In the case of specimens with seven days of the curing period, similar values of friction angle values were obtained while the soil cohesion values

underwent a significant increase. The different amount of pozzolanic reactions that occurred in three and seven days curing periods are attributed to these differences in the cohesion value.

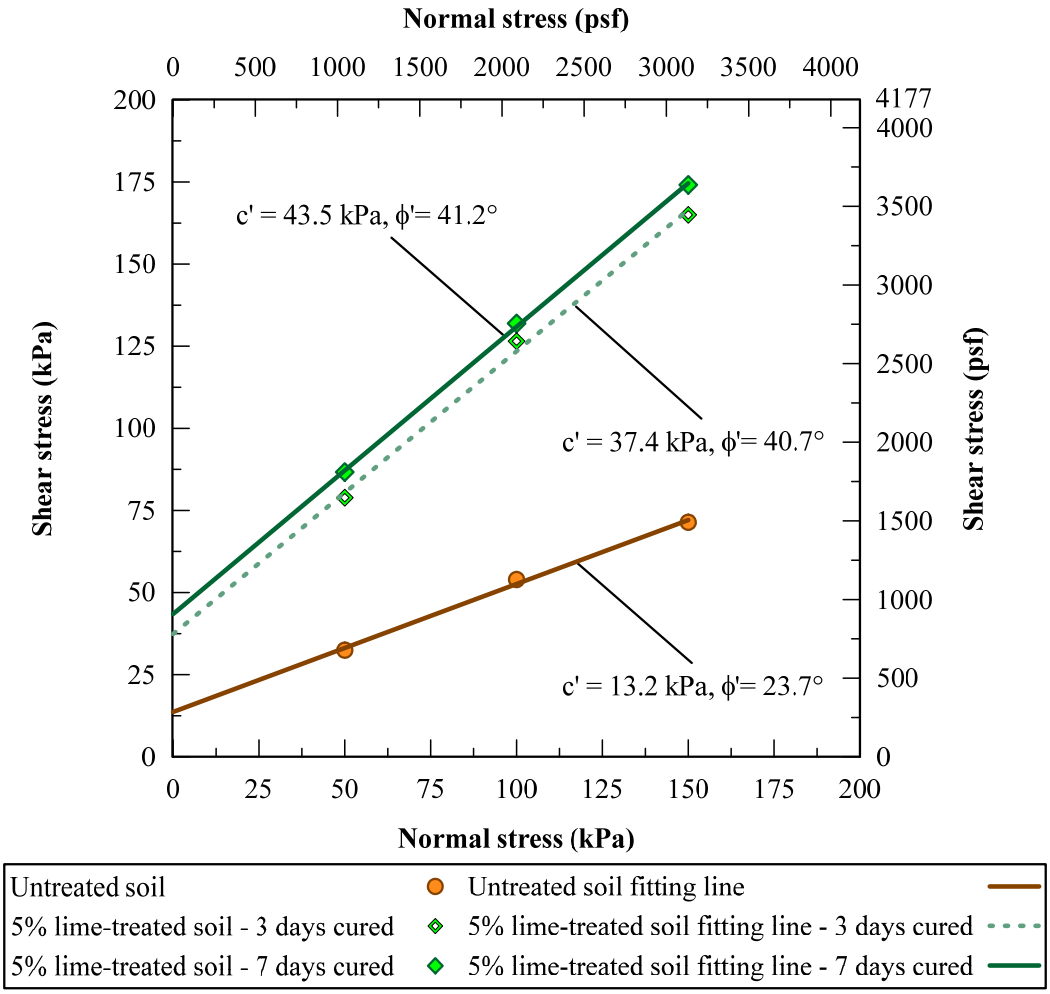

(a)

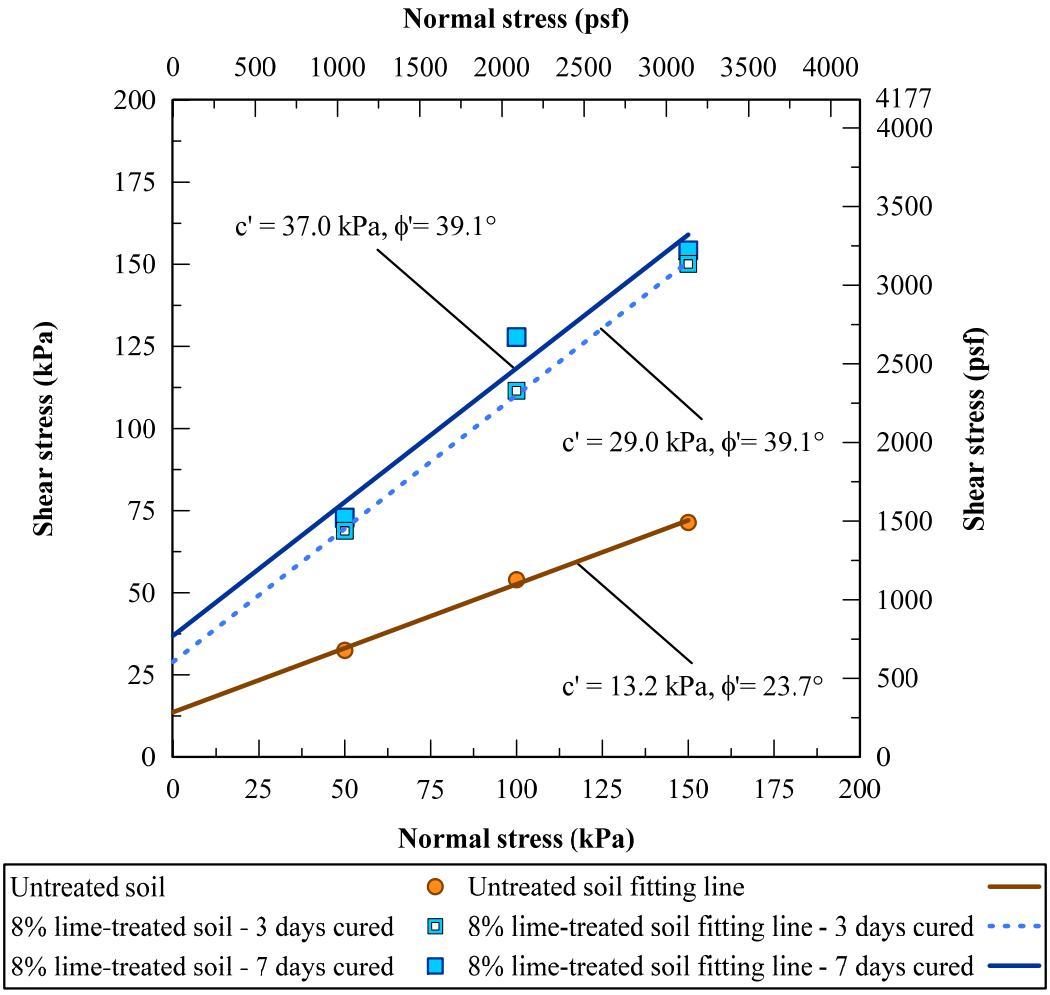

(b)

Figure 4.9 Mohr-Coulomb failure envelopes determined from DS tests for (a) 5% lime-treated soil and (b) 8% lime-treated soil along with the untreated soil

The FSS test results obtained from the TRS test are presented in Figures 4.10a and 4.10b. The results suggest that the weathering cycles degrade the untreated soil strength parameters. Although some of the benefits of lime treatment were negated, there were still considerable high amounts of soil friction angle and

cohesion. In the case of specimens cured for three days, the friction angle of untreated soil obtained from the TRS test was found to increase from 23.4^{o} to 31.0^{o} and 30.5^{o} for 5% and 8% of lime-treated soils respectively. Also, for the same curing period, cohesion intercepts of 1.3 kPa, 5.2 kPa, and 6.6 kPa were obtained for untreated, 5% lime-treated, and 8% lime-treated soils, respectively. For the seven days cured specimens, the measured FSS parameters were found almost equal to the same of three days cured specimens. In FSS conditions, most of the inter-particle cementitious bonding developed during the curing period is damaged and the soil strength improvement is contributed by short-term soil modification and residual cementitious bonding between particles. The obtained results suggested that, even after exposure to weathering cycles, there is a considerable amount of soil friction angle and cohesion in lime-treated soil which can prevent the slope from surficial failures in long term.

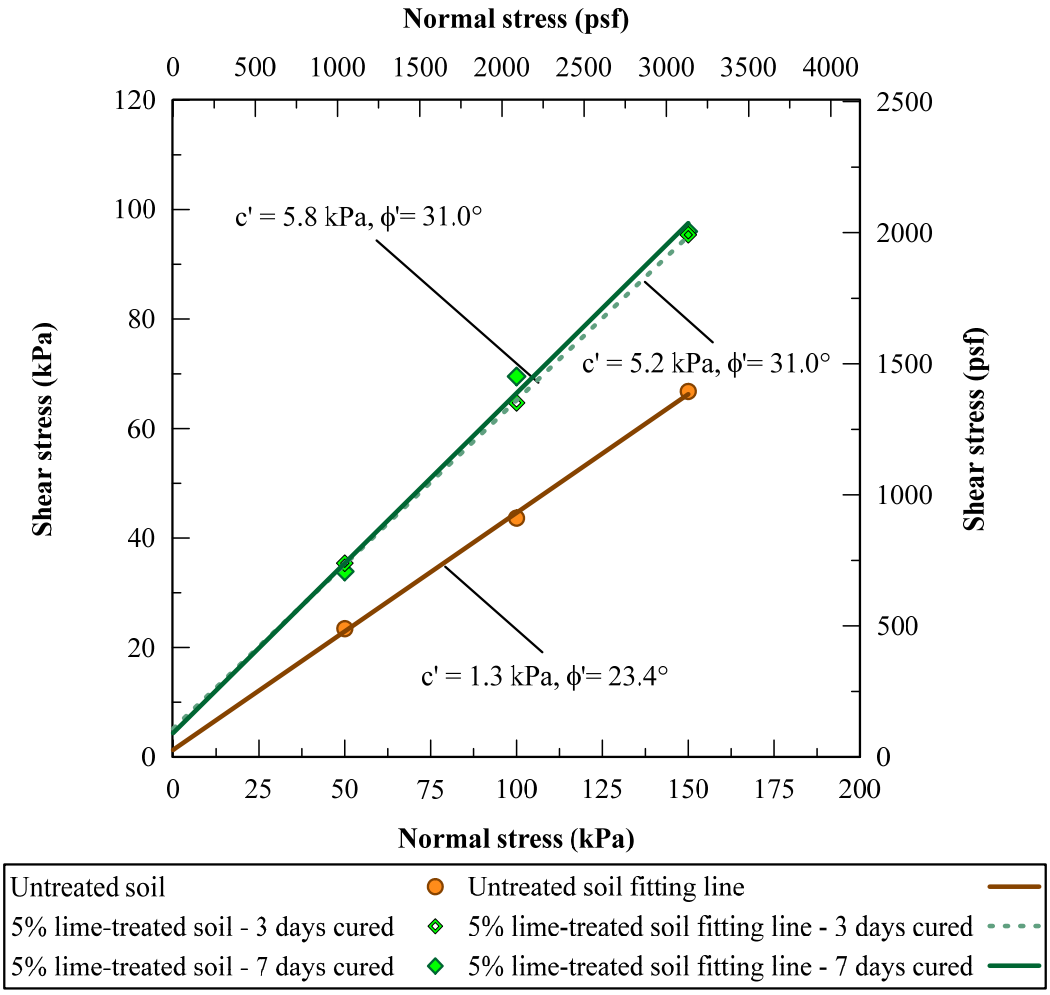
Normal stress (psf)
0
500
1000
1500
2000
2500
3000
3500
4000
120
100
80
60
40
20
0
2500
2000
1500
1000
500
0
Shear stress (kPa)
Shear stress (psf)
c' = 5.8 kPa, ϕ'= 31.0°
c' = 5.2 kPa, ϕ'= 31.0°
c' = 1.3 kPa, ϕ'= 23.4°
0
25
50
75
100
125
150
175
200
Normal stress (kPa)
Untreated soil
Untreated soil fitting line
5% lime-treated soil - 3 days cured
5% lime-treated soil fitting line - 3 days cured
5% lime-treated soil - 7 days cured
5% lime-treated soil fitting line - 7 days cured

(a)

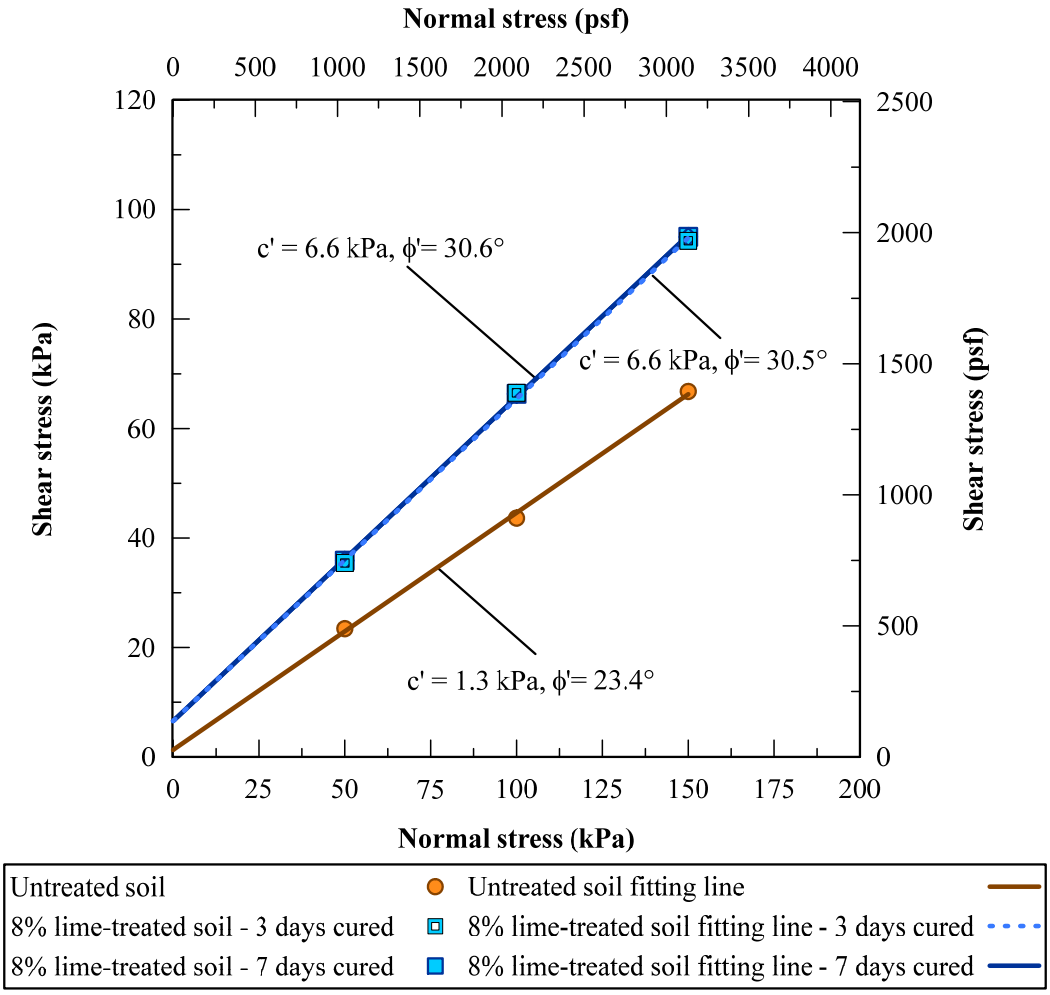

(b)

Figure 4.10 Mohr-Coulomb failure envelopes determined from TRS tests for (a) 5% lime-treated soil and (b) 8% lime-treated soil along with the untreated soil

For a better comparison between parameters of untreated and treated soils, the results of shear strength tests are graphically presented in Figure 4.11 a and Figure 4.11b. There was a significant improvement in peak shear strength value of newly compacted soil samples obtained by conducting DS test and FSS strength

parameters obtained by conducting TRS test on samples which were normally consolidated from slurry for both dosages. These observations showed that 5% lime-treated soil outperformed 8% lime-treated soil which is probably due to lower OMC and higher MDD used for 5% lime-treated soil specimens. Additionally, the higher amount of unreacted lime in 8% lime-treated soil specimens, might have resulted in lower shear strength parameters as the lime additive soil has lower cohesion and friction angle.

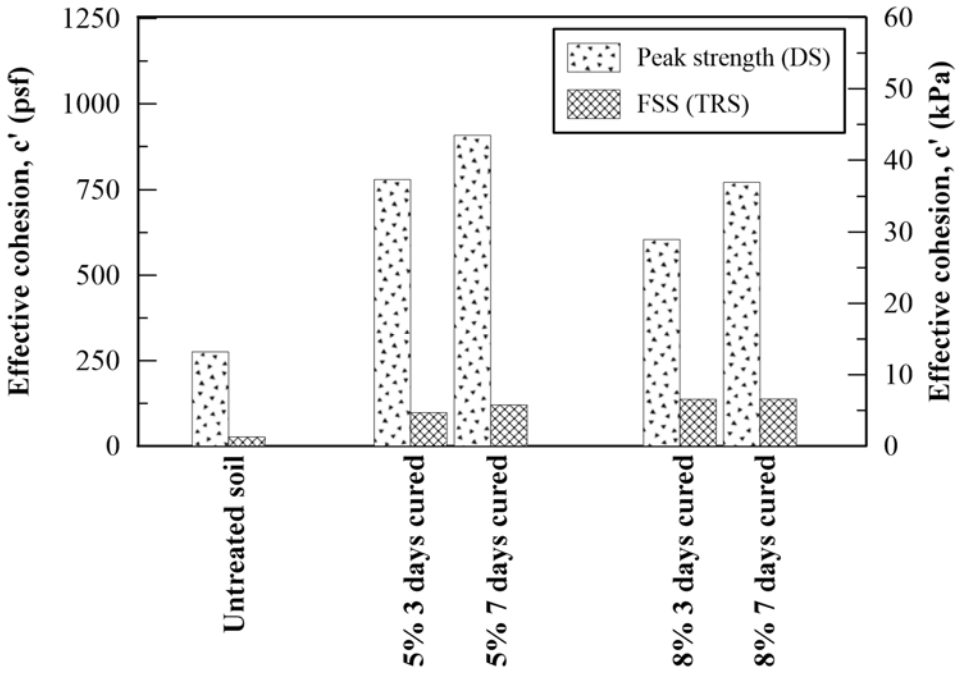

(a)

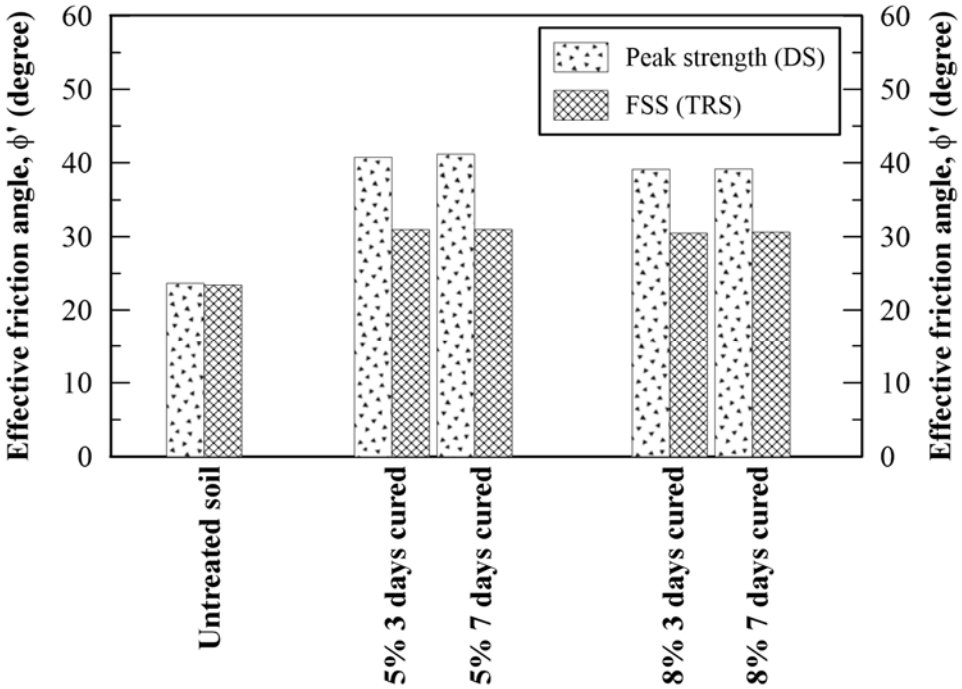

(b)

Figure 4.11 Summary of (a) effective friction angle and (b) effective cohesion values from DS and TRS tests

4.5.3 Soil Water Retention Curve Test Results

This section presents the results of SWRC studies and unsaturated soil properties determined from analysis of SWRC results. The experimental SWRC data, measured in the laboratory, was plotted and best fitted with Fredlund and Xing (1994) function. Figures 4.12a, b, and c present the SWRC test results of untreated, 5% lime-treated, and 8% lime-treated soils, respectively.

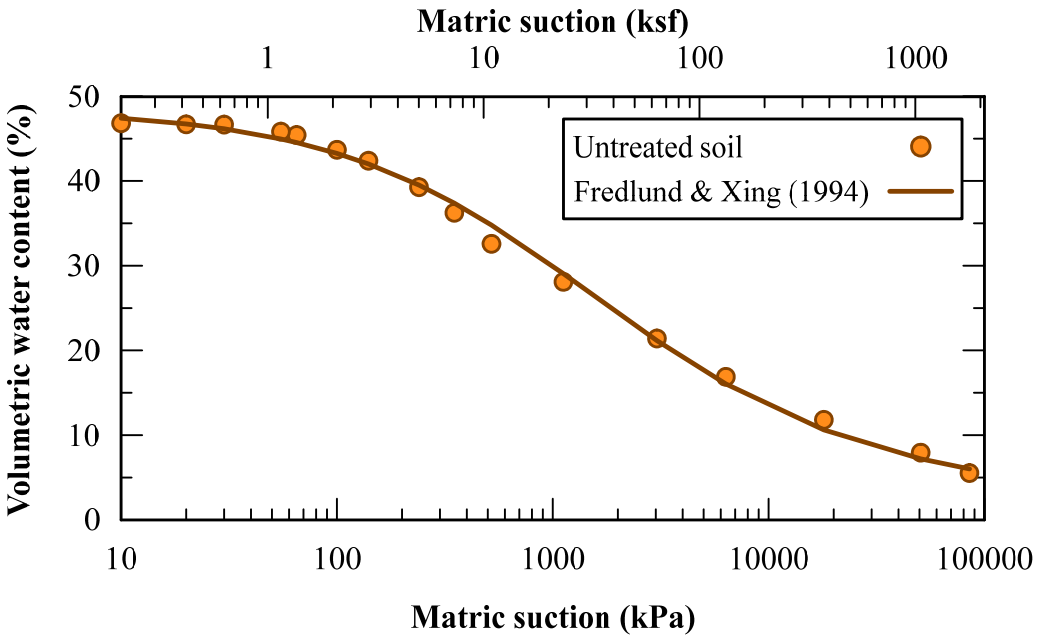
Matric suction (ksf)
1
10
100
1000
Volumetric water content (%)
50
40
30
20
10
0
Untreated soil
Fredlund & Xing (1994)
10
100
1000
10000
100000
Matric suction (kPa)

(a)

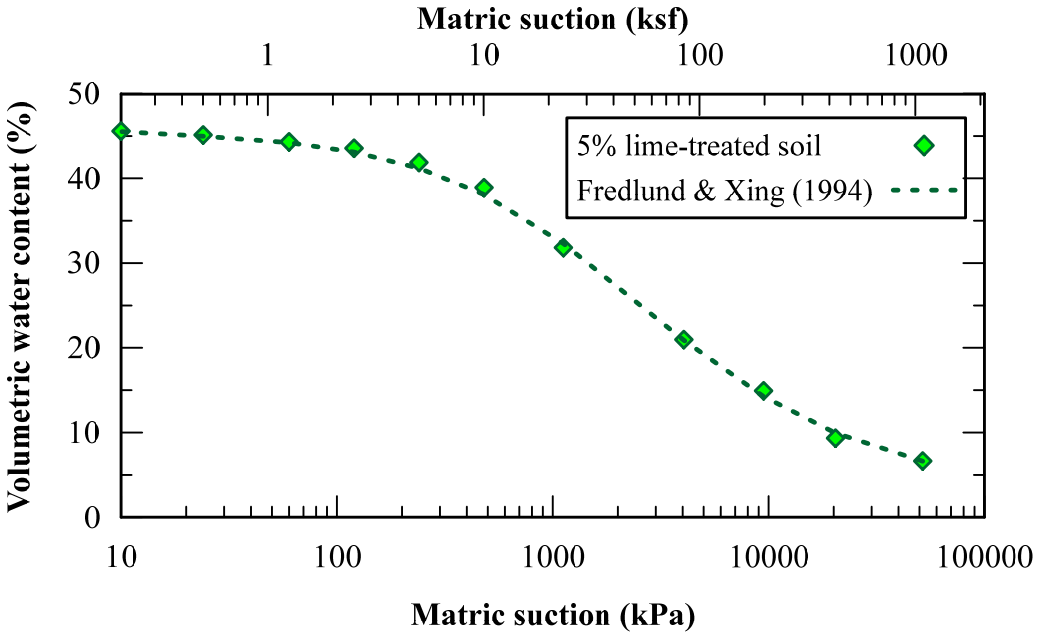
Matric suction (ksf)
1
10
100
1000
Volumetric water content (%)
50
40
30
20
10
0
5% lime-treated soil
Fredlund & Xing (1994)
10
100
1000
10000
100000
Matric suction (kPa)

(b)

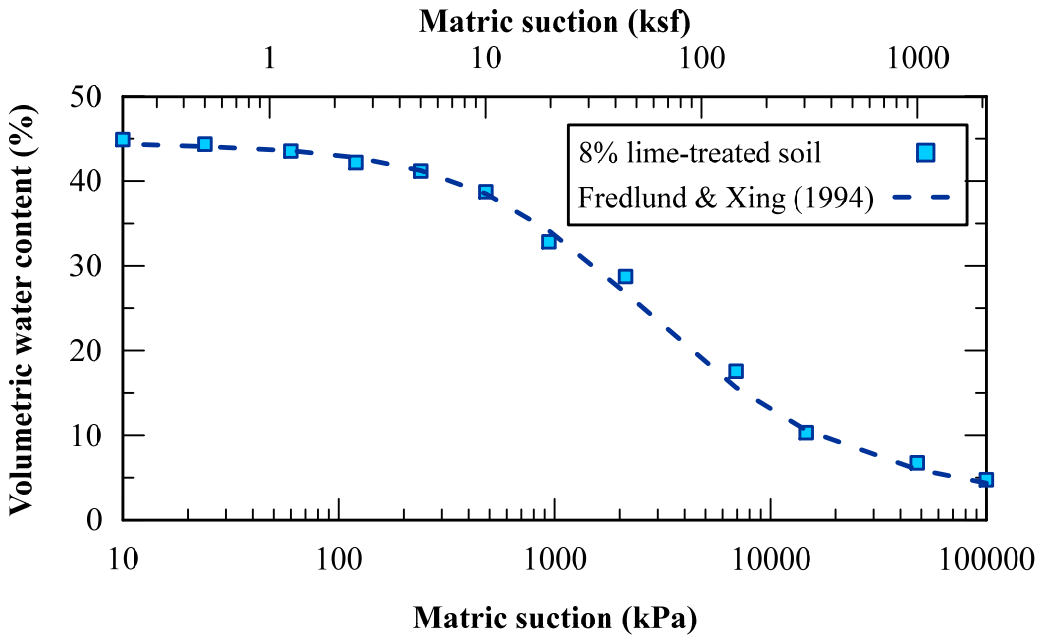

(c)

Figure 4.12 Measured SWRCs of (a) untreated, (b) 5% lime-treated, and (c) 8% lime-treated soils

The summary of these test results and the Fredlung and Xing (1994) formulation constants are presented in Figure 4.13 and Table 4.2, respectively. Test results show that the untreated soil has an air entry value of 95 kPa, which is typically seen for the CH type soil. For the lime-treated soils, the air entry value increased to 230 kPa and 320 kPa for 5% and 8% lime dosages, respectively. This observed change in air entry value after lime treatment was possibly caused by the cementitious gel products during the seven days curing period. The cementitious gel products of CSH have a negative surface charge and high specific surface area due to their porous structures. These characteristics of CSH gels possibly caused

an increase in the AEV. The parameter '*a*', which is closely related to the air entry value of soil, was also found to increase from 940 to 1640 and 1780 for 5% and 8% lime-treated soil respectively.

The SWRC test results indicated that the untreated soil has a '*n'* value of 0.73. This *n* value experienced a moderate increase to 0.90 and 1.02 for 5% and 8% lime-treated soil specimens, respectively. The constant '*n'* is related to the pore size distribution of soil and these observed increases could be attributed to short-term soil lime reactions and flocculation-agglomeration, which leads to a more homogeneous pore size distribution in the lime-treated soil. The untreated soil has '*m'* value of 1.71 whereas, 5% and 8% lime-treated soils have *'m'* values of 1.65 and 1.62, respectively. The constant '*m'* is related to the adsorption characteristics of the soil and these slight decreases showed that the residual water-holding capacity of the untreated soil was not changed significantly.

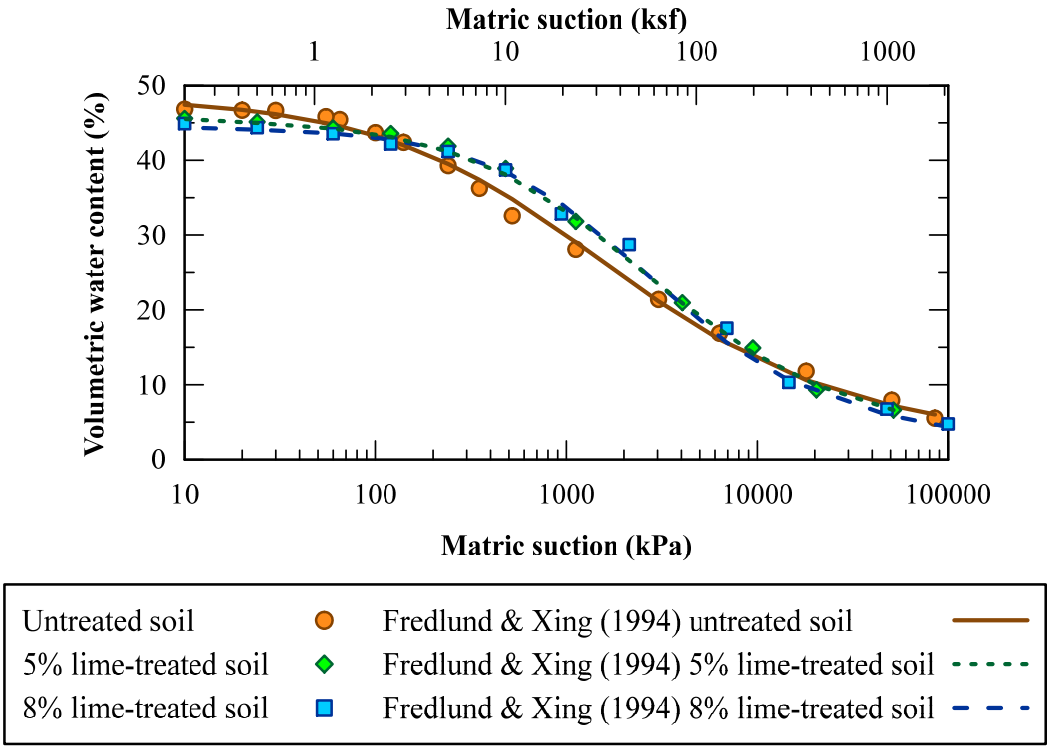

Figure 4.13 SWRCs of untreated, 5%, and (c) 8% lime-treated soils

Table 4.2 Fredlund and Xing (1994) SWRC model parameters

Fredlund and Xing (1994) SWRC Model Constants	**Untreated Soil**	**5% Lime-treated Soil**	**8% Lime-treated Soil**
a	940	1640	1780
n	0.73	0.90	1.02
m	1.71	1.65	1.62

The Fredlund and Xing (1994) parameters were of this study soils used in conjunction with the saturated permeability value of soil to obtain the unsaturated hydraulic conductivity function of untreated and treated soils. These estimated unsaturated soil functions are presented in Figure 4.14. The lime-treated soils

exhibited a higher permeability value than that of untreated soil for all suction values. Post-treatment, soil lime reactions and the flocculation-agglomeration tend to make the soil more friable and results in higher permeability.

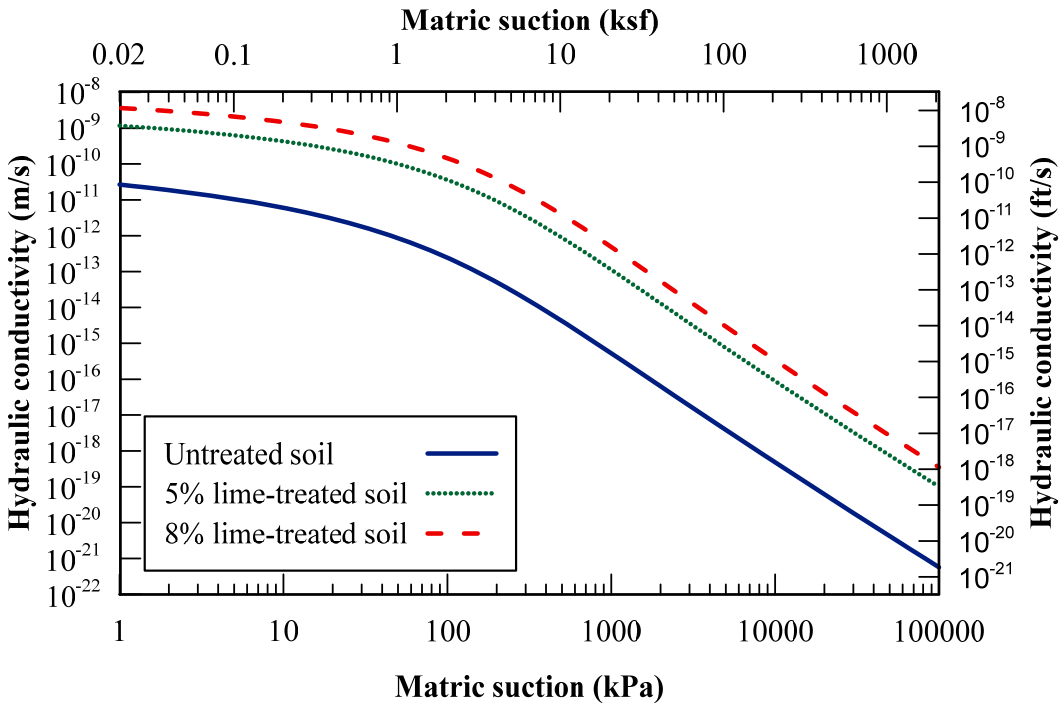

Figure 4.14 Summary of the hydraulic conductivity functions of untreated and 5% and 8% lime-treated soils

4.5.4 Soil Durability and Strength Retention Studies Results

The impact of climatic variation on the durability and strength of the lime-treated soils were determined and these results were compared with untreated soil. The untreated soil experienced 13% volumetric swelling strain and lost its integrity during the first wetting period and ultimately experienced failure. As expected, both 5% and 8% lime-treated soils outperformed the untreated soil in durability

studies. However, 5% lime-treated soil could not withstand the whole 14 cycles and failed during the 8th cycle. Only, 8% lime-treated soil was able to withstand the whole 14 durability cycles. Figures 4.15a, b, c, and d present 8% lime-treated soil after 1, 4, 7, and 14 cycles during durability studies, respectively.

(a)

(b)

(c) (d)

Figure 4.15 The condition of 8% lime-treated soil after (a) first, (b) third, (c) seventh, (d) fourteenth cycles

The volumetric strain changes measured during wet-dry cycles are presented in Figure 4.16. Results of these studies suggested that the lime treatment was successfully able to mitigate volumetric strain changes in soil due to weathering cycles. While the untreated soil underwent 13% volumetric swelling strains during the first wetting period and experienced failure, both the 5% and 8% lime-treated soils experienced only marginal volumetric strains during the first 3 wet-dry cycles. However, starting from the 4^{th} cycle, the benefits of 5% lime treatment on volumetric strain changes started to reduce. In the 7^{th} cycle, the 5% lime-treated soil exhibited approximately 5% swell and shrinkage strains and the soil experienced a failure during the 8^{th} durability cycle. The disintegration of soil,

considerable swell-shrinkage strains, and the breakage of cementitious bonds could be attributed to this failure. The 8% lime-treated soil outperformed the 5% and untreated soil throughout the entire wet-dry durability cycles and experienced insignificant volumetric strain changes during the first 11 cycles. In the 14th durability cycle, the 8% lime-treated soil exhibited approximately 2.5% volumetric swell and shrinkage strains.

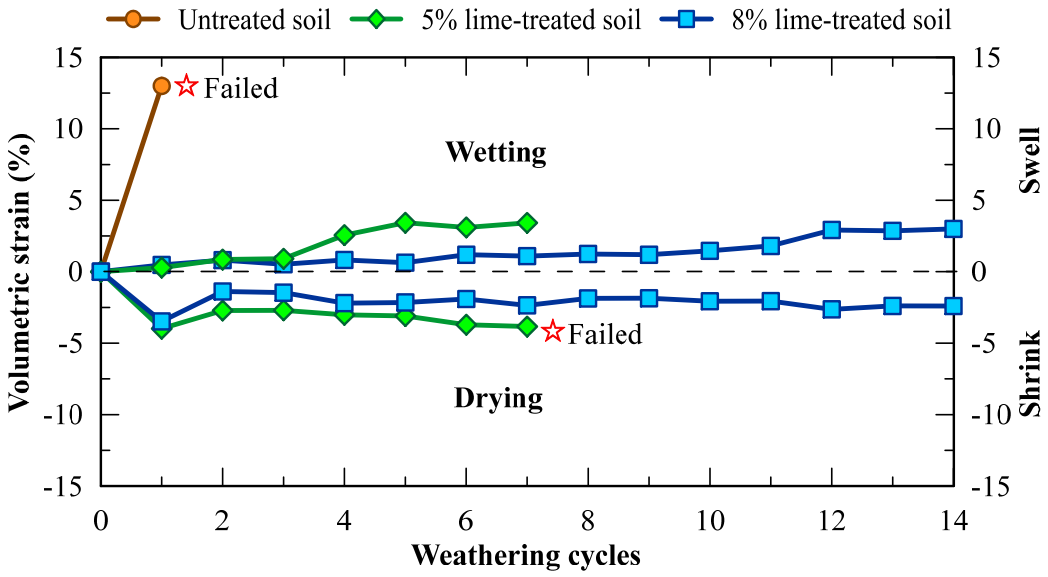

Figure 4.16 Measured volumetric changes for untreated, 5% lime-treated, and 8% lime-treated soils

Similar improvements after lime treatment were observed in the weight loss characteristics of treated soils. Figure 4.17 presents the determined percentage of weight loss during the wet-dry durability cycles. As the untreated soil totally disintegrated during the first wetting cycle its weight loss characteristic could not

be determined. The 8% lime-treated soil outperformed the 5% lime-treated soil and experienced lower weight loss in all the weathering cycles. While the 5% lime-treated soil started to lose a significant amount of weight just after the first cycle, the 8% lime-treated soil started to lose a noticeable amount of weight after the 8th cycle. The better response of 8% lime-treated soil against wetting and dry cycles is possibly due to the formation of more cementitious bonding in the 8% lime-treated soil during the curing and testing period.

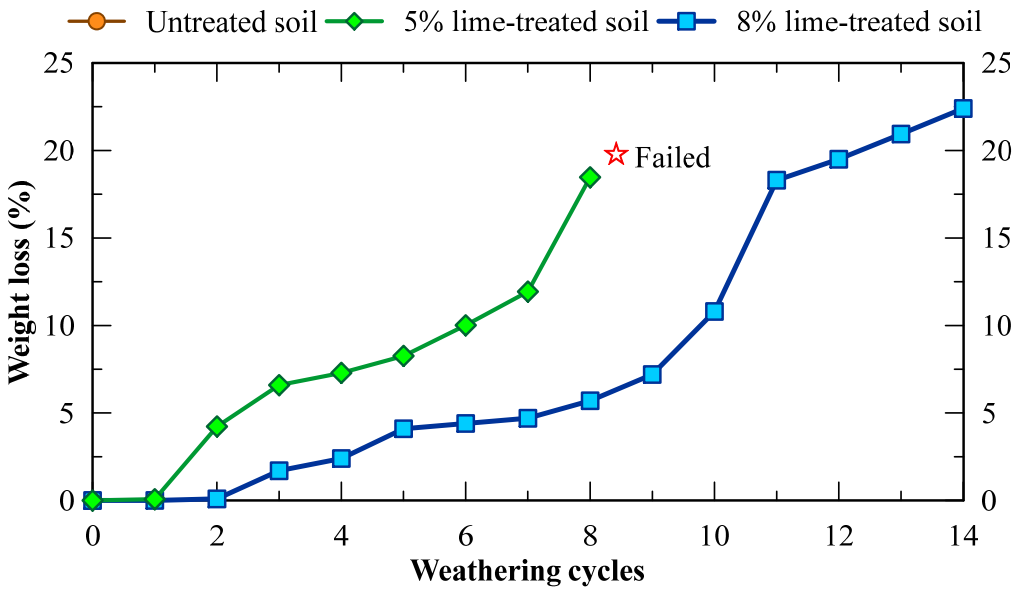

Figure 4.17 Measured weight loss of 5% lime-treated and 8% lime-treated soils during the durability studies

The measured strength retention characteristics of the untreated, 5% lime-treated, and 8% lime-treated soils are shown in Figure 4.18. The results showed that there was a significant improvement in the soil UCS values starting from the

newly compacted condition. The untreated soil UCS value experienced an increase from 319.2 kPa (46.3 psi) to 797.0 kPa (115.6 psi) and 700.0 kPa (101.5 psi) for 5% and 8% lime-treated soils, respectively. Durability studies required oven drying at 71±3°C temperature for 42 hours. Due to this high temperature and long testing periods, a significant UCS value improvement was observed for both 5% and 8% lime-treated soil samples during the first 3 durability cycles. However, after the 3rd cycle, the lime-treated soils started exhibiting a gradual decrease in UCS values which indicate the destructive impacts of the durability cycles.

In the 7th cycle, the UCS value of the 5% lime-treated soil was only 476.5 kPa (69.1 psi) and the soil specimen failed during the 8th cycle. Moreover, the 8% lime-treated soil underwent a lower strength loss rate after the 3rd cycle as compared to 5% lime-treated soil. At the end of the 14th cycle, the 8% lime-treated soil had a UCS value of 450 kPa, which is still higher than the UCS value of untreated soil in the newly compacted conditions.

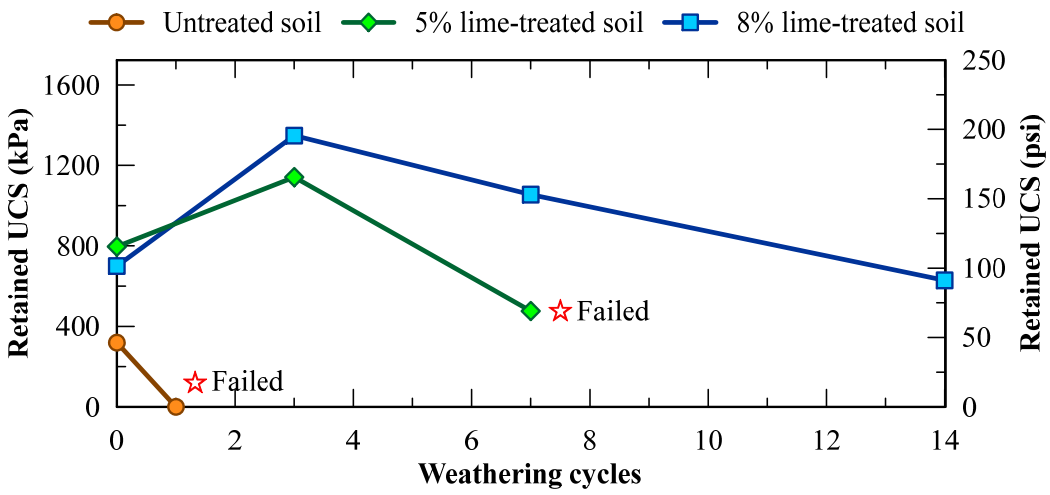

Figure 4.18 Strength retention characteristics of the untreated, 5% lime-treated, and 8% lime-treated soils

4.6 Summary

In this chapter, the soil-mix design studies were presented, and their results were discussed. Several chemical and basic soil characterization tests along with engineering tests were conducted on the untreated and 5% and 8% of lime-treated soils sampled from the embankment of the U.S. 75 Frontage Road. The lime dosage used in the reconstruction work of this slope was chosen based on the analyses of test results of these studies presented in this Chapter. A minimum pH value of 12.4 was targeted as it is needed to sustain long-term pozzolanic reactions after lime treatment. In the present research study, the minimum required dosage of lime stabilizer for the test soil was found to be 5% and the soil mix design studies were conducted for 5% and 8% of the lime dosages.

After lime treatment, the hydraulic conductivity of soil increased approximately by 10 and 50 times for 5% and 8% of treatment dosage respectively. There were significant enhancements in soil peak and FSS strength parameters, particularly in the soil effective cohesion value. The soil cohesion value obtained from the DS test (peak shear strength) increased by 283% and 220% for the 5 and 8% lime-treated soils, respectively, just after the three days curing period. For the FSS condition, this cohesion enhancement was more prominent, and the cohesion value increased by 362% and 508% for the three days cured 5% and 8% lime-treated soils, respectively. Also, the value of the effective friction angle of soil was improved moderately. The friction angle value determined from soil peak strength improved by 171% and 165% in the case of 5% and 8% lime-treated soils.

Moreover, the lime treatment significantly improved the durability and strength retention characteristic of the test soil. While the untreated soil was disintegrating during the 1st wetting period, the 5% and 8% lime-treated soils were able to complete 7 and 14 durability cycles. These results, also, exhibited the importance of incorporating durability studies along with the soil strength studies. Even though the 5% and 8% lime-treated soils had similar improvement in soil peak and FSS, the 5% lime-treated soil endured just for 7 durability cycles, while the 8% lime-treated soil withstood all the 14 durability cycles. These results showed that although the 5% lime satisfied the minimum required pH value and significantly increased the soil strength properties, using 3% extra lime was

required to increase the soil resistance against the inclement weather conditions. Based on the analyses of the results of these studies, the 8% lime treatment was chosen to rehabilitate the failed U.S. 75 Frontage Road slope section.

Chapter 5

NUMERICAL MODELING STUDIES

5.1 Introduction

The assessment of long-term safety of partially saturated slopes under various possible climatic conditions requires knowledge of hydro-mechanical properties of soil and rainfall characteristics. Development of the fractures, fissures, and cracks in soil over a period of time changes its hydro-mechanical properties drastically and further complicates the rainfall infiltration process (Flury et al. 1994; Van Genuchten et al. 1999). Rainfall infiltration induces major slope failures and hence has been studied by many researchers across the world (Ng and Shi 1998, Gasmo et al. 2000, Rahardjo et al. 2007, Kristo et al. 2017, Chan et al. 2021).

The numerical analysis is an economic and efficient method to simulate the behavior of a slope subjected to transient boundary conditions (Yang et al. 2019). The rainfall-induced slope stability analysis can be performed by using either limit equilibrium or finite element/finite difference method (FEM/FDM) based numerical methods. There are many commercial software programs available, which provide rational solutions. Conventional limit equilibrium methods are proven to be reliable and are known to give accurate results (Tsaparas and Toll 2002, Lee et al. 2009, Wang et al. 2011, Le 2013, Matthews et al. 2014,

Ghani et al. 2020). The comparison between the FOS values of slopes computed using the limit equilibrium method and FEM showed a reasonable good agreement (Van Impe and Flores 2007, Khalkhali and Koochaksaraei 2019).

Different chemical treatment methods are attempted to stabilize slope sections that are impacted by slope failures. An attempt has been made here to investigate the long-term performance of one such treated slope, a lime-treated slope rehabilitation work of highway slope section by conducting rainfall-induced slope stability analyses. In this specific research work, the slope stability of lime-treated the U.S. 75 Frontage Road along with the Grapevine and Joe Pool lake dams were investigated. All these slopes, located in North Texas, experienced a similar kind of surficial failures and their surficial slopes were stabilized by using a quick lime treatment method of surficial soil layers.

The long-term stability of these slopes was assessed by incorporating the effect of detrimental changes in the chemico-hydro-mechanical properties of the treated soil due to wet-dry cycles and rainfall events. Therefore, the permanency of the lime treatment method used to repair surficial slope failures were assessed with proper consideration of moisture fluctuations and soil strength reduction. The numerical simulations were carried out using commercially available software of SEEP/W and SLOPE/W that are based on FEM method and limit equilibrium method, respectively.

Numerous parametric studies of slope section with different rainfall intensities and treated soil layer thicknesses were conducted. The necessity of the provision of a proper drainage system was also investigated in the rehabilitated U.S. 75 Frontage Rood slope sections. The material properties of the numerical model were based on the findings of the site investigations and laboratory test results. The geometric configuration details of the slope were obtained from construction and design drawings from TxDOT office in Paris, Texas. The results of the soil mix design studies, presented and discussed in Chapter 4, were used as input parameters in the numerical study of the U.S. 75 Frontage Road slope.

A similar assessment of treated slopes of the Grapevine and Joe Pool lake dams was carried out and the pertaining information of the soil properties and slope geometries were obtained from the works of Dronamraju (2008), Le (2013), and Acharya (2015). The variation in moisture contents in the soils for different rainfall intensities and durations were studied in this research. The compiled rainfall data for the nearest rainfall stations to the test section of the slopes were obtained from the National Oceanic and Atmospheric Administration (NOAA) web site. The following sections include the detailed methodology used in these numerical analysis studies, analysis of the results and findings from these studies.

5.2 Numerical Analyses Studies for U.S. 75 Frontage Road Slope

The numerical analyses primarily aim at the investigation of causes that

led to instability problem in the slope of U.S. 75 Frontage Road. Seepage and slope stability analyses were conducted using the finite element method and limit equilibrium method, respectively. These numerical analyses studies were conducted by using Seep/w and Slope/w software in five main stages:

1. Generating the cross-section of the slope model.
2. Input the material properties into the slope model.
3. Assignment of the initial moisture distribution into slope model.
4. Simulating rainfall studies.
5. Performing unsaturated slope stability analyses.

5.2.1 Development of Numerical Model

In order to conduct numerical studies, a 2-D plane strain model of the slope was developed using the modules of *GEOSTUDIO* software package. The geometry of the slope section was obtained from TxDOT reports and geometrical information was collected during the site visits. In the present numerical analysis, the effects of changes in hydro-mechanical properties of untreated and lime-treated clayey soils due to wet-dry cycles on slope stability was also evaluated. The soil within the surficial layer of the slope is subjected to harsh environmental conditions, particularly from wet and dry cycles. In the long-term period, wetting and drying of soil results in degradation of soil strength and its hydraulic properties. Therefore, the cross-section of the slope was modeled with two different soil layers, a surface soil layer and a deeper soil layer (Figure 5.1).

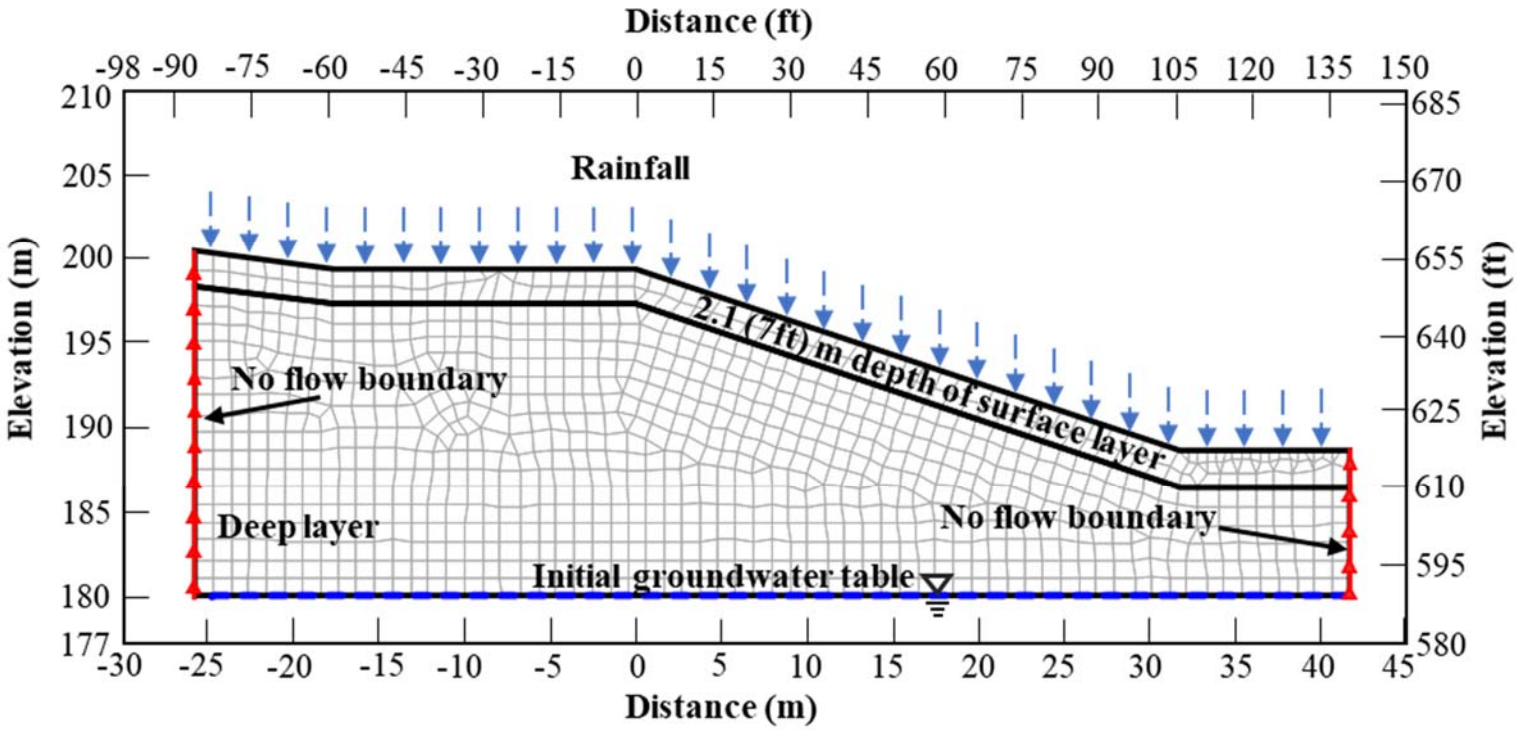

Figure 5.1 Numerical model of U.S. 75 Frontage Road slope section

The site investigations results presented in Chapter 3 showed that the failed slope section has a vertical scarp height of approximately 2.1 m (7 ft). Based on this finding, the surface layer was extended to a depth of 2.1 m from the surface of the slope. The analyses for post-treatment section were conducted using similar geometric configuration. In these analyses, one more additional layer, 8% lime-treated layer, defined with different thickness at the top (30.4 cm, 61.0 cm, 91.4 cm (1 ft, 2 ft, and 3 ft), respectively) was considered and then the long-term performance of the rehabilitated slope was evaluated.

5.2.2 Material Properties

In unsaturated soil condition, matric suction controls the soil strength and hydraulic characteristics of the soil. While defining the soil in a numerical model, it is important to choose a constitutive model which includes the effect of matric suction on its shear strength. In the present numerical study, the extended Mohr-Coulomb model was used to define stress-strain relationship in soil. The formulation of this model, developed by Fredlund (1978), is given below:

$$\tau = c' + (\sigma_n - u_a)\, tan\, \varphi' + (u_a - u_w)\, tan\, \varphi^b \qquad (5.1)$$

Where,

c' is effective cohesion in kPa,

φ' is the effective internal friction angle in degrees,

$(\sigma_n - u_a)$ is net normal stress in kPa,

u_a is pore-air pressure in kPa,

u_w is the pore-water pressure in kPa,

$(u_a - u_w)$ is matric suction in kPa, and

φ^b is an internal friction angle with respect to matric suction.

The contribution of the soil matric suction toward soil strength value is provided by using φ^b value, the internal friction angle due to soil matric suction. It was estimated from the air entry value of soil, in accordance with Zhang et al. (2014) and this φ^b was assigned to the model. Also, the unsaturated hydraulic properties of soil were defined by using the best fitting parameters of Fredlund and Xing (1994) SWRC function and saturated permeability values. The soil properties used in the numerical analysis model along with the best fitting parameters of Fredlund and Xing (1994) are presented in Table 5.1 and Table 5.2, respectively.

Table 5.1 Summary of the soil parameters used in slope stability analyses of U.S. 75 Frontage Road

Soil Type	**Unit Weight (kN/m^3)**	**Peak Shear Strength Parameters**			**FSS Parameters**		
		Test Type	**c' (kPa)**	**ϕ' (°)**	**Test Type**	**c' (kPa)**	**ϕ' (°)**
Untreated	20.3	DS	13.2	23.7	TRS	0	23.4
8% lime-treated	19.7	DS	37	39.1	TRS	6.6	30.6

Table 5.2 Soil permeability, SWRC and Fredlund and Xing (1994) model parameters used in the numerical analysis model of U.S. 75 Frontage Road slope

Soil Type	Saturated Permeability Value (m/s)	SWRC Parameters		Fredlund and Xing (1994) Model Parameters		
		θ_s	ψ_a (kPa)	*a*	*n*	*m*
Untreated	3.0×10^{-10} m/s	48.5	95	940	0.73	1.71
8% lime-treated	1.5×10^{-8} m/s	45.0	150	1780	1.02	1.62

For the short-term condition, the peak shear strength parameters and hydraulic conductivity value of the newly compacted condition of the soil were assigned to the highway slope. In the long-term condition, the FSS parameters and the permeability value of weathered soil were used as input parameters. As the impact of the weathering cycles is limited to the surficial layers of the slope, both peak strength value and permeability value of the newly compacted soil were assigned to underlying soil layers.

5.2.3 Initial Conditions

In the case of unsaturated soil conditions, the initial moisture content distribution in slope is a critical parameter in its stability analyses. Based on the findings of site investigation, the initial soil matric suction distribution in the model was generated in the model by defining the location of the groundwater table. The site investigation studies showed the absence of a groundwater table within the top 15.7 m (51.5 ft) of soil from the surface of the slope. Therefore, the

groundwater table was defined at an elevation of 180 m (590.6 ft) in the numerical analysis model. Additionally, both right and left sides of the model geometry were assigned with a no-flow boundary condition (Q=0).

The software assumes a linear increase in the soil matric suction with the height of soil above the ground water table. This approach usually overestimates the value of matric suction in the surface layer and gives a highly conservative factor of safety for slope. To overcome this limitation of software, the average soil matric suction in the surface layer of the slope was investigated by collecting soil samples. After determining the water content of these soil specimens, the corresponding suction level was estimated using the SWRC of the soil. The results showed a very small matric suction value (20 kPa) within the surface layer of the slope. Therefore, the maximum suction level in the numerical model was limited at 20 kPa to prevent overestimation of unsaturated soil shear strength.

5.2.4 Rainfall Studies

In this study, rainfall-induced slope stability analyses were conducted. The rainfall studies are used to assess the impacts of seepage that occurred in treated slope under expected rainfall events. In these analyses, the effect of rainfall intensity and duration on the pore water pressure (PWP) distribution in the embankment slope was evaluated. After determining the changes in PWP distributions of the slope, the same model was transferred to Slope/W software, to perform slope stability analysis. The most probable rainfall data at the slope

location was collected from NOAA. The numerical analyses were performed for a short (one day), medium (four days), and long (ten days) duration of continuous rainfall. As the highways are planned for a long period of service lives, these estimates were selected for 100 years of average recurrence interval with 90% confidence intervals. The rainfall data collected from NOAA do not provide the hourly distribution of rainfall events, therefore, the corresponding total amount of rainfall is induced with constant rainfall intensities for durations of one, four, and ten days, respectively (Table 5.3).

Table 5.3 Frequency estimates used in the rainfall-induced slope stability analyses for U.S. 75 Frontage Road slope (Perica et al. 2018)

Rainfall Duration (days)	**100 Years Return Period**	
	Total Rainfall Amount (cm/in)	**Rainfall Intensities (cm/s/in/s)**
1	24.8/ 9.78	$2.9x10^{-4}$/ $1.13x10^{-4}$
4	32.3/ 12.7	$9.3x10^{-5}$/ $3.67x10^{-5}$
10	38.6/ 15.20	$4.5x10^{-5}$/ $1.76x10^{-5}$

5.2.5 Slope Stability Analysis

After conducting transient seepage analyses, the FOS of the most critical slip surface of the slope was calculated using the Morgenstern-Price method in the limit equilibrium analysis. The computation of FOS of the slope model was started after specifying the location of probable slip surfaces. After conducting the numerical analyses for the failed untreated slope section, similar analysis processes were repeated on the lime-treated slope sections. These analyses were

conducted with various thicknesses of 30.4 cm, 61.0 cm, and 91.4 cm (1 ft, 2 ft, and 3 ft) of 8% lime-treated surficial layer. In these analyses, the expected long-term performance of lime treatment was investigated, and the optimum thickness of the treated layer was then selected. The lime-treated slope stability analyses were conducted with and without a drainage system under the lime-treated soil section and therefore, the need for a drainage system was studied.

5.3 Numerical Analyses Studies for Grapevine and Joe Pool Lake Dams Slope

One of the main objectives of this research work is to evaluate the long-term performance of lime treatment in slopes. Apart from the U.S. 75 Frontage Highway embankment slope, two dam embankment slopes - Grapevine and Joe Pool lake dams, were also included in the present research study for a comprehensive assessment of lime treatment in different slopes. Both of these dams experienced numerous surficial slope failures, similar to U.S. 75 Frontage Road slope, and were stabilized with lime treatment. The details of slopes and failures are provided in Chapter 3.

The previous UTA researcher studied these slope failures and investigated the performance of several repair methods including the lime treatment method (Dronamraju 2008). The main scope of these studies was assessment and comparison of different slope repair methods. In the present research work, those studies were extended, and the long-term FOS of the dam slopes were calculated

by incorporating the effect of detrimental changes in the hydro-mechanical properties of the treated soil and rainfall events.

The numerical analysis models for Grapevine and Joe Pool lake dams' slopes presented in Figures 5.2a and 5.2b were generated based on the models that were presented by Le (2013). In these numerical analysis models, the topsoil within 1.22 m (4 ft) from the surface was modeled as a surface layer where the degraded soil properties are assigned. Also, the 0.45 m (18 in.) thick surface layer of the slope was generated as 8% lime-treated layer based on the determined treatment thickness. In these models, the soil material and hydro-mechanical properties were compiled from studies of McCleskey (2005), Dronamraju (2008), Le (2013), and Acharya (2015). The soil strength, hydraulic conductivity properties, and unsaturated soil properties used are presented in Tables 5.4 and 5.5.

Le (2013) investigate the moisture variation of the soils in these dams over a period of 4 years (between 2009 and 2012). In this study, the moisture variation of untreated soils at 0.25 m and 0.5 m depths from the surface was determined using two moisture probes and the results are presented in Figures 5.3a and 5.3b for Grapevine and Joe Pool lake dams, respectively.

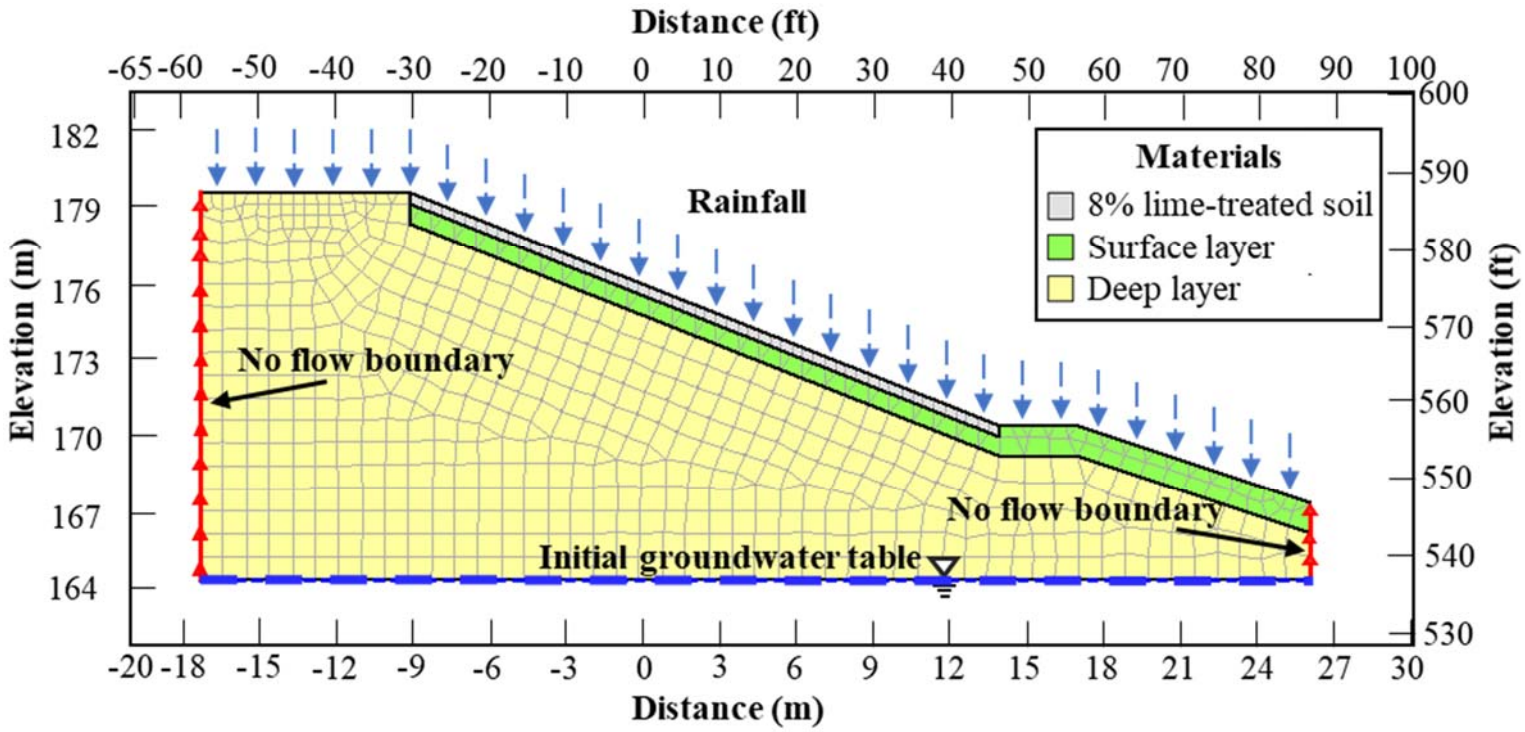
Distance (ft)
-65 -60 -50 -40 -30 -20 -10 0 10 20 30 40 50 60 70 80 90 100
182
179
176
173
170
167
164
Elevation (m)
600
590
580
570
560
550
540
530
Elevation (ft)
Materials
8% lime-treated soil
Surface layer
Deep layer
Rainfall
No flow boundary
No flow boundary
Initial groundwater table
-20 -18 -15 -12 -9 -6 -3 0 3 6 9 12 15 18 21 24 27 30
Distance (m)

(a)

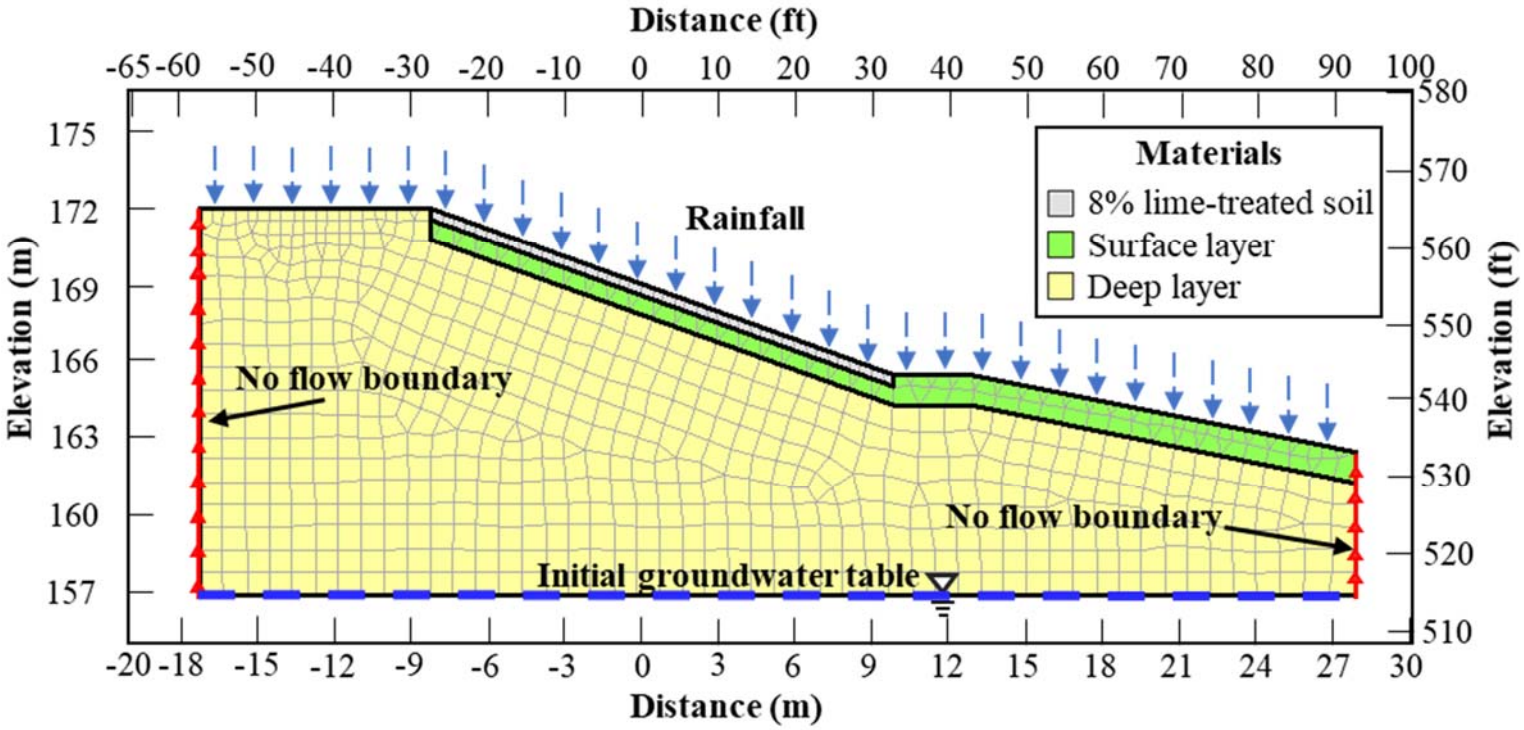

(b)

Figure 5.2 (a) Cross-section of (a) Grapevine dam and (b) Joe Pool lake dam numerical analysis model

Table 5.4 Shear strength properties of slopes of Grapevine and Joe Pool lake dams used in the numerical analyses (Le 2013, Acharya 2015)

Slope	Soil Type	Peak Shear Strength Parameters			FSS Parameters		
		Test type	c' (kPa)	ϕ' (degree)	Test type	c' (kPa)	ϕ' (degree)
Grapevine dam	Untreated	DS	2.4	29.1	TRS	0	18
	8% lime-treated	DS	94.5	32.8	TRS	12.9	38
Joe Pool lake dam	Untreated	DS	4.8	26.2	TRS	0	27
	8% lime-treated	DS	140.6	23.5	TRS	21.9	36.6

Table 5.5 Soil permeability, SWRC and Fredlund and Xing (1994) model parameters used in the numerical analyses models of Grapevine and Joe Pool lake dam slopes (Dronamraju 2008, Acharya 2015)

Slope	Soil Type	Saturated Permeability Value (m/s)	SWRC Parameters		Fredlund and Xing (1994) Model Parameters		
			θ_s	ψ_a (kPa)	*a*	*n*	*m*
Grapevine dam	Untreated	8.1×10^{-6} m/s	43.6	15	70	1.1	1
	8% lime-treated	2.3×10^{-5} m/s	37.2	17	70	1.1	0.85
Joe Pool lake dam	Untreated	2.7×10^{-6} m/s	56.8	38	170	1	1
	8% lime-treated	1.1×10^{-5} m/s	49.2	19	70	1	0.8

In the wet seasons, the 4 years average water contents of the Grapevine and Joe Pool lake dam soils were as high as 34.4% and 43.4%, respectively. The

matric suctions corresponding to these water contents of soil were estimated to be 50 kPa and 138 kPa for Grapevine and Joe Pool lake dam embankment sections, respectively.

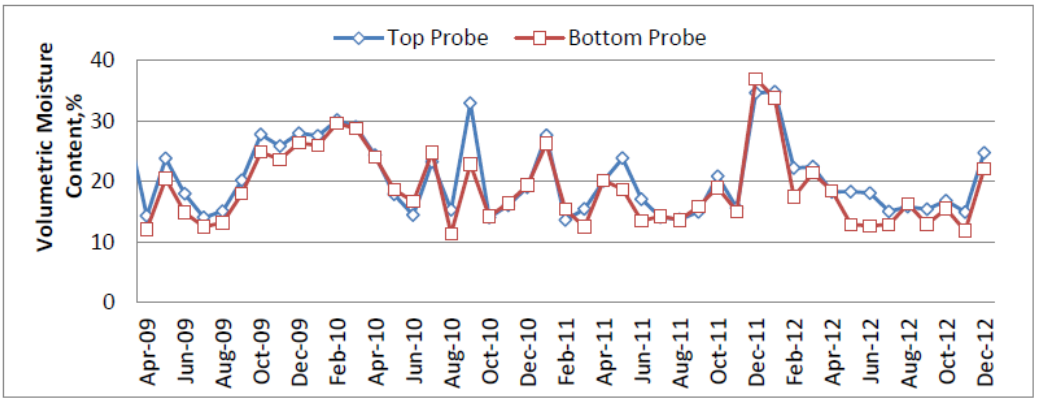

(a)

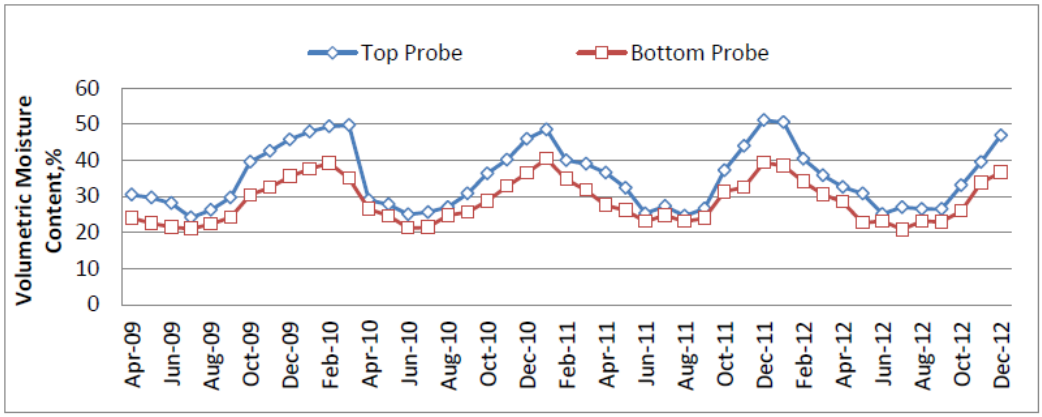

(b)

Figure 5.3 Moisture variation of untreated soils measured in (a) Grapevine and (b) Joe Pool lake dams slope between 2009-2012 (Le 2013)

Therefore, in the numerical analyses, these obtained suction levels were used as the initial matric suction values in the surface layer of slopes and the

maximum suction levels were limited accordingly. Similar numerical analysis processes mentioned in Section 5.2 were repeated for 8% lime-treated section of these dams' slope with compiled rainfall data (Table 5.6). The next section presents the abovementioned rainfall-induced slope stability analysis results.

Table 5.6 Frequency estimates used in the rainfall-induced slope stability analyses for Grapevine and Joe Pool lake dams slope (Perica et al. 2018)

Rainfall Duration (days)	Grapevine Dam		Joe Pool lake Dam	
	Total Rainfall Amount (cm/in)	Rainfall Intensities (cm/s/in/s)	Total Rainfall Amount (cm/in)	Rainfall Intensities (cm/s/in/s)
1	23.1/9.1	$2.7x10^{-4}$/ $1.1x10^{-4}$	24.8/9.5	$2.8x10^{-4}$/ $1.1x10^{-4}$
4	31.0/12.2	$9.0x10^{-5}$/ $3.5x10^{-5}$	32.0/12.6	$9.3x10^{-5}$/ $3.6x10^{-5}$
10	38.1/15.0	$4.4x10^{-5}$/ $1.7x10^{-5}$	38.4/15.1	$4.4x10^{-5}$/ $1.7x10^{-5}$

5.4 Results of Numerical Analyses Conducted on U.S. 75 Frontage Road Slope

Rainfall-induced slope stability analyses were performed to elucidate the impacts of rainfall events on the stability of the embankment slope before and after exposure to weathering cycles. These analyses were repeated for untreated and lime-treated slope sections of U.S. 75 Frontage Road and the results are tabulated in Table 5.7.

The rainfall-induced slope stability analyses conducted on the untreated section of slope facilitated to illustrate the most probable reason for this slope failure. Results of numerical studies showed that for all the rainfall characteristics, the FOS of the critical slip surface of untreated slope before subjecting wet-dry

cycles was sufficient (greater than 1.5). The soils in the slope preserved a considerable amount of matric suction in the surficial layer of slope even after ten days of continuous rainfall and the fluctuation in soil moisture content was limited a shallow depth of 91 cm (3 ft) due to very low permeability value of soil (Figures 5.4a and b). Hence, the significant amount of cohesion value of clayey soil in newly compacted conditions and partially saturated conditions resulted in a deep slip surface with a high FOS value of 2.38.

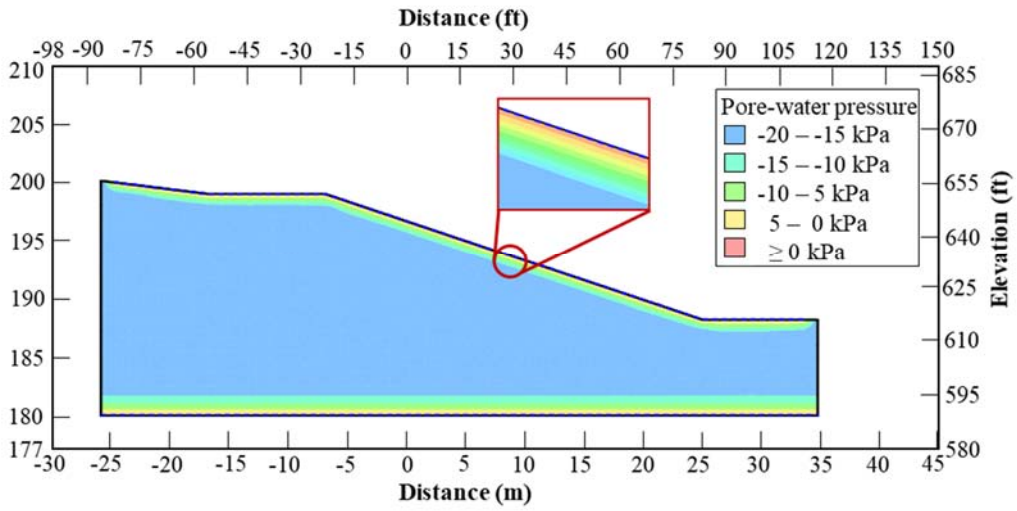

(a)

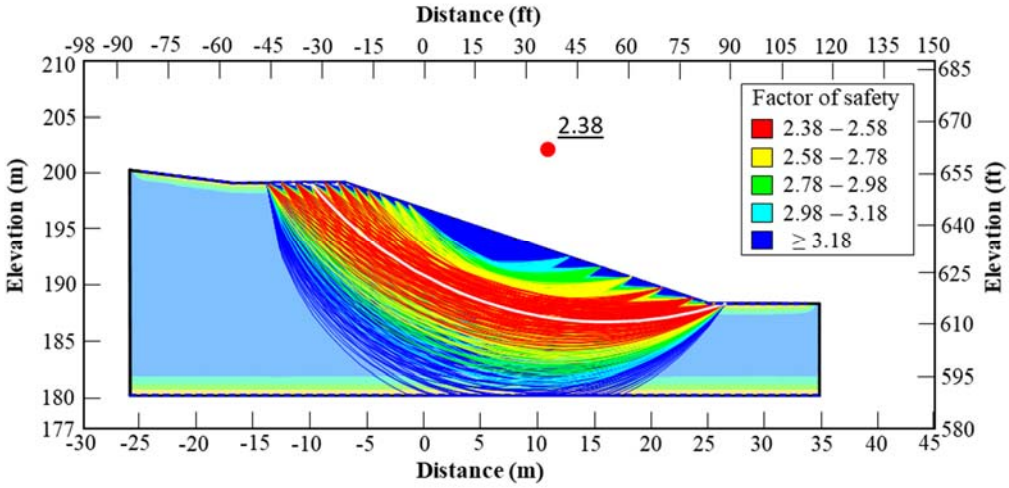

(b)

Figure 5.4 (a) PWP distribution and (b) FOS of untreated U.S. 75 Frontage Road slope after subjecting 91 cm (3 ft) rainfall event in ten days

Table 5.7 Summary of the FOS values of untreated and lime-treated slope sections before and after exposing rainfall events

Drainage System	**Thickness Of Lime-Treated Layer (cm/ft)**	**The Rehabilitated Slope Before Exposing Weathering Cycles**				**The Rehabilitated Slope After Exposing Weathering Cycles**			
		Total Rainfall Amount (cm/in.)				**Total Rainfall Amount (cm/in.)**			
		0	**24.8 / 9.78**	**32.3 / 12.7**	**38.6 / 15.2**	**0**	**24.8 / 9.78**	**32.3 / 12.7**	**38.6 / 15.2**
No	0 (untreated)	2.40	2.39	2.39	2.38	1.97	1.14	0.71	0.67
No	30.5/1.0	2.31	2.30	2.27	2.26	2.09	1.98	1.78	1.21
	61.0/2.0	2.32	2.31	2.29	2.27	2.19	2.09	1.85	1.27
	91.4/3.0	2.34	2.33	2.30	2.29	2.30	2.21	1.95	1.37
Yes	30.5/1.0	2.31	2.30	2.29	2.26	2.23	2.02	1.88	1.40

	61.0/2.0	2.32	2.32	2.31	2.27	2.19	2.14	1.98	1.54
	91.4/3.0	2.34	2.33	2.30	2.29	2.30	2.26	1.98	1.60

It is evident from the analysis results that wet and-dry seasonal cycles had a detrimental effect on the stability of the slope during rainfall events. The FOS value for the most critical slip surfaces decreased to 1.14 from 1.97 after 9.78 in. rainfall in one day. The stability of the slope went further down with an increase in the duration of rainfall. In the case of prolonged rainfalls of four and ten days, the obtained FOS were 0.71 and 0.67, respectively and the slope experienced surficial slope failure (Figure 5.5b). This stability problem can be attributed to the development of positive pore water pressure developed in the surface layer of the slope (perched water table) which degraded the strength of the soil.

Furthermore, the increase in permeability value of soil in the surficial layer allowed rapid water infiltration into the slope during the rainfall event. This rate of rainfall infiltration was slowed down at the underlying deep layer due to the low permeability value of soil which did not experience desiccation cracking and resulted in accumulation of water as shown in Figure 5.5a. The results of this numerical analysis simulation showed similarities with observations recorded from the site. The perched water table (Figure 5.6a) and wet patches (Figure 5.6b) observed during the field investigation visits proved that the formation of positive water pressures in the surface layer of the slope primarily caused this slope failure.

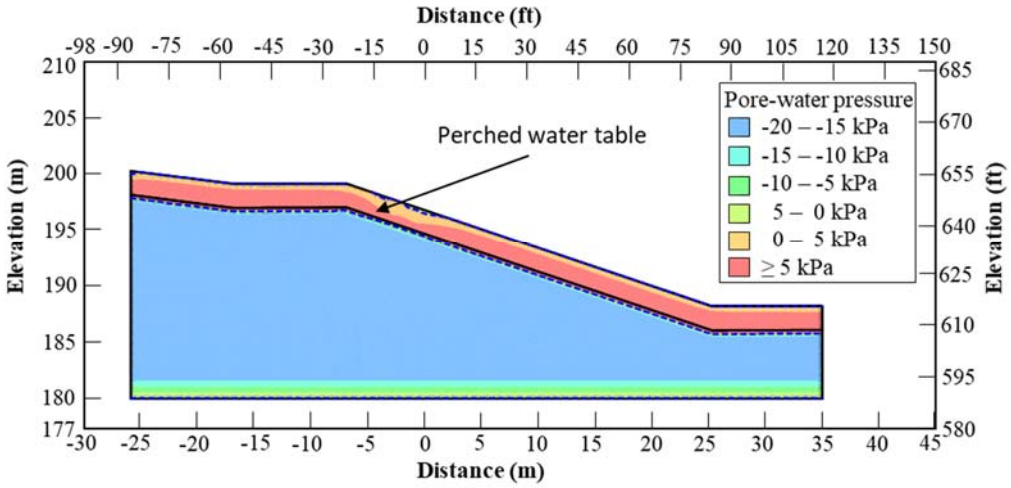

(a)

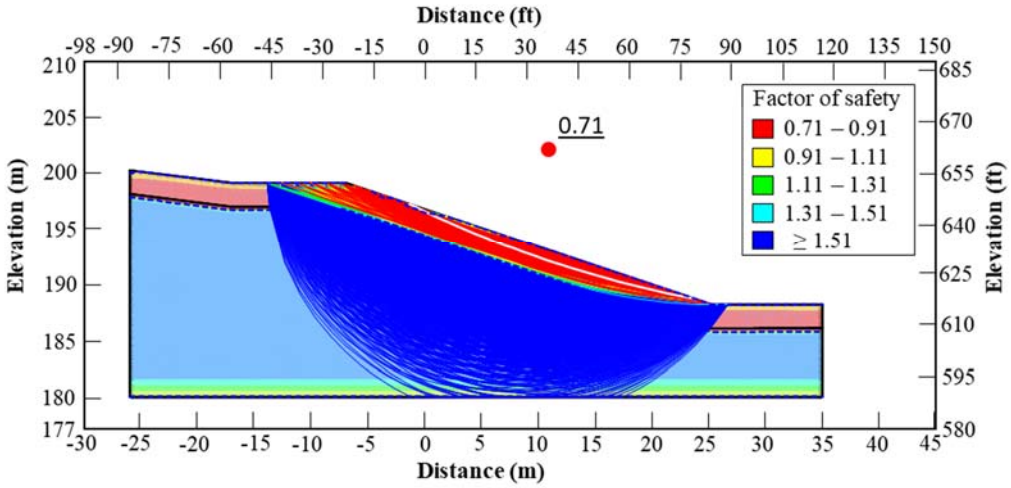

(b)

Figure 5.5 (a) PWP distribution and (b) FOS of untreated U.S. 75 Frontage Road slope after subjecting 32.3 cm (12.7 in.) rainfall event in four days

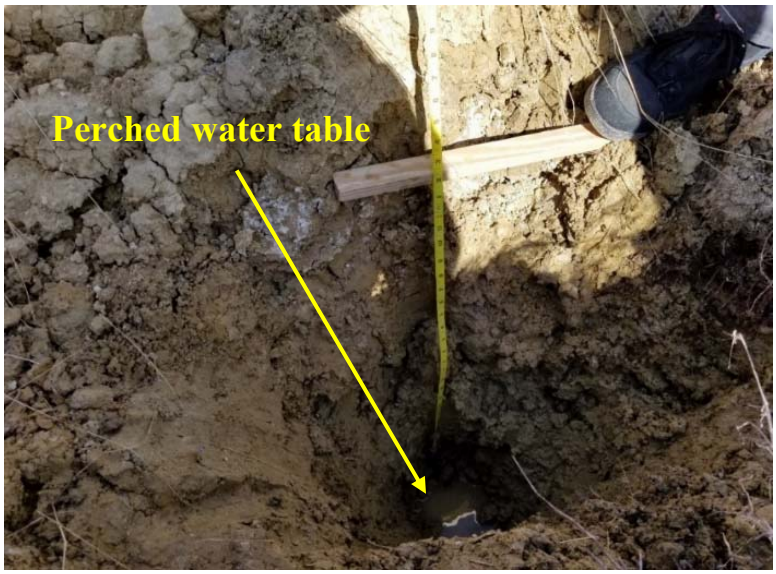

(a)

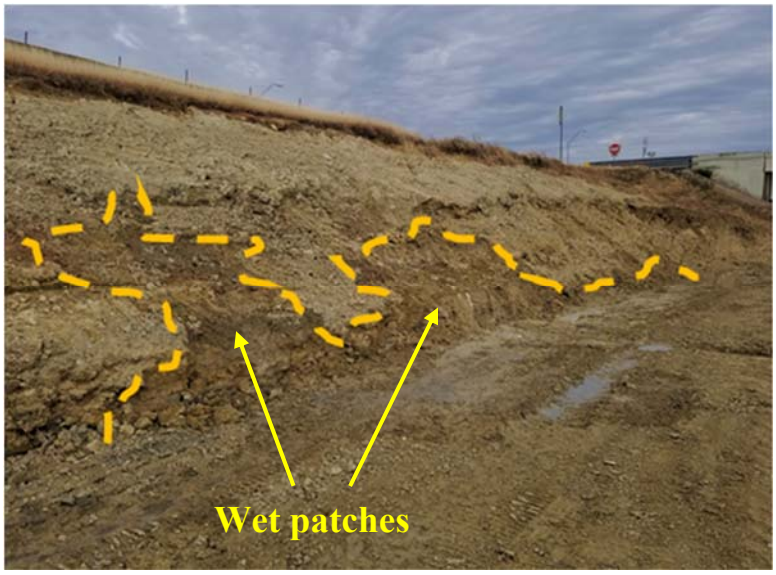

(b)

Figure 5.6 (a) Observed perched water table and (b) wet patches on the slope

The surface layer of the slope was treated with 8% lime with different treatment depths of 30.5, 61.0, and 91.4 cm (1, 2, and 3 ft). In all the cases, lime

treatment resulted in a significant increase in FOS of the critical slip surface. The obtained FOS values for the slope subjected to weathering cycles with and without an underlying drainage system and for different rainfall events are presented in Table 5.7. Prior to a rainfall event, the rehabilitation of the surface layer of the slope increased the most critical FOS from 1.97 to 2.31, 2.32, and 2.34 for 30.5, 61.0, and 91.4 cm thickness of lime, respectively. These safety factors dropped down but remained greater than one even after a rainfall event for all lime treatment depths. The lowest FOS values were obtained after subjecting to 38.6 cm (15.2 in.) rainfall in ten days for the slope that was exposed to the weathering cycles.

Figures 5.7a, b, and c show the obtained PWP variation and FOS for three lime stabilized slopes with thicknesses of 30.5 cm, 61.0 cm, 91.4 cm (1 ft, 2 ft, and 3 ft), respectively. These results showed that, although, exposing to heavy rainfall event leads to a partially saturated surface layer of the slope, the enhanced soil properties, particularly effective cohesion values, of the lime-treated layer prevent the slope from failure.

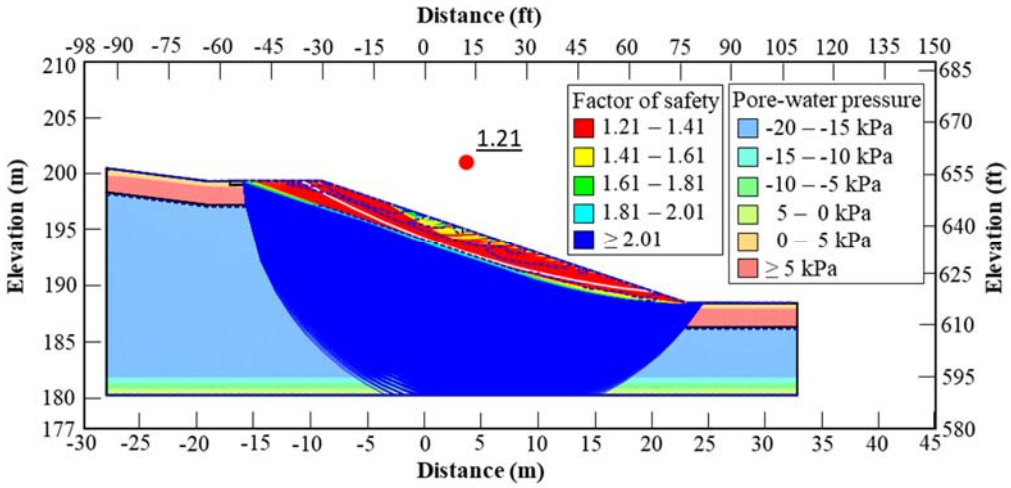
Distance (ft)
-98 -90 -75 -60 -45 -30 -15 0 15 30 45 60 75 90 105 120 135 150
Elevation (m)
210 205 200 195 190 185 180 177
Elevation (ft)
685 670 655 640 625 610 595 580
1.21
Factor of safety
1.21 – 1.41
1.41 – 1.61
1.61 – 1.81
1.81 – 2.01
≥ 2.01
Pore-water pressure
-20 – -15 kPa
-15 – -10 kPa
-10 – -5 kPa
5 – 0 kPa
0 – 5 kPa
≥ 5 kPa
-30 -25 -20 -15 -10 -5 0 5 10 15 20 25 30 35 40 45
Distance (m)

(a)

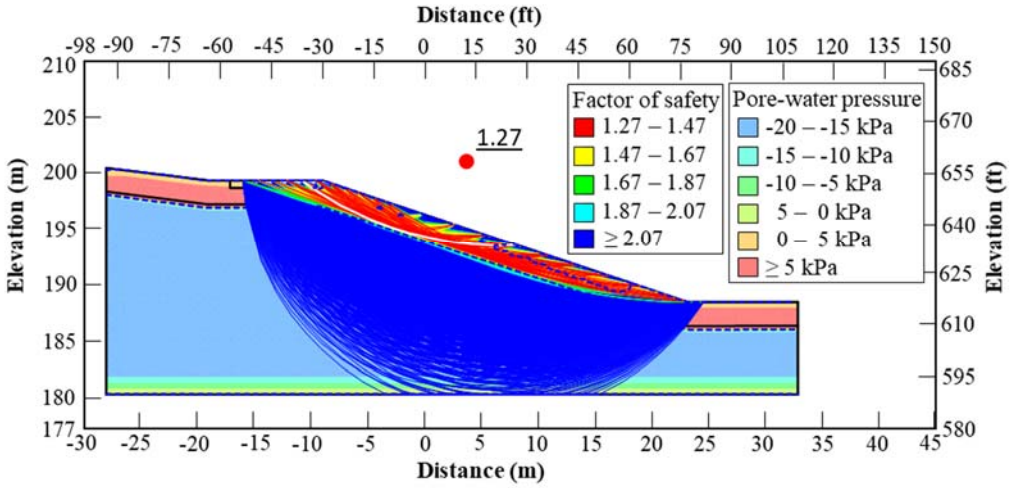
Distance (ft)
-98 -90 -75 -60 -45 -30 -15 0 15 30 45 60 75 90 105 120 135 150
Elevation (m)
210 205 200 195 190 185 180 177
Elevation (ft)
685 670 655 640 625 610 595 580
1.27
Factor of safety
1.27 – 1.47
1.47 – 1.67
1.67 – 1.87
1.87 – 2.07
≥ 2.07
Pore-water pressure
-20 – -15 kPa
-15 – -10 kPa
-10 – -5 kPa
5 – 0 kPa
0 – 5 kPa
≥ 5 kPa
-30 -25 -20 -15 -10 -5 0 5 10 15 20 25 30 35 40 45
Distance (m)

(b)

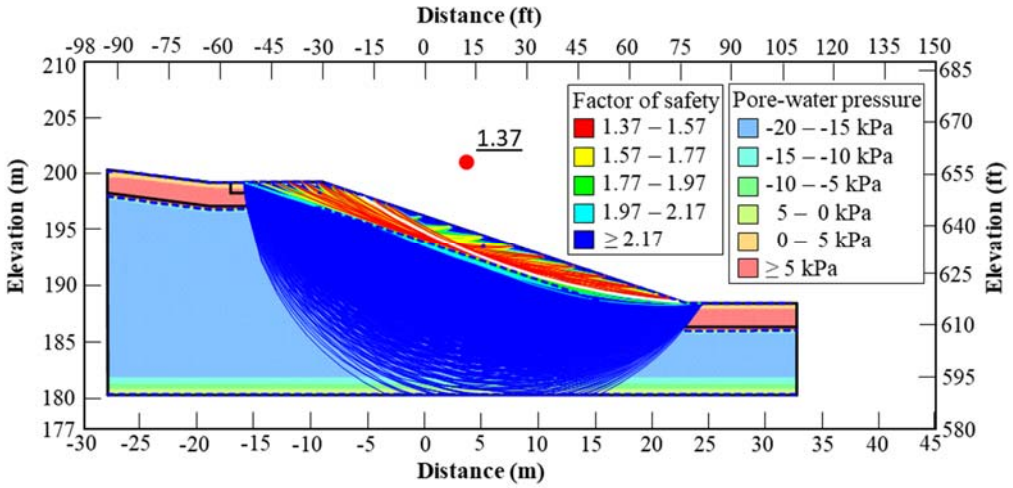

(c)

Figure 5.7 PWP variation and FOS calculated for lime stabilized slopes with thicknesses of (a) 30.5 cm, (b) 61.0 cm, and (c) 91.4 cm after subjecting 38.6 cm (15.2 in.) rainfall in ten days

The increase in FOS values of the critical slip surface of lime-treated slopes obtained with appropriate underlying drainage system was considerable, irrespective of the rainfall intensity and depth of treatment. Figures 5.8a, 5.8b, 5.9a, and 5.9b show the PWP distributions of 61 cm (2 ft) thickness of lime-treated slope section with and without underlying drainage system after subjecting to 38.6 cm (15.2 in.) rainfall events in ten days. The drainage of the rainfall facilitates the preservation of the unsaturated soil zones in the surface layer. Therefore, the soil suction contributed toward the soil strength and enhanced the FOS of the critical slip surface from 1.27 to 1.54 (Figures 5.8a and 5.9a).

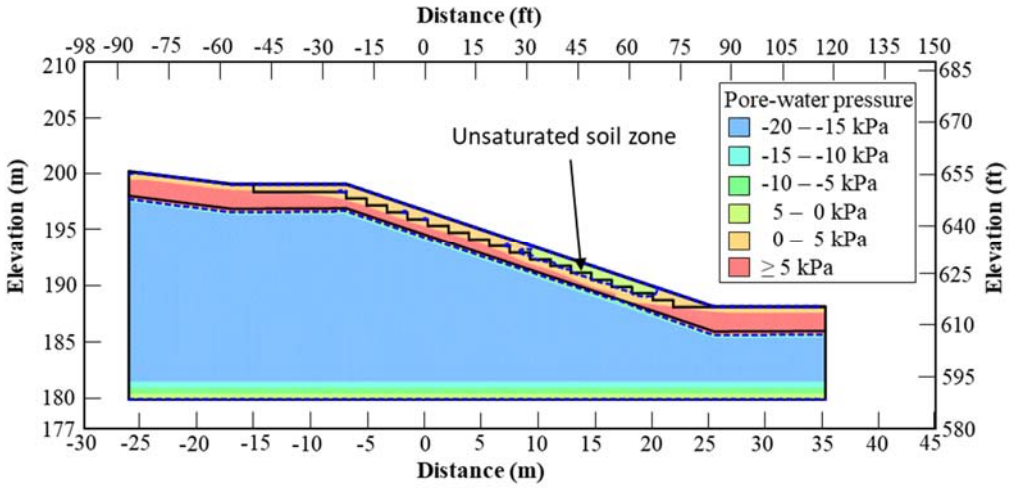

(a)

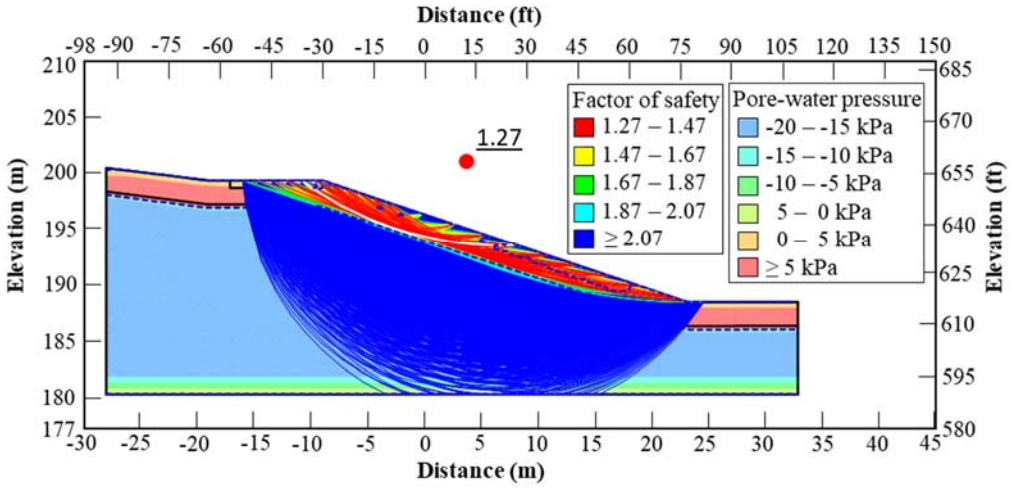

(b)

Figure 5.8 (a) PWP distribution and (b) FOS of 61.0 cm (2ft) lime-treated U.S. 75 Frontage Road slope without underlying drainage system after subjecting 38.6 cm (15.2 in.) rainfall in ten days

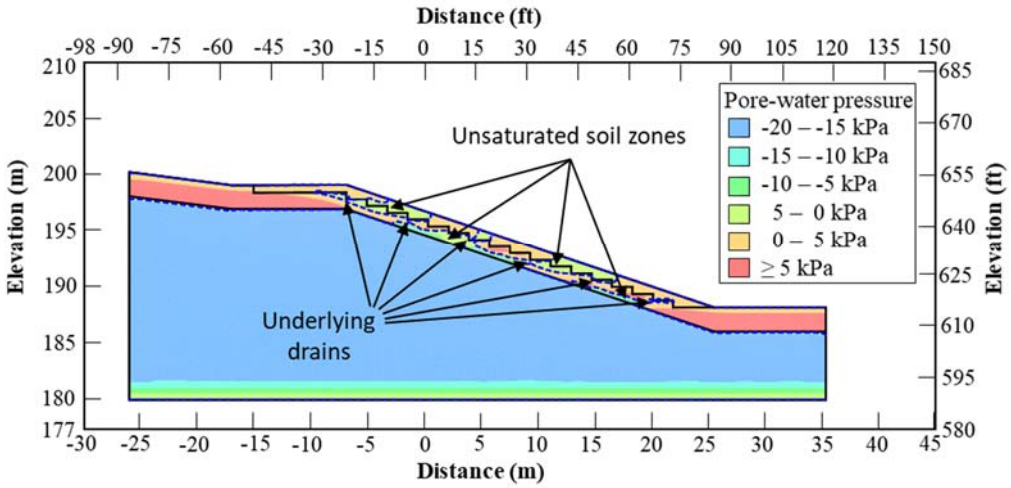

(a)

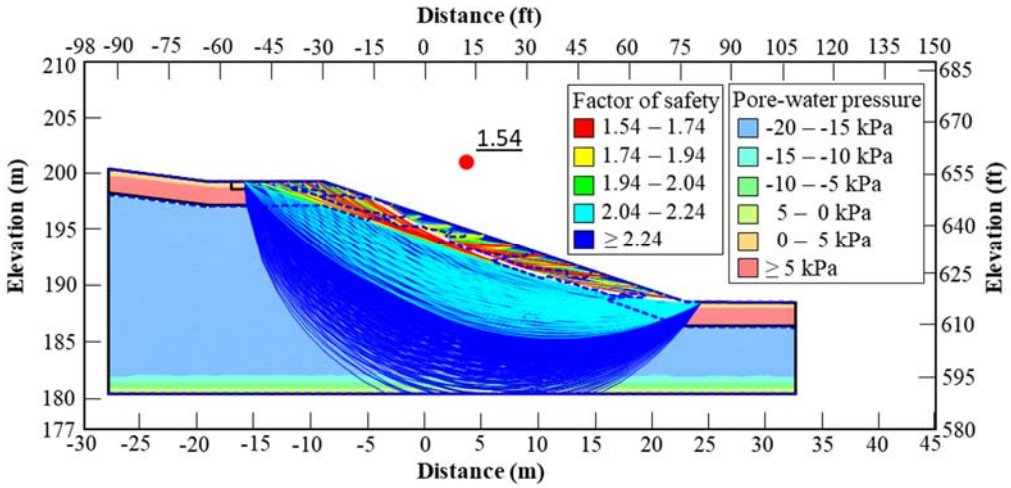

(b)

Figure 5.9 (a) PWP distribution and (b) FOS of 61.0 cm (2ft) lime-treated U.S. 75 Frontage Road slope with underlying drainage system after subjecting 38.6 cm (15.2 in.) rainfall in ten days

The numerical analysis results showed that the underlying drainage system was beneficial to boost the stability of the lime-treated slope. The minimum FOS of 1.5 was obtained with treatment of the top 61 cm (2 ft) of the slope surface with an underlying drainage system, irrespective of rainfall scenarios. Therefore, the 61 cm (2 ft) lime-treated surficial layer with a drainage system below the treated layer was considered the optimum method to rehabilitate this slope. Based on these findings, the construction plan to rehabilitate the slope of the U.S. 75 Frontage Road was prepared and its details are given in Chapter 6. The next section provides the results of numerical analyses studies for lime-treated slope sections of Grapevine and Joe Pool lake dams.

5.5 Results of Numerical Analyses Conducted on Slopes of Grapevine and Joe Pool Lake Dam

Rainfall-induced slope stability analyses were also performed to study the long-term performance of the lime stabilized Grapevine and Joe Pool lake dams' slope after subjected to weathering cycles. The FOS values of the critical slip surfaces and PWP distributions obtained for Grapevine and Joe Pool lake dams are given in Figures 5.10 to 5.13 and 5.13 to 5.17, respectively.

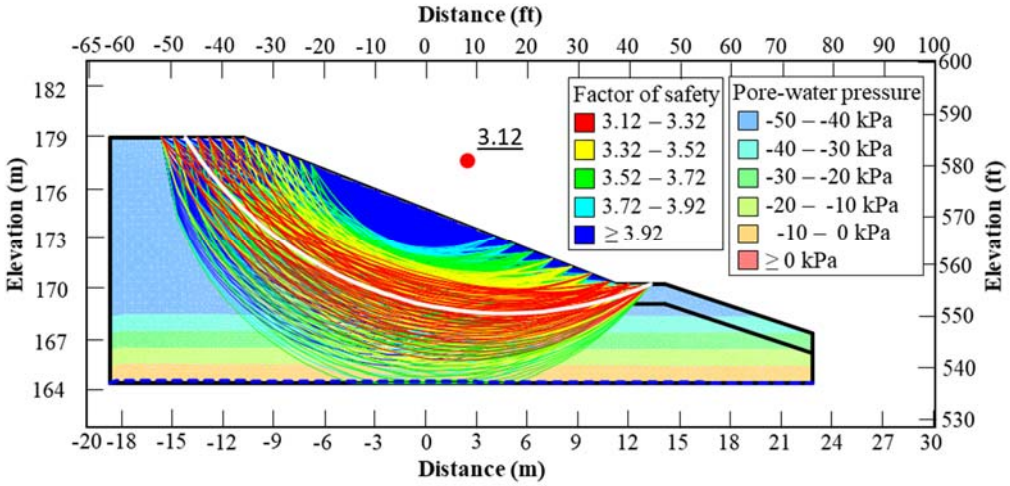

Figure 5.10 PWP variation and FOS of the lime-treated Grapevine dam slope before exposure to rainfall

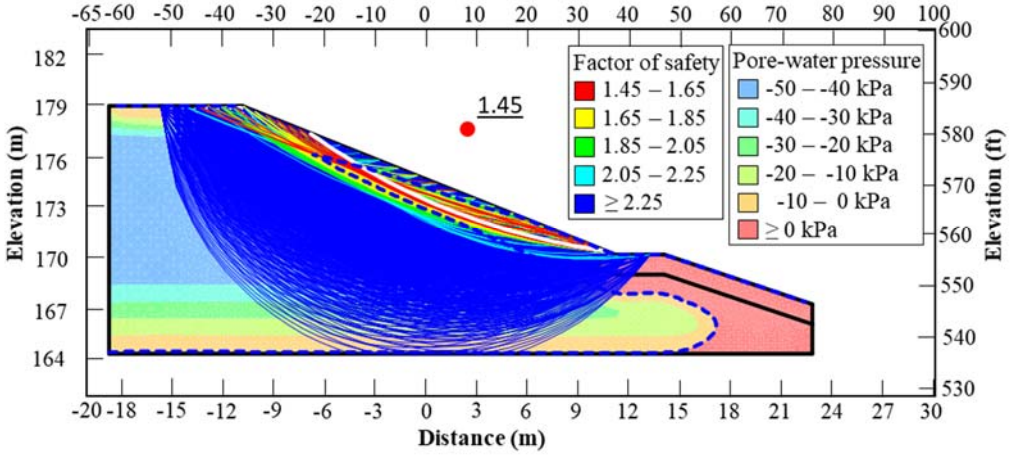

Figure 5.11 PWP variation and FOS of the lime-treated Grapevine dam slope after exposure to 23.1 cm (9.1 in.) rainfall in one day

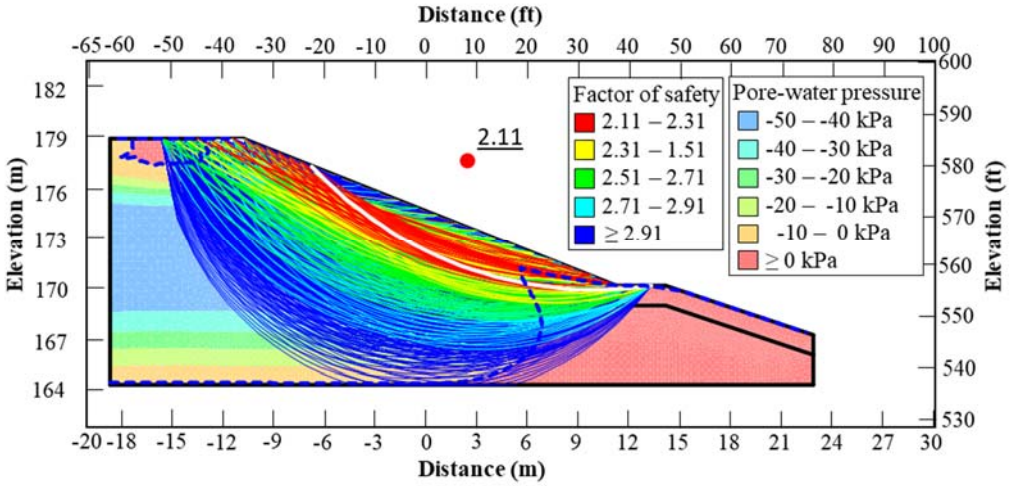

Figure 5.12 PWP variation and FOS of the lime-treated Grapevine dam slope after exposure to 31.0 cm (12.2 in.) rainfall in four days

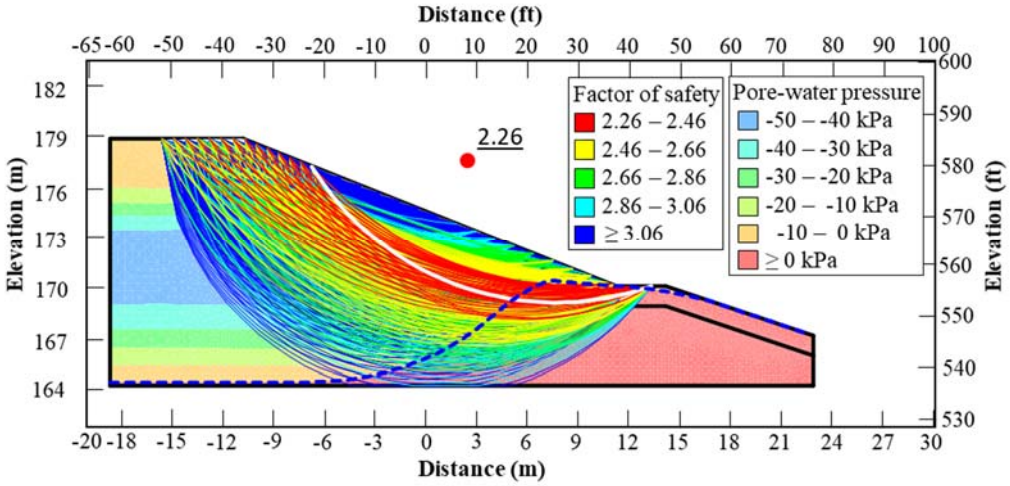

Figure 5.13 PWP variation and FOS of the lime-treated Grapevine dam slope after exposure to 38.1 cm (15.0 in.) rainfall in ten days

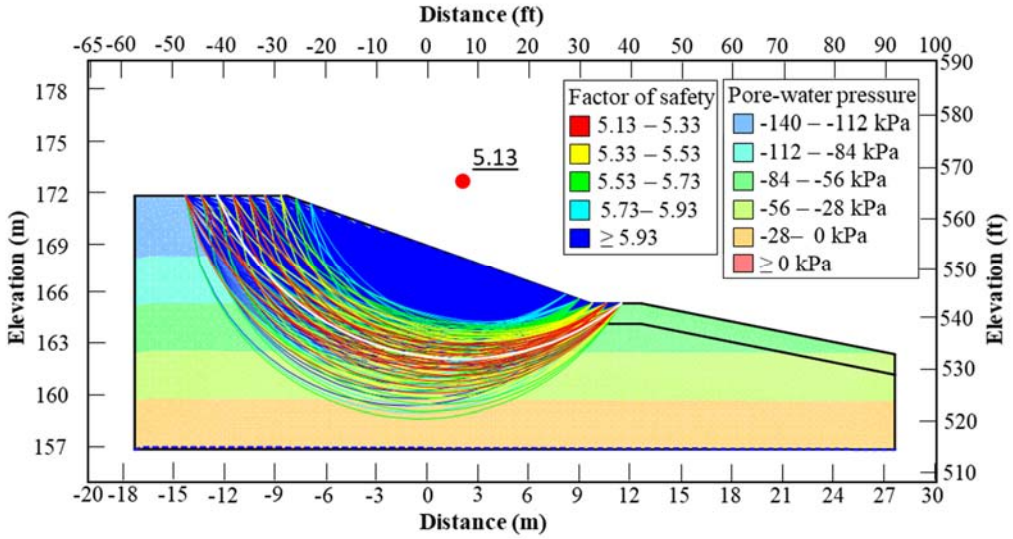

Figure 5.14 PWP variation and FOS of the lime-treated Joe Pool lake dam slope before exposure to rainfall

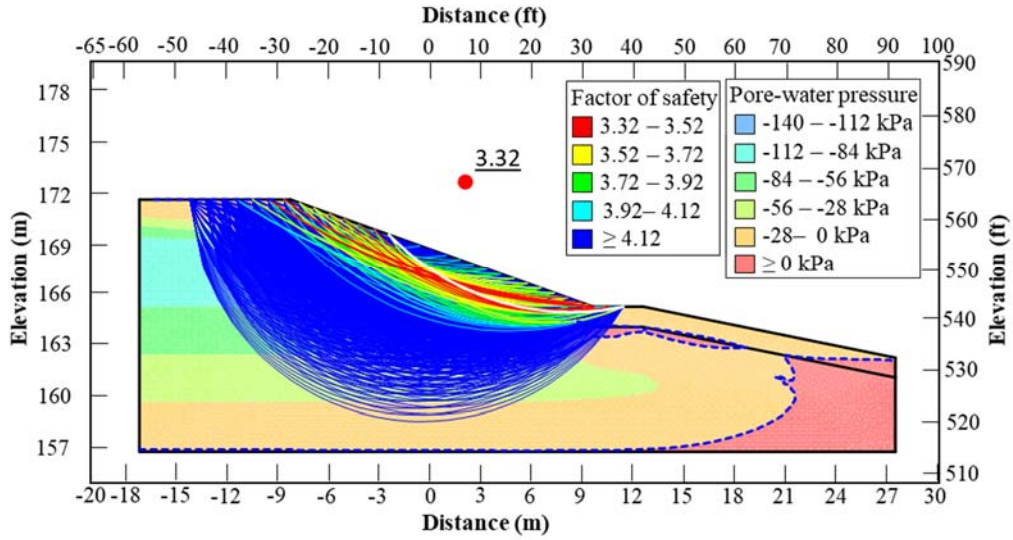

Figure 5.15 PWP variation and FOS of the lime-treated Joe Pool lake dam slope after exposure to 24.8 cm (9.5 in.) rainfall in one day

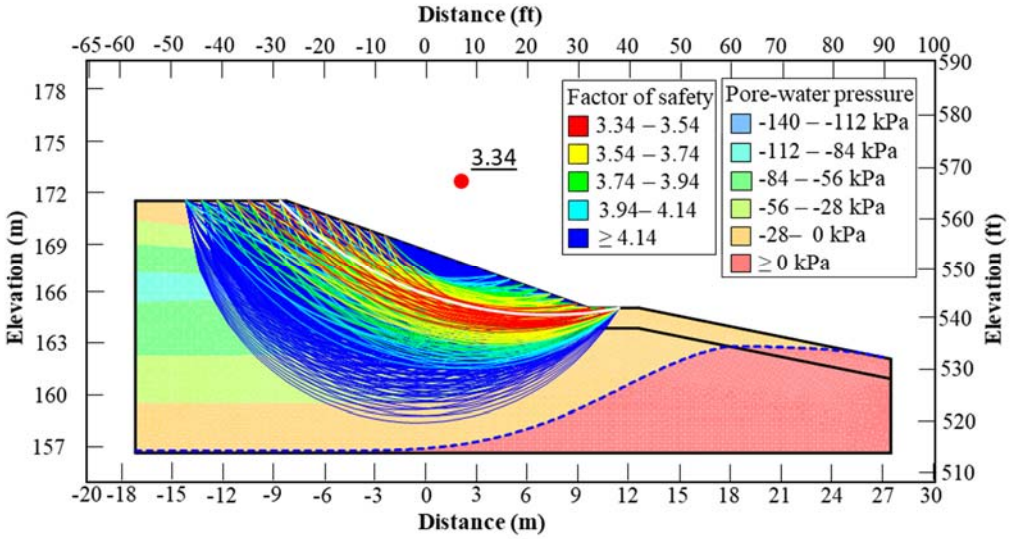

Figure 5.16 PWP variation and FOS of the lime-treated Joe Pool lake dam slope after exposure to 32.0 cm (12.6 in.) rainfall in four days

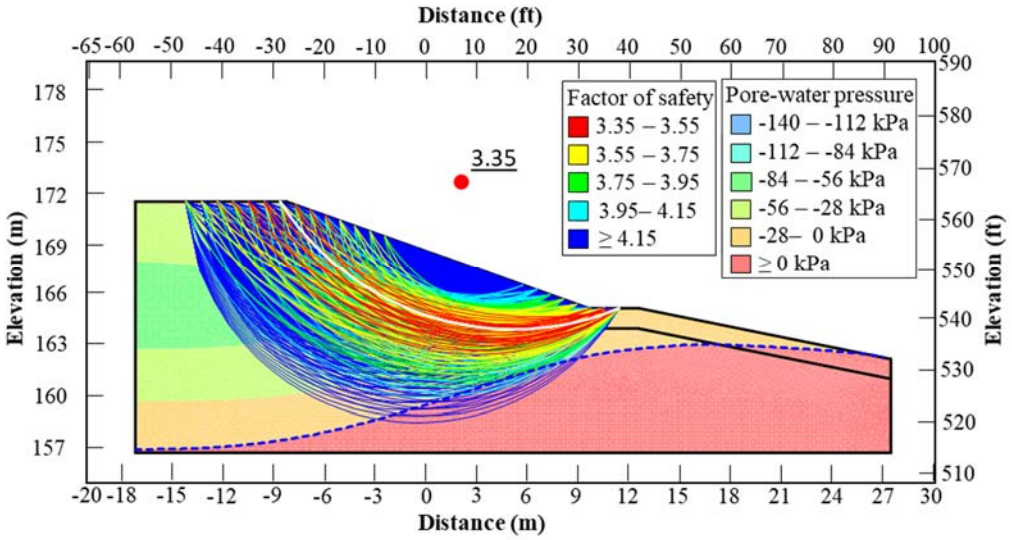

Figure 5.17 PWP variation and FOS of the lime-treated Joe Pool lake dam slope after exposure to 38.4 cm (15.1 in.) rainfall in ten days

Results of numerical studies showed that, in an average wet season, the slopes of Grapevine and Joe Pool lake dam had FOS of 3.12 and 5.13, before the rainfall events, respectively. After applying rainfall boundary conditions, the FOS of the most critical slip surface of these slopes were reduced to 1.45 and 3.32, respectively. Unlike the slope of the U.S. 75 Frontage Road that experienced the most drop in the FOS values after ten days of rainfall, these dams experienced the considerable drop in FOS values due to one day rainfall event with high flux rates of 2.7×10^{-6} m/s (9.1×10^{-6} ft/s) and 2.8×10^{-6} m/s (9.2×10^{-6} ft/s). This difference in results can be attributed to the differences in permeability value of soils.

The soil located in US 75 Frontage Road slope has a low permeability value of 3.02×10^{-10} m/s (9.90×10^{-10} ft/s) while soils in Grapevine and Joe Pool lake slopes have a medium-range permeability value of 8.1×10^{-6} m/s (2.65×10^{-5} ft/s) and 2.7×10^{-6} m/s (8.86×10^{-6} ft/s). In the case of high permeable soil, the soil allows the high intensity rainfall to seep into slope easily. Due to this, the soil experiences rapid saturation and a localized perched water table is formed in the desiccated surficial layer. Thus, the contribution of soil matric suction to strength decreases and results in a decrease in slope safety.

For four days and ten days rainfall events, the FOS of the critical slip surface of Grapevine and Joe Pool lake dams experienced a lower decrease than the same for one day rainfall event. These can be attributed to the water dissipation during the four and ten days of rainfall events. The high permeability of soils from

these dams allowed the infiltrated water to dissipate faster and prevent the slope surface layer from developing perched water table. From the results of these numerical studies on lime-stabilized Grapevine and Joe Pool lake dams' slopes, it can be concluded that the lime treatment work of surficial slope layers is an effective method of providing long-term stability to a slope with reduced surficial slope failures under harsh environmental conditions.

5.6 Summary

In this chapter, a series of rainfall-induced slope stability analyses were performed on the treated slope of the U.S. 75 Frontage Road, Grapevine, and Joe Pool lake dams using the limit equilibrium method. In these analyses, the short-term and long-term performances of slopes were investigated by incorporating the hydro-mechanical properties of the soil before and after exposure to the wet-dry seasonal cycles. The analyses were performed on untreated slope of the U.S. 75 Frontage Road using degraded hydro-mechanical properties to depict the potential reasons for slope failure.

A similar set of analyses were conducted on lime-treated slope models to assess the long-term performance of slopes after treatment. The analyses were conducted for three treated-layer thicknesses of 30.5 cm, 61.0 cm, and 91.4 cm (1 ft, 2 ft, and 3 ft), respectively, and based on these analyses of results, the optimum depth of lime treatment for the rehabilitation work of the U.S. 75 Frontage Road slope was determined.

Results of numerical studies showed that the U.S. 75 Frontage Road experienced shallow failure due to degraded soil hydro-mechanical properties after wetting and drying cycles. Under an intense and prolonged rainfall events (four days or ten days), there was a development of perched water table within the surface layer. This led to soil softening behavior followed by a decrease in mobilized shear strength which ultimately resulted in slope failures. After lime treatment, the slope showed much better performance as the computed FOS value was higher than unity. The minimum FOS values of the treated slope were obtained after ten days of rainfall event.

Treatment of the top 30 cm (1 ft) provided FOS value of 1.2, which was lower than the minimum required FOS of 1.5. The 61cm (2ft) treatment of the surface layer with a proper drainage system provided a minimum FOS of 1.54 under any rainfall events. In addition to the slope of US 75 Frontage Highway embankment, the long-term performance of lime stabilized slopes of Grapevine and Joe Pool lake dams' embankments were also assessed, which showed similar enhanced FOS values. The rainfall-induced unsaturated slope stability analysis with consideration of the effect of wet-dry cycles on properties of soil, provided sufficient FOS values when surficial soils were treated with lime additive.

Chapter 6

REHABILITATION, FIELD MONITORING AND LIFE CYCLE COST BENEFIT ANALYSIS

6.1 Introduction

The failed slope section of U.S. 75 Frontage Road was considered for a novel rehabilitation method using the lime treatment of surficial finite depth of soil, and the construction work for this repair was carried out at the site during the time period between July 2019 and May 2020. This chapter provides the details of field operations carried out for rehabilitation of the failed slope section. Based on the results from earlier laboratory and numerical studies, reported in Chapter 4 and Chapter 5, both design and construction plans were fully prepared and executed. These studies suggested that the use of 8% lime in soil was sufficient to enhance its strength, durability, and volumetric change characteristics, as well as improve the long-term stability of the slope. Moreover, provision of an underlying drainage system in the slope was recommended to further enhance the embankment section stability.

The performance of lime treatment field design and construction works was evaluated by using field instrumentation studies, total station and light detection and ranging (LIDAR) surveys. The variation in moisture content of embankment subsoil under varying climatic conditions (wet-dry seasons) was

recorded by moisture probes installed in the slope during the construction. Additionally, the deformation of the lime-treated slope was obtained by conducting both total station and LIDAR surveys. Also, the economic feasibility of the U.S. 75 Frontage Road slope rehabilitation work using the lime additive was evaluated by conducting life cycle cost and benefit analysis (LCCBA). The overall required cost expenditure and benefits of this method over a life cycle period was calculated and compared.

6.2 Rehabilitation of the Failed U.S. 75 Frontage Road

6.2.1 Construction Plan

The cross-section details of the lime-treated slope section of U.S. 75 Frontage Road is presented in Figure 6.1. Lime treatment was carried out on the surficial slope layer with a thickness of 61 cm (2 ft). The treated soil layer was then covered with a 15 cm (6 in.) thick layer of topsoil to facilitate vegetation growth at the slope surface after the construction. To enhance frictional resistance between untreated and treated soil layers, the embankment benching as shown in Figure 6.1 was provided in untreated soil layer with 90º angle cuts. This benching also eliminated existing slickened slide planes and facilitated the repair works by providing horizontal layers in the slope. Below the lime-treated layer, a total of 6 longitudinal perforated drainpipes were installed along the slope at 5.5 m (18 ft) spacing to drain infiltrated water out of the slope. The next section presents the construction steps followed in the slope treatment and field construction work.

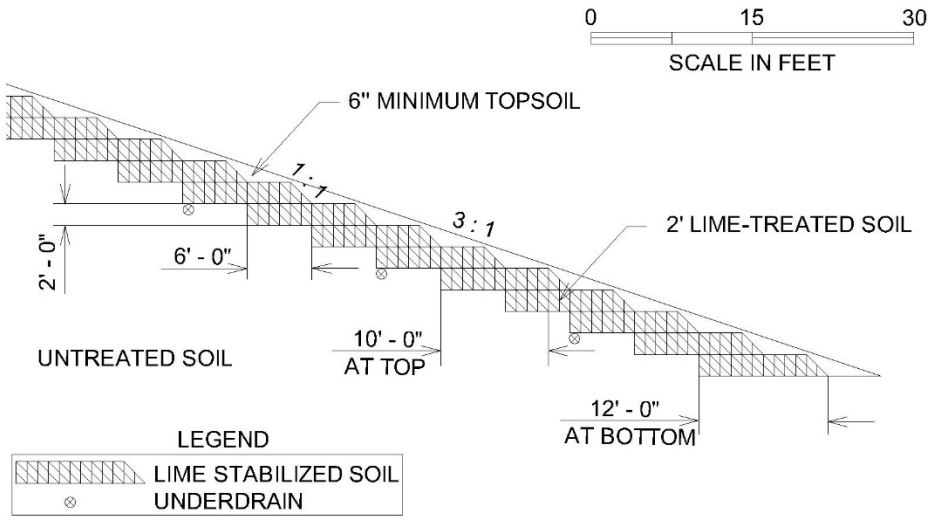

Figure 6.1 Plan details of lime-treated slope section of the U.S. 75 Frontage Road

6.2.2 Construction Steps

6.2.2.1 Excavation Phase

Before the start of construction in July 2019, the major portion of the failed section of the slope was extended to approximately 45.7 m (150 ft) in longitudinal direction with 1.8 m (6 ft) failure depth (Figure 6.2). Along with that, a minor failure occurred on each side of the failed portion of the slope due to impact of weathering cycles. The total failed section of slope was extended to 134.7 m (442 ft) in longitudinal direction and the failed debris reached to the toe of the slope (Figure 6.3). To optimize the excavation work and increase ease of constructability, an excavation plan was prepared and executed as shown in Figure 6.4. The excavation was carried out by making cuts of small angles to facilitate

material transportation by dump trucks. As the debris was reused in the construction, it was stocked at designated stock area in an adjacent farmland. Along with the slope debris, the topsoil of the slope was also excavated and stored separately to prevent mixing of the vegetation and organic soil in the lime-treated soil zone.

Figure 6.2 Failed portion of slope

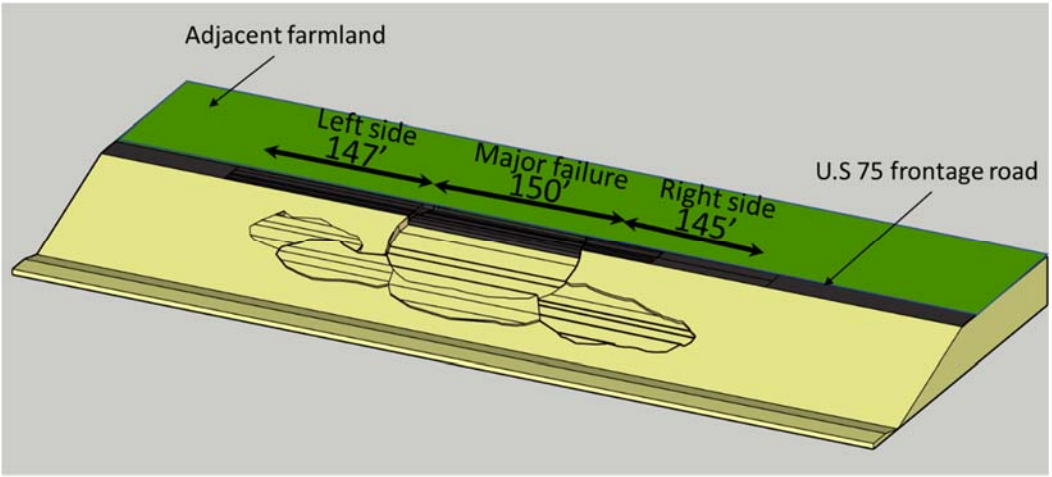

Figure 6.3 Schematic of failed slope of U.S. 75 Frontage Road

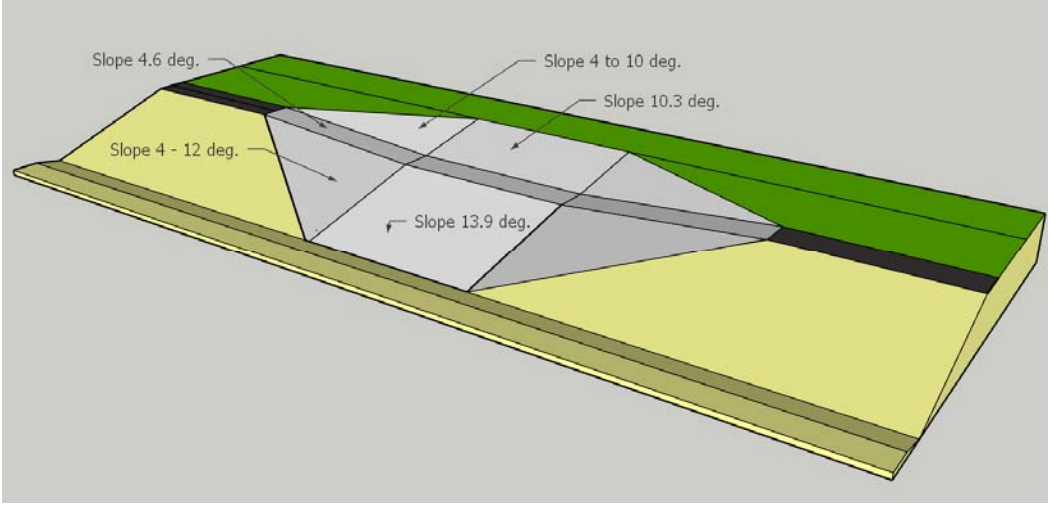

Figure 6.4 Excavation plan adopted for the failed slope

6.2.2.2 Lime Treatment

In this task, quicklime (Calcium Oxide (CaO)) was used to stabilize the soil from the failed slope zone. Quick lime was brought to the construction site in bulk amounts from the manufacturer with tanker tracks and was then hydrated in

portable lime slakers (Figure 6.5a). During the hydration of lime, an exothermic reaction takes place between water and quicklime, which converts CaO to $Ca(OH)_2$. The hydration process was continued for approximately an hour, and once it was over, the hydrated lime was transferred to the construction site using trucks (Figure 6.5b).

At the field site, lime treatment work was started from the toe area of the slope. In order to provide a better interlocking between the untreated soil and treated layer, the existing untreated soil layer was benched by providing a vertical cut of 0.61 m (2 ft) height with the help of a motor grader machine and crawler dozer (Figure 6.6a). The excavated soil was transferred back to the slope, dumped in lifts of 0.61 m (2 ft) in height and 3.65 m (12 ft) in width (Figure 6.6b), and was graded using a crawler dozer (Figure 6.6c).

(a)

(b)

Figure 6.5 (a) Portable lime slaker and (b) transportation of hydrated lime

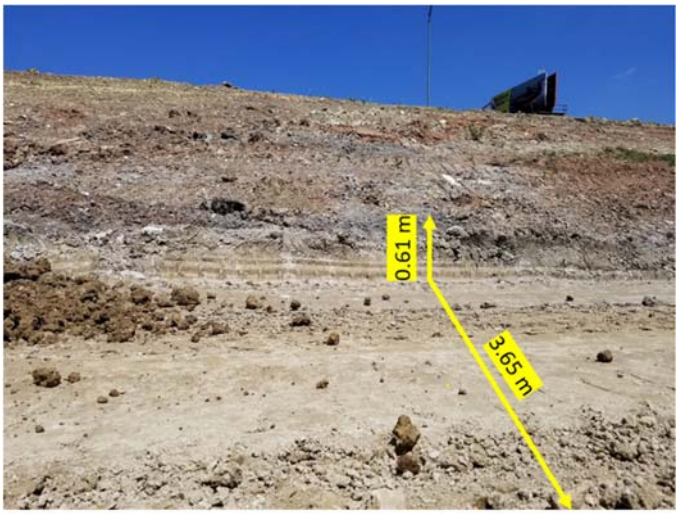

(a)

(b) (c)

Figure 6.6 (a) Benched slope section, (b) transportation of untreated soil, and (c) grading the untreated soil layer

Before mixing the lime slurry with untreated soil, a windrow was built with a crawler dozer to prevent flow of lime slurry from the sides (Figure 6.7a). The lime slurry was then transferred and poured on the untreated soil layer by using a

distributor truck (Figure 6.7b). To maintain the homogeneity and uniform distribution of lime in soil, the slurry was simultaneously blended in soil using a rotary mixer (Figure 6.7c). After a thorough mixing of the lime slurry and soil blend, the lime-treated layer was compacted (0.3 m in height) using a sheepsfoot type roller (Figure 6.7d). The entire surface of the slope section was treated by following the aforementioned process.

(a) (b)

(c) (d)

Figure 6.7 (a) Windrow to prevent lime slurry runoff from sides, (b) application of hydrated lime slurry, (c) mixing of lime slurry in soil with rotary mixer machine,

and (d) compaction of lime-treated layer with a sheepsfoot type roller

6.2.2.3 Installation of Drainage System

Horizontal drains are often used to lower down the water levels in the slope and to improve its stability. Because of the ease of installation and relatively high installation speed, horizontal drain is a preferred choice in any slope stabilization project. In the current slope rehabilitation project, 6 longitudinal PVC perforated pipes were placed beneath the lime-treated soil layer along the slope at 5.5 m (18 ft) spacing. As shown in Figure 6.8a, the PVC drainpipe was placed in a trench of 0.3m (1ft) width and 0.3 m (1ft) depth. The surface area of trench was covered with geotextile material, and the space between drainpipe and geotextile was filled with Type B filter material to prevent clogging of the drainage system.

The schematic view of the treated slope section, with all components of the drainage system, is presented in Figure 6.8b. In order to ensure free flow of water under gravity, the drains were placed at a 0.2% fall to the north side. The ends of all longitudinal drains were connected to a lateral non-perforated underdrain pipe of 152.4 mm (6 in.) diameter. Therefore, rainfall water collected by longitudinal drains will migrate to lateral drainpipe and ultimately drain out to roadside drain. A concrete head wall with a galvanized wire mesh system was built at the outlet of lateral drainpipe to prevent wild creatures or trash into the drainage system.

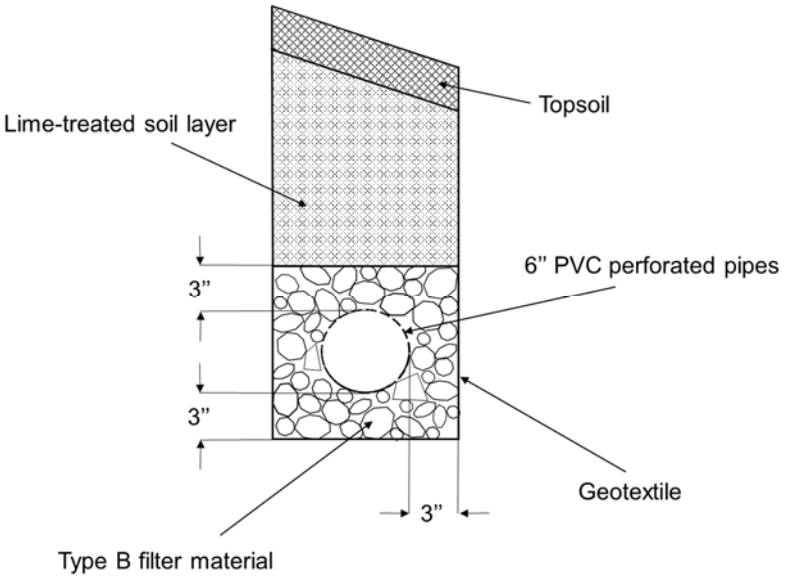

(a)

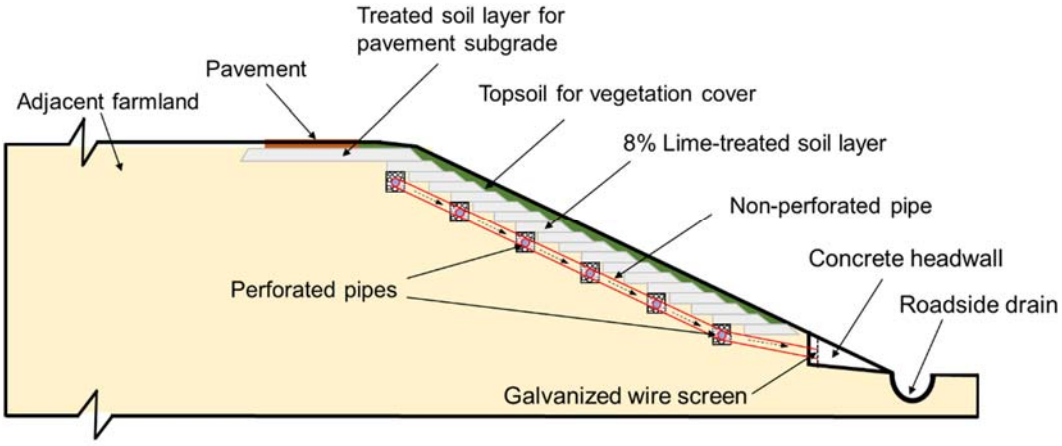

(b)

Figure 6.8 (a) Cross section of underdrain in trench and (b) schematic view of drainage system in the slope

Figure 6.9 shows the installation process of perforated pipes in the longitudinal direction. The underdrains were installed just before the placement of

the lime-treated soil layer. Figure 6.10 shows the connection between longitudinal and lateral drainpipes, and another PCV pipe was provided to flush out the drains in case of potential soil clogging. The exit points of these flushing pipes were kept on the surface of slope with moveable lids.

Figure 6.9 Installation of longitudinal underdrains

Figure 6.10 Connection of longitudinal and lateral drainpipes

6.3 Quality Control and Assurance Studies

During the slope rehabilitation work, the quality control and assurance studies were conducted using site inspections and quick laboratory tests. Several 1D swell-shrinkage strain tests, DS tests, pH control tests were conducted on the field treated soil samples, and the water content and dry density of samples were determined. All the laboratory tests conducted on field samples were performed as per the procedures mentioned in Chapter 4. These results were compared with results of soil-mix design studies to assess the quality of field construction. Table 6.1 presents the targeted and achieved results of rehabilitation work of U.S. 75 Frontage Road. The results of tests conducted in the laboratory and field showed a reasonably good agreement, confirming that the lime stabilization closely simulated the laboratory mixing process.

Table 6.1 Results of field quality control and assurance studies

Value	**Soil Unit Weight & Water Content**		**Swell-Shrinkage Characteristic**		**Soil Peak Strength Parameters**	
	MC (%)	**DUW kN/m^3 (pcf)**	**1D Swell Strain (%)**	**1D Shrinkage Strain (%)**	**c' kPa (psf)**	**ϕ' (deg)**
Laboratory Samples	23.0	15.8 (100.8)	0.37	10.7	37.0 (772.8)	39.1
Field Samples	23.7	14.9 (95.1)	0.25	10.0	30.9 (645.4)	42.9

6.4 Measurement of Field Moisture Fluctuation

One of the main objectives of lime treatment work of soil is to prevent the development of desiccation cracks and intrusion of water into deeper layers of soil. The fluctuation in moisture content of lime-treated soil during or following a rainfall event was monitored by using moisture probes. During the construction, three probes were placed in the slope at depth of 0.45 (1.5 ft), 0.76 m (2.5 ft), and 1.68 m (5.5 ft) from the ground surface (Figure 6.11). To record the moisture data, a data logger was safely placed under the nearby bridge and was connected to all the probes with cables. These cables were encapsulated with PVC pipes to prevent them from getting damaged from the construction activities (excavation or mixing of soil) (Figure 6.12). The moisture data was recorded every 15 minutes automatically in a data logger and was transferred to a laptop during site visits. The moisture fluctuation in soil of rehabilitated slope was measured for a period of 17 months (from December 2019 to May 2021).

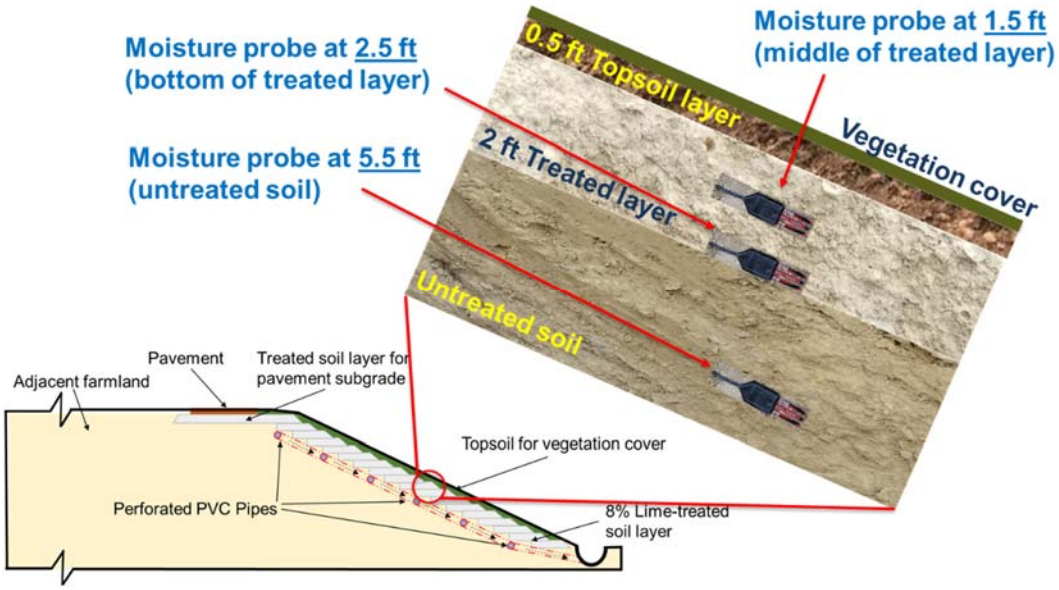

Figure 6.11 Schematic representation of location of moisture probes

(a) (b)

Figure 6.12 Installation of moisture probes (a) at depth of 0.45 m (2.5ft) at middle of treated soil and (b) at depth of 1.68 m (5.5 ft) at untreated soil

The rainfall data at the nearest rainfall station to slope section of U.S. 75 Frontage Road for the period between December 2019 to May 2021 was obtained from NOAA for and is shown in Figure 6.13. In this period, a total of 133.6 cm (52.6 in.) rainfall was recorded, and the highest daily rainfall (10.8 cm (4.25 in.)) was observed on 9-1-2020. Also, the wettest month was May 2020 (25.96 cm (10.22 in.)) and the driest month was December 2019 (2.76 cm (1.08 in.)). In this investigation period, while the months of March, April, and May 2020 represent the wettest season (52.15 cm (20.53 in.)), July, October, November, and December 2020 represent the dry seasonal condition (13.85 cm (5.45 in.)).

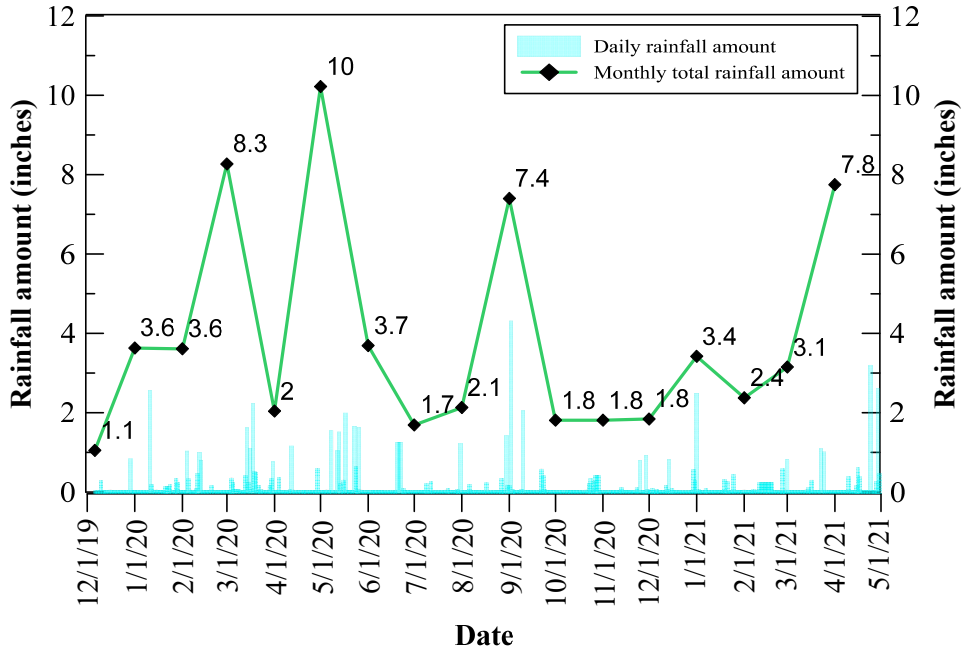

Figure 6.13 Recorded monthly rainfall data for U.S. 75 Frontage Road

To compare the moisture variation at different depths of the slope, the results from all 3 moisture probes are plotted together in Figure 6.14. The plots show that the trend of moisture variation in lime-treated layer at 0.45 m (1.5ft) and 0.76 m (2.5ft) depth was quite similar throughout the observation period. The bottom of lime-treated soil layer was found to have a lower moisture content than the same of the middle of treated layer. During a rainfall event, the increase in moisture content of soil was minimum in the untreated soil layer. These observations suggest that the moisture intrusion into slope in the lime-treated surficial layer was limited and took a longer time to infiltrate into deeper layers.

Based on moisture probes data, the soil at the middle and bottom of the lime-treated layer was found to reach nearly 100% saturation once and twice, respectively, during the monitoring period. Unlike the treated layer, soil in untreated layer was never completely saturated during any rainfall event throughout the observing period. This phenomenon showed that the wetting front was not able to reach into the deeper layer (untreated soil) which implies the absence of desiccation cracks. Results also showed that the moisture content of untreated soil was decreased by 5.44% over a period of 17 months. This can be attributed to presence of drainage system under the lime-treated layer. Most of the moisture infiltrate during the rainfall was discharged by drainage system before it seeped down into untreated layer. Based on these findings, it can be concluded that

the overlying lime-treated layer successfully shields the untreated soil from wet-dry seasonal cycles and prevents moisture intrusion into the slope subsoils.

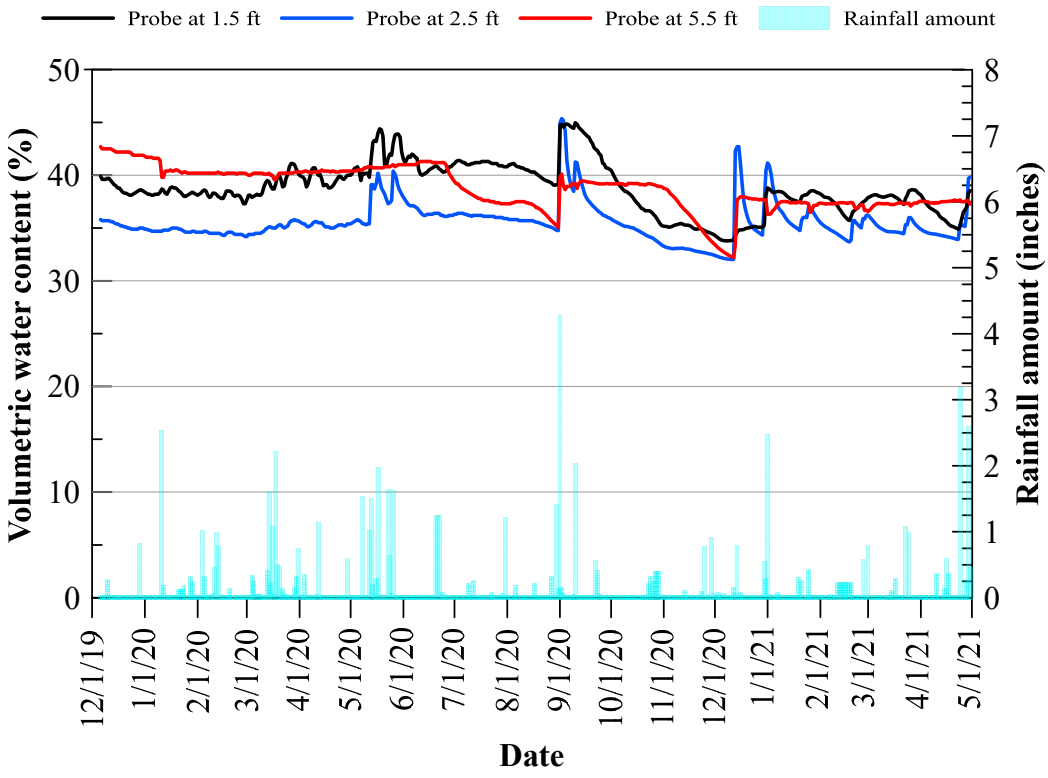

Figure 6.14 Obtained moisture content data from probes at 0.45 m (1.5 ft), 0.76 m (2.5 ft), and 1.68 m (5.5 ft)

6.5 Monitoring of the Vertical Ground Movements

The vertical deformation of the slope due to swelling and shrinkage of soil was monitored by conducting routine field surveys. These post-construction elevation surveys were performed using a total station and LIDAR equipment on the treated slope section. The first elevation survey was carried out on 10th October 2020, and the subsequent surveys were performed monthly. Using the filed

surveys, swell-shrinkage performance of the treated slope section was evaluated. The following section presents details of the survey methods followed.

6.5.1 Total Station Surveys

The total station survey is one of the preferred surveying methods that have been widely used by many agencies. This equipment contains a distance measuring device, theodolite, and a data collector. The elements of total station are presented in Figure 6.15. With the help of total station, the three-dimensional coordinates (X, Y, and Z coordinates) of a single survey point can be determined. The surveying is conducted with an operator who uses total station and takes readings and another person who hold the prism pole. The prism pole is placed on the designated survey points, and the three-dimensional coordinates of each survey point are calculated with respect to fixed reference point. After determining the coordinates, the elevation of the survey points can be calculated using the following equation (Wang 2017).

$$H_T = H_s + H_I \pm L\sin\left(\frac{\pi}{2} - V\right) - H_R \quad (6.1)$$

Where,

H_T= Elevation of survey point,

H_s = Elevation of reference point,

H_I = Height of installed total station,

L = Slope distance between total station and prism,

H_R = Height of placed prism, and

V = Vertical angle between total station and prism (Figure 6.15).

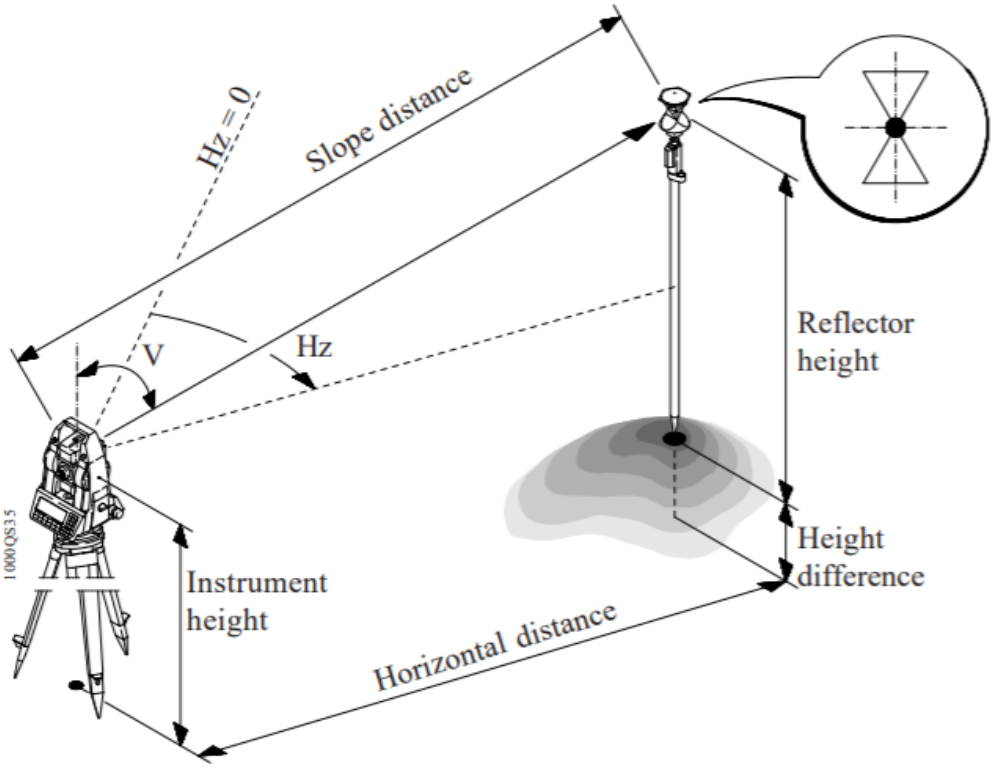

Figure 6.15 Total station surveying elements (Leica 2006)

In this study, total station surveys were performed to obtain deformations in both the treated slope section and shoulder of the pavement. A grid of survey points with 5 columns and 6 rows was formed with longitudinal spacing of 100 ft and lateral spacing of 25. Figure 6.16a shows the schematic view of survey design with notation used in this study. The benchmark point was set at a nearby bridge abutment with fixed elevation, and the vertical movements (swell-shrink strains)

of the survey points were measured with periodic site visits (Figures 6.16b and 6.16c).

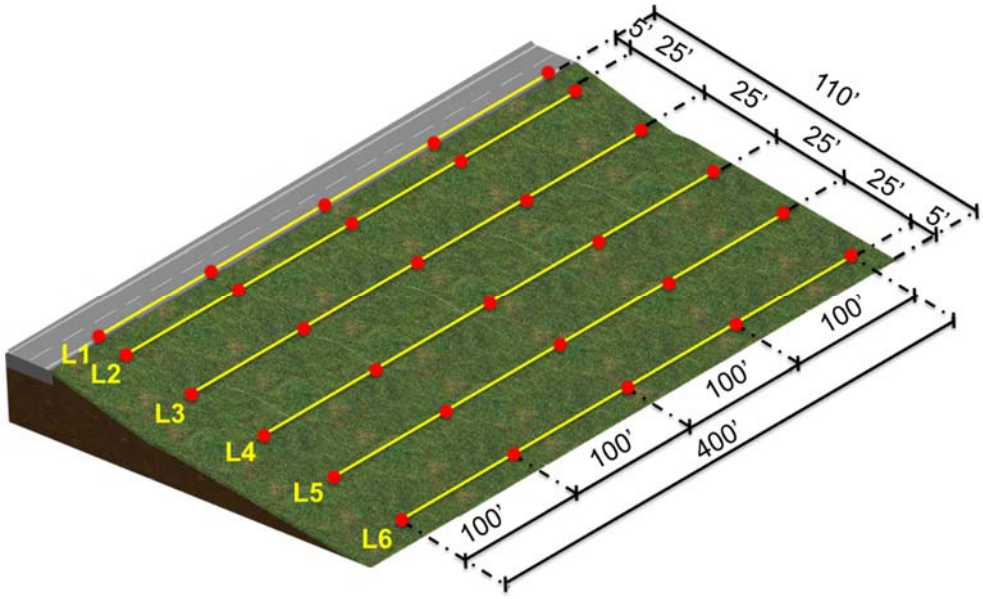

(a)

(b)

(c)

Figure 6.16 (a) Schematic showing arrangement of survey points, (b) a survey point on slope, and (c) total station surveying

6.5.2 LIDAR Surveys

3D terrestrial LIDAR surveying is one of the newest technological developments which can be used to measure the ground movement. The active remote sensing technology of the LIDAR includes a group of sensors to locate the objects, global positioning system receivers, and altimeter (Lefsky et al. 2002). By conducting LIDAR scan, all the objects in 3D space can be covered, and the ground movements can be tracked efficiently and accurately (Shafikhani 2018). In 3D LIDAR technology, a stream of focused laser beams is emitted using a rotating mirror towards the target object in scanned place. These reflected signals are received by the receiver units, and a dense point cloud of the scanned object is produced by calculating the elapsed time between the received and emitted pulses (Campbell and Wynne 2011). Based on the quality and resolution settings selected by operator, several hundred million of points can be stored in a single scan. The time required for each scan can vary from several minutes to couple of hours depends on the selected these settings, the geometry, and size of scanned area.

Before performing a LIDAR scan, it is necessary to plan and prepare the survey such that the entire area needed to be covered can be scanned with a minimum number of LIDAR scanning sets with a specified quality setting. These setting can be obtained from equipment manuals or can be determined by following a trial and error approach (Shafikhani 2018). After conducting a set of LIDAR scans, all the scans are aligned and registered in a single project point

cloud using a computer program. The different project point clouds are rotated to the same coordinate system with a help of fixed reference points, and the displacements of the scanned objects with respect to other scans are determined.

Unlike the total station survey, which is time intensive and requires to stop to traffic, LIDAR surveying can be performed in less time and without traffic interruption (Shafikhani 2018). Therefore, in this research work, an approximately 10,452 ft^2 of area including stabilized slope section and pavement was scanned by LIDAR surveys. Figure 6.17a shows the area of slope where vertical deformations were calculated using LIDAR scans. The optimum LIDAR surveying plan was prepared based on the scanned site area as per Shafikhani (2018). For each survey, a total of 6 LIDAR scans were performed with a ¼ resolution and 4x quality settings.

LIDAR scans were conducted using the 6 spheres of radius 11.4 cm (4.5 in.), and registration of each individual scans in a single point clouds were accomplished using these artificial reference points (Figure 6.17b). Rotation of project clouds are also used achieved using the same size 3 spheres with a fixed elevation placed on the nearby bridge abutment. The registration and rotation of scans was performed by using the Scene software, and determination of relative elevation displacement were computed using the Builder add-ons. The next section provides the results obtained from these surveying works.

(a) (b)

Figure 6.17 (a) LIDAR surveying area and (b) LIDAR surveying on the treated slope section

6.5.3 Vertical Deformation Results

The elevation surveys were carried out periodically by using the same survey points each time, and an average change in elevation of slope surface was calculated. The results from the survey conducted using total station are presented in Figure 6.18. Along with it, the variation in moisture content of the untreated soil at 1.68 m (5.5 ft) depth is also presented. The results show that during the observation period of 7 months (between October 2020 to May 2021), the newly stabilized slope section performed exceptionally well. The vertical deformations were very small and never exceeded 25.4 mm (1 in.) during this period. Also, it was observed that change in elevation of ground was related to variation in moisture content of the untreated soil. It implies that there was negligible swelling-

shrinkage observed in treated slope, and the deformation of slope can be attributed to the small fluctuations in moisture content of untreated soil.

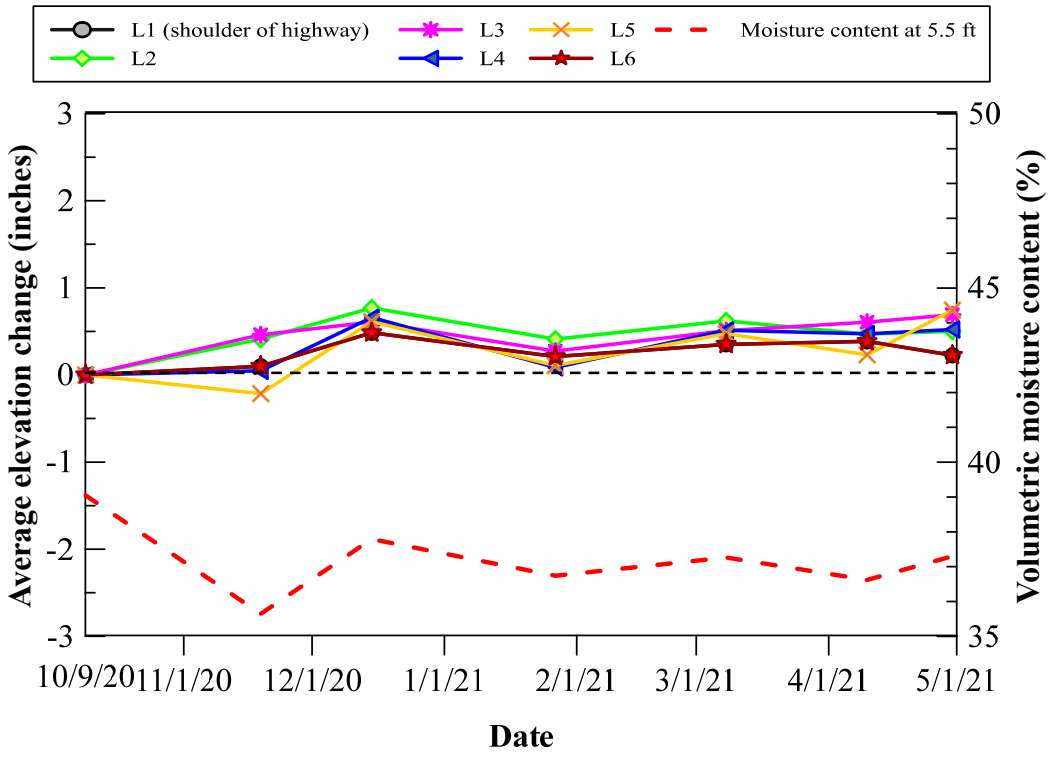

Figure 6.18 Elevation changes measured on shoulder of pavement and slope and variation of untreated soil moisture content at 5.5 ft

Throughout the observation period, the crest of slope was found to experience the maximum swelling deformations than any other part of the slope. The magnitude of deformation was found to decrease down the slope with minimum deformations at the toe of slope. This phenomenon can be attributed to higher infiltration in the crest than toe of a slope. Similar observations are noted in the literature (Gasmo et al. 2000). The water in the crest of slope seeps

downwards towards the toe of the slope allow more water to infiltrate. Also, the results of total station surveys showed that the vertical deformation measured on the pavement structure (L1, shoulder of pavement) was generally lower than the deformations measured on the slope surface. This phenomenon can be attributed to higher overburden pressure due to presence of pavement structure and the lower permeability values of hot mixed concrete asphalt (HMCA) than the soil in the surficial layer of slope. This lower permeability value possibly caused lesser infiltration into the soil below the pavement structure than soil present in the surficial layer of slope.

After processing the LIDAR scans using a computer software, the processed survey scans of the embankment slope and the pavement structure were prepared. The obtained heatmaps of elevation of treated slope section for different period of LIDAR surveys are shown in Figures 6.19a, b, c, and d. The heatmaps were used to calculate the changes in elevation of the entire scanned area. These results showed that surface of the newly stabilized slope did not experience any significant elevation changes due to environmental factors.

These results also suggest that the newly stabilized slope preserved its global stability and did not experience erosion during the rainfall events. Due to fluctuation in thickness of vegetation cover with time, the precise calculation of deformation on the slope surface with the LIDAR surveys was difficult. Therefore,

the LIDAR surveys were used to determine the elevation changes on middle of each lane of the pavement section as shown in Figure 6.20.

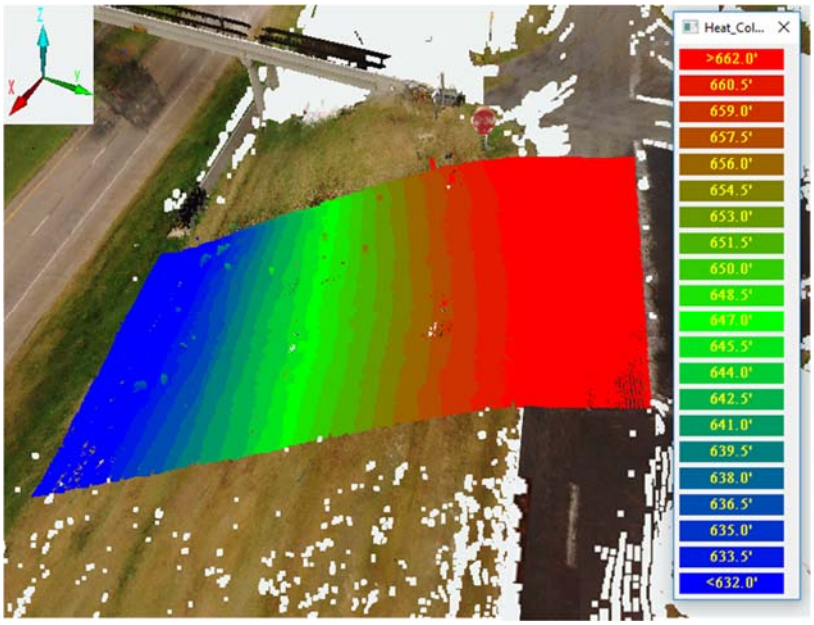

(a)

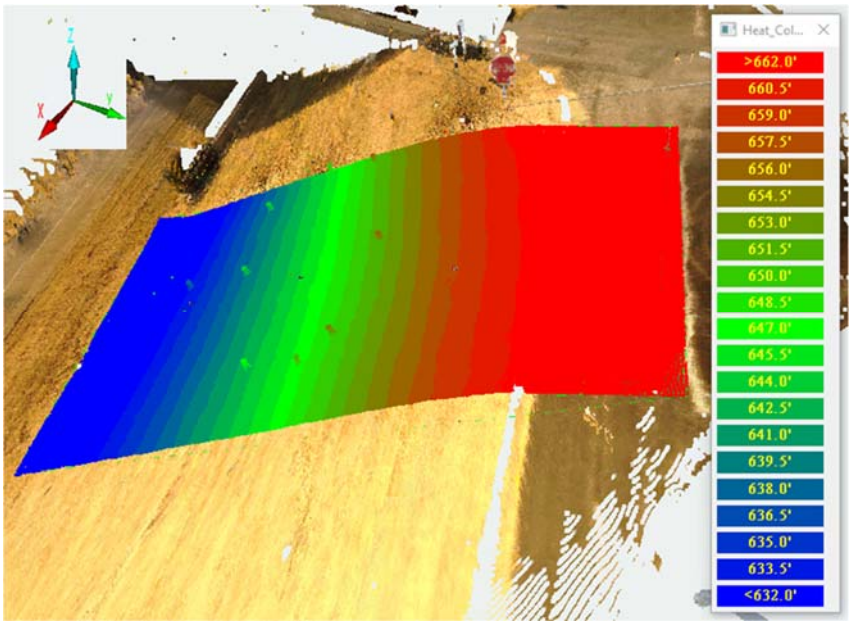

(b)

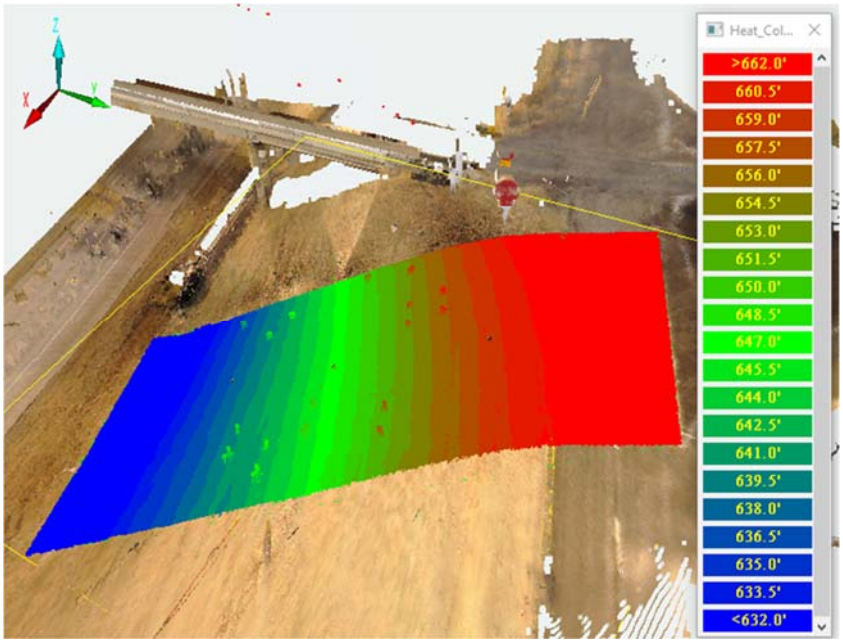
Heat_Col...
>662.0'
660.5'
659.0'
657.5'
656.0'
654.5'
653.0'
651.5'
650.0'
648.5'
647.0'
645.5'
644.0'
642.5'
641.0'
639.5'
638.0'
636.5'
635.0'
633.5'
<632.0'

(c)

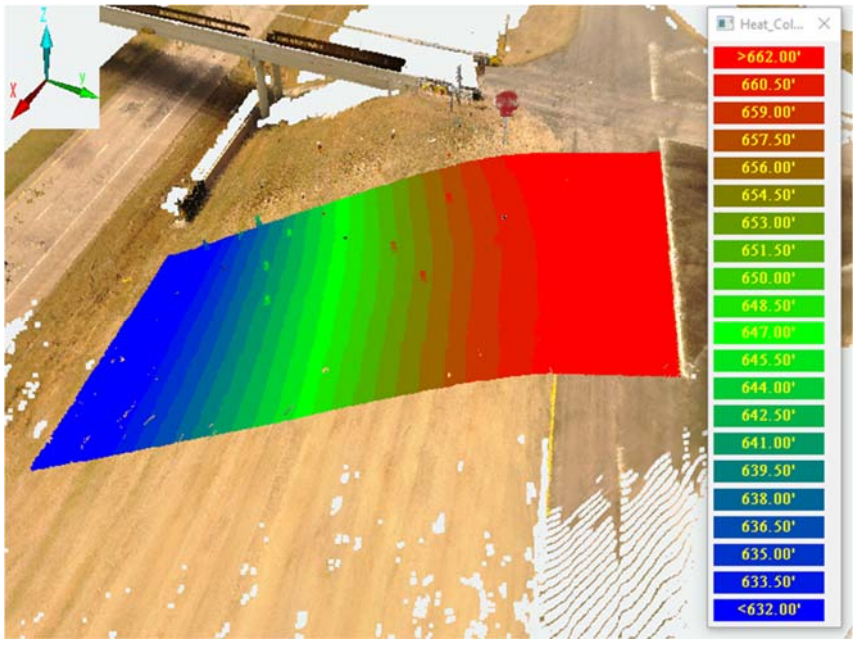
Heat_Col...
>662.00'
660.50'
659.00'
657.50'
656.00'
654.50'
653.00'
651.50'
650.00'
648.50'
647.00'
645.50'
644.00'
642.50'
641.00'
639.50'
638.00'
636.50'
635.00'
633.50'
<632.00'

(d)

Figure 6.19 Heatmaps of the elevation of the slope section for (a) November 2020 (b) December 2020, (c) January 2021, and (d) March 2021

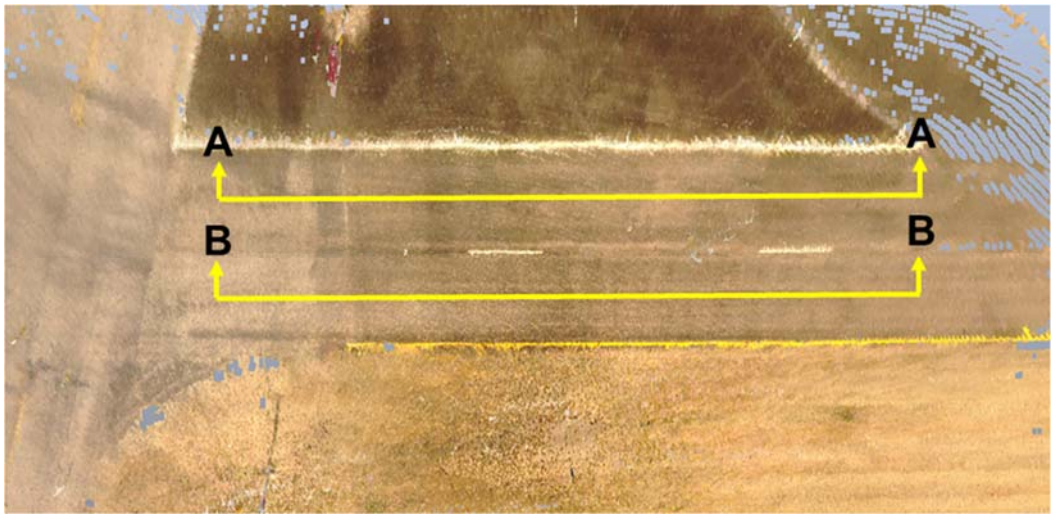

Figure 6.20 Elevation monitoring section of pavement of the U.S. 75 Frontage Road

Figure 6.21 presents the results of vertical deformation determined on pavement section from LIDAR surveys. The results show that there was insignificant value of approximately 12.7 mm (0.5 in.) in vertical swell-shrinkage deformation observed on the pavement section over a period of 7 months. Also, the effects of wet-dry cycle on the lane of close the slope section was found higher than the other lane during most of the observation period. As the lane farther from the slope (Section AA) was having a wide shoulder area, the moisture infiltration was lower than the lane close to slope. Hence, Section AA was found to experience less swelling-shrinkage induced deformation due to rainfall events.

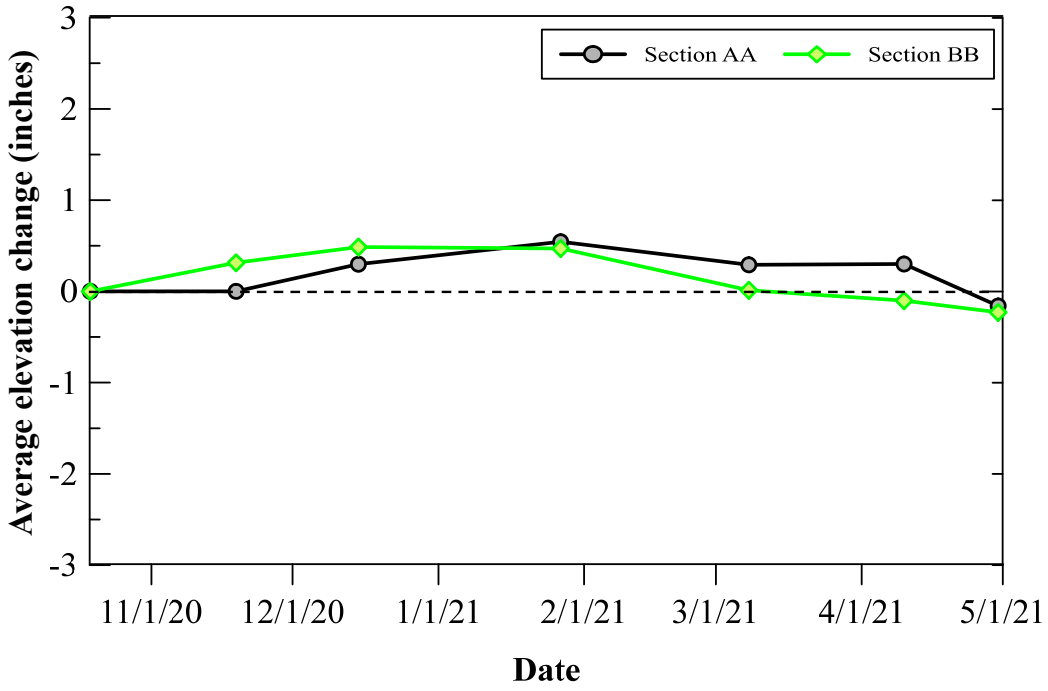

Figure 6.21 Measured elevation changes of the pavement of the U.S. 75 Frontage Road

Measured swelling and shrinkage induced vertical ground movements showed that the lime-treated slope performed exceptionally well during the 7 months of monitoring period. Throughout the monitoring period, the slope and pavement section of the U.S. 75 Frontage Road experienced vertical deformations less than 25.4 mm and 12.7 mm (1.0 and 0.5 in.), respectively. Also, the negligible fluctuation in the moisture content of underlying untreated layer confirms the absence of the desiccation cracks in surficial soil after the lime treatment. Hence, based on the results of overall field investigation studies, it was concluded that,

the lime treatment of the surficial soils of the slope of U.S. 75 Frontage Road enhanced the resiliency of the embankment slope and provided stability in the field conditions under seasonal wet-dry cycles. The next section details the overall expected cost related expenditures and benefits of this slope rehabilitation project for a 50-year life cycle period.

6.6 Life Cycle Cost and Benefit Analysis

6.6.1 Introduction

Each year, numerous surficial slope failures occur on embankments built with a moderate-to-high swelling potential clayey soil. The state department of transportation (DOT) agencies spend millions of dollars annually to repair these failures. According to the TxDOT (2019), the annual cost of repair of failed slopes in 2018 was around 28.5 million dollars in the state of Texas. In most of the cases, failed slopes are repaired by reconstructing and compacting the slope with the same soil without any stabilization method. This method is generally preferred as it involves few resources, low construction cost, and time. The main drawback of this method is that it does not improve engineering properties of soils, hence recurring failures occur in the slope. (McCleskey Jr 2005, Saftner et al. 2017, Shahandashti et al. 2019).

It has been reported that around 55% of total slope failures in the state of Texas are recurring failures, and approximately $15.6 million is spent annually to repair them (Shahandashti et al. 2019). Results of the laboratory tests, numerical

studies, and field monitoring studies conducted for U.S. 75 Frontage Highway slope showed that the lime treatment can be effectively used in rehabilitation of failed slopes to prevent recurring failures. The lime treatment increases the resilience of slope and provides a promising long-term stability.

While selecting a slope rehabilitation method, the overall life cycle expected costs and benefits analysis is given a proper consideration. For the current research project, the economic viability of the proposed lime treatment method was evaluated by performing a comprehensive life cycle cost and benefit analysis (LCCBA) tool. In this analysis, the costs and benefits of initial construction, major maintenance works, user costs and traffic delay costs caused by the rebuilding and compaction method and lime treatment method are determined and compared for a selected analysis period. These analyses will eventually help decision makers in the selection of a feasible and economical rehabilitation method for embankment slopes.

6.6.2 Methodology

The costs and benefits of lime treatment in the current project were estimated based on available data and reasonable assumptions. As the embankment slopes are generally designed for a long period of service life, the LCCBA analyses were performed considering the 50 years of period starting from the year of 2020. The future capital cost was reported using the time value of

money, and all the future expenses were converted to today's present value (PV) by using a discount rate. PV was calculated using the following equation:

$$\text{PV} = C \text{ x } \frac{1}{(1+i)^n} \tag{6.2}$$

Where,

C = cost of the activity,

i = discount rate, and

n = years of expenditure.

The acceptable value of discount rate in LCCBA usually lies between 3% and 5% (Walls III and Smith 1998). In this study, discount rate of 4% was selected based on recommendations of Little (1995). The summation of all expected costs and benefits of the lime treatment work were calculated as a present value by using following equation:

$$\text{PV} = C_0 + \sum_{n=1}^{N} \frac{C_n}{(1+0.04)^n} \tag{6.3}$$

Where,

C_0 = Cost of the immediate activity which was invested in year of 0 (2020),

N = the considered life cycle period,

i = discount rate, and

n = years of expenditure.

The calculation of present value of total cost (PV_c) and present value of total benefits (PV_b) was primarily based on following categories:

1) Agency costs (AC) – includes the cost related to initial construction work, the future maintenance and rehabilitation works over the considered analysis period.
2) User costs – that cover traffic delays and related vehicle operating costs due to the maintenance work.

The PV_c of the lime treatment method of rehabilitation basically consists of initial immediate construction cost of lime repair work, and the user costs during the repair work. As lime treatment provides resilience to the slope, there was not any future maintenance and operation costs involved in calculation of present value of total costs. Recurring shallow slope failure are frequently observed in the slopes which are repaired using rebuilding and compacting method.

Stauffer and Wright (1984) reported that slope having ratio of 3H:1V or steeper and with soil having LL over 50 is likely experience failure in future and on an average, a such slopes experience failure in 19.4 years. Therefore, in the case of U.S. 75 Frontage Road slope, it is reasonable to assume 2 failures within the next 50 years of service life. As the previous slope failure also damaged the overlying pavement structure, it was assumed that at least one of the failures in future will damage the overlying pavement structure. Therefore, in the calculation of PV_b, the initial cost of repair in the rebuild and compaction method, the expected damage on the overlying pavement structure, pavement damage related traffic delays, and vehicle operating costs were included.

After calculating PV_c and PV_b for the project, the benefit to cost ratio (BCR), also known as profitability index, of the lime repair work of slope was calculated by using Equation 6.4. Based on the results the economical aspect of the lime treatment slope repair project was assessed. The BCR value represents that the economical and profitable aspects of the project in long-term basis. The following section presents the results of the LCCBA conducted for the lime treatment repair work of U.S. 75 Frontage Road.

$$\text{BCR} = \frac{PV_b}{PV_c} \tag{6.4}$$

6.6.3 Life Cycle Cost and Benefit Analysis of Lime-Treated Slope

6.6.3.1 Costs Estimation

The LCCBA of the current lime-treated project was conducted on a portion of failed section of U.S. 75 frontage road slope which had longitudinal extent of 150 ft, width of 110 ft and an average failure depth of 3.5 ft. For this project, a total of 57,726 ft^3 of untreated soil was excavated, and around 133 tons of hydrated lime slurry was mixed with untreated soil for lime treatment. Over the treated layer, a 6 in. thick layer of topsoil of was placed over an area of 16,500 ft^2. Also, underdrain PVC pipes (900 ft in total) were installed in treated slope section to enhance its stability.

The cost of expenses such as traffic safety and control (i.e., installation and removing the of object makers, traffic barriers etc.) were determined for the of

slope section based on the average unit price spend for the entire project. The cost of regular maintenance operation for the overlying vegetation cover (trimming) conducted by state DOT is not included in this analysis as it is the same for untreated and lime-treated slope sections.

The maintenance cost for treated slope is considered negligible in this project as the numerical analysis showed that the treated slope section will not experience failure even under harsh environmental conditions. The quantities and cost information for repair works of slope, provided by the TxDOT Paris office and contractor of the project, are presented in Table 6.2. For the current lime treatment project, the calculated total cost for repair of 16,500 ft^2 of slope area was $142,386. The life cycle cost of lime treatment repair method with the provision of underdrain systems was calculated as $8.63/$ft^2$.

Table 6.2 Summary of cost estimation of the lime treatment slope rehabilitation method

Activity	Cost ($)
Total costs of excavation work	$25,667
Total cost of compaction	$38,500
Cost of lime slurry used	$25,303
Mixing and labor cost of lime treatment	$9,167
Material and labor cost of underdrain pipes	$22,500
Furnishing and placing of topsoil	$5,500
Seeding, watering, and labor cost of vegetation cover	$9,286
Traffic safety and control measurement cost	$6,463
Total cost	$142,386

6.6.3.2 Benefits Estimation

The main benefit of lime treatment method is the prevention of recurring failures in slope. The study conducted on slope failures observed in Texas by Stauffer and Wright (1984) showed that the untreated soil embankment slopes built with high plasticity clays typically experience failures between 11 to 31 years after construction with a mean value of 19.4 years. Therefore, for slope repaired using rebuilding and compaction method, it was assumed that at least 2 recurring failures will occur in 50 years of analysis period. These failures were assumed to occur 20 years and 40 years after the repair work. The repair cost of slides usually ranges from US$10,000 for temporary repairs to over US$100,000 for thorough repairs (Das et al 2018).

In this study, the cost of repairing the slope of U.S. 75 Frontage Road without lime treatment was calculated as $85,416. The untreated slope failures after 20 and 40 years later are assumed to cause damage to overlying pavement structure, therefore, pavement reconstruction costs were also included as a benefits of lime treatment repair method. The pavement section considered in this section is having dimensions of 150x 24 ft. The pavement section has 76.2 mm (3 in.) of hot mixture asphalt concrete (HMAC), under laid by 256.5 mm (10 in.) flexible base, and then 203.2 mm (8 in.) of 8% lime-treated subgrade. The costs of pavement repair works were calculated and is tabulated in Table 6.3. This calculated value was added to PV_b of lime treatment repair work.

Table 6.3 Repair cost of pavement damaged due to underlying slope failure

Activity	Total Cost ($)
Total costs dispose of existing pavement structure	$8,400
Total cost of material and compaction cost of subbase	$6,250
Material cost of lime slurry	$1,848
Mixing and labor cost of lime treatment	$1,350
Backfilling pavement edges	$27,750
Total cost of HMCA material and labor	$11,726
Total cost	$57,324

Due to pavement damage, the U.S. 75 Frontage Road was closed to traffic which caused traffic delays and extra vehicle operation costs. Hence, the user cost related to pavement damage was considered for in this study. The estimation of total time of traffic interruption was calculated based on the timeline of current project. The entire slope and pavement repair work for 1,100 ft long slope section was completed in 172 days. Please note that 172 days includes the excavation, compaction, building of pavement structure, furnishing and placing of topsoil, seeding and watering of vegetation cover, traffic safety and handling measurements. In the LCCBA of current project, the time of completion was approximated by considering the total project duration with the proportional length of the section considered in the analysis. Using this approach, time required for repairing 150 ft of slope was approximated to be 25 days.

The U.S. 75 Frontage Road is a low volume road with a yearly passing traffic of 31,058 cars and projected yearly traffic growth of 2%. As the distribution

of different type of vehicle passing from this road was not available, this information was estimated based on the results from the Habibzadeh-Bigdarvish et al. (2019), which was performed on Texas DOT conditions. The estimated traffic and its distribution for U.S. 75 Frontage Road in 2060 is presented in Table 6.4. Due to the 25 days of traffic interruption, the vehicle users would be required to use alternate roads which would increase the road trip by about 4.6 miles or 7 minutes of vehicle drive. The value of hourly travel delay information of the trucks and vehicles was adopted from Habibzadeh-Bigdarvish et al. (2019) and presented in the Table 6.5.

Table 6.4 Estimated traffic conditions of U.S. 75 Frontage Road in 2060

Traffic Data	**Value**
Average daily total number of vehicle and trucks pass	207
Average daily number of truck pass	10
Average number of daily non truck vehicle pass	197
Average daily traffic of personal travel (93.7%)	185
Average daily traffic of business travel (6.3 %)	12

Table 6.5 Hourly value of travel time estimated per vehicle (Habibzadeh-Bigdarvish et al. 2019)

Item	**Value ($/veh-hr.)**
Vehicle drive for personal purpose	$44.60
Vehicle drive for business purpose	$34.35
Truck drive	$19.84

The expected total cost of travel delays occurred due to repair work activities was calculated by multiplying the number of vehicle pass, the extended

travel time, and the unit cost of hourly travel time ($/hr) value is tabulated in Table 6.6.

Table 6.6 Estimated user cost due to the future traffic delay in 2060

Item	Cost ($)
Value of traffic delay for drive of personal purpose	$24,065
Value of traffic delay for drive of business purpose	$1,202
Value of traffic delay for truck drive	$579
Total costs	$25,846

As the route extension causes extra consumption of fuel, the additional vehicle operation costs were also included in the LCCBA as a user cost. In this study the average fuel consumptions for a truck and car were used as 6.1 miles per gallons (MPG) and 22.3 MPG, respectively (U.S. Dept. of Transportation 2019). With an average of $2.69 gas price and $3.06 diesel price the vehicle operation costs were calculated and is presented in Table 6.7 (U.S Energy Information Administration 2019).

Table 6.7 Estimated additional vehicle operation costs due to the pavement damage in 2060

Type	MPG	Unit Price ($/miles)	Total Cost of Additional Vehicle Operation Cost ($)
Non-truck drive	22.3	0.12	$2,719
Truck drive	6.1	0.50	$575
		Total cost	$3,294

The PV_b of the lime-treated slope rehabilitation work was calculated by including all the expected agency and user costs. The calculated PV_b for this project are tabulated in Table 6.8.

Table 6.8 Present value of benefits (PV_b) of lime-treated slope rehabilitation method

Year	**Activity**	**Cost ($)**	**Present Value ($)**
0	Initial repair cost	$85,416	$85,416
20	Recurring slope failure repair	$85,416	$38,983
20	Repair cost of pavement structure	$57,324	$26,162
20	Traffic delay cost on users	$17,467	$7,972
20	Additional vehicle operation cost on users	$2,238	$1,021
40	Recurring slope failure repair	$85,416	$17,791
40	Repair cost of pavement structure	$57,324	$11,940
40	Traffic delay cost on users	$25,846	$5,383
40	Additional vehicle operation cost on users	$3,294	$686
		Total	$195,354

For total repaired area of 16,500 ft^2, the life cycle benefits of lime treatment repair method was calculated as 11.83$/$ft^2$ which resulted in BCR value of 1.37. In one life cycle period of 50 years, the overall benefits of lime treatment method in slope outweighed its cost by 37%. Considering millions of dollars has been spent annually by the government agencies to maintain and repair their embankment slopes, 37% savings with application of lime-treatment method yields a very significant amount of capital saving. This result shows that apart from

increasing resilience of slope, the lime treatment rehabilitation method provides an economical solution for repairing failed slopes.

Once the construction workforce is highly familiar with the proposed rehabilitation procedures and equipment related to this method, this rehabilitation method can be conveniently and quickly applied with the help of advance construction machines in the field. Taking all these factors into account, lime treatment method was found as a cost effective, resilient, and viable rehabilitation method for failed slopes. By using this method, the state agencies can save a significant amount of money and provide a resilient infrastructure.

6.7 Summary

This chapter presents the details of the rehabilitation work of the failed slope section U.S. 75 Frontage Road using the lime treatment. All the phases of construction including excavation, lime treatment, and installation of drainage system were discussed in detail. After the construction, the performance of lime treatment section was monitored by using field instrumentation and survey techniques. Moisture probes, installed during construction, were used to capture fluctuation in moisture content soil with time. The vertical deformation of slope was obtained by conducting total station and LIDAR surveys. Post treatment field investigations showed that the lime treatment effectively reduces the moisture intrusion in the soil and prevents excessive swelling or shrinkage of soil. Also, the treated slope section underwent less than an inch swelling within 7 months of

investigation period. Based on this field monitoring results, the application of lime treatment method on U.S. 75 Frontage Road was assessed as successful.

Moreover, the economic feasibility of lime treatment work was evaluated by performing life cycle cost and benefit analysis. For the present study, the BCR for the lime treatment rehabilitation method was calculated as 1.37. This value indicates that rehabilitation of failed slope using lime treatment resulted in 37% saving for a life cycle period of 50 years. Although the initial cost of repair in lime treatment method is high, the maintenance cost and operational cost are almost negligible. The findings of this chapter have demonstrated that the proposed research solution using lime stabilized slope repair method is a resilient, economically viable and promising slope repair method.

Chapter 7

SUMMARY, FINDINGS AND FUTURE RESEARCH DIRECTIONS

7.1 Summary

In this research, an attempt has been made to evaluate the long-term effectiveness of the lime treatment method in mitigation of surficial slope failures. Three different expansive clayey slopes sections (U.S. 75 Frontage Road slope, Joe Pool lake and Grapevine dam embankment slopes) were considered and of which two dam embankments had experienced surficial failures in the past and were stabilized with lime treatment method. All these sections are considered in the present study.

A forensic analysis was first conducted to determine the causes of surficial failure of U.S. 75 Frontage Road slope by incorporating the effects of the weathering cycles and rainfall events on the soil properties and slope stability, respectively. The assessment of lime treatment method for stabilization of slope the U.S. 75 Frontage Highway was carried out as per a framework developed in this study. This framework includes determination of long-term engineering properties of the treated soil, analysis of stability of slope under different environmental conditions using a numerical method, and field monitoring post construction.

A comprehensive experimental program was planned to determine the long-term strength parameters and durability characteristics of both untreated and treated soils under different wet and dry cycles. The soil-mix design studies for the rehabilitation work of U.S. 75 Frontage Road slope were conducted with different stabilizer treatment dosages and curing periods. The peak and FSS shear strength properties of untreated and treated soils were determined by using direct shear and torsional ring shear tests. Laboratory durability tests were then performed on lime-treated soils under wet and dry cycles to investigate the long-term performance of lime treatment method and also to determine the optimum dosage of lime, along with their strength properties, and hydraulic related properties of soils including permeability and SWRC data.

The long-term performance of three lime stabilized slopes were then studied by conducting rainfall-induced transient seepage and unsaturated slope stability analyses using FEM and LEM methods, respectively. The effect of weathering cycles on the safety of slope was studied by using the FSS parameters in the numerical model. In this study, besides the U.S. 75 Frontage Highway slope embankment, the long-term performance of lime-stabilized embankment slopes of Grapevine and Joe Pool dams were also studied using similar numerical analysis method. The stabilities of these slopes were again evaluated by considering the expected rainfall characteristics for these slope locations and incorporating the

effects of the changes in hydro-mechanical properties of soils in the numerical modeling.

The post-construction performance of the newly stabilized U.S. 75 Frontage Road slope was evaluated by using field instrumentation and surveys. The moisture content variation in slopes under varying climatic conditions (wet-dry seasons) was investigated by moisture probes installed during the construction process. Additionally, the swell-shrinkage induced deformations of the lime-treated slopes were obtained by conducting both total station and LIDAR surveys. Moreover, the long-term economic feasibility of the lime stabilized slope method was also determined by performing life cycle cost analyses and benefits studies for the slope rehabilitation works of the Frontage Road. Based on these studies, the following salient findings are inferred.

7.2 Summary of Findings

1. The soil from the U.S. 75 Frontage Road slope was found to have a high plasticity index value of 37% and swelling and shrinkage strains of 7.2% and 17.7%, respectively. These results show the embankment soil's susceptibility to development of desiccation cracks from weathering cycles.
2. In the long-term FSS condition, there is a significant reduction in the shear strength properties of untreated soil due to the weathering cycles. This reduction in shear strength of soil is primarily because of loss of its

cohesion due to cyclic wet-dry cycles. In FSS condition, the friction angle of soil decreased slightly, while the cohesion intercept became was small and almost negligible (close to zero). The low shear strength of the embankment soil near surface results in surficial slope failures.

3. Forensic analyses conducted on the failed slopes of the U.S. 75 Frontage Highway showed the presence of the desiccation cracks in the surficial layers of clayey soils leading to an increase in soil permeability, which eventually resulted in high rainfall water infiltration. The infiltrated water accumulated in the desiccated surficial layers resulting in a perched water table. The development of perched water table during the prolonged precipitation and along with a degradation in soil properties were the causes of the surficial slope failures along the U.S. 75 Frontage Road highway.
4. The soil mix design studies show that the lime treatment significantly enhanced both the peak and FSS parameters of soil. After the lime treatment, the cohesion intercept parameters from DS tests results (peak strength) significantly increased by upto more than 3 times while the friction angle was increased by upto 1.7 times. Also, in FSS conditions, the lime treatment increased the cohesion value and friction angle of soil by upto 5.1 and 1.3 times those of untreated soil, respectively. This observation indicates that the lime-treated soil exhibits a significant shear

strength even after cyclic weathering cycles. The presence of the small amount of cohesion intercept in lime-treated soil can mitigate the development of surficial slope failures.

5. The hydraulic conductivity of soil highly influences the slope stability under different rainfall characteristics. The high permeable soils of Grapevine and Joe Pool dam slopes allowed faster infiltration whereas, the low permeable soil of the U.S. 75 Frontage Road slope limited the water percolation. These results suggest that for a slope with low permeable soil, a long duration and less intense rainfall event is more critical than a short duration and intense rainfall event.
6. The estimation of lime dosage from standard pH tests and Eades and Grim method do not consider the destructive impacts of wet-dry cycles on properties of soil. Durability and strength retention laboratory tests in the soil-mix design studies are found crucial in determination of the optimum dosage of lime stabilizer for any lime treatment project.
7. The numerical analyses studies conducted on all rehabilitated slope sections yielded a minimum FOS value of 1.45 under any rainfall conditions and related characteristics. These results highlight the efficacy of the lime treatment in providing long-term stability to a slope subjected to harsh environmental conditions.

8. The rainfall induced slope stability analyses of the U.S. 75 Frontage Road highlighted the importance of providing an underlying drainage system in a slope. Results showed that the factor of safety of slope was increased by upto 21% after installation of drainage system which mitigates the development of perched water table in the surficial layer of the slope.
9. Post treatment field investigations showed that the lime treatment effectively reduced the moisture intrusion into the underlying untreated soil layers. Results showed that the moisture content of untreated soil was decreased by 5.44% over a period of 17 months. Lime treatment prevents the development of desiccation cracks in the surficial soil layer and this protects the untreated underlying soil layers from the effects of rainfall events.
10. The results of field surveys showed that application of lime treatment on the surface layer of a slope efficiently reduces the swelling and shrinkage induced deformations in the slope and pavement structure. Results showed that the slope section underwent less than an inch of swelling within 7 months of the current monitoring period. Because of the lime treatment and a subsurface drainage system at the embankment site, the underlying untreated soil layer exhibits low swelling from reduced moisture infiltration.

11. The life cycle cost and benefit analysis conducted for the slope rehabilitation works of the U.S. 75 Frontage Road showed that the expected overall benefits of the lime stabilized slope are 37% more than the expected expenditures for the 50 years of life cycle period. Though the initial application costs of lime stabilization was found to be high, the expected maintenance and operational costs are low and almost negligible. Apart from its advantages including easy constructability on wide range of clayey soils, and strong resiliency and promising slope stability performance so far, the lime stabilization of surficial slopes proven to be an economical method for repairing of slopes.

7.3 Future Research Needs

As a part of future research needs, the following recommendations are suggested:

1) The field investigating studies shall be conducted for longer periods and robust numerical models of the rainfall infiltration and deformation characteristic of lime-treated slope are needed.
2) The actual long-term strength and permeability of lime-treated soils shall be determined by conducting laboratory tests on the soil samples collected from the field and the obtained strength data can be correlated with FSS parameters.

3) The impacts of the lime treatment on the permeability value of soils can be better depicted by conducting pore size distribution and microstructural studies on the treated soils.
4) The strength improvement characteristics of lime-treated soils observed in the FSS conditions can be studied using the microstructural studies.

REFERENCES

Abrams, T.G., and Wright, S.G. 1972. A survey of earth slope failures and remedial measures in Texas.

Abramson, L.W., Lee, T.S., Sharma, S., and Boyce, G.M. 2001. Slope stability and stabilization methods. John Wiley & Sons.

Acharya, R. 2015. Enhanced Shrinkage Characterization of Clayey Soils, P.h.D dissertation, University of Texas at Arlington.

Adem, H.H., and Vanapalli, S.K. 2013. Constitutive modeling approach for estimating 1-D heave with respect to time for expansive soils. International Journal of Geotechnical Engineering, 7(2): 199–204. doi:10.1179/1938636213Z.00000000024.

Akcanca, F., and Aytekin, M. 2014. Impact of wetting–drying cycles on the hydraulic conductivity of liners made of lime-stabilized sand–bentonite mixtures for sanitary landfills. Environmental earth sciences, 72(1): 59–66. Springer.

Al-Ani, T., and Sarapää, O. 2008. Clay and clay mineralogy. Physical-chemical Properties and Industrial Uses,.

Al-Dakheeli, H., and Bulut, R. 2019. Interpretation of Desiccation Soil Cracking in the Framework of Unsaturated Soil Mechanics.

Al-Mukhtar, M., Khattab, S., and Alcover, J.-F. 2012a. Microstructure and geotechnical properties of lime-treated expansive clayey soil. Engineering

geology, 139: 17–27. Elsevier.

Al-Mukhtar, M., Khattab, S., and Alcover, J.-F. 2012b. Microstructure and geotechnical properties of lime-treated expansive clayey soil. Engineering Geology, 139–140: 17–27. doi:10.1016/j.enggeo.2012.04.004.

Al-Mukhtar, M., Lasledj, A., and Alcover, J.-F. 2010. Behaviour and mineralogy changes in lime-treated expansive soil at 20°C. Applied Clay Science, 50(2): 191–198. doi:10.1016/j.clay.2010.07.023.

Al-Rawas, A.A., and Goosen, M.F.A. 2006. Expansive soils: recent advances in characterization and treatment. Taylor & Francis.

Al-Rawas, A.A., Hago, A.W., and Al-Sarmi, H. 2005. Effect of lime, cement and Sarooj (artificial pozzolan) on the swelling potential of an expansive soil from Oman. Building and Environment, 40(5): 681–687. Elsevier.

Albrecht, B.A., and Benson, C.H. 2001. Effect of Desiccation on Compacted Natural Clays. Journal of Geotechnical and Geoenvironmental Engineering, 127(1): 67–75. American Society of Civil Engineers. doi:10.1061/(ASCE)1090-0241(2001)127:1(67).

Anderson, D.C., Brown, K.W., and Thomas, J.C. 1985. Conductivity of compacted clay soils to water and organic liquids. Waste Management & Research, 3(4): 339–349. Elsevier.

Association, N.L. 2004. Lime-treated soil construction manual: Lime stabilization and lime modification. The Association.

Au, S.W.C. 1998. Rain-induced slope instability in Hong Kong. Engineering Geology, 51(1): 1–36. Elsevier.

Azmi, M., Ramli, M.H., Hezmi, M.A., Mohd Yusoff, S.A.., and Alel, M.N.A. 2019. Estimation of Soil Water Characteristic Curves (SWCC) of mining sand using soil suction modelling. IOP Conference Series: Materials Science and Engineering, 527: 012016. doi:10.1088/1757-899X/527/1/012016.

Bagherzadeh Khalkhali, A., and Kabiri Koochaksaraei, M. 2019. Evaluation of Limit Equilibrium and Finite Element Methods in Slope Stability Analysis-Case Study of Zaremroud Landslide, Iran. Computational Engineering and Physical Modeling, 2(3): 1–15. Pouyan Press.

Banerjee, A. 2017. Response of Unsaturated Soils Under Monotonic and Dynamic Loading over Moderate Suction States. Doctoral Dissertation, The University of Texas at Arlington, Arlington, Texas.

Barton, C.D., and Karathanasis, A.D. 2002. Clay minerals. Encyclopedia of Soil Science. Marcel Dekker, Inc. AH rights reserved.

Bell, F.G. 1996. Lime stabilization of clay minerals and soils. Engineering geology, 42(4): 223–237. Elsevier.

Bell, F.G., and Culshaw, M.G. 2001. Problems soils: a review from a British perspective. *In* Problematic Soils: Proceedings of the Symposium held at the Nottingham Trent University on 8 November 2001. Thomas Telford Publishing. pp. 1–35.

Benson, C.H. 2001. Effect of Desiccation on Compacted Natural Clays. 0241(March). doi:10.1061/(ASCE)1090-0241(2001)127.

Berg, R.R., Collin, J.G., Taylor, T.P., and Watts, C.F. 2020. Case history on failure of a 67 M tall reinforced soil slope. Geotextiles and Geomembranes,. doi:10.1016/j.geotexmem.2020.06.003.

Bhaskar, P., Boluk, B., Banerjee, A., Shafikhani, A., and Puppala, A. 2019a. Unsaturated Soils. *In* Geo-Congress 2019. American Society of Civil Engineers, Reston, VA. pp. 773–783.

Bhaskar, P., Boluk, B., Banerjee, A., Shafikhani, A., and Puppala, A. 2019b. Effect of Lime Stabilization on the Unsaturated Hydraulic Conductivity of Clayey Soil in Texas. *In* Geo-Congress 2019. American Society of Civil Engineers, Reston, VA. pp. 773–783.

Bhaskar, P. 2020. Transient seepage and slope stability analysis in partially saturated earthen dam, P.h.D dissertation, University of Texas at Arlington.

Bhattacharja, S., and Bhatty, J. 2003. Comparative performance of portland cement and lime stabilization of moderate to high plasticity clay soils. Portl. Cem. Assoc,.

Boluk, Burak, Anand J. Puppala, Sayantan Chakraborty, and Puneet Bhaskar. "Forensic Analyses and Rehabilitation of a Failed Highway Embankment Slope in Texas." Transportation Research Record (2021): 0361198121996359.

Bordoloi, S., Ni, J., and Ng, C.W.W. 2020. Soil desiccation cracking and its characterization in vegetated soil: A perspective review. Science of The Total Environment, 729: 138760. doi:10.1016/j.scitotenv.2020.138760.

Boynton, S.S., and Daniel, D.E. 1985. Hydraulic Conductivity Tests on Compacted Clay. Journal of Geotechnical Engineering, 111(4): 465–478. American Society of Civil Engineers. doi:10.1061/(ASCE)0733-9410(1985)111:4(465).

de Brito Galvão, T.C., Elsharief, A., and Simões, G.F. 2004. Effects of Lime on Permeability and Compressibility of Two Tropical Residual Soils. Journal of Environmental Engineering, 130(8): 881–885. doi:10.1061/(ASCE)0733-9372(2004)130:8(881).

Broms, B., and Boman, P. 1977. Stabilization of soil with lime–soil columns. Design Handbook, 2nd Edn., Royal Institute of Technology, Stockholm, Sweden,.

Burger, C.A., and Shackelford, C.D. 2001. Soil-water characteristic curves and dual porosity of sand–diatomaceous earth mixtures. Journal of geotechnical and geoenvironmental engineering, 127(9): 790–800. American Society of Civil Engineers.

Caballero, S., Acharya, R., Banerjee, A., Bheemasetti, T. V., Puppala, A.J., and Patil, U. 2016. Sustainable Slope Stabilization Using Biopolymer-Reinforced Soil. *In* Geo-Chicago 2016. American Society of Civil Engineers, Reston,

VA. pp. 116–126.

Cai, F., and Ugai, K. 2004. Numerical analysis of rainfall effects on slope stability. International Journal of Geomechanics, 4(2): 69–78. American Society of Civil Engineers.

Campbell, J.B., and Wynne, R.H. 2011. Introduction to remote sensing. Guilford Press.

Castellanos, B.A. 2014. Use and measurement of fully softened shear strength. Virginia Tech.

Castellanos, B.A., Brandon, T.L., and VandenBerge, D.R. 2016. Use of fully softened shear strength in slope stability analysis. Landslides, 13(4): 697–709. Springer.

Chakraborty, S., and Nair, S. 2018. Impact of curing time on moisture-induced damage in lime-treated soils. International Journal of Pavement Engineering,: 1–13. doi:10.1080/10298436.2018.1453068.

Chan, Y.E.C., Ng, Q.L., Satyanaga, A., and Rahardjo, H. 2021. Regional Stability and Adaptation Measures against Rainfall-Induced Slope Failures. Environmental Geotechnics,: 1–16. doi:10.1680/jenge.20.00089.

Chen, D.H., and Won, M. 2007. Field Investigations of Cracking on Concrete Pavements. Journal of Performance of Constructed Facilities, 21(6): 450–458. doi:10.1061/(ASCE)0887-3828(2007)21:6(450).

Collin, J.G., Loehr, J.E., and Hung, C.J. 2008. Slope Maintenance and Slide

Restoration Reference Manual for NHI Course 132081, prepared for FHWA. *In* Report FHWA NHI-08-098.

Collins, B.D., and Short, R. 2006. Testing and Evaluation of Driven Plate Piles in Full-Size Test Slope: New Method for Stabilizing Shallow Landslides.

Congress, S.S.C., and Puppala, A.J. 2020. Evaluation of UAV–CRP Data for Monitoring Transportation Infrastructure Constructed over Expansive Soils. Indian Geotechnical Journal, 50(2): 159–171. doi:10.1007/s40098-019-00384-4.

Corathers, L.A., and Apodaca, L.E. 2017. 2017 Minerals Yearbook U.S. Department of the Interior U.S. Geological Survey LIME [ADVANCE RELEASE] ; US Department of the Interior. US Geological Survey: Virgina, VA, USA, April,.

Daneshmand, S., Huat, B., ASADI, A., and Farshchi, I. 2011. Slope Stability Analysis with Applicability of Lime in Capillary Barrier Effects. Electronic Journal of Geotechnical Engineering, 16.

Daniel, D.E. 1984. Predicting Hydraulic Conductivity of Clay Liners. Journal of Geotechnical Engineering, 110(2): 285–300. doi:10.1061/(ASCE)0733-9410(1984)110:2(285).

Daniel, D.E., and Wu, Y.-K. 1993. Compacted clay liners and covers for arid sites. Journal of Geotechnical Engineering, 119(2): 223–237. American Society of Civil Engineers.

Das, B.M., and Shukla, S.K. 2013. Earth anchors. J. Ross Publishing.

Day, R.W. 1996a. Design and Repair for Surficial Failures, Practice Periodical on Structural Design and Construction. August.

Day, R.W. 1996b. Design and repair for surficial slope failures. Practice Periodical on Structural Design and Construction, 1(3): 83–87. doi:10.1061/(ASCE)1084-0680(1996)1:3(83).

Day, R.W. 1999. Geotechnical and foundation engineering: design and construction. McGraw-Hill Professional.

Day, R.W., and Axten, G.W. 1989. Surficial Stability of Compacted Clay Slopes. Journal of Geotechnical Engineering, 115(41. Day, R. W., and G. W. Axten. Surficial Stability of Compacted Clay Slopes. Journal of Geotechnical Engineering, Vol. 115, No. 4, 1989, pp. 577–580. https://doi.org/10.1061/(ASCE)0733-9410(1989)115:4(577).): 577–580. American Society of Civil Engineers. doi:10.1061/(ASCE)0733-9410(1989)115:4(577).

DEATON III, H. 1984. Tieback Wall Stabilization of Railroad Embankments. Transportation Research Record, 1030: 29.

Deer, W.A. 2011. Rock-forming minerals. Geological Society of London.

Deng, L., Yuan, P., Liu, D., Annabi-Bergaya, F., Zhou, J., Chen, F., and Liu, Z. 2017. Effects of microstructure of clay minerals, montmorillonite, kaolinite and halloysite, on their benzene adsorption behaviors. Applied Clay Science,

143: 184–191. doi:10.1016/j.clay.2017.03.035.

Dronamraju, V.S. 2008. Studies on field stabilization methods to prevent surficial slope failures of earthfill dams. The University of Texas at Arlington.

Duncan, J.M., and Wright, S.G. 2005. Soil strength and slope stability. John Wiley & Sons.

Eades, J.L., and Grim, R.E. 1966. A quick test to determine lime requirements for lime stabilization. Highway research record, (139).

El-Rawi, N.M., and Awad, A.A.A. 1981. Permeability of lime stabilized soils. Transportation Engineering Journal of ASCE, 107(1): 25–35. ASCE.

Elsbury, B.R., Daniel, D.E., Sraders, G.A., and Anderson, D.C. 1990. Lessons learned from compacted clay liner. Journal of Geotechnical Engineering, 116(11): 1641–1660. American Society of Civil Engineers.

Escario, V., and Saez, J. 1986. The shear strength of partly saturated soils. Geotechnique, 36(3): 453–456. Thomas Telford Ltd.

Evans, G., L., and Bell, D., H. 1981. Chemical Stabilization Odloes", New Zealand, 10th ICSMFE, Stockholm, 3, 649-658. [19] Guney, Y., Sari, D., Cetin, M. ve Tuncan, M., 2007."Impact of Cyclic Wetting-Drying on Swelling Behavior of Lime-Stabilized Soil", Building and …. 10th ICSMFE, New Zealand.

Fabius, M., Bo, M.W., and Villegas, B. 2008. Stabilization Of A 30 M High Riverbank In Canada With Nails, Plates And Roots. Missouri University of

Science and Technology.

Fay, L., Akin, M., and Shi, X. 2012. Cost-effective and sustainable road slope stabilization and erosion control. Transportation Research Board.

Fickies, R.H., Fakundiny, R.H., and Mosley, E.T. 1979. Geotechnical analysis of soil samples from test trench at Western New York Nuclear Service Center. West Valley, New York, New York State Geological Survey, NUREG/Cft-0644, 21.

Fleming, R.L., Sills, G.L., and Steward, E.S. 1992. Lime stabilization of levee slopes. *In* Proceedings Second Interagency Symposium On Stabilization Of Soils And Other Materials, Metairie, LA.

Fredlund, D.G., and Krahn, J. 1977. Comparison of slope stability methods of analysis. Canadian geotechnical journal, 14(3): 429–439. NRC Research Press.

Fredlund, D.G., Morgenstern, N.R., and Widger, R.A. 1978. The shear strength of unsaturated soils. Canadian geotechnical journal, 15(3): 313–321. NRC Research Press.

Fredlund, D.G., and Rahardjo, H. 1993. Soil Mechanics for Unsaturated Soils. John Wiley & Sons, Inc., Hoboken, NJ, USA.

Fredlund, D.G., Rahardjo, H., and Fredlund, M.D. 2012. Unsaturated Soil Mechanics in Engineering Practice. John Wiley & Sons, Inc., Hoboken, NJ, USA.

Fredlund, D.G., Xing, A., and Huang, S. 1994. Predicting the permeability function for unsaturated soils using the soil-water characteristic curve. Canadian Geotechnical Journal, 31(4): 533–546. doi:10.1139/t94-062.

Gamez, J.A., and Stark, T.D. 2014. Fully Softened Shear Strength at Low Stresses for Levee and Embankment Design. Journal of Geotechnical and Geoenvironmental Engineering, 140(9): 06014010. American Society of Civil Engineers. doi:10.1061/(ASCE)GT.1943-5606.0001151.

Garg, N., and Maji, S. 2014. A critical review of principal traffic noise models: Strategies and implications. Environmental Impact Assessment Review, 46: 68–81. Elsevier Inc. doi:10.1016/j.eiar.2014.02.001.

Gasmo, J.M., Rahardjo, H., and Leong, E.C. 2000. Infiltration effects on stability of a residual soil slope. Computers and geotechnics, 26(2): 145–165. Elsevier.

Gay, G., and Schad, H. 2000. Influence of cement and lime additives on the compaction properties and shear parameters of fine grained soils. Otto-Graf-Journal, 11: 19.

Gedney, D.S., and Weber Jr, W.G. 1978. Design and construction of soil slopes. Transportation Research Board Special Report, (176).

Van Genuchten, M.T., Schaap, M.G., Mohanty, B.P., Simunek, J., and Leij, F.J. 1999. Modeling flow and transport processes at the local scale. Modelling of transport process in soils at various scales in time and space. Wageningen

Pers., Wageningen, the Netherlands,: 23–45. Citeseer.

George, A.M., Chakraborty, S., Das, J.T., Pedarla, A., and Puppala, A.J. 2018. Understanding Shallow Slope Failures on Expansive Soil Embankments in North Texas Using Unsaturated Soil Property Framework. *In* PanAm Unsaturated Soils 2017. American Society of Civil Engineers, Reston, VA. pp. 206–216.

Ghani, A.N.C., Taib, A.M., and Hasbollah, D.Z.A. 2020. Effect of rainfall pattern on slope stability. *In* Geotechnics for Sustainable Infrastructure Development. Springer. pp. 887–892.

Ghobadi, M.H., Abdilor, Y., and Babazadeh, R. 2014. Stabilization of clay soils using lime and effect of pH variations on shear strength parameters. Bulletin of Engineering Geology and the Environment, 73(2): 611–619. doi:10.1007/s10064-013-0563-7.

Gofar, N., Lee, M.L., and Kassim, A. 2007. Stability of unsaturated slopes subjected to rainfall infiltration. *In* Proceedings of the Fourth International Conference on Disaster Prevention and Rehabilitation. pp. 158–167.

Gofar, N., and Rahardjo, H. 2017. Saturated and unsaturated stability analysis of slope subjected to rainfall infiltration. MATEC Web of Conferences, 101: 05004. doi:10.1051/matecconf/201710105004.

Habibzadeh-Bigdarvish, O., Yu, X., Lei, G., Li, T., & Puppala, A. J. (2019). Life-Cycle cost-benefit analysis of Bridge deck de-icing using geothermal heat

pump system: A case study of North Texas. Sustainable cities and society, 47, 101492.

Harris, J.P., Sebesta, S., and Scullion, T. 2004. Hydrated lime stabilization of sulfate-bearing vertisols in Texas. Transportation Research Record, 1868(1): 31–39. SAGE Publications Sage CA: Los Angeles, CA.

He, S. 2019. Chemical Stabilization of Expansive Soils Using Liquid Ionic Soil Stabilizers (LISS). P.h.D dissertation, University of Texas at Arlington.

He, S., Yu, X., Banerjee, A., and Puppala, A.J. 2018. Expansive Soil Treatment with Liquid Ionic Soil Stabilizer. Transportation Research Record: Journal of the Transportation Research Board,: 036119811879299. doi:10.1177/0361198118792996.

Hedayati, M. 2016. Rainfall induced distress in low volume pavements. Civil and Environmental Engineering.

Highland, L., and Bobrowsky, P.T. 2008. The landslide handbook: a guide to understanding landslides. US Geological Survey Reston.

Hilf, J.W. 1956. An investigation of pore water pressure in compacted cohesive soils.

Holtz, D.R. and Kovacs, D.W. (1981) An Introduction to Geotechnical Engineering. Prentice-Hall, Inc.

Holtz, R.D., and Schuster, R.L. 1996. Stabilization of soil slopes. Landslides: Investigation and Mitigation, edited by: Turner A. K. and Schuster RL,

Transportation Research Board, Special Report, 247: 439–473.

Hotineanu, A., Bouasker, M., Aldaood, A., and Al-Mukhtar, M. 2015. Effect of freeze–thaw cycling on the mechanical properties of lime-stabilized expansive clays. Cold Regions Science and Technology, 119: 151–157. doi:10.1016/j.coldregions.2015.08.008.

Hoyos, L.R., Puppala, A.J., and Chainuwat, P. 2004. Dynamic properties of chemically stabilized sulfate rich clay. Journal of Geotechnical and Geoenvironmental Engineering, 130(2): 153–162. American Society of Civil Engineers.

Van Impe, W.F., and Flores, R.D.V. 2007. Underwater Embankments on Soft Soil: A Case History. CRC Press.

Jafari, N., Puppala, A., Chakroborty, S., and Boluk, B. 2019a. Integrated Full-Scale Physical Experiments and Numerical Modeling of the Performance and Rehabilitation of Highway Embankments.

Jafari, N.H., Puppala, A., Boluk, B., Cadigan, J.A., Chakraborty, S., Bheemasetti, T., and Pleasant, J.E. 2019b. Predicting the Performance of Highway Embankment Slopes. MATEC Web of Conferences, 271(2001): 02007. doi:10.1051/matecconf/201927102007.

Jafari, N.H., Puppala, A., Boluk, B., Cadigan, J.A., Chakraborty, S., Bheemasetti, T., and Pleasant, J.E. 2019c. Predicting the Performance of Highway Embankment Slopes. MATEC Web of Conferences, 271: 02007.

doi:10.1051/matecconf/201927102007.

Johnson, K.A., and Sitar, N. 1990. Hydrologic conditions leading to debris-flow initiation. Canadian Geotechnical Journal, 27(6): 789–801. NRC Research Press.

Jones Jr, D.E., and Holtz, W.G. 1973. Expansive soils-the hidden disaster. Civil Engineering, 43(8).

Jones, L.D., and Jefferson, I. 2012. Expansive soils. ICE Publishing.

Julina, M., and Thyagaraj, T. 2019. Quantification of desiccation cracks using X-ray tomography for tracing shrinkage path of compacted expansive soil. Acta Geotechnica, 14(1): 35–56. Springer.

Kassim, K.A., and Uuey, C.S. 2000. Consolidation characteristics of lime stabilised soil. Malaysian Journal of Civil Engineering, 12(1).

Kayyal, M.K., and Wright, S.G. 1991. "Investigation of Long-Term Strength Properties of Paris and Beaumont Clays in Earth Embankments." Research Report 1195-2F, Center for Transportation Research, The University of Texas at Austin.(November 1991) 125 pgs.

Khan, M.S., Hossain, S., Ahmed, A., and Faysal, M. 2017. Investigation of a shallow slope failure on expansive clay in Texas. Engineering Geology, 219: 118–129. Elsevier B.V. doi:10.1016/j.enggeo.2016.10.004.

Khattab, S.A., Al-Mukhtar, M., and Fleureau, J.-M. 2007. Long-term stability characteristics of a lime-treated plastic soil. Journal of materials in civil

engineering, 19(4): 358–366. American Society of Civil Engineers.

Klein, C., and Hurlbut, C.S. 1993. Systematic mineralogy part IV: Silicates. Manual of mineralogy,: 366–467. John Wiley and Sons New York.

Kleppe, J., and Olson, R. 1985. Desiccation Cracking of Soil Barriers. *In* Hydraulic Barriers in Soil and Rock. ASTM International, 100 Barr Harbor Drive, PO Box C700, West Conshohocken, PA 19428-2959. pp. 263-263–13.

Kodikara, J., and Costa, S. 2013. Desiccation Cracking in Clayey Soils: Mechanisms and Modelling. pp. 21–32.

Kodikara, J.K., Nahlawi, H., and Bouazza, A. 2004. Modelling of curling in desiccating clay. Canadian Geotechnical Journal, 41(3): 560–566. doi:10.1139/t04-015.

Konrad, J., and Ayad, R. 2011. Desiccation of a sensitive clay: Field experimental observations. Canadian Geotechnical Journal, 34: 929–942. doi:10.1139/t97-063.

Kota, P.B.V.S., Hazlett, D., and Perrin, L. 1996. Sulfate-bearing soils: problems with calcium-based stabilizers. Transportation research record, 1546(1): 62–69. SAGE Publications Sage CA: Los Angeles, CA.

Kristo, C., Rahardjo, H., and Satyanaga, A. 2017. Effect of variations in rainfall intensity on slope stability in Singapore. International Soil and Water Conservation Research, 5(4): 258–264. doi:10.1016/j.iswcr.2017.07.001.

Kumar, P., and Singh, S.P. 2008. Fiber-reinforced fly ash subbases in rural roads. Journal of transportation engineering, 134(4): 171–180. American Society of Civil Engineers.

Le, M. 2013. Investigations to develop field stabilization methods to mitigate surficial slope failures. Civil & Environmental Engineering.

Le, M., Puppala, A.J., and Pedarla, A. (n.d.). Effect of Compost Soil Treatment on Surficial Slope Stability in Fully Softened Condition. *In* IFCEE 2015. pp. 2748–2757.

Lee, L.M., Gofar, N., and Rahardjo, H. 2009. A simple model for preliminary evaluation of rainfall-induced slope instability. Engineering Geology, 108(3–4): 272–285. Elsevier. doi:10.1016/j.enggeo.2009.06.011.

Lees, G., Abdelkater, M.O., and Hamdani, S.K. 1982. Effect of the clay fraction on some mechanical properties of lime-soil mixtures. Highway Engineer, 29(11).

Lefsky, M.A., Cohen, W.B., Parker, G.G., and Harding, D.J. 2002. Lidar remote sensing for ecosystem studies: Lidar, an emerging remote sensing technology that directly measures the three-dimensional distribution of plant canopies, can accurately estimate vegetation structural attributes and should be of particular inte. BioScience, 52(1): 19–30. American Institute of Biological Sciences.

Leica. 2006. TPS - System 1000 System.

Leong, E.-C., Tripathy, S., and Rahardjo, H. 2003. Total suction measurement of unsaturated soils with a device using the chilled-mirror dew-point technique. Geotechnique, 53(2): 173–182. Thomas Telford Ltd.

Leong, E.C., and Rahardjo, H. 1997a. Permeability functions for unsaturated soils. Journal of geotechnical and geoenvironmental engineering, 123(12): 1118–1126. American Society of Civil Engineers.

Leong, E.C., and Rahardjo, H. 1997b. Review of Soil-Water Characteristic Curve Equations. Journal of Geotechnical and Geoenvironmental Engineering, 123(12): 1106–1117. doi:10.1061/(ASCE)1090-0241(1997)123:12(1106).

Li, W.C., Lee, L.M., Cai, H., Li, H.J., Dai, F.C., and Wang, M.L. 2013. Combined roles of saturated permeability and rainfall characteristics on surficial failure of homogeneous soil slope. Engineering Geology, 153: 105–113. doi:10.1016/j.enggeo.2012.11.017.

Little, D.N. 1995. Stabilization of pavement subgrades and base courses with lime.

Locat, J., Trembaly, H., and Leroueil, S. 1996. Mechanical and hydraulic behaviour of a soft inorganic clay treated with lime. Canadian geotechnical journal, 33(4): 654–669. NRC Research Press.

Louati, F., Trabelsi, H., Jamei, M., and Taibi, S. 2018. Impact of wetting-drying cycles and cracks on the permeability of compacted clayey soil. European Journal of Environmental and Civil Engineering,: 1–26. doi:10.1080/19648189.2018.1541144.

M. A. Al-Kiki, I., A. K. Al-Juari, K., and A. A. Khattab, D.S. 2008. Strength, Durability And Hydraulic Properties Of Clayey Soil Stabilized With Lime And Industrial Waste Lime. AL-Rafdain Engineering Journal (AREJ), 16(1): 102–116. doi:10.33899/rengj.2008.44026.

Maher, M.H., and Gray, D.H. 1990. Static response of sands reinforced with randomly distributed fibers. Journal of Geotechnical Engineering, 116(11): 1661–1677. American Society of Civil Engineers.

Mallela, J., Quintus, H. Von, and Smith, K. 2004. Consideration of lime-stabilized layers in mechanistic-empirical pavement design. The National Lime Association, 200: 1–40.

Matthews, C., Farook, Z., and Helm, P. 2014. Slope stability analysis–limit equilibrium or the finite element method. Ground Engineering, 48(5): 22–28.

McCallister, L.D., and Petry, T.M. 1992. Leach tests on lime-treated clays. Geotechnical testing journal, 15(2): 106–114. ASTM International.

McCleskey Jr, K.L. 2005. Experimental investigations to select stabilization methods to mitigate embankment desiccation cracks in order to reduce slope failures. The University of Texas at Arlington.

McCleskey, K.L.J. 2005. Experimental investigations to select stabilization methods to mitigate embankment desiccation cracks in order to reduce slope failures. The University of Texas at Arlington.

McDowell, C. 1959. Stabilization of soils with lime, lime-fly ash and other lime

reactive materials. Highway Research Board Bulletin, 231(1): 60–66.

Mitchell,]. K., Fundamentals of Soil Behavior, John Wiley and Sons, Inc. 1976.

Mizal-Azzmi, N., Mohd-Noor, N., and Jamaludin, N. 2011. Geotechnical approaches for slope stabilization in residential area. Procedia Engineering, 20: 474–482. Elsevier.

Moni, M.M., and Sazzad, M.M. 2015. Stability analysis of slopes with surcharge by LEM and FEM. International Journal of Advances in Structural and Geotechnical Engineering, 4(4): 216–225.

Morris, P.H., Graham, J., and Williams, D.J. 1992. Cracking in drying soils. Canadian Geotechnical Journal, 29(2): 263–277. NRC Research Press.

Mukherjee, S. 2012. Applied mineralogy: applications in industry and environment. Springer Science & Business Media.

Nahlawi, H., and Kodikara, J.K. 2006. Laboratory experiments on desiccation cracking of thin soil layers. Geotechnical and Geological Engineering, 24(6): 1641–1664. doi:10.1007/s10706-005-4894-4.

Nalbantoglu, Z., and Tuncer, E.R. 2001. Compressibility and hydraulic conductivity of a chemically treated expansive clay. Canadian geotechnical journal, 38(1): 154–160. NRC Research Press.

Nelson, D., and Allen, W.L. 1974. Sawdust as lightweight fill material. United States. Federal Highway Administration. Offices of Research and ….

Nelson, J.D., and Miller, D.J. 1992. Expansive soils : problems and practice in

foundation and pavement engineering. J. Wiley.

Nerincx, N., Bonelli, S., Puiatti, D., Herrier, G., Fry, J.-J., Tourment, R., and Nicaise, S. 2016. Impact of lime-treated soils performance on design of earthfill dikes.

Neubauer Jr, C.H., and Thompson, M.R. 1972. Stability properties of uncured lime-treated fine-grained soils.

Ng, C.W.W., and Menzies, B. 2014. Advanced unsaturated soil mechanics and engineering. CRC Press.

Ng, C.W.W., and Shi, Q. 1998. A numerical investigation of the stability of unsaturated soil slopes subjected to transient seepage. Computers and geotechnics, 22(1): 1–28. Elsevier.

Norrish, K. 1954. The swelling of montmorillonite. Discussions of the Faraday Society, 18: 120. doi:10.1039/df9541800120.

Ola, S.A. 1978. Geotechnical properties and behaviour of some stabilized Nigerian lateritic soils. Quarterly Journal of Engineering Geology and Hydrogeology, 11(2): 145–160. doi:10.1144/GSL.QJEG.1978.011.02.04.

Omidi, G.H., Thomas, J.C., and Brown, K.W. 1996. Effect of desiccation cracking on the hydraulic conductivity of a compacted clay liner. Water, Air, and Soil Pollution, 89(1–2): 91–103. doi:10.1007/BF00300424.

Onur, M.I., Tuncan, M., Evirgen, B., Ozdemir, B., and Tuncan, A. 2016. Behavior of Soil Reinforcements in Slopes. Procedia Engineering, 143: 483–489.

doi:10.1016/j.proeng.2016.06.061.

Ooi, T.A., and Tee, C.H. 2011. Advance in geogrid reinforced slopes in Malaysia. Geotechnical Engineering, 42(1): 9.

Padilla, J.M., Perera, Y.Y., Houston, W.N., and Fredlund, D.G. 2005. A new soil-water characteristic curve device. Proceedings of the advanced experimental unsaturated soil mechanics, EXPERUS,: 15–22.

Patel, A. 2019. Geotechnical Investigations and Improvement of Ground Conditions. Elsevier.

Pedarla, A., Chittoori, S., and Puppala, A.J. 2011. Influence of Mineralogy and Plasticity Index on the Stabilization Effectiveness of Expansive Clays. Transportation Research Record: Journal of the Transportation Research Board, 2212(1): 91–99. doi:10.3141/2212-10.

Perica, S., Pavlovic, S., Laurent, M.S., Trypaluk, C., Unruh, D., Martin, D., and Wilhite, O. (n.d.). NOAA Atlas 14: Precipitation Frequency Atlas of the United States Volume 10: Northeastern States.

Prozzi, J.A., and Luo, R. 2007. Using Geogrids to Minimize Reflective Longitudinal Cracking on Pavements over Shrinking Subgrades. Transportation Research Record: Journal of the Transportation Research Board, 2004(1): 99–110. doi:10.3141/2004-11.

Punthutaecha, K., Puppala, A.J., Vanapalli, S.K., and Inyang, H. 2006. Volume Change Behaviors of Expansive Soils Stabilized with Recycled Ashes and

Fibers. Journal of Materials in Civil Engineering, 18(2): 295–306. doi:10.1061/(ASCE)0899-1561(2006)18:2(295).

Puppala, A.J. 2016. Advances in ground modification with chemical additives: From theory to practice. Transportation Geotechnics, 9: 123–138. Elsevier.

Puppala, A.J., Chittoori, B.C.S., Talluri, N., Le, M., Bheemasetti, T., and Thomey, J. 2013. Stabilizer Selection for Arresting Surficial Slope Failures: A Sustainability Perspective. *In* Geo-Congress 2013. American Society of Civil Engineers, Reston, VA. pp. 1465–1474.

Puppala, A.J., Congress, S.S.C., and Banerjee, A. 2019a. Research Advancements in Expansive Soil Characterization, Stabilization and Geoinfrastructure Monitoring. pp. 15–29.

Puppala, A.J., Congress, S.S.C., and Banerjee, A. 2019b. Research Advancements in Expansive Soil Characterization, Stabilization and Geoinfrastructure Monitoring. pp. 15–29.

Puppala, A.J., Congress, S.S.C., Talluri, N., and Wattanasanthicharoen, E. 2019c. Sulfate-Heaving Studies on Chemically Treated Sulfate-Rich Geomaterials. Journal of Materials in Civil Engineering, 31(6): 04019076. doi:10.1061/(ASCE)MT.1943-5533.0002729.

Puppala, A.J., Intharasombat, N., and Vempati, R.K. 2005. Experimental studies on ettringite-induced heaving in soils. Journal of Geotechnical and Geoenvironmental Engineering, 131(3): 325–337. American Society of Civil

Engineers.

Puppala, A.J., Manosuthikij, T., and Chittoori, B.C.S. 2014a. Swell and shrinkage strain prediction models for expansive clays. Engineering Geology, 168: 1–8. doi:10.1016/j.enggeo.2013.10.017.

Puppala, A.J., Manosuthkij, T., Nazarian, S., and Hoyos, L.R. 2011. Threshold moisture content and matric suction potentials in expansive clays prior to initiation of cracking in pavements. Canadian Geotechnical Journal, 48(4): 519–531. doi:10.1139/t10-087.

Puppala, A.J., Mohammad, L.N., and Allen, A. 1996. Engineering behavior of lime-treated Louisiana subgrade soil. Transportation Research Record, 1546(1): 24–31. SAGE Publications Sage CA: Los Angeles, CA.

Puppala, A.J., Talluri, N., and Chittoori, B.C.S. 2014b. Calcium-based stabiliser treatment of sulfate-bearing soils. Proceedings of the Institution of Civil Engineers - Ground Improvement, 167(3): 162–172. doi:10.1680/grim.13.00008.

Puppala, A.J., Talluri, N., Congress, S.S.C., and Gaily, A. 2018. Ettringite induced heaving in stabilized high sulfate soils. Innovative Infrastructure Solutions, 3(1): 72. doi:10.1007/s41062-018-0179-7.

Tiwari, B., & Ajmera, B. (2011). A new correlation relating the shear strength of reconstituted soil to the proportions of clay minerals and plasticity characteristics. Applied Clay Science, 53(1), 48-57.

Qi, Y., Wang, Z., Xu, H., and Yuan, Z. 2020. Instability Analysis of a Low-Angle Low-Expansive Soil Slope under Seasonal Wet-Dry Cycles and River-Level Variations. Advances in Civil Engineering, 2020. Hindawi.

Qiang, X., Hai-jun, L., Zhen-ze, L., and Lei, L. 2014. Cracking, water permeability and deformation of compacted clay liners improved by straw fiber. Engineering Geology, 178: 82–90. Elsevier.

Qiang, Y., and Chen, Y. 2015. Experimental Research on the Mechanical Behavior of Lime-Treated Soil under Different Loading Rates. Advances in Materials Science and Engineering, 2015: 1–10. doi:10.1155/2015/862106.

Quang, N.D., and Chai, J.C. 2015. Permeability of lime- and cement-treated clayey soils. Canadian Geotechnical Journal, 52(9): 1221–1227. doi:10.1139/cgj-2014-0134.

Rahardjo, H., Leong, E.C., and Rezaur, R.B. 2008. Effect of antecedent rainfall on pore-water pressure distribution characteristics in residual soil slopes under tropical rainfall. Hydrological Processes: An International Journal, 22(4): 506–523. Wiley Online Library.

Rahardjo, H., Li, X.W., Toll, D.G., and Leong, E.C. 2001. The effect of antecedent rainfall on slope stability. *In* Unsaturated Soil Concepts and Their Application in Geotechnical Practice. Springer. pp. 371–399.

Rahardjo, H., Ong, T.H., Rezaur, R.B., and Leong, E.C. 2007a. Factors controlling instability of homogeneous soil slopes under rainfall. Journal of Geotechnical

and Geoenvironmental Engineering, 133(12): 1532–1543. American Society of Civil Engineers.

Rahardjo, H., Ong, T.H., Rezaur, R.B., and Leong, E.C. 2007b. Factors Controlling Instability of Homogeneous Soil Slopes under Rainfall. Journal of Geotechnical and Geoenvironmental Engineering, 133(12): 1532–1543. doi:10.1061/(asce)1090-0241(2007)133:12(1532).

Rahimi, A., Rahardjo, H., and Leong, E.-C. 2011. Effect of Antecedent Rainfall Patterns on Rainfall-Induced Slope Failure. Journal of Geotechnical and Geoenvironmental Engineering, 137(5): 483–491. doi:10.1061/(ASCE)GT.1943-5606.0000451.

Rahimi, A., Rahardjo, H., and Leong, E. 2015. Effects of soil – water characteristic curve and relative permeability equations on estimation of unsaturated permeability function. Soils and Foundations, 55(6): 1400–1411. Elsevier. doi:10.1016/j.sandf.2015.10.006.

Rajasekaran, G., and Narasimha Rao, S. 2002. Permeability characteristics of lime treated marine clay. Ocean Engineering, 29(2): 113–127. doi:10.1016/S0029-8018(01)00017-8.

Ran, Q., Hong, Y., Li, W., and Gao, J. 2018. A modelling study of rainfall-induced shallow landslide mechanisms under different rainfall characteristics. Journal of Hydrology, 563: 790–801. Elsevier.

Rao, S.M., Reddy, B.V. V, and Muttharam, M. 2001. The impact of cyclic wetting

and drying on the swelling behaviour of stabilized expansive soils. Engineering geology, 60(1–4): 223–233. Elsevier.

Rapp, G.R. 2002. Archaeomineralogy. Springer Science & Business Media.

Rayhani, M.H., Yanful, E.K., and Fakher, A. 2007. Desiccation-induced cracking and its effect on the hydraulic conductivity of clayey soils from Iran. Canadian Geotechnical Journal, 44(3): 276–283. doi:10.1139/t06-125.

Reddy, K.R. 2002. Engineering properties of soils based on laboratory testing. Department of Civil and Materials Engineering. University of Illinois, Chicago,.

Le Runigo, B., Ferber, V., Cui, Y.-J., Cuisinier, O., and Deneele, D. 2011. Performance of lime-treated silty soil under long-term hydraulic conditions. Engineering geology, 118(1–2): 20–28. Elsevier.

Sabtan, A.A. 2005. Geotechnical properties of expansive clay shale in Tabuk, Saudi Arabia. Journal of Asian Earth Sciences, 25(5): 747–757. doi:10.1016/j.jseaes.2004.07.003.

Saftner, D., Carranza-Torres, C., and Nelson, M. 2017a. Slope Stabilization Guide.

Saftner, D., Carranza-Torres, C., and Nelson, M. 2017b. Slope stabilization and repair solutions for local government engineers. Minnesota Department of Transportation.

Saleh, A.A., and Wright, S.G. 1997. Shear strength correlations and remedial measure guidelines for long-term stability of slopes constructed of highly

plastic clay soils.

Sapkota A. 2019. Effect Of Modified Moisture Barriers On Slopes Stabilized With Recycled Plastic Pins. P.h.D dissertation, University of Texas at Arlington.

Shafikhani, A. 2018. A New Approach for Performance Evaluation of Bridge Infrastructure Using Terrestrial Lidar and Advanced Mathematical Modeling. P.h.D dissertation, University of Texas at Arlington.

Shahandashti, M., Hossain, S., Khankarli, G., Zahedzahedani, S.E., Abediniangerabi, B., and Nabaei, M. 2019. Synthesis on Rapid Repair Methods for Embankment Slope Failure.

Sharma, A.K., and Sivapullaiah, P. V. 2016. Ground granulated blast furnace slag amended fly ash as an expansive soil stabilizer. Soils and Foundations, 56(2): 205–212. Elsevier.

Skempton, A.W. 1948. The rate of softening in stiff-fissured clays, with special reference to London clay. *In* Proc of the 2nd Int, Conf. Soil Mech. & Found. Engineering. p. 50.

Skempton, A.W. 1964. Long-term stability of clay slopes. Geotechnique, 14(2): 77–102.

Skempton, A.W. 1970. First-time slides in overconsolidated clays. Geotechnique, 20(3): 320–324.

Skempton, A.W. 1977. Slope stability of cuttings in Brown London Clay. *In* In Proceedings of the Ninth International Conference on Soil Mechanics

Foundation Engineering Held in Tokyo, Japan 3 1977,. pp. 261–270.

Song, Z., Zhang, D., Mao, Y., Mu, Y., Zhang, K., and Zhang, Q. 2020. Behavior of Lime-Stabilized Red Bed Soil after Cyclic Wetting-Drying in Triaxial Tests and SEM Analysis. Advances in Materials Science and Engineering, 2020: 1–12. doi:10.1155/2020/4230519.

Steward, J.E., and Ribera, J.M. 1995. Launched Soil Nails: New Method for Rapid Low-impact Slope Repairs. *In* Proceeding of the Sixth International Conference on Low-Volume Roads. pp. 25–29.

Szendefy, J. 2013. Impact of the soil-stabilization with lime. *In* Proceedings of the 18th international conference on soil mechanics and geotechnical engineering, Paris. pp. 2601–2604.

Taliaferro, S. 2016. Review of Recent ODOT Geotechnical Research & Construction Projects.

Tang, C.-S., Cui, Y.-J., Tang, A.-M., and Shi, B. 2010. Experiment evidence on the temperature dependence of desiccation cracking behavior of clayey soils. Engineering Geology, 114(3–4): 261–266. Elsevier.

Tang, C.-S., Shi, B., Liu, C., Suo, W.-B., and Gao, L. 2011. Experimental characterization of shrinkage and desiccation cracking in thin clay layer. Applied Clay Science, 52(1–2): 69–77. doi:10.1016/j.clay.2011.01.032.

Taylor, D.W. 1937. Stability of earth slopes. J. Boston Soc. Civil Engineers, 24(3): 197–247.

Terzaghi, K. 1936. Stability of slopes of natural clay. Proc. lst. ICSMFE, Harvard, 1936, 1: 161–165.

Thompson, M.R. 1965. Shear strength and elastic properties of lime-soil mixtures.

Titi, H.H., and Helwany, S. 2007. Investigation of vertical members to resist surficial slope instabilities. Wisconsin. Dept. of Transportation. Bureau of Technical Services.

Tripathy, S., and Rao, K.S.S. 2009. Cyclic swell–shrink behaviour of a compacted expansive soil. Geotechnical and Geological Engineering, 27(1): 89–103. Springer.

Tsaparas, I., Rahardjo, H., Toll, D.G., and Leong, E.C. 2002. Controlling parameters for rainfall-induced landslides. Computers and geotechnics, 29(1): 1–27. Elsevier.

Tsaparas, I., and Toll, D.G. 2002. Numerical analysis of infiltration into unsaturated residual soil slopes. *In* Proceedings of the 3rd International Conference on Unsaturated Soils, Recife, Brazil. Swets & Zeitlinger, Lisse. pp. 755–762.

Ural, Nazile 2018. The importance of clay in geotechnical engineering. IntechOpen,.

USDA Forest Servi. 1994. Application Guide for Launched Soil Nails. No. EM 7170-12A. Washington, D.C.

Vanapalli, S.K., Sillers, W.S., and Fredlund, M.D. 1998. The meaning and

relevance of residual state to unsaturated soils. *In* 51st Canadian Geotechnical Conference. sn. pp. 4–7.

Velde, B. 1995. Composition and Mineralogy of Clay Minerals. *In* Origin and Mineralogy of Clays. Springer Berlin Heidelberg, Berlin, Heidelberg. pp. 8–42.

Walls III, J., and Smith, M.R. 1998. Life cycle cost analysis in pavement design-interim technical bulletin. United States. Federal Highway Administration.

Wang, D. 2017. Application and evaluation of non-destructive testing methods for buried pipes.

Wang, M., Kong, L., Zhao, C., and Zang, M. 2012. Dynamic characteristics of lime-treated expansive soil under cyclic loading. Journal of Rock Mechanics and Geotechnical Engineering, 4(4): 352–359. doi:10.3724/SP.J.1235.2012.00352.

Wang, Z.F., Li, J.H., and Zhang, L.M. 2011. Influence of cracks on the stability of a cracked soil slope. *In* Proc., 5th Asia-Pacisif Conf. on Unsaturated Soils (AP-UNSAT 2011). pp. 721–728.

Wei, X., Gao, C., and Liu, K. 2020. A Review of Cracking Behavior and Mechanism in Clayey Soils Related to Desiccation. Advances in Civil Engineering, 2020: 1–12. doi:10.1155/2020/8880873.

Williams, H.F.L. 2003. Urbanization pressure increases potential for soils-related hazards, Denton County, Texas. Environmental Geology, 44(8): 933–938.

doi:10.1007/s00254-003-0836-8.

Witczak, M.W. 1972. Relationships between physiographic units and highway design factors. NCHRP Report, (132).

Wright, S.G., Zornberg, J.G., and Aguettant, J.E. 2007. The Fully Softened Shear Strength of High Plasticity Clays. Project No. 0-5202-3, Center for Transportation Research, The University of Texas at Austin, (August 2007): 132 pgs.

Xian, Z., Hao, Y., Zhao, Y., and Song, S. 2017. Quantitative determination of isomorphous substitutions on clay mineral surfaces through AFM imaging: A case of mica. Colloids and Surfaces A: Physicochemical and Engineering Aspects, 533: 55–60. doi:10.1016/j.colsurfa.2017.08.024.

Yang, R., Huang, J., Griffiths, D., and Sheng, D. 2019a. Effects of desiccation cracks on slope reliability. *In* Proceedings of the 7th International Symposium on Geotechnical Safety and Risk (ISGSR).

Yang, R., Xiao, P., and Qi, S. 2019b. Analysis of Slope Stability in Unsaturated Expansive Soil: A Case Study. Frontiers in Earth Science, 7. doi:10.3389/feart.2019.00292.

Yeo, S.-S., and Hsuan, Y.G. 2010. Evaluation of creep behavior of high density polyethylene and polyethylene-terephthalate geogrids. Geotextiles and Geomembranes, 28(5): 409–421. doi:10.1016/j.geotexmem.2009.12.003.

Yesiller, N., Miller, C.J., Inci, G., and Yaldo, K. 2000. Desiccation and cracking

behavior of three compacted landfill liner soils. Engineering Geology, 57(1–2): 105–121. Elsevier.

Yong, R.N., and Warkentin, B.P. 1975. Soil Properties and Behaviour. Elsevier.

Zhai, Q., and Rahardjo, H. 2015. Estimation of permeability function from the soil – water characteristic curve. Engineering Geology, 199: 148–156. Elsevier B.V. doi:10.1016/j.enggeo.2015.11.001.

Zhang, F., and Fredlund, D.G. 2015. Examination of the estimation of relative permeability for unsaturated soils. 2087(May): 2077–2087.

Zhang, J., Zhu, D., and Zhang, S. 2020. Shallow slope stability evolution during rainwater infiltration considering soil cracking state. Computers and Geotechnics, 117: 103285. doi:10.1016/j.compgeo.2019.103285.

Zhang, L.L., Fredlund, D.G., Fredlund, M.D., and Wilson, G.W. 2014. Modeling the unsaturated soil zone in slope stability analysis. Canadian Geotechnical Journal, 51(12): 1384–1398. NRC Research Press. doi:10.1139/cgj-2013-0394.

Zhao, S., Shi, Z., Peng, M., and Bao, Y. 2020. Stability Analysis of Expansive Soil Slope Considering Seepage Softening and Moistening Expansion Deformation. Water, 12(6): 1678. doi:10.3390/w12061678.

Zhao, Y., Yi, H., Jia, F., Li, H., Peng, C., and Song, S. 2017. A novel method for determining the thickness of hydration shells on nanosheets: A case of montmorillonite in water. Powder Technology, 306: 74–79.

doi:10.1016/j.powtec.2016.10.045.

Zhou, A.-N., Sheng, D., and Carter, J.P. 2012. Modelling the effect of initial density on soil-water characteristic curves. Géotechnique, 62(8): 669–680. Thomas Telford Ltd.